2016

The Role of Microrna in Cardioprotection: Ischemic Preconditioning and Mesenchymal Stem Cell Paracrine Effects

Kristin Luther
Loyola University Chicago

LOYOLA UNIVERSITY CHICAGO

THE ROLE OF MICRORNA IN CARDIOPROTECTION: ISCHEMIC PRECONDITIONING AND MESENCHYMAL STEM CELL PARACRINE EFFECTS

A DISSERTATION SUBMITTED TO

THE FACULTY OF THE GRADUATE SCHOOL

IN CANDIDACY FOR THE DEGREE OF

DOCTOR OF PHILOSOPHY

PROGRAM IN PHARMACOLOGY

BY

KRISTIN LUTHER

CHICAGO, ILLINOIS

DECEMBER 2016

ACKNOWLEDGEMENTS

I would like to thank all of the people who made this dissertation possible, starting with the University of Cincinnati department of Pharmacology. I would like to thank the faculty for their excellent teaching and research rotation experiences. I would also like to acknowledge the department of Pharmacology at Loyola for making me welcome there during the second half of my graduate training. I appreciate all the help I have received along the way from professors and fellow students who shared their equipment, ideas, and expertise with me.

I thank my mentor Dr. Keith Jones, for the excellent training I received in his lab, and for the advice and opportunities he's given me over the past five years. I would also like to thank all of the Jones lab members, past and present, for making the lab a great place to work. A special thank you to Dr. Lauren Haar, for helping me in so many ways, especially for the birthday cakes. I would also like to thank Dr. Michael Tranter for mentoring me starting on my first day in the Jones lab. Thanks to Myc McGuinness for all of his hard work, training, and contributions to the Jones lab large and small. I would like to acknowledge Faryal Mallick who contributed to this dissertation by collecting and submitting the IPC and sham mouse heart tissue samples for the sequencing project.

Next I would like to thank my committee members for their support and helpful suggestions to advance the project. Their expertise made a huge difference to the quality of the finished work. Thanks also to our collaborator, Dr. Reineke, for working with us on the RNA-binding polymers.

Last but not least, I most sincerely appreciate the people in my personal life who supported me through the Ph.D. process, first and foremost my husband Sean for his constant support and encouragement. I would also like to thank my parents and friends for listening, commiserating, and celebrating with me throughout this process.

TABLE OF CONTENTS

LIST OF TABLES

LIST OF FIGURES

LIST OF ABBREVIATIONS

3'-UTR	3 prime untranslated region
ADRC	adipose derived regenerative cells
Ago-2	argonaute 2
Akt	Ak (mouse strain) transforming
ATF5	activating transcription factor 5
BCA	bicinchoninic acid
Bck-XL	B-cell lymphoma-extra large
Bcl-2	B-Cell CLL/Lymphoma 2
BDM	butanedione monoxime
BMMNC	bone marrow mononuclear cells
C-terminal	carboxy terminal
CDC	cardiosphere derived cell
CM	conditioned medium
CMV	cytomegalovirus
CSC	cardiac stem cell
DAPI	4',6-diamidino-2-phenylindole
DMEM	Dulbecco's modified Eagle medium
ECG	electrocardiogram
EGFP	enhanced green fluorescent protein
eNOS	endothelial nitric oxide synthase

EPC	endothelial progenitor cell
ER	endoplasmic reticulum
ERK1/2	extracellular regulated kinase-1 and -2
ESCRT	endosomal sorting complexes required for transport
FACS	fluorescence assisted cell sorting
FADD	Fas associated death domain
FasL	Fas ligand
FBS	fetal bovine serum
GAPDH	glyceraldehyde 3-phosphate dehydrogenase
GATA4	GATA binding protein 4
Grp78/BiP	78 kDa glucose-regulated protein
GW182	trinucleotide repeat containing 6A
HEK293T	human embryonic kidney 293T
HGF	hepatocyte growth factor
Hif-1	hypoxia inducible factor
hnRNPA2B1	Heterogeneous ribonuclear protein A2B1
HPC	hypoxic preconditioning
HRS	hepatocyte growth factor–regulated tyrosine kinase substrate
HS	heat shock
HSC	hematopoietic stem cell
Hsc70	heat shock cognate 71 kDa protein
Hsp110	heat shock protein 105 kDa
Hsp20	heat shock 20 kDa protein

Hsp22	heat shock 22 kDa protein
Hsp27	heat shock 27 kDa protein
Hsp40	heat shock 40 kDa protein
Hsp70	heat shock 70kDa protein
Hsp90	heat shock 90kDa protein
HUVEC	human umbilical vein endothelial cells
I/R	ischemia/reperfusion
ICAM	intracellular adhesion molecule 1
IkBα	NF-κB inhibitor alpha
ILV	intraluminal vesicle
IPC	ischemic preconditioning
LAD	left anterior descending artery
LDH 1	actate dehydrogenase
Mecp2	methyl CpG binding protein
MI	myocardial infarction
miRNA	micro-ribonucleic acid
MMP	matrix metalloproteinase
MOMP	mitochondrial outer membrane permeabilization
MP	microparticles
MPTP	mitochondrial permeability transition pore
MSC	mesenchymal stem cell
MVB	multivesicular body
N-terminal	amino terminal

NADPH	nicotinamide adenine dinucleotide phosphate
NEF	nucleotide exchange factor
NF-kB	nuclear factor of kappa light polypeptide gene enhancer in B cells
NMVM	neonatal murine ventricular myocytes
NO	nitric oxide
NOX4	NADPH oxidase 4
OGD	oxygen glucose deprivation
PBS	phosphate buffered saline
PCI	percutaneous intervention
PDCD4	programmed cell death 4
PDGF	platelet-derived growth factor
Pdia6	protein disulfide isomerase 6
PI	propidium iodide
PKC	protein kinase C
Pol II	RNA polymerase II
PTEN	phosphatase and tensin homologue mutated on chromosome 10
PTP1	protein tyrosine phosphatase 1
RIPA	radioimmunoprecipitation assay
RISK	reperfusion injury salvage kinase
RNS	reactive nitrogen species
ROS	reactive oxygen species
SERCA	sarco/endoplasmic reticulum Ca2+ ATPase
simI/R	simulated ischemia/reperfusion

SMAC	diablo homolog, mitochondrial
SR	sarcoplasmic reticulum
STAT	signal transducer and activator of transcription
Stc-1	stanniocalcin 1
TGF-b	tumor growth factor b
TIMP	tissue inhibitor of metalloproteinase
TSG101	tumor susceptibility gene 101 protein
TTC	triphenyl tetrazolium chloride
TUNEL	terminal deoxynucleotidyl transferase dUTP nick end labeling
VEGF	vascular endothelial growth factor
Vps4	vacuolar protein sorting 4 homolog

ABSTRACT

Changes in gene expression and protein levels are an important aspect of cardioprotection in which short non-coding RNA known as miRNA may play a key regulatory role. We investigated the functions of several miRNAs in the context of two cardioprotective stimuli, ischemic preconditioning (IPC) and mesenchymal stem cell (MSC) paracrine effects. We hypothesized that downregulation of a set of miRNAs (miR-148a/b, miR-30b, and let-7a*) augments expression of protective heat shock proteins during IPC, and that MSC exosomes transfer miR-21 to cardiomyocytes, resulting in downregulation of pro-apoptotic genes and reduction of infarct size.

IPC increased the level of Hsp70, Hsp90, and Hsp40 family members within 6 hours as measured by qPCR and Western blot. Luciferase reporter assays and miRNA mimic transfection and knockdown were used to confirm effects of miR-148a/b, miR-30b, and let-7a* on translation. Combinations of miRNAs had more pronounced effects than single miRNAs alone. Pretreatment with wild type exosomes, but not those lacking miR-21, reduced cell death *in vitro*, and decreased infarct size in mice. The wild type exosomes, and miR-21 mimic, decreased protein levels of the miR-21 target genes Fas Ligand, Programmed Cell Death 4, Phosphatase and Tensin Homolog, and Pellino1.

In conclusion, a small set of miRNAs may act synergistically as regulatory nodes in a heat shock protein expression network after IPC. Future studies will test whether manipulation of this set of miRNAs can induce cardioprotection. miR-21 plays a key role in pro-survival paracrine effects mediated by MSC exosomes. Future studies will test whether MSC exosomes mediate regeneration as well as cardioprotection.

CHAPTER 1

INTRODUCTION

THE ROLE OF MICRORNA IN ISCHEMIC PRECONDITIONING

Myocardial Infarction and Ischemia/Reperfusion Injury

It is estimated that 735,000 Americans experience a myocardial infarction (MI) each year[1]. MI occurs when a coronary artery is obstructed by an atherosclerotic plaque, clot, or vasospasm, causing the myocardium to be deprived of oxygen and nutrients, which is known as ischemia. Patients experience chest pain, nausea, dizziness, and fatigue. Most patients are admitted to the hospital 2.5 to 3 hours after onset of symptoms. The clinical treatment for MI is to re-open the artery through percutaneous intervention (PCI) or provide thrombolytic therapy. After the artery is re-opened, reperfusion of the myocardium occurs. While timely reperfusion is crucial to limit infarct size, reperfusion itself causes further injury, accounting for 30 to 50% of the cumulative damage[2, 3], which is known as ischemia/reperfusion (I/R) injury. During the next hours and days, the infarcted tissue is broken down in a process known as coagulation necrosis, and then neutrophils and macrophages infiltrate and phagocytose the dead cells. Next, granulation tissue forms, ultimately giving rise to a collagenous acellular scar within 6 to 8 weeks[4]. Complications from MI include heart failure, arrhythmia, future MI, angina pectoris, stroke, and sudden death[1]. Likelihood of these

complications is directly linked to the infarct size, so treatments to reduce this are of great clinical interest.

During ischemia ATP levels fall due to lack of oxygen, which is required for oxidative phosphorylation. Cardiomyocytes switch to anaerobic glycolysis, which leads to acidosis, or accumulation of H^+ ions. These cause the membrane sodium-hydrogen exchanger to overload the cell with Na^+, which in turn causes Ca^{2+} overload because of reverse operation of the sodium-calcium exchanger. Lack of ATP prevents the Na^+/K^+-ATPase pump from correcting the imbalance, resulting in osmotic swelling. Likewise, the sarco/endoplasmic reticulum Ca^{2+}-ATPase (SERCA) pump can no longer efficiently pump Ca^{2+} into the sarcoplasmic reticulum (SR), leading to further cytosolic Ca^{2+} accumulation. Increases in cytosolic Ca^{2+} cause necrosis in cardiomyocytes through activation of proteases and mitochondrial damage.

Restoration of blood flow re-introduces oxygen, and oxidative phosphorylation resumes. The renewed presence of ATP during cytosolic Ca^{2+} overload causes hypercontracture, and normalization of pH leads to opening of the mitochondrial permeability transition pore (MPTP). This causes mitochondrial uncoupling, generation of oxygen free radicals, and activation of apoptosis. Furthermore, due to the abundance of reduced metabolic substrates that accumulated during ischemia, a burst of reactive oxygen species (ROS) and reactive nitrogen species (RNS) are generated by the resumption of oxidative phosphoryation. These damage other proteins, and misfolded proteins accumulate, inducing the endoplasmic reticulum (ER) stress response. Autophagy increases during I/R injury, but it is unclear whether this is beneficial or detrimental.

Cells die from I/R injury primarily due to both necrosis and apoptosis. Necrosis is a form of loosely regulated accidental cell death, and occurs during ischemia from osmotic swelling and compromised membrane integrity. Rupture of cardiomyocytes is pro-inflammatory and leads to the release of biomarkers of MI, such as Troponin I and creatinine kinase, into the bloodstream.

Apoptosis, on the other hand, is the tightly regulated process wherein cells die while breaking down their components, which remain membrane-bound. Morphologically, the cell shrinks and its chromatin condenses before the nucleus fragments. Then the cell separates into apoptotic bodies. Phosphatidylserine is exposed on the external leaflet of the membrane, which is a signal for the apoptotic body to be phagocytosed, thus no cellular contents are released and inflammation does not occur.

Both extracellular and intracellular signals can lead to initiation of apoptosis during I/R injury. Extrinsic apoptosis is caused by the binding of a death inducing ligand, for example, Fas ligand (FasL) to a cell surface receptor such as Fas, leading to receptor trimerization, which recruits adapters such as Fas-associated death domain protein (FADD). FADD organizes the death inducing signaling complex by recruiting procaspase-8 or -10, causing them to be cleaved and thus activated[5]. FasL/Fas signaling is well accepted to play a role in apoptosis in the contexts of MI and post-infarction remodeling[6-8].

Intrinsic apoptosis can be initiated in the heart by I/R injury due to prolonged activation of the ER stress response[9-13] or mitochondrial damage, or Ca^{2+} overload. It is regulated by the mitochondria through the MPTP and the association of pro-apoptotic Bcl proteins, which form channels in the outer membrane, leading to mitochondrial outer

membrane permeabilization (MOMP). Cytochrome c leaks from these channels and together with the adaptor protein Apaf-1, caspase-9, and ATP forms the apoptosome. This activates caspase-9, leading to cleavage of downstream caspases and execution of apoptosis. It is also regulated by the endoplasmic reticulum through activation of caspase-12 during the ER stress response, which can activate caspase-9 independently of the apoptosome[14]. Both extrinsic and intrinsic apoptotic pathways begin with the activation of apical caspases and converge upon activated "executioner" caspases-3 and -7.

Ischemic Preconditioning

Ischemic preconditioning (IPC) is an endogenous cardioprotective response to brief, non-lethal bouts of ischemia and reperfusion. Initially discovered in 1986 by Murry *et al*. in dogs[15], it was subsequently demonstrated in many species, including rodents[16, 17], rabbits[18] and pigs[19]. Together with the risk associated with repeatedly occluding the culprit artery (which is likely to be atherosclerotic and fragile), the unpredictable nature of MI has limited the direct translation of IPC to the clinic for this condition, despite clinical trials supporting that it is protective in the context of planned cardiac surgeries such as coronary artery bypass grafting and elective PCI[20]. Furthermore, it led to the investigation of ischemic post-conditioning, in which a blocked coronary artery is re-opened repetitively after an ischemic episode, which ameliorates reperfusion injury[21-23]. It also laid the groundwork for the study of remote ischemic preconditioning (RIPC), in which preconditioning occurring in one vascular bed confers protection to an area at risk in a subsequent I/R injury[24, 25].

IPC consists of two phases, an early and a late phase[26, 27]. The early phase is effective immediately after preconditioning, and lasts 1 to 3 hours. It results from activation of G-protein coupled receptors including the opioid, bradykinin, and adenosine receptors, leading to kinase cascades that activate protein kinase C (PKC) and lead to mitochondrial K_{ATP} channel opening. These kinases, known as reperfusion injury salvage kinases (RISK), include Akt (also known as protein kinase B) and extracellular regulated kinase-1 and -2 (ERK1/2)[28]. Protective levels of autophagy and mitophagy, the autophagy of mitochondria, are also triggered[29-32]. Furthermore, cellular ATP levels are preserved during I/R injury in preconditioned cardiomyocytes[33]. These events act together to protect cells against prolonged I/R injury occurring within a few hours after IPC.

By contrast, the late phase of IPC takes effect 12 to 24 hours after an IPC stimulus, and lasts 3 to 4 days. Late IPC relies on synthesis of protective proteins[34, 35]. PKC and the mitochondrial K_{ATP} channel appear to act as important bridges between early and late IPC[36]. Signaling that takes place during the early phase of protection results in the activation of transcription factors such as NF-κB[37, 38], Hif-1α[39], STAT-3[40] (potentially STAT-5 in man[41]), and others, which reprogram gene expression. Proteomic studies have revealed several functional groups of proteins that are upregulated to allow the heart to adapt to ischemia. These include metabolic enzymes, anti-oxidative proteins, chaperones, and cytoskeletal components[42, 43]. The requirement for some of these proteins, including heat shock protein 70 (Hsp70)[38], has been established through use of knockout mice, revealing that IPC's reduction in infarct size cannot occur in the absence of that protein.

Chaperone expression after IPC is a key aspect of cardioprotection because it directly counteracts one of the mechanisms of I/R injury, the accumulation of damaged and misfolded proteins. The heat shock protein (HSP) family includes many genes that work together in the heat shock and unfolded protein response pathways to fold nascent, unfolded, or damaged proteins. Hsp70 and Hsp90 bind exposed hydrophobic regions of unfolded proteins and catalyze ATP to refold them. Hsp40 stimulates Hsp70's ATPase activity, increasing the rate of refolding, and some family members can also bind unfolded proteins directly.

Hsp20 The small heat shock protein family includes Hsp27, αA-crystallin, αB-crystallin, Hsp20 and Hsp22, among others[44, 45]. Under normal conditions, these form large, inactive multimers. Under stress, phosphorylation causes them to disperse as homodimers, and bind to unfolded proteins, preventing aggregation. They do not themselves refold the proteins, but allow them to be refolded by Hsp70. Hsp20 has been demonstrated to be highly cardioprotective against I/R injury in mice[46-49]. Hsp27 and αB-crystallin are also protective through stabilization of cytoskeletal and sarcomeric structures[50-52]. Overexpression of Hsp27 reduced infarct size in an isolated perfused heart model compared with wild-type littermates[53]. Highlighting the importance of normal small HSP function, a mutation in αB-crystallin was shown to result in desmin-related cardiomyopathy due to aggregation of unfolded pre-amyloid oligomers along with impaired autophagy and mitochondrial function[54-56].

Hsp40 The DnaJ/Hsp40 family has over 20 members in mammals, perhaps as many as 41 in man, which can be categorized into 3 groups based on their structure[57]. They all share the J domain, through which they interact with the ATPase domain of

Hsp70. Types I and II have the J domain and a Gly/Phe rich region which allows them to bind to short hydrophobic stretches of unfolded or nascent proteins. Type III DnaJ proteins lack the Gly/Phe region, and may or may not bind to client proteins[58]. In addition to these activities, they also assist in the process of endocytosis through disassembly of clathrin coats, translocation of ribosomes to the endoplasmic reticulum, and delivery of proteins to the proteasome for degradation. The functional diversity of this family derives from subtle differences in the structure of the different family members, which affect their cellular localization, and the Hsp70 family members and client proteins with which they can associate[58, 59].

Several DnaJ family members are expressed in the heart. In H9c2 cells, a cardiac cell line, *Dnaja1, Dnaja4*, and *Dnajb1* were shown to be inducible by heat shock. These co-localize in the cytosol with Hsp70, and after heat shock, they both translocate to the nucleus. Overexpression of Hsp70 alone increased cell survival upon prolonged heat shock, and when Hsp70 and either Dnaja1 or Dnaja4 were co-overexpressed, this effect was increased[60]. The results of this study suggest that these DnaJ family members are co-chaperones with Hsp70 and act together to protect cardiomyocytes from stress. In a swine model of I/R injury, Hsp40 (pig Dnaj-like protein, *pDJA1*) was increased slightly during ischemia, and to a greater extent during the early hours of reperfusion[61]. Furthermore, expression of this protein in neonatal rat cardiomyocytes protected them from staurosporine-induced apoptosis. Little is known about expression of Hsp40 family members in the heart during IPC, but it was found to increase during cerebral IPC, along with Hsp70[62]. A previous publication from our lab identified Dnaja1 as being significantly upregulated at the mRNA level 3h after IPC in the mouse heart[38]. This

effect was partially reliant on NF-κB, because in the dominant negative 2M mouse model, which cannot activate NF-κB, the increase was blunted significantly.

Hsp70 Structurally, Hsp70 proteins consist of an N-terminal ATP binding domain and a C-terminal peptide binding domain connected by a flexible linker. The peptide domain, in turn, consists of the substrate binding domain and a helical lid region. The substrate binding domain interacts with hydrophobic 5 amino acid stretches of unfolded client proteins. When ATP is bound, the conformation is such that the peptide binding domain interacts loosely with client proteins, binding and releasing them rapidly. After ATP hydrolysis (stimulated by the DnaJ co-chaperone), Hsp70 binds stably to the protein, preventing aggregation[58]. Release of the client protein requires interaction with a nucleotide exchange factor (NEF), such as Hsp110, recycling Hsp70 to the ATP bound open state. Once released, the client protein has a chance to fold correctly, or be re-captured by Hsp70. There are both inducible and constitutively expressed Hsp70 family members. The constitutively expressed proteins are known as Hsc70, and are continually present to fold nascent proteins in the cytosol and ER. Grp78/BiP has the dual role of being both a chaperone and a sensor of ER stress.

The inducible Hsp70s were among the first proteins to be recognized as effectors of late IPC[63]. In a transgenic mouse model, overexpression of Hsp70 was shown to be sufficient on its own to induce cardioprotection as evidenced by reduced infarct size and enhanced contractile function in the isolated perfused heart[64]. Furthermore, targeted knockout of both inducible Hsp70 family members (Hsp70.1 and Hsp70.3) prevents infarct size reduction in late IPC[38, 65], though it has no effect on early IPC[65].

Hsp70.1 and Hsp70.3 are identical proteins in man, but in the mouse, Hsp70.1 has the insertion of a proline residue in the lid region of its peptide binding domain. The effect of this change on the function of the protein is unknown, but our group has shown that Hsp70.1 is not required for IPC, and that Hsp70.1 knockout mice have significantly smaller infarcts compared with wild-type mice, indicating that murine Hsp70.1 is injurious in the context of I/R injury[38]. However, we also showed that in the context of permanent occlusion, Hsp70.1 is protective[66]. It remains to be seen whether this is a unique aspect of murine Hsp70.1 amino acid sequence, or is due to differential regulation, and whether this extends to other mammals.

Hsp90 Like Hsp70, Hsp90 can hydrolyze ATP and actively refold misfolded proteins. Hsp90 has two family members, Hsp90A and Hsp90B, which are constitutively expressed and further increase upon heat shock. Hsp90 has an N-terminal ATPase domain, followed by a stretch of charged residues, and a C-terminal dimerization domain. The exact features of the client proteins that Hsp90 binds are under investigation. Like Hsp70, Hsp90 functions through cyclical ATP/client protein binding, hydrolysis, and release. The ATP bound form of Hsp90 is closed and tightly binds the client protein. The cofactor P23 stabilizes the ATP bound state and assists in folding. Then Hsp90 hydrolyzes ATP and releases the protein, which can be re-bound if necessary. Hsp90 and Hsp70 can work together; the protein Hop can transfer substrates from Hsp70 to Hsp90.

Hsp90 was shown to increase after heat shock or metabolic preconditioning (consisting of exposure to lactic acid and 2-deoxy D-Glucose at pH 6.8), which was protective in cultured adult rat cardiomyocytes upon prolonged heat shock or ischemia

[67]. Other than enhancing protein homeostasis, one proposed mechanism for cytoprotection is that Hsp90, along with Hsp70 and αB-crystallin prevent the release of apoptotic factors such as SMAC/Diablo from the mitochondria[68]. Furthermore, Hsp90 has been shown to be required for proper functionality of other cardioprotective proteins. For example, it was shown to target the mitoK_{ATP} channel to the mitochondrial membrane in order to mediate hypoxic preconditioning *in vitro*[69], and to co-localize with eNOS after anesthetic preconditioning and IPC in a rabbit model, which was required for eNOS function[70].

Regulation of HSP expression in IPC HSP expression is controlled by the activation of the heat shock factor (HSF) family of transcription factors, which includes HSF-1 through -4. Other transcription factors are now known to play important roles as well, including NF-κB. Using a cardiac-specific dominant negative mouse model of NF-κB activation, mediated by overexpression of inhibitor of κB α (IκBα) which cannot be phosphorylated, we showed that Hsp70 protein does not increase in the heart during late IPC, which was associated with failure of IPC to reduce infarct size in these mice[38]. It is also becoming clear that microRNA (miRNA) plays a role in gene expression during late IPC in general, and in the expression of HSPs specifically.

MicroRNA

MicroRNAs (miRNAs) are short 19-22 base RNA molecules that influence transcription and translation of mRNA in many circumstances. Most often, they exert their activity by binding to the 3' untranslated region (3'-UTR) of target mRNAs and cause translational silencing and degradation. The first miRNA was discovered in *C. elegans* in 1993[71]. Since that time, the number of miRNAs and their predicted targets

have expanded until now it is believed that most protein-coding genes are subject to regulation by miRNA[72].

Like mRNAs, miRNA genes are transcribed by Pol II, producing a precursor known as the pri-miRNA. This is then cleaved by Drosha within the microprocessor complex into a hairpin structure known as pre-miRNA, and exported from the nucleus. Subsequently, it is cleaved by Dicer into a short double stranded RNA duplex, which is incorporated into the RNA-induced silencing complex (RISC), and one strand is removed[73]. The mature miRNA within the RISC is associated with Argonaute-2 (Ago-2), which has endonuclease activity, and regulates its mRNA targets through complimentary base pairing, in a process known as RNA interference. A few simple rules form the basis of much accurate target prediction[72]. Nucleotides 2-7 of the miRNA are known as the seed sequence. These nucleotides pair perfectly, or nearly perfectly, with a sequence in the 3'-UTR of the target mRNA. Predicted targets that are conserved across multiple species are more likely to be functional. Lastly, effective repression usually occurs at sites that are away from the middle of long UTRs, and that have higher local AU content, which affects accessibility[72, 74]. It is believed that whether the mRNA will be degraded or only silenced is based on the extent of base pairing that occurs outside of the seed sequence[75].

Because miRNAs are so short, and because base pairing does not have to be perfectly complimentary, each miRNA is predicted to have numerous mRNA targets, and likewise, most mRNAs are predicted to be regulated by numerous miRNAs. This suggests the interesting possibility that miRNAs could act as nodes in a network of gene regulation, such that changes in the level of one miRNA could affect the expression of

many functionally related genes. Indeed it has been suggested that this is the case[76, 77]. If miRNAs can be identified that regulate groups of protective genes, manipulating one or more of them could have strong protective effects, which would be of interest clinically. Synergistic physiological effects between two or more miRNAs in the heart have been reported. For instance, Pisano *et al.* showed that miR-499 and miR-133 synergistically induced differentiation of embryonic stem cells to cardiomyocytes[78], and Zhu *et al*. demonstrated that miR-21 and miR-1 act synergistically to reduce cell death from oxidative stress[79].

The roles of a few miRNAs in IPC have been identified. For instance, the miR-144/451 family was shown to be required for IPC, when increased expression downregulates Rac-1. This downregulation reduces the activation of NADPH oxidase, reducing the generation of reactive oxygen species[80]. Similarly, miR-21 has been found to increase in multiple forms of cardioprotection, including ischemic pre- and post-conditioning as well as isofluorane-induced preconditioning[81, 82], downregulating the expression of pro-apoptotic genes such as Programmed Cell Death 4[83], PTEN[84] and FasL[85].

Meanwhile, other miRNAs have been found to decrease during IPC, in order to derepress protective genes. For example, miR-199 is downregulated by IPC, allowing the transcription factor HIF-1α to accumulate and activate pro-survival gene expression[86]. We have shown that miR-711 and miR-378* both decrease after IPC to allow increased expression of their target, Hsp70[87]. Three hours after IPC, miR-711 and 378* were both found to be decreased in heart tissue, whereas Hsp70.3 mRNA was increased ~25-fold. Through use of the 2M dominant negative IκB mouse, we

determined that the increase in Hsp70.3 as well as the decrease in miR-711 are dependent on NF-κB activation. Luciferase assays confirmed that these miRNAs target the 3'-UTR of Hsp70.3, and transfection of synthetic miRNA mimics confirmed that both of these miRNAs can downregulate Hsp70.3 protein[87]. It was further demonstrated that transfection of HL-1 cells with an inhibitor of miR-378* could induce expression of Hsp70 (unpublished data). However, it is not known whether a set of miRNAs regulates the expression of related sets of genes, such as HSPs, in IPC. ***A goal of this work is to identify miRNAs that could act as regulatory nodes for numerous heat shock protein family members during IPC (Results p67).*** This was accomplished through use of mRNA and miRNA sequencing, *in vitro* targeting analysis, 3'-UTR reporter assays, and gain- and loss-of-function techniques to test miRNA effects on expression of HSPs.

miRNA as a Paracrine Mediator from Myocardium to Transplanted Mesenchymal Stem Cells

Endogenous Regenerative Potential of the Myocardium

In the mammalian heart during cardiac development, cardiomyocytes increase in number after birth for a short time (a few days in mice, a few months in humans), and then further growth of the heart is achieved by increases in cell size[88]. During the very early postnatal period of cardiomyocyte cell division, it was demonstrated in mice that a surgical wound to the apex of the heart could heal completely, whereas a similar wound occurring one week after birth causes fibrosis and permanent damage[89]. Using a fate mapping approach, the source of the cells that regenerated the wound was shown to be neighboring cardiomyocytes, indicating that early on, cardiomyocytes are capable of proliferation.

After the postnatal period of cardiomyocyte proliferation, cardiomyocytes increase dramatically in size but cease dividing. In order to accomplish this physiological growth, it appears that mammalian cardiomyocytes must replicate their DNA[90]. In rodents, cardiomyocytes undergo karyokinesis but not cytokinesis, leading to a predominant population of binucleate cardiomyocytes (wherein each nucleus is diploid), beginning at approximately 4 days of age through adulthood[91]. In humans, cardiomyocytes also replicate their DNA during the pre-adolescent growth phase (8-12 years of age), but undergo neither karyokinesis nor cytokinesis. Thus the majority (60%) of cardiomyocytes in the healthy heart over age 7 are tetraploid but mononucleate[92, 93], with about 25% of cardiomyocytes being binucleate, and very small percentages of tri- and tetranucleated cells[94]. In hypertrophied hearts, ploidy increases such that octaploid nuclei predominate, with a small fraction of nuclei observed to be up to 32-ploid. Increases in myocyte cell number have also been documented in grossly hypertrophied hearts, weighing over twice the normal heart weight[95].

After development, there is limited capacity for further cell division. The degree of cell turnover within the heart is debated within the field, because different methods suggest different rates of turnover[96]. Genetic approaches in combination with "pulse-chase" experiments have provided some insight into the rate of proliferation in mice. One such experiment labeled cardiomyocyte nuclei with transgenic expression of β-galactosidase (driven by the cardiomyocyte-specific α-myosin heavy chain promoter) and newly synthesized DNA with radioactive thymidine. These researchers found a low baseline level of cell division of 0.0005%, which increased to 0.0083% after cryoinjury[97]. In another study[98], cardiomyocyte nuclei were permanently labeled, and

then mice were infarcted or subjected to pressure overload. In the control mice, the percentage of cardiomyocytes with labeled nuclei remained constant at 83%, while in the injured mice, the percentage decreased to 68% in the border zone after MI and 76% in the remote region or under pressure overload, indicating that new myocytes had arisen from a non-cardiomyocyte source. This may have been resident cardiac stem cells (CSCs) or circulating multipotent stem cells mobilized from the bone marrow. By performing in situ hybridization for Y-chromosomal DNA in combination with immunohistochemistry for cardiomyocyte markers in sex-mismatched heart transplant patients, it has been demonstrated that cells from the host become cardiomyocytes in the transplanted heart, albeit at low levels (≤1% of cardiomyocytes)[99, 100]. In man, relying on environmental levels of ^{14}C that have fluctuated over time to label the DNA of cardiomyocytes, Bergmann *et al*. found that turnover does occur in the adult heart at estimated rates of 1% in young adulthood, decreasing to 0.4% in the aging heart[101]. The fact that regeneration can occur in neonatal and even adult hearts, albeit to a very limited extent, raises the possibility that this endogenous capacity could be enhanced experimentally and perhaps therapeutically.

Stem Cell Therapy for Regeneration of the Myocardium

It is clear that the endogenous potential for repair is insufficient to replace the millions of cardiomyocytes lost during MI. This was the rationale for the first experiments using stem cell transplantation as a therapeutic. It was hypothesized that the stem cells would engraft and differentiate into cardiomyocytes, replacing the lost cells and helping to improve heart function. A number of different types of cells have been

explored for their regenerative potential, including embryonic and adult stem cells. The first of these was the skeletal myoblast.

Skeletal Myoblasts In 1992, Marelli *et al*.[102] transplanted autologous skeletal satellite myoblast cells into cryoinjured canine hearts. In this and other subsequent studies, researchers found that the skeletal myoblasts remained viable and gave rise to grafts of striated muscle tissue in the recipient heart. In fact, studies in animal models showed that these grafts had the capacity to become quite large, affecting the shape and function of the heart. Furthermore, they failed to express gap junction proteins after transplantation, indicating that they did not establish functional electrical coupling with neighboring cardiomyocytes[103]. Clinical trials initially reported improvements in ejection fraction and heart function[104], but these were not sustained, while the risk of arrhythmia persisted at 4 year follow-up[105]. It is thought that the initial improvements may have been due to remodeled scar formation or improved elasticity of the ventricular wall in the area of injury.

Bone Marrow Mononuclear Cells (BMMNC), a heterogeneous population that includes hematopoietic stem cells (HSC) and endothelial progenitor cells (EPC), as well as other types of precursors, have also been explored in the context of transplantation for MI. In 2001, Piero Anversa's group isolated c-kit positive (c-kit+) bone marrow stem cells from enhanced green fluorescent protein (EGFP) expressing donor mice, and injected them into recipient mice's myocardium 3-5 hours after infarction. Nine days later, they found that these stem cells had formed new myocardial tissue which occupied 68% of the infarct zone and was comprised of mainly cardiomyocytes, with GFP^+ endothelial cells and smooth muscle cells also noted[106]. Fernandez-Aviles *et al*. also

showed that human bone marrow cells isolated from patients post MI could engraft and differentiate into cardiomyocytes when cultured on slices of cryoinjured mouse heart tissue[107]. In the same study, they transplanted the autologous bone marrow cells into the patients' hearts approximately 2 weeks after MI. This resulted in reduction of ventricular remodeling and improvements in regional and global left ventricular function. Other studies pointed to angiogenesis as the main benefit of BMMNC transplantation in animal studies[108, 109]. In light of these encouraging results, clinical trials were quickly initiated, and showed modest functional benefits in man[110]. Even as clinical trials were underway, debate arose about the mechanism of the observed benefits.

At issue were both the persistence and capacity of the transplanted stem cells to differentiate into cardiomyocytes or other therapeutically relevant cell types. Scherschel *et al*. injected a series of different bone marrow derived stem cell populations, including one that matched those used by Anversa's group in their 2001 publication, into infarcted mouse hearts. As before, these cells were tracked by EGFP expression. After 9 to 10 days, they sacrificed the mice and used two-photon laser scanning microscopy to detect intracellular Ca^{2+} currents in the host and donor cells, which were found in clusters within the infarct and border zone. None of the >3000 donor cells tested exhibited Ca^{2+} transients[111]. In this study and others[112-114], engrafted HSC failed to express cardiac tissue markers or adopt cardiomyocyte morphology. Furthermore, while engraftment was consistently detected at day 9, by week 4 after injection most of the cells were gone[112, 113].

In light of the growing body of data that showed convincing improvements in heart function, without a corresponding amount of engraftment or transdifferentiation[115],

the paracrine hypothesis became widely accepted as an important mechanism of action[116]. This hypothesis suggests that stem cells release factors that exert effects on the injured myocardium including cardioprotection, angiogenesis, and decreased scar size. It is unclear whether paracrine effects also result in myogenesis, and if so whether the source of new myocytes is cell division of existing cardiomyocytes or differentiation of resident cardiac stem cells.

Cardiac Stem Cells and Cardiosphere Derived Cells Evidence for resident cardiac stem cells (CSCs) was initially presented in 2002 by Hierlihy, *et al*.[117]. They isolated a population of cells with stem-cell like properties from the adult mouse myocardium by fluorescence assisted cell sorting (FACS). This population, which constituted ~1% of the total cells sorted, could be expanded through colony formation and differentiated into cardiomyocytes *in vitro*. Beltrami *et al.*[118] further described CSCs as small, immature cells that could be found in clusters within the normal aging rat heart. They express c-kit as well as some genes involved in cardiac development and differentiation including *Nkx2.5* and *MEF2C*. Some also expressed mature cardiomyocyte markers such as α-sarcomeric actin. In culture, the CSCs formed multicellular spheroids in suspension. When media was changed to differentiation media (containing dexamethasone), the spheroids attached and cells differentiating into cardiomyocytes, smooth muscle cells, and endothelial cells migrated out of the spheroids. Furthermore, over 20 days after injection into infarcted rat hearts, the CSCs persisted and appeared to contribute new myocytes throughout the infarct zone, generating an average 48 mm^3 of tissue that reduced the size of the infarct from 70% of the ventricle to 48%[118].

Similarly, Messina *et al.* found that CSCs emigrated from small pieces of human and mouse heart tissue and formed so-called "cardiospheres" in suspension culture, and that the cardiospheres could give rise to new cardiomyocytes and other cardiac cell types when transplanted into the infarcted myocardium. Immediately after permanent ligation of the LAD, cardiospheres were injected at 4 left ventricular sites. Eighteen days later, mice were sacrificed and the hearts sectioned and analyzed. Bands of regenerating myocardium with varying degrees of organization and thickness were observed throughout the infarcted area, which stained positive for a human nuclear marker (indicative of the human source of the cardiosphere derived cells) and cardiomyocyte markers myosin heavy chain, connexin-43, or the capillary markers α-smooth muscle actin and platelet endothelial cell adhesion molecule[119]. Scar size, as assessed by H&E staining after 18 days, was not reduced significantly, but the anterior wall was significantly thicker and fractional shortening was improved as assessed by echocardiography.

Based on preclinical data showing regeneration as well as capacity for *ex vivo* expansion, cardiosphere derived cells (CDCs) presented an opportunity to transplant autologous stem cells after MI. The Phase I CADEUCEUS trial[120], conducted by Marban and colleagues, showed that this procedure was safe, and that after 1 year scar size was decreased, while muscle mass increased[121]. However, data from animal studies later supported that CDCs act primarily through paracrine mechanisms without long-term engraftment[122, 123]. Regeneration, which persisted long after the transplanted cells were cleared, was observed to result from proliferation of existing cardiomyocytes as well as recruitment of endogenous CSCs to differentiate[124]. Because the transplanted

cells do not remain in the heart, and have low immunogenicity, it may be possible to transplant allogeneic CDCs as a readily available "off the shelf" therapeutic, for which the ALLSTAR Phase I/II clinical trial is currently recruiting (identifier, NCT01458405).

Mesenchymal Stem Cells (MSCs) are another population of cells that reside in the bone marrow as well as many other organs and tissues[125], including the heart[126]. They were originally identified as a rare population of bone marrow stromal cells with the capability to adhere to tissue culture plastic and differentiate into different lineages when transplanted *in vivo*[127]. Their role in the bone marrow is to support hematopoietic stem cells by maintaining the population of osteoblasts, adipocytes, and reticular cells which comprise their niche[125]. Their role in other organs is not completely understood because their low numbers make labeling and tracking them technically challenging. Other than plastic adherence and the capacity for self-renewal and differentiation into mesodermal lineages (adipogenic, osteogenic, and chondrogenic), the International Society for Cellular Therapy defines MSCs by the expression of certain cell-surface epitopes. In man these are CD73, CD90, and CD105 in the absence of CD34, CD45, HLA-DR, CD14 or CD11b, CD79a, or CD19. In mice, MSCs are positive for Sca-1, CD29, CD44, CD105, and/or CD106, without CD11b, CD45, Flk1, CD31, CD34, CD90, or c-kit[128-131].

In 2000, Wang *et al*.[132] were the first to transplant MSCs into the heart using a rat model. In the absence of ischemia or other injury, they injected *ex vivo* expanded MSCs labeled with DAPI into the right ventricle, and looked 4 days to 12 weeks later to determine whether they survived and differentiated into cardiomyocytes. At 4 days, they observed numerous $DAPI^+$ cells with an immature stem cell like phenotype. After 4

weeks, they found a few labeled cells remaining, which had incorporated within the myocardium and adopted the same appearance as the surrounding cardiomyocytes. Immunohistochemistry of 6 week frozen sections showed the expression of sarcomeric myosin heavy chain and connexin 43 proteins in the DAPI labeled cells, suggestive of differentiation and functional electromechanical coupling. That MSCs could differentiate into cardiomyocytes *in vitro* by exposure to the DNA demethylating agent 5-azacytidine had been recently reported[133], and *in vivo* differentiation was noted subsequently in healthy and infarcted myocardium[134, 135]. Studies in animal models over the next 5 years indicated that transplantation of MSCs into hearts with I/R injury resulted in improvements in heart function, reduced remodeling, and angiogenesis[135-140]. In these studies, MSCs were transplanted 1 week after MI, with the exception of Shake *et al.*,[135] who transplanted them 2 weeks after, and Kinnaird *et al.*,[137] whose model was a hindlimb ischemia model of angiogenesis.

MSCs from bone marrow and adipose tissue have been used in clinical trials for treatment of acute MI as well as ischemic and non-ischemic heart failure. Bone marrow derived MSCs have been tested in phase I and phase II trials with administration within 1 week of MI. These studies show decreased arrhythmias, improved ejection fraction (EF), reduced hypertrophy, heart failure, and rehospitalizations for cardiac complications[141, 142]. Adipose derived MSCs have been tested in a small trial for acute MI, and showed reduced scar formation and improved perfusion[143]. More commonly, MSCs have been investigated in the setting of ischemic cardiomyopathy. In clinical trials such as POSEIDON, TAC-HFT, and PROMETHEUS, it has been shown that even after

chronic ischemia, MSCs can reduce scar size by 30-50%, and enhance contractility, angiogenesis, and functional capacity of the patients (reviewed in [144]).

The Mechanism of Action of MSC Transplantation is now understood to involve a number of different processes. As with BMMNCs and CSCs, permanent engraftment and retention in the myocardium occur at very low levels[134], and numerous studies support that release of paracrine factors is an important component of MSCs' effects[116]. Firstly, angiogenesis leading to improvement of myocardial perfusion and contractile function is well recognized to occur. MSCs release angiogenic cytokines such as vascular endothelial growth factor (VEGF), which act on endothelial cells to form new capillaries[136]. Preconditioning with hypoxia for 24h prior to transplantation of MSCs further enhanced their angiogenic properties through upregulation of VEGF, the VEGF receptor Flk1, and erythropoietin. The preconditioning treatment also increased expression of the pro-survival proteins Bcl-2, Bcl-xL, and Hif-1, which protected the MSCs from apoptosis after transplantation, enhancing their effects[145].

MSCs also reduce fibrosis via paracrine mechanisms. In an isoproterenol-induced heart failure model, transplantation of MSCs almost completely restored heart function after 1 month, and reduced fibrosis. This may have been mediated through the release of hepatocyte growth factor (HGF) from the MSCs, as supported by the finding that HGF was expressed in the MSCs and that MSC transplantation increased HGF mRNA and protein levels in the heart[146]. The MSCs also mediated reduction of mRNA levels of collagens I and III, and MMP-2 and -9 in the myocardium. This group then showed data in support of a similar role for the antifibrotic protein adrenomedullin in the same animal model. Additionally, they showed inhibition of cardiac fibroblast

proliferation *in vitro* and decreased expression of collagen I and III by exposure to MSC conditioned medium[147]. Another experiment on fibroblasts exposed to MSC conditioned medium[148] showed that it enhanced the expression of matrix metalloproteinases (MMP) -2 and -9, while downregulating tissue inhibitor of metalloproteinase 2 (TIMP2) and confirmed the decrease in fibroblast viability. Based on the paracrine roles of VEGF and HGF in angiogenesis and anti-fibrosis, a recent study[149] tested whether adenovirally-mediated overexpression of these factors in transplanted MSCs would enhance these beneficial effects in a porcine model. The results showed that HGF overexpression was more effective than VEGF overexpression at reducing scar mass and improving ejection fraction, and equally effective at increasing blood vessel density and perfusion. This may be due to slightly improved survival of the HGF-overexpressing MSCs *vs.* those overexpressing VEGF. Overexpression of either protein improved survival compared with the unmodified MSCs.

Another important paracrine role of transplanted MSCs is stimulation of endogenous neomyogenesis by boosting cardiac stem cell function and stimulating existing cardiomyocytes to divide. MSC injection has been shown to increase the number of endogenous c-kit+ CSCs as well as mitotic cardiomyocytes[150]. Furthermore, co-culture of CSCs with MSCs increases the viability, proliferation, and differentiation of the CSCs[150], and transplantation of a combination of CSCs and MSCs was shown to be more effective than either cell type alone with regard to infarct size, contractility, and engraftment of the transplanted cells in the infarcted myocardium[151]. Thus it is clear that MSCs and CSCs interact in a biologically meaningful way; just as MSCs support the HSC niche in the bone marrow, perhaps they support CSCs in the heart.

Lastly, MSCs may act through direct cardioprotection. Many MSC transplantation protocols involve transplanting the cells within hours of the experimental MI, thus the observed reduction in infarct size (and associated functional benefits) may not be myogenesis or regeneration, but prevention of cell death. This is supported by experiments in which MSC conditioned medium (CM), administered near the time of reperfusion during experimental MI, exerts cardioprotective effects. To test the paracrine effects of CM from regular or AKT-overexpressing MSCs, Gnecchi *et al*.[152] exposed the MSCs to hypoxia for 12 hours, concentrated their CM, and injected this or either type of MSC into the rat heart 1 hour after reperfusion. The Akt-overexpressing MSCs and their CM decreased infarct size by 62% and 45% respectively, as measured by triphenyl tetrazolium chloride (TTC) staining at 72h. Their finding indicates that cardioprotective factors are secreted into the media of hypoxic MSCs, and that Akt activation increases this effect (regular MSCs and their CM showed only modest reductions in infarct size). They found that the combination of Akt overexpression and hypoxia treatment upregulated VEGF, HGF, insulin like growth factor (IGF-I), and thymosin-β4 (TB4). Binding of these factors to their receptors on cardiomyocytes leads to cardioprotection through activation of Akt. Other protective factors that have been identified include adrenomedullin, interleukin-11, erythropoietin, and fibroblast growth factor-2[116]. Timmers *et al*. injected CM 5 minutes prior to reperfusion in a pig model, and observed a 60% reduction in infarct size, which was assessed 4h after reperfusion[153]. Fractionation of the CM revealed that the protective factor was >1000 kDa in size, and subsequent studies showed that it was in fact exosomes.

MSC Exosomes Exosomes are small 60-120 nm membrane-bound vesicles that are produced and stored within cells in the multivesicular body (MVB). They are released constitutively by most cell types by exocytosis and can be taken up by other cells in a paracrine or endocrine fashion, through endocytosis. Within the target cell, they can release their contents by fusion with the membrane of the MVB. In addition to cytokines and trophic factors, MSCs (as well as other stem cell types) release exosomes, which are taken up by cardiomyocytes and contain many known cardioprotective proteins, bioactive lipids, and RNA[154-157]. MSC exosomes are the focus of Section 3.

Preconditioning the Heart: A Technique to Enhance Stem Cell Survival?

Enhancing MSC engraftment and viability in the host myocardium would doubtless extend and magnify their paracrine effects, and thus is of interest clinically. While techniques for preconditioning MSC prior to transplantation into the infarcted heart have been extensively investigated[145, 158-161], less is known about communication from the heart to the stem cell.

There is evidence that inducing cardioprotection at the time of MSC transplantation has beneficial effects on MSC survival. Hypothesizing that poor engraftment is caused by I/R injury to the heart, one group[162] sought to reduce this through postconditioning, injecting GFP^+ MSCs 2h later. They found that after 4 weeks, the number of surviving MSCs in the postconditioned hearts was twice that of the control hearts. Capillary density was increased, and functional parameters such as ejection fraction were significantly improved. They attributed these effects to improvement of the cardiac microenvironment, *i.e.,* reduced release of inflammatory cytokines. Another method of cardiac conditioning is electroacupuncture, which appears

to protect the heart through both nervous system activation[163] and release of soluble factors[164]. When electroacupuncture was added to MSC transplantation, Zhang *et al*.[165] observed better engraftment after 4 weeks, as well as reduced fibrosis, increased capillary density, and improved heart function compared to MSC alone. These studies indicate that the preconditioned heart can better support stem cell engraftment, through modification of factors released by the infarcted myocardium. In isolated perfused heart studies in which the heart is preconditioned, coronary effluent can be collected, warmed, reoygenated, and perfused through a naïve heart, which induces cardioprotection in this heart[166]. The identity of the factor(s) released from the heart is not known. However, it has been reported that IPC leads to recruitment of bone marrow stem cells via SDF-1α/CXCR4 signaling, and that infiltration of the myocardium by mobilized bone marrow stem cells is an important mediator of the late phase of IPC[167]. Thus preconditioning of the heart changes the signals that it releases, and bone marrow stem cells are sensitive to some of these. The heart may have an important though poorly understood role in releasing hormones and other signals to the rest of the body.

Cardiac exosomes, first characterized in the media of isolated rat cardiomyocytes by Gupta and Knowlton[168], may be a key aspect of these signals. Exosomes carry protein and RNA cargo representative of the parent cell, but the contents can change to reflect its biological state in response to some stimuli. HL-1 cells, an atrial cardiomyocyte cell line, release exosomes that can be taken up by cardiac fibroblasts[169]. Using microarrays, the mRNA and DNA content of the exosomes was identified. Then fibroblasts were treated with whole conditioned medium, the exosome fraction, and the exosome-depleted conditioned medium to examine the effects of the entire HL-1 secretome, HL-1

exosomes, and other soluble factors, respectively, on fibroblast gene expression. The exosome fraction induced more significant changes in gene expression than did the soluble factors (161 vs. 96 changes), including both up- and downregulated genes. Stimulation of the HL-1s with growth factors TGF-β2 and PDGF-BB partially changed the mRNA content of the exosomes[170]. About 40% of the transcripts remained constant despite the treatments, while a small number of transcripts were shared between both growth factor treatments, and others were unique to each growth factor. This likely resulted from activation of some shared transcription factors and other transcription factors unique to the TGF or PDGF signaling pathways, or changes in the exosomal packaging of transcripts may be involved.

Previous work in the Jones lab showed that miR-711 and miR-378* decreased 3h after IPC[87]. Further experiments (Jones lab, unpublished observations) showed that these miRNAs were also decreased in the serum of these mice after IPC compared with sham controls, which suggests that the heart is the source of these miRNAs under control conditions. Because miRNA was analyzed from whole serum, it is currently unknown whether these miRNAs were contained in the exosome fraction. However, these findings prompted us to explore whether changes in the miRNA profile of cardiomyocytes were reflected in the exosomes released by them.

Thus while cardiomyocytes are generally not considered to be secretory cells, they do communicate via the release of soluble factors and exosomes with many different cell types in a paracrine and endocrine fashion. It is not known whether IPC changes the profile of miRNA or mRNA found in cardiomyocyte derived exosomes, or whether these exosomes can be taken up by transplanted MSCs, resulting in enhanced

viability. ***One of the goals of the work presented in this dissertation was to test whether HL-1 exosome content changes with preconditioning and if this mediates protective effects in the MSCs (see Results, p102).*** We preconditioned HL-1 cells with a 1-hour exposure to hypoxia in an ischemia mimetic solution, a treatment that markedly reduces cell death upon a subsequent prolonged ischemia 18-24h later (see Results, Figure 8). Then we collected total RNA from the cells and exosomes and sequenced its mRNA and miRNA content to determine whether protective RNA products increased in the exosomes. These results shed light on the cellular mRNA and miRNA profile of Hl-1 cells and their exosomes, and indicate that exosomal content is tightly regulated.

miRNA in Stem Cell Mediated Paracrine Effects on the Myocardium

While extracellular miRNA has been found within a number of different carriers, including ribonucleoprotein complexes, lipoproteins, and extracellular vesicles (including microparticles and exosomes)[171], here we focus on its paracrine transfer via exosomes.

Exosome Biogenesis and Transfer

Exosome biogenesis occurs through inward budding of the membrane of an organelle known as the multivesicular body (MVB), forming intraluminal vesicles (ILVs). There are two classes of MVBs within cells: one is destined for degradation, and the other fuses with the plasma membrane, releasing the ILVs that then become exosomes. The formation of ILVs that become exosomes is not completely understood yet, but it may involve endosomal sorting complex required for transport (ESCRT) complexes, which are involved in formation of ILVs that are destined for degradation. ESCRT-0 associates with cargo proteins in the endosomal membrane. HRS (hepatocyte

growth factor–regulated tyrosine kinase substrate), a component of ESCRT-0, recruits TSG101 of the ESCRT-I complex, which mediates membrane budding into the MVB. Then ESCRT-II or another protein, Alix, recruits the ESCRT-III complex, which pinches off the vesicle, releasing it into the MVB containing a small amount of cytosol and its cargo. Then Vps4, an ATPase, dissociates the ESCRT machinery, which is recycled. It is interesting to note that HRS is phosphorylated after stimulation with HGF, known for its anti-fibrotic effects[146, 149, 152], but the effect of this phosphorylation on exosome production has not been described. siRNA-mediated knockdown of some components of this pathway, such as HRS and Tsg101, decreased exosome production in HeLa cells[172]. However, there are ESCRT-independent biogenesis mechanisms as well, involving oligomerization of syndecan and interaction with Alix and CD63[173].

Regarding the origin of the endosome that gives rise to the MVB, Tan *et al*.[174] showed that in MSCs it is derived from endocytosis at lipid raft microdomains in the plasma membrane. Labeled transferrin was endocytosed via the transferrin receptor, a prototypical recycling receptor, and later released in exosomes, indicating a recycling endosome had given rise to the MVB in which those exosomes were produced. Furthermore, labeled Cholera Toxin B, which binds to lipid raft associated GM1 gangliosides, was also found in exosomes, indicating that lipid rafts were endocytosed and included in the MVB. Exocytosis requires the small GTPase Rab and is likely mediated by as yet unidentified SNARE (soluble N-ethylmaleimide-sensitive fusion protein-attachment protein receptor) complexes at the plasma membrane[175].

The uptake of exosomes by target cells involves the interaction of specific proteins in the exosomal and cellular membrane, in a cell-type dependent fashion. For

example, interactions between intercellular adhesion molecule 1 (ICAM1) and integrins (i.e., αvβ3 or α3β5) have been shown to mediate exosome uptake in dendritic cells, endothelial cells, and pancreatic cells. CD9 and CD81 can also interact with integrins to mediate uptake. Other important molecules include galectins, annexin, and heparan sulfate proteoglycans[176, 177]. The potential specificity of the protein interactions involved in exosome uptake raises the interesting possibility that exosomes could be engineered to deliver therapeutic cargo to targeted cell types. Indeed one group showed that they could modify a protein normally found in exosomes (Lamp2b) to include a neuron-specific peptide that could target them to the brain, where they delivered siRNA directed against a gene product potentially involved in Alzheimer's disease[178]. Exosomes are taken up by endocytic processes, including clathrin mediated endocytosis, macropinocytosis, phagocytosis, and lipid raft endocytosis[179, 180], and then trafficked to different locations within the cell, including phagolysosomes, late endosomes, and the nucleus. They can release their contents through fusion with the membranes of these structures, which is more likely to occur at a slightly acidic pH. Tsg101 and Alix may also mediate this process[181]. Direct fusion of exosomes with the plasma membrane of target cells has also been reported[182].

It should also be noted that exosome-mediated signaling also occurs at the plasma membrane, inducing responses independent of uptake. In a recent study, researchers isolated exosomes from plasma of rats and healthy human volunteers, and tested its effects on I/R injury models including *in vitro*, isolated perfused heart, and *in vivo* rat hearts. Finding that the exosomes from both rats and humans decreased infarct size and decreased cell death dose dependently *in vitro* in the absence of being

internalized, the authors investigated signaling pathway activation. They found a rapid and transient increase in ERK1/2 phosphorylation, as well as phosphorylation of Hsp27 at a p38 site. They determined that TLR4 on the cardiomyocyte cell surface was activated by Hsp70 on the cell surface of the plasma exosomes, resulting in activation of Hsp27 as the effector of cardioprotection[183]. Another group found that MSC exosomes bear enzymatically active CD73, which forms extracellular adenosine from adenine nucleotides; this adenosine activates adenosine receptors on cardiomyocytes, causing Akt activation[155].

Exosomal Protein Content

Many proteomic and genomic studies have been performed on exosomes of various sources, and much of this data is now available on a public resource website known as ExoCarta[184]. Exosomes are enriched in the proteins required for their biosynthesis, such as components of the ESCRT machinery, as well as tetraspanins. Other proteins include cytoskeletal proteins, ribosomal proteins, metabolic enzymes, and lipid bound proteins such as annexin[177]. The manner in which cells distribute specific protein cargo to exosomes is an area of active investigation. In the case of the metabolic enzyme glyceraldehyde 3-phosphate dehydrogenase (GAPDH), Hsc70 associates with a specific amino acid sequence of the cargo protein (KFERQ), as well as phosphatidylserine on the MVB outer membrane, thus delivering GAPDH as the ILVs form[185]. Other reports stress the importance of tetraspanins in sorting proteins to exosomes. For example, in CD81 knockout mice, the exosomal proteome lacked a set of proteins known to interact with CD81[186]. Likewise, CD9 and CD63 have been shown to

mediate the loading of metalloproteinase CD10 and LMP1 (latent membrane protein), respectively[187, 188].

The protein content of exosomes has been shown to counteract several hallmarks of myocardial injury. First, exosomes contain all of the ATP-producing glycolytic enzymes including GAPDH, phosphoglycerate kinase, phosphoglucomutase, enolase, and pyruvate kinase. These enzymes are depleted after I/R injury[189], slowing metabolic recovery after ischemia, but treatment with MSC exosomes administered intravenously 5 minutes prior to reperfusion increased ATP and NADH levels, presumably through transfer of glycolytic enzymes[155]. Furthermore, proteomic data from this group and others showed that exosomes contain antioxidant enzymes such as glutathione S-transferase and peroxiredoxin, which reduce oxidative stress, another mechanism of I/R injury. Furthermore, it is well known that exosomes contain Hsp70, the transfer of which could assist cardiomyocytes with the response to damaged proteins.

Exosomal RNA content

mRNA Content It is clear that mRNA transported from one cell type to another can be translated and gives rise to a functional protein in the recipient cell. In 2007 Valadi *et al.* showed that when human mast cells took up murine mast cell exosomes, the murine mRNAs were translated into proteins[190]. This mRNA transfer may have therapeutic implications, as the transfer of growth factor receptor mRNA via exosomes was later found to be a mechanism by which MSCs induce regeneration in damaged renal epithelial cells[156].

The process of mRNA and miRNA incorporation into exosomes appears not to be random, based on many studies of expression in parent cells and their exosomes. For

example, Valadi *et al.* characterized mRNA and miRNA in mouse and human mast cells, and showed that some sequences are enriched in exosomes, while others, despite high expression in the parent cells, are excluded[190]. Selective RNA incorporation in exosomes may be a combination of the nucleotide sequence and tertiary structures formed by the mRNA, through which RNA binding proteins with the capacity to interact with the MVB could mediate exosome loading. Sequences known as "zipcode sequences" are found in the 3'-UTR of mRNAs; ribonuclear protein complexes bind them and transport the mRNA to the correct cellular location, where it is released and translated[191-193], implying that there may be a zipcode sequence that directs mRNAs to the MVB for incorporation in exosomes. Through comparison of the mRNA profile of glioblastoma multiforme cells and their exosomes, Bolukbasi *et al.* identified the top 20 most enriched transcripts in exosomes. By aligning their 3'-UTRs, they found a concensus zipcode sequence, which is 25 nucleotides in length, and forms a stem-loop structure with the core nucleotide concensus sequence "CTGCC." They cloned the zipcode sequence into the 3'-UTR of enhanced green fluorescent protein (EGFP), and found that its presence caused EGFP mRNA to be incorporated into exosomes. They noted the presence of a miRNA binding site within the zipcode sequence, miR-1289, and found that overexpression of this miRNA further increased loading of the EGFP mRNA into exosomes, suggesting a cooperative role for this miRNA in binding to the (as yet unidentified) ribonuclear protein which transports it. Furthermore, overexpression of miR-1289 enhanced the loading of endogenous mRNAs bearing the zipcode sequence, confirming this synergy[194].

miRNA Content As with mRNA, miRNA may be loaded into exosomes by proteins that bind to certain motifs. Alignment of miRNA sequences enriched in exosomes vs. cells identified two such motifs present in the exosomal-enriched miRNA (GGAG and CCCU), which induced sorting to exosomes regardless of changes in cellular activation state in T cells[195]. Heterogeneous ribonuclear protein A2B1 (hnRNPA2B1) mediated the exosomal loading. Another group showed that when macrophages are activated, a subset (5%) of miRNAs within exosomes is significantly changed. They showed that this was due to changes in their target mRNA levels upon activation[196]. Comparing exosomes from transfected HEK293T cells overexpressing miR-146a *vs.* untransfected cells, sequencing data showed that despite marked increases in this miRNA, the rest of the exosomal miRNA profile was maintained[197]. Even comparing exosomes from different cell types, several commonalities among the most exosomal-enriched miRNAs were noted, implying that some miRNAs are universally exported. For example, miR-451 was among the most exported miRNA in the majority of the datasets. In the case of miR-451 and several other preferentially exported miRNAs, Ago2 rather than Dicer plays an important role in biogenesis of the mature miRNA, as shown by reduction in their level in Ago2 knockout mice. This implies that this type of processing somehow targets them to exosomes. miRNA-bound Ago2 has been shown to localize within GW bodies at the MVB membrane. GW182, the protein within GW bodies from which they take their name, is sorted into MVBs. A fraction of miRNA/Ago2 complexes may also be sorted into MVBs for lysosomal degradation or secretion in exosomes, but Ago2 was detected at low levels within exosomes[198]. More

research is needed to elucidate how Ago2 and other miRNA binding proteins connect miRNA processing to its loading into exosomes.

Stem cell exosomes from various types of stem cells contain miRNA with protective or regenerative effects on I/R injured myocardium. Two recent studies on exosomes derived from cardiac stem cell sources, CDCs and CSCs, showed they contain miRNAs that decrease apoptosis and increase vessel density after I/R injury. In the CDC exosomes, miR-146a had a key role through suppression of components of the toll like receptor and tumor growth factor-β pathways, as well as a pro-oxidative stress protein, NOX4. Treating the infarcted heart with a miR-146a mimic reproduced some, but not all, of the effects of CDC-derived exosomes, and exosomes lacking miR-146a (by anti-sense knockdown in the parent cells) could still suppress apoptosis[199]. Thus miR-146a is an important contributor to their benefits, but not the only factor involved. In human CPC exosomes, several miRNAs were enriched compared with non-therapeutically active fibroblast exosomes, including miR-210, miR-132, miR-146a, and miR-181[200]. The authors focused on miR-210, a well-known cardioprotective miRNA, and miR-132 through overexpressing the miRNAs *in vitro*, performing functional assays for apoptosis and tube formation (an indicator of angiogenic activity) as well as analysis of expression of their target genes. MiR-210 downregulated ephrin A3 and PTP1 in HL-1 cells and decreased apoptosis; miR-132 downregulated RasGap-p120 in HUVECs and induced tube formation. Human CD34+ stem cells have also been shown to mediate cardiac repair through release of exosomes. The exosomes contain angiogenic miRNA including miR-126 and miR-130a[201], though their targets and contribution to angiogenesis have not yet been tested. Like CSC exosomes, exosomes from iPSC were also shown to

contain miR-210 as well as miR-21, and to reduce markers of I/R injury such as TUNEL staining and cleaved Caspase-3 when injected into the mouse heart just after induction of ischemia. Changes in expression of the target genes of miR-210 and miR-21 were not investigated, but incubation of H9c2 with iPSC exosomes did show that the levels of these miRNAs increased, indicating that the exosomes delivered these cardioprotective miRNAs[202].

Two studies have investigated cardioprotective miRNA within MSC exosomes. The first tested the effect of preconditioning the source MSCs with hypoxia on the miRNA profile and beneficial effects of their exosomes. They found a 4.5-fold enrichment of miR-22 in the exosomes after hypoxic preconditioning and went on to show that miR-22 targets methyl CpG binding protein (Mecp2)[203]. In support of a role for Mecp2 in I/R injury, they showed that knockdown of Mecp2 via siRNA or miR-22 mimic in the heart decreased apoptosis after I/R injury. Lastly, they showed that the exosomes from preconditioned MSCs decreased infarct size and fibrosis in a mouse model, and miR-22 knockdown in the MSCs and their exosomes partially abrogated this effect, indicating an important role for miR-22 (though Mecp2 levels in the heart after exosome treatment were not shown and the role in I/R injury of Mecp2 is unknown). The second study compared the protective effects of MSC exosomes from MSCs overexpressing the transcription factor GATA4 with null-transfected MSCs, and found the former to be more protective, possibly through enhanced content of miR-19 and miR-451[204]. Specifically, both types of exosomes were found to downregulate PTEN and Bim, but the exosomes from GATA4-MSCs were more effective.

In summary, miRNA within stem cell exosomes is increasingly recognized to mediate well known aspects of stem cell paracrine effects, including decreased apoptosis of cardiomyocytes and angiogenesis. A number of protective miRNAs have been researched within stem cell exosomes, and some of their mRNA targets and associated mechanisms have been elucidated. However, cardioprotective miRNA in MSC exosomes has not been extensively investigated and there is currently no data regarding exosomal mRNA in the context of paracrine cardioprotection or regeneration. ***The goal of this part of the project (see Results p109) was to characterize the mRNA and miRNA profiles of MSC exosomes and test the functional contribution of miR-21***, a promising candidate which emerged from this profile, to cardioprotection. As discussed in Section 1, it downregulates a number of proteins involved in cell death in cardiomyocytes and other cell types, including PDCD4, FasL, PTEN. It is also predicted to target Peli1, which may be injurious in the context of I/R injury[205].

We found miR-21 to be the most highly expressed miRNA in MSC exosomes, but this is not the first description of its presence there. Wang *et al*.[202] described it as being enriched in iPSC exosomes *vs.* non-therapeutically active fibroblast exosomes, and Feng *et al*.[203] noted both its presence in MSC exosomes at baseline and a significant 3.3-fold increase after hypoxic preconditioning. However, whether miR-21 within MSC exosomes contributes significantly to their protective effect, and the proteins targeted by exosomally-delivered miR-21 are unknown. To test this hypothesis, we isolated MSCs from miR-21a knockout (miR-21a KO) mice and compared their exosomes with those of WT MSCs. Subsequently, we examined gene expression *in vitro* and *in vivo* after treatment with miR-21, WT exosomes, and miR-21 KO exosomes.

SUMMARY OF GOALS AND HYPOTHESES

Due to the prevalence and poor prognosis associated with myocardial infarction, it is important to find new cardioprotective strategies that could lead to therapeutic advances. There are two philosophies about how to improve outcomes after myocardial infarction. The first is to trigger endogenous cardioprotective pathways such as that active in IPC, to prevent the loss of cells. The other is to regenerate the myocardium by boosting its endogenous limited regenerative potential, or replace the lost cells with differentiated stem cells. However, there may be more mechanistic overlap between these two approaches than is currently appreciated. For example, stem cells and their exosomes may act to trigger endogenous cardioprotection, and IPC may boost the capability of stem cells (both endogenous and transplanted) to regenerate the myocardium. Thus it is useful to investigate both of these approaches together and seek commonalities, such as key roles for miRNA in mediating and communicating protective effects.

Goal 1

To identify miRNAs that could act as regulatory nodes for numerous heat shock protein family members during IPC. We know that individual miRNAs are regulated by IPC, contributing to protective gene expression during late IPC, and that miRNAs can act to regulate functionally related sets of genes, so the first section is driven by the hypothesis that *certain miRNAs act to regulate the expression of HSPs including Hsp40/Dnaj proteins, Hsp70, and Hsp90 in response to preconditioning.*

Goal 2

To test whether HL-1 exosome content changes with preconditioning and if this mediates protective effects in the MSCs. Evidence suggests that preconditioning causes

the release of protective factors from the myocardium, and that changes in secreted factors may mediate improved stem cell engraftment. The hypothesis of this section was that preconditioning of cardiomyocytes leads to increased exosomal loading of protective miRNA, which exerts pro-survival effects on transplanted MSC.

Goal 3

To characterize the transcriptome of MSC exosomes and test the functional contribution of their highly enriched miRs to cardioprotection. Because mRNA and miRNA transferred by exosomes have been shown to be functional in recipient cells, and MSC exosomes are known to be cardioprotective, we hypothesized that a significant part of their cardioprotective effects are mediated through transfer of protective mRNA and/or miRNA, specifically miR-21, which we found to be the most highly represented miRNA in the exosomes.

CHAPTER 2

MATERIALS AND METHODS

METHODOLOGY

Animals

The following types of mice were purchased from Jackson Labs (Bar Harbor, ME): C57Bl/6J (stock # 000664), B6;129SF2/J (stock # 101045), and miR-21 null (B6;129S6-^{Mir21atm1Yoli}/J, stock # 016856) and were maintained according to the guidelines set forth by the NIH in the Guide for the Care and Use of Laboratory Animals (GCULA) and Loyola University Chicago's Institutional Animal Care and Use Committee.

Ischemic Preconditioning and Ischemia/Reperfusion Injury

Ischemic preconditioning was achieved by reversible ligation of the left anterior descending (LAD) coronary artery as previously described[206]. Mice were anesthetized by intraperitoneal injection of sodium pentobarbital (90 mg/kg) and intubated to maintain a respiratory rate of 100±5/minute using a mini-ventilator (Harvard Apparatus, Cambridge MA). A lateral thoracotomy was performed between the 2nd and 3rd ribs to access the heart, and the LAD artery was occluded 2-4 mm from the tip of the left auricle by tightening a suture (8-O nylon) against a short, thin piece of silicon tubing. Six cycles of 4-minute occlusion and 4-minute reperfusion were performed. The heart was monitored by ECG and visual changes (blanching) to confirm that ischemia occurred.

Subsequently, the chest was closed and mice were allowed to recover until the time point of interest for investigation of gene expression changes.

To induce ischemia/reperfusion injury, similar procedures were performed, with the LAD being occluded for 45 minutes, followed by reperfusion and recovery overnight[206]. Characteristic ECG changes included widening of the QRS complex, T wave inversion, and ST segment changes characteristic of myocardial infarction. The suture used to occlude the LAD was left in place.

TTC Staining and Infarct Size Assessment

As previously described[206], 24 hours after I/R injury, mice were euthanized using sodium pentobarbital, the chest was re-opened, and the aorta was cannulated with polyethylene-10 tubing. Triphenyltetrazolium chloride (TTC) 1% solution in PBS was perfused through the heart and coronary arteries including the LAD. Enzymes active in viable tissue reduce TTC to a formazan compound with a red color, while dead tissue in the infarct zone remains unstained. To determine the area at risk, the suture on the LAD was tightened once again, and a 5% solution of phthalo blue pigment (Heucotech, Fairless Hills PA) in PBS was perfused through the heart, staining only the areas of the heart that were not at risk.

After staining, hearts were frozen and sectioned into 1 mm slices from just below the suture to the apex of the heart (4 to 5 slices total). These slices were imaged using a Nikon camera and the total area, infarct area, and area at risk were determined digitally in NIH ImageJ by tracing the entire heart section, white area, and red area (including white areas within), respectively. Then, using the weight of the slices, the percent of the

heart at risk as well as the percent of the risk area that was infarcted were calculated according to the accepted method of Fishbein *et. al*[207].

Pericardial Sac Injections

Mice were anesthetized and the chest opened as previously described in Section 2.2. Injections into the pericardial sac were performed using a 50µl Hamilton syringe (Hamilton Company, Newport Beach CA)[208] with a custom removable needle (25 gauge, 1" length with a tip beveled at 45º). The chest was then closed and mice were periodically re-positioned until they recovered from the anesthesia, to ensure the injected solution reached all areas of the heart equally. The volume of the injection was based on the mouse's weight to control for proportional differences in the size of the heart, and was 1 µl/g of body weight.

Culture of Cardiac Cell Lines

HL-1 transformed murine atrial cardiomyocytes were cultured according to established conditions[209] with approval for use granted by Dr. Claycomb. They require the specially formulated Claycomb growth medium (Sigma-Aldrich, St. Louis MO), containing 10% FBS (of particular pre-tested lots) and norepinephrine (100 µM), and must be grown on a gelatin-fibronectin coated substrate. Furthermore, it is recommended that they be passaged at a 1:3 ratio and not be allowed to become underconfluent (personal communication, Dr. May Lam). Under these conditions, HL-1s maintain a differentiated contractile phenotype and can be serially passaged and recovered from frozen stocks[209].

H9c2(2-1) rat cardiac myoblast cells[210] were purchased from ATCC and cultured according to ATCC's recommendations. They were maintained in Dulbecco's Modified

Eagle Medium (DMEM) supplemented with 10% FBS, penicillin (100 U/mL), streptomycin (100 ug/mL), and L-glutamine. All cells were maintained at 37ºC in humidified incubators with 5% CO_2.

Culture of Primary Neonatal Mouse Ventricular Myocytes

Neonatal mouse ventricular myocytes (NMVM) were obtained from 1 to 3 day old wildtype or miR-21 null pups as described by Ehler *et al.*[211]. In accordance with institutional guidelines, the pups were cooled on ice prior to decapitation with a sharp scalpel and removal of the heart. Hearts were then washed in phosphate buffered saline (PBS) without Ca^{2+} or Mg^{2+} containing 20 mM 2,3-Butanedione monoxime (BDM, Sigma-Aldrich, St. Louis). BDM prevents the myocytes from contracting during the isolation procedure, enhancing viability and yield. Then the hearts were minced into small pieces and incubated in 10 mL isolation medium (Hank's buffered salt solution without Ca^{2+} or Mg^{2+} containing 20 mM BDM, 0.0125% trypsin) overnight at 4ºC on a rocking platform.

The next day, the hearts were digested using a collagenase/dispase enzyme mix (Roche #10269638001, 15 mg in 10 mL L15 Medium containing 20 mM BDM) for 25 minutes at 37ºC. The fragments were then gently triturated to release the cells. Any fragments that didn't disperse were then enzymatically digested once more. The cell suspension was then pipetted over a 100 µm cell strainer and centrifuged at 100xg to pellet the cardiomyocytes. These were resuspended in plating medium (65% DMEM high glucose, 19% M-199, 10% horse serum, 5% fetal calf serum, 1% penicillin-streptomycin). Then cells were plated for 1-2 hours on uncoated plastic to allow attachment of endothelial cells and fibroblasts, before plating the cardiomyocytes into

12- or 6-well plates pre-coated with gelatin-fibronectin or collagen at a density of 1.5 x 10^5 cells per cm^2. The next day, medium was changed to maintenance medium (78% DMEM high glucose, 17% M-199, 4% horse serum, 1% penicillin/streptomycin, 1 μM AraC, 1 μM isoproterenol). Cardiomyocytes became adherent and began to spontaneously contract. They were then cultured for an additional 1 to 5 days.

In order to test the purity of the cardiomyocyte population, immunocytochemistry was performed for Troponin I, a myocyte-specific protein. Cells were fixed in paraformaldehyde, rinsed in PBS, and then permeabilized using Triton-X100 (0.1% in PBS) for 10:00. Cells were then washed again and blocked using 3% BSA, 0.1% Tween20 in PBS, for 30:00. Cardiomyocytes were then labeled using a rabbit anti-mouse antibody to Troponin I (Abcam, San Francisco, CA #ab47003) diluted 1:400 in blocking buffer for 1 hour. After washing, the cells were then incubated with goat anti-rabbit secondary antibody labeled with Alexa Fluor 594 (Thermo Fisher Scientific, Waltham MA, #R37117) as well as DAPI to label nuclei. After washing, cells were imaged using the Cytation3 with the DAPI and Texas Red filters. The isolation procedure resulted in 89±7% Troponin I^+ cells (Figure 1).

Figure 1. Primary Neonatal Cardiomyocytes

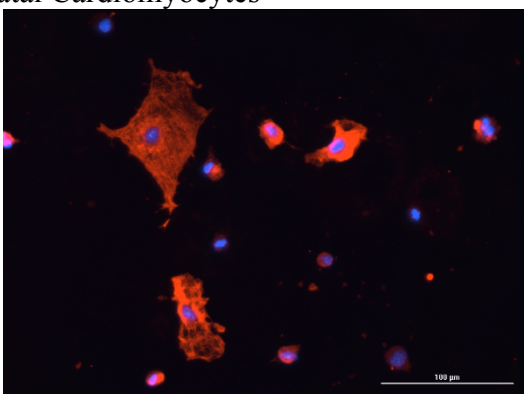

Three days after plating, immunocytochemistry was performed to determine the percentage of cells positive for Troponin I (red fluorescence) out of the total number of cells, labeled with DAPI.

After day 3, the NMVMs were treated with MSC exosomes overnight to assess exosome uptake by flow cytometry and exosomes' effects on gene expression and viability upon OGD challenge.

Culture of Primary Mesenchymal Stem Cells

Mesenchymal stem cells were obtained from mouse bone marrow as well as bone chips of the femur and tibia. Female wildtype B6;129 and miR-21 null mice (on a B6;129 background) were used at age 8-10 weeks. The bones were cleaned of muscle and connective tissue, and the ends were clipped to expose the marrow, which was flushed from the bone using a 27-gauge needle as described previously[129] in isolation medium consisting of RPMI-1640 with 9% FBS, 9% horse serum, 100 U/mL penicillin, 100 µg/mL streptomycin, and 12 µM L-glutamine (Thermo Fisher Scientific, Waltham)[128]. RPMI discourages the expansion of hematopoietic stem cells. Each long bone was flushed with 5 mL of isolation media into a 50 mL conical tube. The cell suspension was strained over a 70 µm cell strainer, and then plated into T75 flasks. Non-adherent cells were removed by rinsing with PBS and medium was replaced. This

washing was repeated every 3 to 4 days for 4 weeks or until cells became confluent. They were released from the flask with 0.25% Trypsin-EDTA for 2 minutes and re-plated into a new flask. Cells that remained attached were discarded. The passage 1 cells were then allowed to grow, with media replacement twice per week. Over 2 to 4 weeks, colonies of rapidly multiplying cells became evident. When these became numerous and/or large in size, the cells were again passaged and plated in expansion media, consisting of Iscove modified Dulbecco medium (IMDM) with 9% FBS, 9% horse serum, 100 U/mL penicillin, 100 μg/mL streptomycin, and 12 μM L-glutamine.

Because MSCs have also been described to reside within compact bone as well as bone marrow[130], the flushed bones were cut into small pieces and placed in 10 cm^2 culture dishes containing isolation medium. By the next day, cells began to migrate out of the chips and attach to the plastic. The bone chips were left in the dishes for 1 week, and then removed. These cells were then cultured in the same way as the bone marrow derived MSCs; MSCs derived from bone marrow and bone chips showed no differences in morphology, surface marker expression or proliferative potential in our hands.

To validate the isolation procedure as generating a pure population of MSCs, three assays were performed. First, their capacity for self-renewal and proliferation was assessed by the colony forming unit (CFU) assay, in which 100 cells are plated in expansion media in a 60 mm culture dish. These were incubated for 3 weeks, and then colonies were stained in 3% crystal violet in methanol for 20:00 at room temperature[128]. Then the colonies were counted to determine how many of the original 100 cells could give rise to a rapidly dividing colony. This number increased with passaging until by passage 10, over 100 colonies had formed.

Figure 2. Mesenchymal Stem Cell Colonies

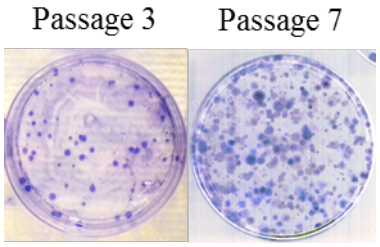

100 cells were plated in expansion media and incubated for 3 weeks. Colonies were then stained with Crystal Violet solution and counted. At passage 3, there were an average of 62 colonies. At passage 7, there were >200 colonies, indicating that the proliferative potential of the cells increased with passaging.

Next we assessed their capacity to differentiate into three different lineages: adipocytes, chondroblasts, and osteoblasts. This was done using commercially available kits from Cyagen (Santa Clara, CA) according to the manufacturer's instructions (adipogenic differentiation, GUXMX-90031; chondrogenic differentiation, GUXMX-90041, and osteogenic differentiation GUXMX-90021). Briefly, adipogenic differentiation is induced by the addition of insulin, 3-isobutyl-1-methylxanthine (IBMX), rosiglitazone, and dexamethasone to the basal culture media. Chondrogenic differentiation is induced by dexamethasone, TGF-β, and ITS+ supplement (insulin, transferrin, and sodium selenite) in media containing sodium pyruvate, ascorbate, and proline. Osteogenic differentiation was induced by adding β-glycerophosphate to basal media containing ascorbate. We confirmed that the MSCs could differentiate into all three lineages (Figure 3).

Figure 3. Differentiation of MSCs

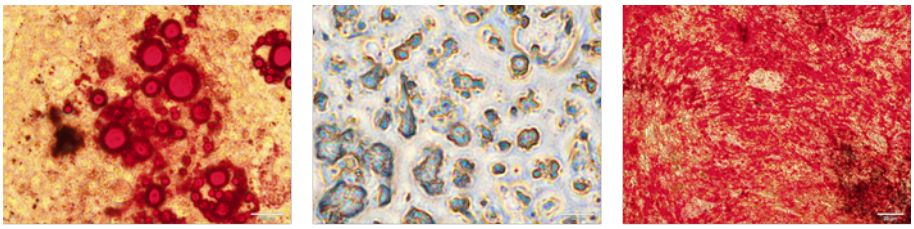

Adipogenic Chondrogenic Osteogenic

Passage 5 MSCs were differentiated to three different mesodermal lineages, adipogenic, chondrogenic, and osteogenic. Specific stains were used to confirm differentiation. Adipocytes were stained with Oil Red O, which stains lipids. Chondrocytes formed a cartilaginous matrix pellet within the culture tube, which was stained with toluidine blue. Calcium deposits produced by osteocytes were stained with Alizarin red.

Lastly, we examined the surface epitopes of the cells to confirm the presence of known MSC markers and the absence of hematopoietic and leukocyte markers. The cells were detached using Accutase (which preserves surface proteins better than trypsin), and counted. $1x10^6$ cells were labeled with the antibodies in Table 1 for 45:00 on ice in flow cytometry buffer (PBS with 1% BSA, 25 mM HEPES, and 10 U/mL DNAse). The negative control was unstained cells.

Table 1. Antibodies to Cell Surface Markers

Marker	Fluorescent label	Wavelength (ex/em)	Dilution/10^6 cells	Associated cell type
CD44	Allophycocyanin	645/660	1 µl	MSC
Sca-1	Pacific Blue	410/455	5 µl	MSC
CD-29	Phycoerythrin	496/575	1 µl	MSC
CD45	Phycoerythrin-Cy7	496/565	1 µl	Hematopoietic stem cell
CD11b	Brilliant Violet 510	405/510	5 µl	Leukocyte

After labeling, cells were washed twice, re-suspended in 1 mL of flow cytometry buffer and passed over a 70 µm cell strainer into Falcon tubes for sorting. The live single cell population was gated and 10,000 events were counted. The results were analyzed in FlowJo and displayed as overlaid frequency histograms of stained vs. negative control

cells to show the percentage of cells positive for each surface marker. The resulting immunophenotype was $CD29^+$, $CD44^+$, $Sca1^+$, $CD45^-$, $CD11b^-$, (see Figure 4) which is consistent with the mesenchymal phenotype and the absence of hematopoietic stem cells[128-130].

***In Vitro* Models and Viability Assays: Hypoxic Preconditioning (HPC) and Simulated Ischemia Reperfusion Injury (simI/R)**

HL-1 cells were preconditioned by exposure to ischemia mimetic solution (in mM: 125 NaCl, 8 KCl, 1.2 KH_2PO_4, 1.25 $MgSO_4$,1.2 $CaCl_2$, 6.25$NaHCO_3$, 5 sodium lactate, 20 HEPES, pH 6.6 at 37ºC)[29] for 1 hour in a hypoxic chamber (Biospherix, Parish NY). Oxygen was replaced by nitrogen until the oxygen level reached ≤0.5%, while CO_2 was maintained at 5%. After 1 hour cells were reoxygenated and the ischemia mimetic solution was replaced with growth media. Simulated ischemia reperfusion injury (simI/R) was induced by exposure to glucose and serum free DMEM and placement in the hypoxic chamber for 1.5 to 3 hours (Figure 5). The optimal time for each experiment was estimated based on a series of time courses performed with the cells plated at different densities.

Then growth medium was replaced and cells were returned to normal growth conditions. For H9c2 cells, simI/R was performed by incubation in the hypoxic chamber for 15 to 18 hours in ischemia mimetic solution; a longer ischemia time was required to induce cell death in H9c2 cells than in HL-1s.

Figure 4. Surface Epitopes of MSCs

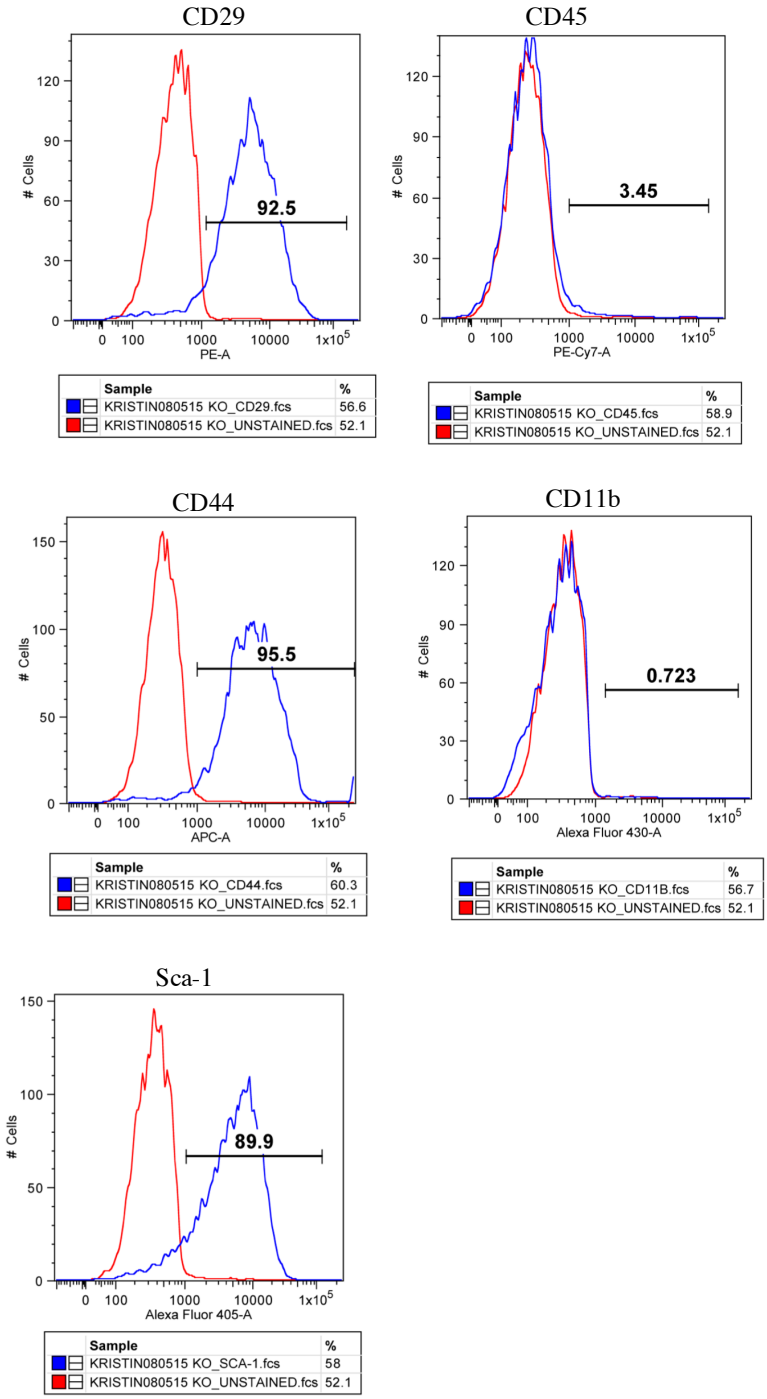

Passage 10 MSCs were released with Accutase and labeled with fluorescently conjugated primary antibodies for the surface markers CD29, CD44, Sca-1, CD11b, and CD45. Unlabeled cells were used as negative controls (red line), and the fluorescence intensity of the labeled cells was compared to this (blue line). A shift to the right indicates increased fluorescence intensity, signifying that that the antigen is expressed by the cells.

Figure 5. Time to 50% Cell Death from SimI/R Changes with Confluence in HL-1 Cells

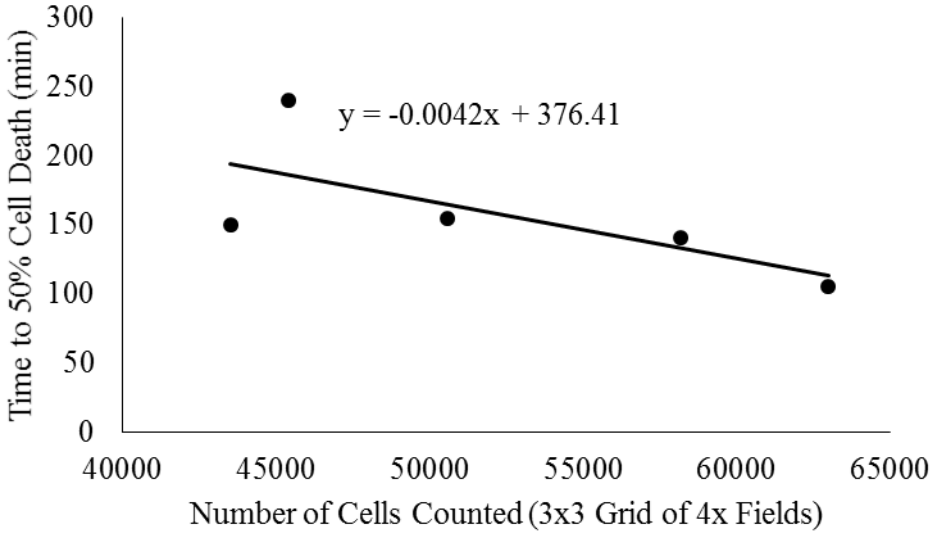

The optimal duration of simI/R was determined to be a function of confluence of the cells because as HL-1 cells become more confluent, the time needed to kill approximately 50% of them decreases. HL-1 cells were plated at different densities and grown overnight. The following day, simI/R time courses of 0, 60, 120, 180, and 240 minutes were performed, and viability was determined by Hoechst/PI uptake assay (see section 2.9), allowing determination of the time to 50% cell death. N=6/condition.

Three methods were employed to assess cell death after simI/R: (1) lactate dehydrogenase (LDH) release into the media, (2) uptake of Hoechst 33342 (Life Technologies H3570) and propidium iodide (PI, Life Technologies p3566) fluorescent dyes, and (3) GF-AFC fluorescence (Promega Madison WI, Cell-titer Fluor kit, #G6080), an indication of cellular metabolic activity. LDH release was assessed using a kit from Clontech (Palo Alto CA, #630117) according to the manufacturer's instructions with the modification of using a standard curve of 0 to 25 U/mL LDH (Sigma-Aldrich, St. Louis, #L3888-500UN). The principle of the assay is that NAD+ is reduced to NADH/H+ by the LDH catalyzed conversion of lactate to pyruvate. In the second step, a catalyst included in the reaction mixture (diaphorase) transfers H/H+ from NADH/H+ to

the tetrazolium salt INT, which is reduced to a formazan dye which can be detected at a wavelength of 490 nm.

Cells were re-oxygenated after simI/R in phenol red free DMEM containing glucose and serum. Because serum contains a baseline level of LDH activity, a media blank must also be included when serum is present in the reperfusion media. Phenol red in the media interferes with reading of the assay because it contributes to absorbance readings at 490 nm. Culture medium was diluted 1:10 in a final volume of 100 µl per well in a 96-well plate in duplicate. Then 100 µl of freshly prepared reaction mixture was added and the plate was incubated for 30:00 at room temperature, protected from light. Then absorbance at 490 nm was measured using the Cytation3 and units of LDH activity were calculated based on the standard curve and dilution factor.

Another measure of cell death is the labeling of dead cells with PI. Live cells exclude PI, but it enters dead cells and stains DNA. All cells take up Hoechst 33342, which also stains DNA. Using these dyes in combination provides the ratio of dead cells to all cells. After post-simI/R reoxygenation for at least 1 hour (we found similar results between 1 hour and 18h after reoxygenation), cells were exposed to reperfusion media, containing PI and Hoechst diluted to 2 µg/mL and 0.2 µg/mL respectively, and allowed to take up the dyes for 30 min in the incubator. Then the cells were imaged using the Cytation3 with the Texas Red filter to detect dead cells (PI^+) and the DAPI filter to detect all cells ($Hoechst^+$). The Gen5 software for the plate reader was programmed to count these cells and export the count for each well to Excel. To determine the percentage of cells that survived the simI/R challenge, this assay can be performed prior

to the simI/R to determine the number of cells present in the well at the beginning, allowing one to control for differences in plating or growth kinetics.

Exosome Preparation and Quantification of Uptake

Exosomes were pelleted from conditioned media of MSC and HL-1 cells by centrifuging the media at three different speeds as described in Table 2 according to the protocol described by Thery *et al.*[212]. Expansion media (per section 2.7) was made with exosome depleted serum when exosomes were being isolated. Exosome depleted serum was made by ultracentrifugation of FBS for 90:00 at 100,000 x g.

Table 2. Centrifugation Procedure for Exosome Isolation

Step	Type of tube	Volume /tube	Speed (xg)	Time (min)	Component pelleted
1	Falcon Conical	50 mL	2000	20	Cells
2	Oak Ridge High Speed	30 mL	10,000	30	Microvesicles
3	Beckman Ultra Bottle assembly	60 mL	100,000	70	Exosomes

After the exosomes were pelleted, they were resuspended in PBS and re-pelleted to wash. If multiple tubes of media were used in step 3, the exosomes were pooled prior to washing. After pelleting them once more, a protein assay was performed so that a consistent concentration of exosomes could be used in subsequent experiments. The size of the pelleted vesicles was 70 to 105 nm, as determined using dynamic light scattering on a Zetasizer. Furthermore the vesicles were positive for the exosomal marker proteins Tsg101 and CD9[212, 213] by Western blot.

Figure 6: Characterization of MSC Exosomes

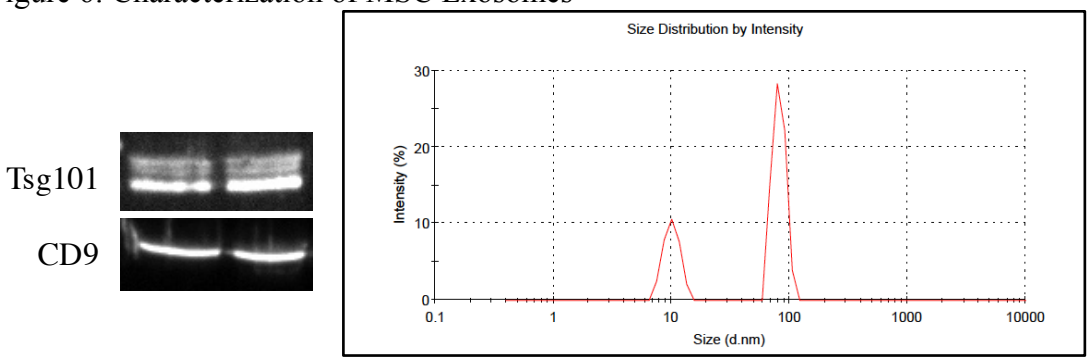

Western blot shows the presence of CD9 and Tsg101, and dynamic light scattering shows the size of the vesicles to be consistent with that of exosomes. Note, the peak at 10 nm was also present in the PBS used to re-suspend the exosomes.

To count the exosomes and confirm that various cell types take them up, exosomes were labeled with PKH26 (Sigma-Aldrich, St. Louis) according to the manufacturer's recommendations. The exosome pellet was re-suspended in 1 mL of diluent provided with the labeling kit, and an equal volume of PKH26 dye in diluent was added (4 µl in 1 mL). This was mixed well by pipetting up and down, and labeling carried out for 3 minutes with gentle agitation once per minute. Then an equivalent volume of exosome free FBS was added to stop the reaction and the labeled exosomes were washed in 50 mL PBS to remove excess unbound PKH26 dye. After this wash, the exosome pellet appeared pink. Exosomes were resuspended in PBS and diluted into the growth media of the cells being studied (HL-1, H9c2, MSC, and NMVM cells were tested). Cells were incubated overnight, then lifted with Accutase Cell Detachment Solution (Thermo Fisher Scientific, Waltham), pelleted, and re-suspended in cell sorting buffer for analysis by traditional flow cytometry or Amnis Image Stream.

Protein Isolation and Quantification

Protein was extracted from cells in RIPA buffer (Santa Cruz Biotechnology, Santa Cruz CA, #sc-24948A) containing freshly added PMSF, Na_3VO_4, and a protease

inhibitor cocktail, according to the manufacturer's recommendations. Medium was removed and cells were washed twice in cold PBS. Then 100-200 µl of RIPA buffer were added per well (depending on confluence of cells) and cells were lysed for 15:00 at 4ºC on a rocking platform. Next cells were scraped and lysates were incubated for 30 to 60 minutes on ice before centrifuging to pellet debris at 10000 x g for 15:00 at 4ºC. Lysates were transferred to a new tube and frozen at -80ºC or further analyzed by protein concentration assay and western blotting.

To extract protein from the mouse heart, the heart was removed and washed well in ice cold PBS to remove blood. The left ventricle was dissected, rinsed once more, and snap frozen in liquid nitrogen. It was then powdered using a tissue crusher (also cooled in liquid nitrogen) and suspended in 300 µl RIPA buffer. The homogenate was then processed using a dounce homogenizer until uniform. Lysates were then incubated 30 to 60 minutes on ice, and the remainder of the protein extraction carried out as previously described. Lysates were stored in aliquots of 100 µl each at -80ºC.

Protein concentration was determined using the bicinchoninic acid (BCA) method (kit from Thermo Fisher Scientific, Waltham). Cell lysates were diluted 1:4, while heart tissue samples were diluted 1:20 in RIPA buffer. Standards were also diluted in RIPA buffer ranging from 125 to 2000 µg/mL and a RIPA buffer blank was performed. The BCA working reagent was added to 20 µl diluted sample or standard, and the 96-well plate was incubated covered at 37ºC for 30:00. It was then allowed to cool to room temperature and absorbance was read at 562nm.

Western Blotting

Ten to fifteen µg of protein were heated at 95ºC for 10:00 in 2x or 4x Laemmli buffer before separation on a 10 or 12% polyacrylamide gel. Proteins were then electro-transferred to nitrocellulose membranes and transfer was confirmed by Ponceau staining. Membranes were blocked in 5% dry milk (w/v) in tris buffered saline containing 0.1% Tween20 (TBS-T) for 1 hour. Then they were incubated with primary antibody (see Table 3) diluted in blocking buffer overnight or for 2 hours at room temperature, washed, and then incubated in HRP conjugated secondary antibody, also diluted in blocking buffer, for 1 hour at room temperature. After washing, chemiluminescent bands were digitally detected using the Bio-Rad ChemiDoc imager using ECL or SuperSignal West Dura reagent kits (Thermo Fisher Scientific, Waltham). A series of images were acquired and the exposure just prior to oversaturation was used for quantitation. Images of the membranes were exported as TIF files from the Image Lab software, and densitometry was performed in ImageJ to assess relative band intensities.

Table 3. Primary Antibodies

Antibody	Source & cat#	Dilution	Appropriate secondary antibody
Hsp70	Santa Cruz Biotechnology, Santa Cruz, sc-24	1000	Mouse (1:2000)
Hsp90	Thermo Fisher Scientific, Waltham, PA3-013	2000	Rabbit (1:5000)
Dnaja1	Thermo Fisher Scientific, Waltham, ms-225-p0	2000	Mouse (1:2000)
Dnajb4	Santa Cruz Biotechnology, Santa Cruz, sc-100711	1000	Mouse (1:2000)
Actin	Sigma-Aldrich, St. Louis, A2066-.2ML	2000	Rabbit (1:5000)
β-actin	Thermo Fisher Scientific, Waltham, MA5-15739	2000	Mouse (1:2000)
PDCD4	Cell Signaling, D29C6	1000	Rabbit (1:5000)

PTEN	Cell Signaling	1000	Rabbit (1:5000)
FasL	Abcam, ab68338	500	Rabbit (1:5000)
Peli1	Abcam, ab13812	1000	Rabbit (1:5000)
TSG101	Santa Cruz Biotechnology, Santa Cruz, sc-7964	500	Mouse (1:2000)
CD9	Santa Cruz Biotechnology, Santa Cruz, sc-9148	1000	Rabbit (1:5000)

RNA Isolation

Three hours after IPC, mice were euthanized by CO_2 inhalation. Hearts were removed, washed in PBS, and the ischemic zone was dissected out and snap frozen in liquid nitrogen. It was then homogenized using a tissue grinder in 1 mL Qiazol and extracted using the miRNEasy mini kit (Qiagen, Germantown MD) according to the manufacturer's instructions, including DNAse digestion.

RNA was extracted from cells in Qiazol (Qiagen, Germantown) and isolated by phase separation and isopropanol precipitation, DNAse treated, and re-isolated. Alternatively, the miRNEasy kit (Qiagen, Germantown) was used. For exosomes resuspended in PBS, Trizol LS (Thermo Fisher Scientific, Waltham) was used to isolate RNA by phase separation and isopropanol precipitation according to the manufacturer's recommendations, with DNAse treatment and re-isolation.

Reverse Transcription

RNA concentration and purity was determined using a NanoDrop or Take3 plate on the Cytation3. A consistent amount of RNA was used for each cDNA synthesis reaction, with a maximum amount of 2 μg. For analysis of miRNA, the miScript II RT kit (Qiagen, Germantown, #218161) was used; for analysis of mRNA, the High Capacity

RNA-to-cDNA kit was used (Thermo Fisher Scientific, Waltham, #4387406). For either kit, the reaction consisted of input RNA, water, enzyme, and nucleotide mix, in a 20 µl total volume. This was held at 37ºC for 60 minutes, heated to 95ºC for 5 minutes, and then cooled to 4ºC. For short-term storage, cDNA was kept at -20 ºC, and for long term storage at -80ºC.

Real-Time PCR

Separate protocols were used to analyze mRNA and miRNA expression. For mRNA analysis, primers were designed in house for the gene of interest; the sequences are listed in Table 4. The reaction consisted of 5 µl cDNA (diluted 1:10 in nuclease-free water), 0.25 µl each of forward and reverse primers, 4.5 µl water and 10 µl 2x SYBR Green Master Mix in a total volume of 20 µl. The SYBR Green Master Mix also contained ROX dye as a passive reference. For analysis of miRNA, miScript primers were purchased from Qiagen (Germantown). The reaction, in a 22 µl volume, consisted of 2 µl cDNA (diluted 1:10 in nuclease free water), 2 µl universal primer, 4 µl water, and 10 µl 2x SYBR Green Master Mix.

Real-Time PCR was performed on an AriaMX instrument using the following thermal cycling parameters: hot start 10:00 at 95ºC, followed by 40 cycles of denaturing for 15s at 95ºC, annealing for 30s at 55ºC, and extending for 30s at 70ºC with fluorescent data collection occurring at this step. After the 40 cycles of amplification, a melt curve was performed to ensure the synthesis of a single product (one peak). Data analysis was performed as previously described [87, 214] with normalization to U6 for miRNA and 18S for mRNA. Primers were designed using Vector NTI, and ordered from

IDT (Coralville, IA), with the exception of Hsp90aa1 and Dnajb4, which were purchased from Qiagen (Germantown).

Table 4. Sequences of Real-time PCR primers

Gene	**Sense primer**	**Anti-sense primer**
Hsp70.1	GAAGACATATAGTCTAGCTGCCCAGT	CCAAGACGTTTGTTTAAGACACTTT
Hsp70.3	GGCCAGGGCTGGATTACT	GCAACCACCATGCAAGATTA
Dnaja1 3'	GGTGAAGGAGACCAAGAACCAGGA	TTGACAATCTGACCTGGATGAGAGG
Dnajb1 3'	ATGTTTGCTGAGTTCTTCGGTGGC	CCGCTGTAGATCTCTTCAAGGGAGAC
18S	AGTCCCTGCCCTTTGTACACA	CCGAGGGCCTCACTAAACC
PTEN	GGCCAACCGATACTTCTCTCC	CTGGATCAGAGTCAGTGGTGT
PDCD4 total, mouse	TGGTGGGCCAGTTTATTGCT	CCAGATCCCCACACACTGTC
PDCD4 total rat	TACCGCATTTCCACCACGAG	GCACAGAGTATGAGTGTGGGAC
PDCD4 v1 mouse	GCACAGCAACTCTTACAGTCTTAG	CGGTGGTTCCTCTTCTGTCC
PDCD4 v3 mouse	CAAGAACAGATCTCAACTGGAACAT	ACCGGGTTCGTTTTTCCAGT
PDCD4 v1 rat	GAAGGAGATGGAGGTCGTCTTAAACC	AGGTGGTTACTCTTCGGTCCCT
PDCD4 v3 rat	CCAAGAACAGATCTCAATTGGAACGT	GTAGAAAAATAGATGTTCCAGCCACC
Peli1	GTGAATGTCCTATGTGTAGGTCTGTT	CCTTGTTCACCAGCCAACTGAT
FasL	GGCTCCTCCAGGGTCAGTTTTT	CATTCCAACCAGAGCCACCAG

Generation of Luciferase Reporter Plasmids

Luciferase reporter plasmids were constructed as previously described[87]. Using primers to murine genomic DNA, the 3'-UTR of the gene of interest was amplified. See Table 5 for the sequences of cloning primers for each plasmid. Then the pGL4 plasmid (Promega, Fitchburg, Wisconsin) was linearized using appropriate restriction enzymes to

create the desired overhang sequences. The pGL4 plasmid expresses luc2 (a modified luciferase with mammalian codon replacement) driven by the constitutively active cytomegalovirus (CMV) promoter. The 3'-UTR sequence was ligated into the plasmid immediately following the luc2 sequence and the plasmid was re-circularized. *E. coli* bacteria were transformed with the plasmid by standard heat shock protocol, allowed to recover for 1 hour, and plated on agarose. Several colonies were transferred to Terrific broth (Sigma-Aldrich, St. Louis) and grown overnight under penicillin selection (100 μg/mL) at 37ºC in a rotary shaker. DNA was extracted using a DNA isolation kit according to the manufacturer's instructions. Each plasmid was tested by restriction analysis and sequencing.

The resulting construct provides high expression of luc2 that is regulated by the 3'-UTR of the gene of interest. When co-transfected with miRNA that binds to the 3'-UTR, translational repression and reduced luciferase activity occur, confirming that the miRNA regulates the target gene through interaction with its 3'-UTR.

Table 5. 3'-UTR Cloning Primers

3'-UTR	Forward primer (5'- to 3')	Reverse primer (5'- to 3')
Hsp70.3	GGTGGATTAGAGGCCTCTG CTGGCTCTCCCGGTGCT	GGTGGTACCCGGCCGGCCT GTTGTCAGTTCTCACCT
Hsp70.1	GGTGGATTAGAGGCCTCTG CTGGCTCTCCCGGTGTG	GGTCCTGAGTGGCCGGCCC AGGAACCACATGGTGGCT
Hsp90aa1	AAGATCGCCGTGTAGGTCA CCAGAACTATGTGTTTGCTT ACCTT	GTCTGCTCGAAGCGGGTGT GCTGGGGAAGAGAGGATGT C
Dnajb4	AAGATCGCCGTGTAGGATG AGAAGAACCTTGCTATCCA TAGTTTGA	GTCTGCTCGAAGCGGCTGG GCACAGCTCCACGGTG
PDCD4	AAGATCGCCGTGTAGGCAC AGCAACTCTTACAGTCTTAG G	GTCTGCTCGAAGCGGAGCA GGTTCTGTCTCAAGAAGCA
FasL	AAGATCGCCGTGTAGAAGA AAAAGCATTTTAAAATGAT	GTCTGCTCGAAGCGGGAGG AAAGAAACTAGACAGAAGA

	CTACTATTCTTTATCATGGGCA	GAGGGGAAA

Dnaja1 has a very long 3'-UTR (>2000 bp) that proved difficult to clone into the pGL4 reporter plasmid. Therefore, we outsourced the purchase of this reagent from GeneCopoeia.

Transfection and Luciferase Assay

H9c2 cells were plated at a density of $1x10^4$ cells/well in 96-well plates. The next day, they were incubated in Opti-MEM (Thermo Fisher Scientific, Waltham) without FBS (serum starved) for 1 hour and then co-transfected with plasmid DNA and RNAi (miRNA mimics, negative control or positive control siRNA) using Lipofectamine 2000 (Thermo Fisher Scientific, Waltham). RNAi and lipofectamine were complexed using the recommended ratio of 1 µl lipofectamine per 20 pmol RNAi. When dose curves of miRNA were being performed, the total molarity was held constant, with negative control siRNA used to compensate. DNA was complexed separately from the RNA, at the recommended ratio of 2.5 µl lipofectamine per µg of DNA. The final volumes of complexed RNA and DNA were 25 µl each per well. The Opti-MEM used to starve the cells was removed, the RNA and DNA were combined, and 50 µl were added to each well. The transfection was carried out for 4 hours, followed by addition of 50 µl per well of DMEM containing 20% FBS for a final FBS concentration of 10%, and recovered overnight. The next day, 100 µl per well of Steady Glo Luciferase Reagent (Promega) were added, the plate was incubated at room temperature for 5 minutes to ensure complete lysis of cells. The contents of each well were transferred to corresponding wells of an opaque white plate for reading of luminescence on the Cytation3.

RNA and miRNA-Sequencing

Sequencing was performed on two sets of samples, (1) IPC *vs.* sham mouse hearts; (2) HPC *vs.* normoxic HL-1 cells and their exosomes as well as wildtype MSCs and their exosomes. For the first set, three hours after sham or IPC, mouse hearts were removed and the ischemic zone dissected as described previously[38]. Total RNA was isolated by phase separation, and purity and concentration determined by absorbance readings at 260 and 280 nm using a NanoDrop. For the second set of samples, HL-1 cells underwent HPC and were allowed to recover for 18h. RNA was isolated by phase separation from the cells and exosomes pelleted from the conditioned media. To increase the yield of RNA from the exosomes, 5 µl Glyco Blue (Thermo Fisher Scientific, Waltham) were added during the isopropanol precipitation step. RNA was also isolated from untreated wildtype MSC and their exosomes for sequencing.

The first two sets of samples were provided to the University of Cincinnati genomics core facility for miRNA-Seq and RNA-Seq. Quality control was performed to ensure RNA integrity and presence of small RNA by Agilent Bioanalyzer, and cDNA libraries were prepared using the NEBNext Small RNA Library Prep Set for Illumina. Then the libraries were analyzed on an Illumina HiSeq 2000 instrument to yield 50 base pair single end reads.

Bioinformatic Analysis of Sequencing Data

Raw data from the Illumina in the FASTQ file format was uploaded to Galaxy, an open source web-based platform for data-intensive biomedical research, and "groomed" to prepare it for downstream analysis. Quality control was performed using the application FastQC. This program provides the quality of the data for each

nucleotide read in the form of a Phred quality score. Because this score is logarithmically related to the probability of an error, quality scores over 30 are predicted to result in 99.9% accuracy of reads (the probability of an incorrect base call is 1 in 1000). An example from our data is shown in Figure 7.

Figure 7: Example of Phred Quality Score Data

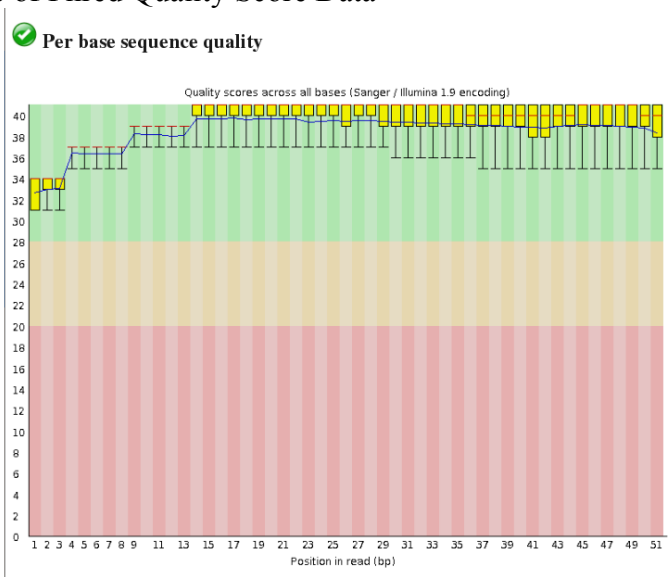

After ensuring that the quality scores were consistently over 30, adapters were trimmed and the resulting sequencing reads were aligned to the mouse genome (build GRCm38) to determine their identity using TopHat2, which has the advantage of being able to map reads that span exon junctions[215], producing a BAM file containing the read alignments which mapped to genes. Reads were counted using the Python package HTSeq, then analyzed by making a series of pairwise comparisons between the groups using a Bioconductor package called DESeq[216]. For the mRNA experiments, information about the function of the genes was provided by GO term analysis.

For miRNA, quality control and grooming were carried out as for the mRNA files. Then they were aligned to the mouse genome using BowTie (v. 0.12.8) and analyzed by DESeq.

***In silico* Targeting Hypothesis Generation Using Cytoscape**

MicroRNAs that are predicted to target each protein of interest were identified using the MiRanda targeting algorithm[217] on microRNA.org[74]. Stringent parameters were used for the prediction, such that only conserved sites with good mirSVR scores (a model to predict efficiency of sites[218]) were included. Noting that some microRNAs had common targets, we visualized the network as follows using Cytoscape, an open-source biological network visualization program. For the heat shock proteins, each microRNA was entered into an Excel spreadsheet formatted with the microRNAs in one column and gene targets in the next column. In Cytoscape, the "Import Network From File" dialog was opened and this Excel file was chosen. The microRNA (column 1) was chosen as the "source," the interaction was left as Default, and the protein (column 2) was chosen as the "target."

The resulting network showed all of the heat shock proteins and 414 miRNAs predicted to target them. Because we are interested in miRNAs that act as nodes in a network, regulating numerous genes, we eliminated miRNAs that only targeted 1 or 2 genes, and kept those that targeted 3 or more. Of these, 3 miRs were chosen for follow-up based on reasonable expression levels in the heart and HL-1 cells (some were expressed very low or not at all), as well as a decrease in the expression level being noted after protective stimuli such as IPC[83, 219, 220] or HPC (herein).

Statistical Analysis

For normally distributed data with equal variance, comparisons between two conditions were made using student's T test, and between 3 or more conditions using the ANOVA test with Bonferroni's correction for multiple comparisons. Group size was determined by performing power analysis with a desired β of >0.8. Differential expression in the sequencing data was analyzed by determining the dispersion and the mean of each gene's reads within groups and between groups in the application DESeq.

EXPERIMENTAL LIMITATIONS

Luciferase Assay Limitations

Luciferase reporters expressing the full length 3'-UTR are useful for determining whether the miRNA binding site is accessible within the 3D structure formed by the RNA of the 3'-UTR, but because the sequence for luciferase is substituted for the actual gene, the structure of the mRNA may be different than it is for the endogenous transcript. Also, expression of the reporter is driven by a constitutively active promoter, leading to production of a very high number of copies of the mRNA/3'-UTR. In such cases, the machinery responsible for splicing and alternative polyadenylation which can occur in the 3'-UTR, affecting the presence of miRNA binding sites, could be overwhelmed, and the 3'-UTR may not be processed the same as it would be with endogenous levels of gene expression. Furthermore, the number of copies of the miRNA which are transfected is also extremely high, which could affect how endogenous miRNAs are loaded within RISC complexes. As such, reporter assays can answer the question of whether it is possible for a miRNA to repress a gene through its 3'-UTR, but whether the endogenous transcript is a true target must be determined empirically.

Limitations of Mimic Transfection and miRNA Knockdown Assays

After transfection, the change in miRNA level is much greater in magnitude (as measured by real time PCR) than that which occurs endogenously in response to cardioprotective stimuli. The results can also be affected by transfection efficiency. Furthermore, the transfection process can affect cell viability, and recovery from transfection could be a stressor that induces heat shock protein expression. This is why we always used a negative control siRNA rather than non-transfected cells as controls. However, to get around these concerns, stable cell lines would need to be generated.

Imaging-based Viability Assay Limitations

With the overnight exosome pre-treatment *in vitro*, we often noted a mild proliferative effect on the H9c2 cells. This was the rationale for counting viable cells immediately before and after OGD. If they had been only counted after OGD, the greater number present would have led to an overestimation of the protective effect because the greater number present before OGD wouldn't be taken into account. Instead we used the viable count before and after to calculate the percent survival, and found that a smaller percentage were lost after the WT exosome treatment. This conclusion is based on the assumption that under conditions of oxygen and glucose withdrawal, the H9c2 cells no longer divide. It is possible that the same fraction of cells was killed by the OGD challenge, and what we have termed a protective effect here is actually the result of increased cell division, which compensated for those lost. Without experiments that used proliferation inhibitors in the media, or pulse-chase experiments to label newly synthesized DNA, it is not possible to discern between the two.

CHAPTER 3

RESULTS

THE ROLE OF MICRORNA IN ISCHEMIC PRECONDITIONING

Preconditioning and I/R Injury *In Vivo* and *In Vitro*

Late ischemic preconditioning results in reduction of infarct size from 40.6% in sham controls to 21.4% of the area at risk[38]. Previous work from the Jones lab established a role for miR-711 and miR-378* acting in conjunction with alternative polyadenylation to regulate the expression of Hsp70.3, a cardioprotective gene that is required for late IPC[38, 87]. Using Hl-1 cells, we established *in vitro* models of hypoxic pre-conditioning (HPC) and simulated ischemia/reperfusion injury (simI/R) in order to test the roles of other miRNAs and heat shock protein family members. When HPC was performed 24h prior to simI/R, cell death was dramatically reduced. Furthermore, the amount of lactate dehydrogenase (LDH) released into the media was decreased (Figure 8).

Figure 8. Simulated Ischemia/Reperfusion Injury and Hypoxic Preconditioning

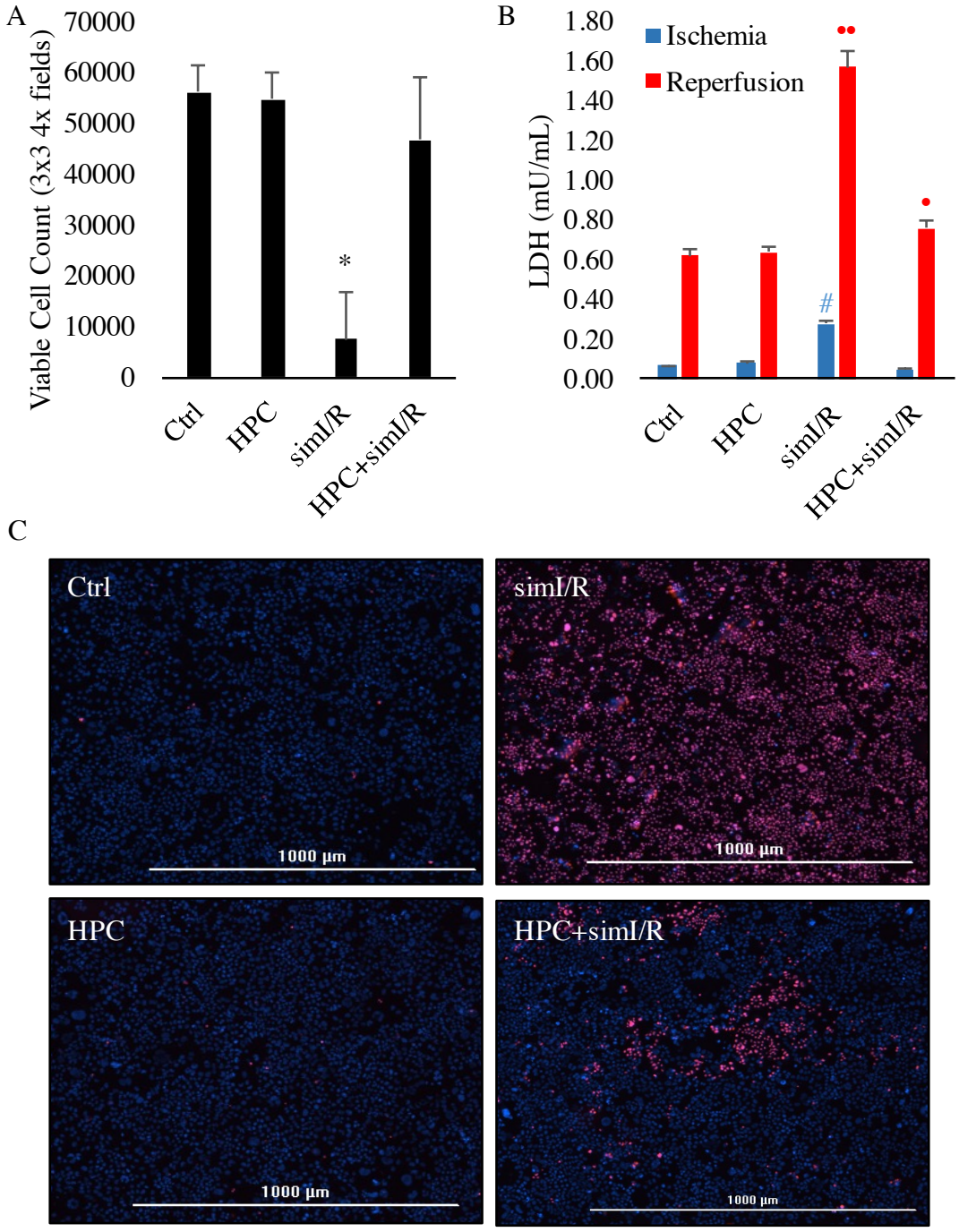

A. Confluent 6-well plates of HL-1 cells were preconditioned by 1 hour of hypoxia in ischemia mimetic solution and then returned to normal culture conditions overnight. The next day they were subjected to simI/R by exposure to hypoxia for 2.5 hours followed by 1h reoxygenation. All and dead cells were then counted by staining with Hoechst and PI, respectively, to obtain the viable cell count (n=6). *$P<0.001$ *vs*. Ctrl. B. Cells were treated as in part A and culture media from ischemia and reperfusion steps

was assayed for LDH released from cells (n=3). #*P*<0.001 *vs.* Ischemia Ctrl, •*P*=0.029 *vs.* Ctrl, ••*P*<0.001 *vs.* Reperfusion Ctrl. C. Representative 4x images used to calculate the values in A. Hoechst labels all nuclei blue, while PI labels nuclei of dead cells red. Double-labeled dead cells appear purple.

Gene Expression after IPC

Previous work in the Jones lab established a profile of genes that are regulated 3h after IPC through microarray analysis. We built upon this data set by performing deep sequencing for mRNA and miRNA on new sham and IPC heart tissue samples, also collected at 3h post IPC (n=2/group). Table 6 shows a comparison of the fold changes detected in the microarray data and the sequencing data for those genes that were significantly differentially expressed in both assays. In general, the fold changes are in agreement in direction (i.e., expression increases or decreases in both) but the magnitude was greater in the RNA-Seq data. Seven out of the 61 genes were heat shock protein family members, including Hsp40 (*Dnaj* family members), Hsp70, Hsp90 (*Hsp90aa1*), and chaperonin (*Hspd1*), underscoring the importance of this group of proteins in IPC. For the complete list of significant mRNA changes in the sham *vs.* IPC sequencing data, see Appendix A.

Table 6. Comparison of Microarray and Sequencing Data on Mouse Heart Tissue 3h Post-IPC

Symbol	Gene Name	Array	RNA-Seq
Adamts1	a disintegrin-like and metallopeptidase (reprolysin type) with thrombospondin type 1 motif, 1	2.83	4.10
Akap2	A kinase (PRKA) anchor protein 2	1.55	1.92
Atf3	activating transcription factor 3	3.37	17.08
Bag3	Bcl2-associated athanogene 3	1.38	4.09
Cnksr1	connector enhancer of kinase suppressor of Ras 1	1.33	2.82
Cnksr3	Cnksr family member 3	1.43	1.99
Ctps	cytidine 5'-triphosphate synthase	1.28	1.75

Dnaja1	*DnaJ (Hsp40) homolog, subfamily A, member 1*	*2.48*	*7.09*
Dnaja4	*DnaJ (Hsp40) homolog, subfamily A, member 4*	*1.39*	*2.32*
Dnajb1	*DnaJ (Hsp40) homolog, subfamily B, member 1*	*2.1*	*8.38*
Dnajb4	*DnaJ (Hsp40) homolog, subfamily B, member 4*	*2.72*	*3.50*
Ell2	elongation factor RNA polymerase II 2	2.2	3.79
Entpd5	ectonucleoside triphosphate diphosphohydrolase 5	-1.77	-1.74
Errfi1	ERBB receptor feedback inhibitor 1	1.79	1.84
Fgl2	fibrinogen-like protein 2	2.26	3.46
Frat2	frequently rearranged in advanced T-cell lymphomas 2	2.78	5.23
Frmd6	FERM domain containing 6	1.52	2.45
Gadd45b	growth arrest and DNA-damage-inducible 45 beta	-1.35	2.09
Gp49a	glycoprotein 49 A	1.49	1.88
Hmox1	heme oxygenase (decycling) 1	1.77	3.09
Hsp90aa1	*heat shock protein 90kDa alpha (cytosolic), class A member 1*	*3.08*	*9.14*
Hspa1b	*heat shock protein 1B*	*8.53*	*690.66*
Hspd1	*heat shock protein 1 (chaperonin)*	*1.75*	*1.67*
Il1r1	interleukin 1 receptor, type I	1.4	1.68
Il1r2	interleukin 1 receptor, type II	1.46	3.66
Il4ra	interleukin 4 receptor, alpha	1.45	2.04
Kcnb1	potassium voltage gated channel, Shab-related subfamily, member 1	1.34	-1.81
Kcnq1	potassium voltage-gated channel, subfamily Q, member 1	-1.37	-1.72
Kctd6	potassium channel tetramerisation domain containing 6	1.38	2.74
Klf6	Kruppel-like factor 6	1.39	1.94
Ky	kyphoscoliosis peptidase	-2.06	-2.40
Lilrb4	leukocyte immunoglobulin-like receptor, subfamily B, member 4	2.02	2.03
Maff	v-maf musculoaponeurotic fibrosarcoma oncogene family, protein F (avian)	1.35	3.01
Mum1l1	melanoma associated antigen (mutated) 1-like 1	2.65	5.92
Nfil3	nuclear factor, interleukin 3, regulated	1.62	2.00
Nle1	notchless homolog 1 (Drosophila)	2.31	4.47
Nt5e	5' nucleotidase, ecto	2.21	2.55
Nts	neurotensin	1.58	2.53
Odc1	ornithine decarboxylase, structural 1	1.88	1.84
Paqr7	progestin and adipoQ receptor family member VII	-1.53	-2.03

Pde4b	phosphodiesterase 4B, cAMP specific	1.66	2.24
Pgm1	phosphoglucomutase 1	1.4	2.11
Phlda1	pleckstrin homology-like domain, family A, member 1	1.76	6.16
Ptx3	pentraxin related gene	2.36	5.68
Rassf1	Ras association (RalGDS/AF-6) domain family 1	1.25	2.39
S100a8	S100 calcium binding protein A8 (calgranulin A)	1.43	4.40
Sat1	spermidine/spermine N1-acetyl transferase 1	1.45	1.93
Sbno2	strawberry notch homolog 2 (Drosophila)	1.77	3.90
Sema6d	sema domain, transmembrane domain (TM), and cytoplasmic domain, (semaphorin) 6D	1.35	1.90
Serpinh1	serine (or cysteine) peptidase inhibitor, clade H, member 1	1.78	4.66
Slc20a1	solute carrier family 20, member 1	1.32	1.68
Slc35b2	solute carrier family 35, member B2	-1.39	-1.84
Smad1	MAD homolog 1 (Drosophila)	1.42	1.85
Sphk1	sphingosine kinase 1	2.61	12.52
Stip1	stress-induced phosphoprotein 1	1.47	2.80
Tcta	T-cell leukemia translocation altered gene	-1.83	-1.67
Tec	cytoplasmic tyrosine kinase, Dscr28C related (Drosophila)	1.49	2.68
Thbd	thrombomodulin	1.45	1.99
Tpm3	tropomyosin 3, gamma	1.44	1.80
Txnrd1	thioredoxin reductase 1	1.42	2.01
Unc45b	unc-45 homolog B (C. elegans)	1.34	2.55

Fold changes between sham and IPC. Array data are a pooled n of 3, while sequencing data n=2 mice/group. The above genes are those that were significantly different in both assays. Bold-faced genes are heat shock protein family members.

Gene ontology analysis of the upregulated genes suggested a number of regulatory themes, many of which are known to be important contributors to ischemic preconditioning (Table 7). For example, sets of genes that are regulated by NF-κB and heat shock factors 1 and 2 are increased; these transcription factors are well known to mediate protective gene expression in IPC[37, 38, 70, 221, 222]. Additionally, genes related to nitric oxide biosynthesis are upregulated; NO is well known to be an important cardioprotective factor[27, 70, 223, 224]. There was also enrichment of general categories such

as response to wounding, and inflammation/immune response. Many of the upregulated gene sets were associated with GO terms related to chaperone function, such as "protein refolding" and "response to heat" which is consistent with literature published about IPC since shortly after its discovery[33, 63, 64].

Table 7. Functional Enrichment from RNA-Seq Analysis

Description	**#Genes**	**P Value**
Genes upregulated by NF-kappa B (Human)	97	1.38E-29
protein refolding	11	8.79E-28
response to unfolded protein	50	1.41E-25
positive regulation of protein import into nucleus, translocation	12	3.99E-24
Genes with promoter regions [-2kb, 2kb] around transcription start site containing the motif NGAANNWTCK which matches annotation for HSF2: heat shock transcription factor 2	201	5.15E-23
positive regulation of nitric oxide biosynthetic process	29	2.26E-23
Up-regulated at any timepoint following TNFa treatment, only with functional NF-κB (Human)	17	1.34E-22
chaperone mediated protein folding requiring cofactor	14	1.70E-22
immune response	532	6.77E-22
chaperone-mediated protein folding	22	2.62E-21
Genes with promoter regions [-2kb, 2kb] around transcription start site containing the motif RGAANNTTC which matches annotation for HSF1: heat shock transcription factor 1	375	8.63E-21
response to wounding	505	7.40E-21
inflammatory response	316	7.30E-20
regulation of cytokine production	287	4.77E-18
regulation of nitric oxide biosynthetic process	37	9.29E-18
'de novo' posttranslational protein folding	17	1.37E-17
nitric oxide biosynthetic process	44	1.75E-15
nitric oxide metabolic process	48	5.28E-15
unfolded protein binding	80	6.91E-15
Protein processing in endoplasmic reticulum	159	1.48E-14
response to heat	50	2.53E-13
intracellular protein kinase cascade	633	4.84E-13

The 20 most significantly enriched gene ontology (GO) terms are shown. The heat shock response and protein folding constitute major aspects of the heart's response to IPC.

Based on the list of heat shock protein family members (HPSs) that were significantly increased in Table 6, we validated their expression in the heart after IPC through qPCR (Figure 9) and Western blot (Figure 10). The pattern of expression of the genes correlated closely with that of the sequencing data, with low Hsp70 expression at baseline that was highly inducible after IPC, while comparatively higher expression of *Hsp90aa1* and *Dnajb4* were observed at baseline, which also increased after IPC. Western blot showed that 6h after IPC, expression of Dnaja1 and Dnajb4 were increased by 4.9- and 6.5-fold respectively, while Hsp70 (antibodies currently available cannot discern between Hsp70.1 and Hsp70.3) increased by 12.5-fold. Hsp90 showed a trend towards an increase which did not reach statistical significance (Figure 10). By 24h after IPC, Hsp70 was the only protein that remained elevated.

Figure 9. Validation of HSP RNA-Seq Data by qPCR

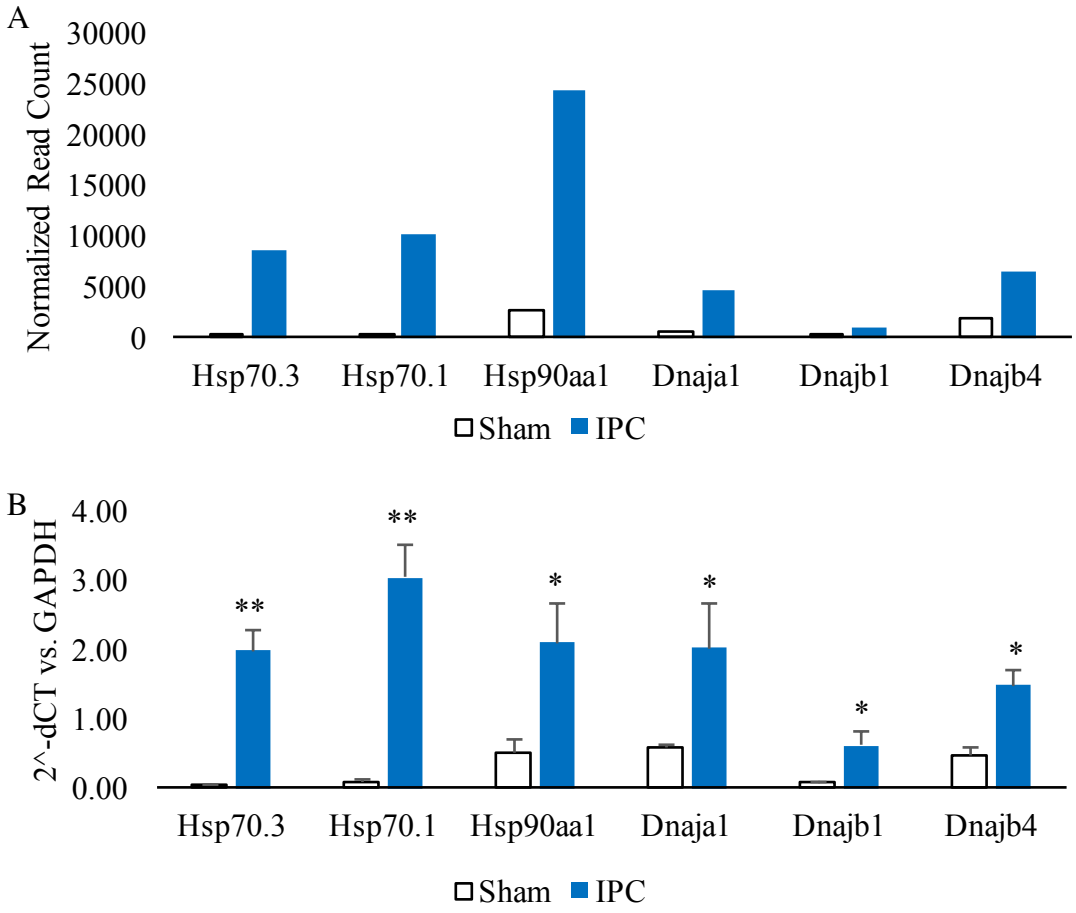

A. The average read count of the HSPs from Table 6 chosen for follow-up, in sham and IPC samples. B. Expression of the HSPs normalized to GAPDH, n=4-5 mice/group. *P<0.05 *vs*. sham **P <0.001 *vs*. sham by t-test.

Figure 10. HSP Protein Levels 6 and 24h after IPC

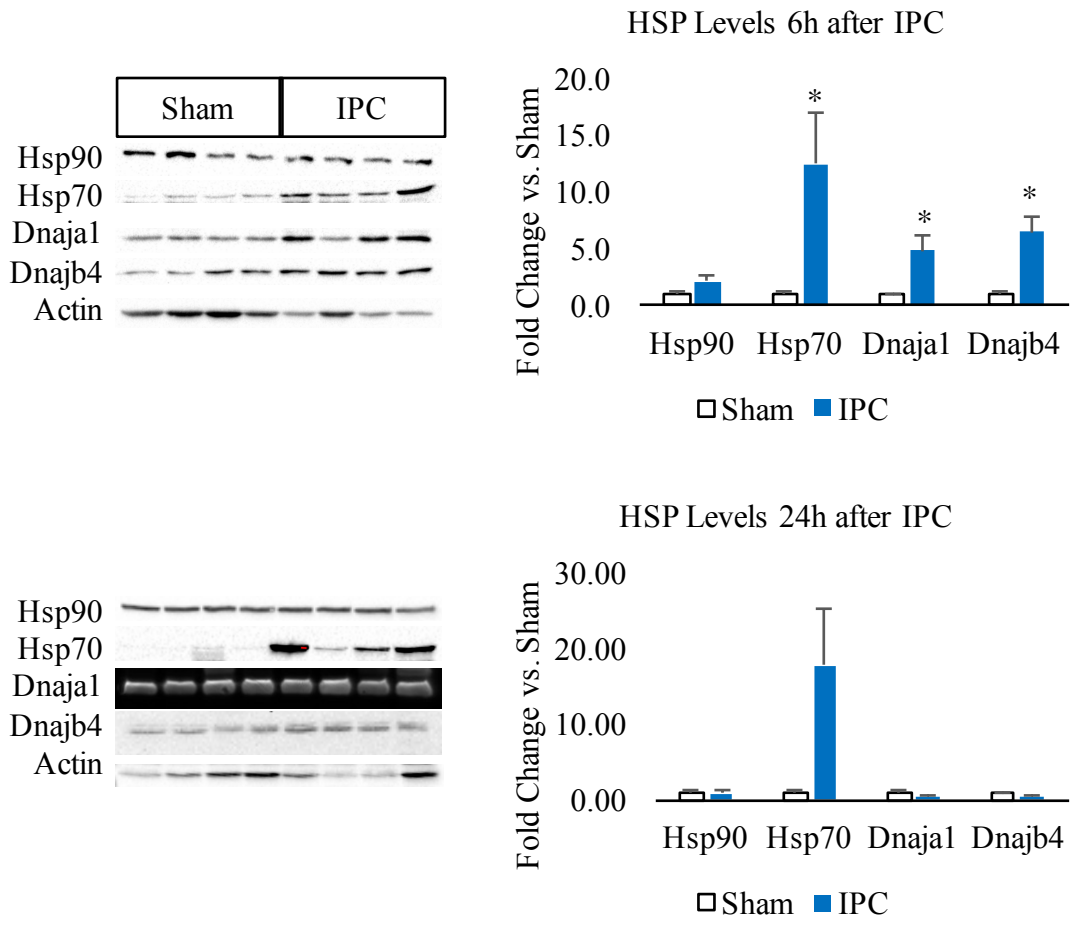

Protein was extracted in RIPA buffer from the ischemic zone of the LV 6 and 24h after IPC (n=4 mice/group). Ten μg of protein were analyzed by Western blot for the above proteins. Band intensities were normalized to Actin and are displayed as the fold change *vs.* Sham. *$P<0.05$ *vs.* Sham by t-test.

Comparison of Gene Expression After IPC and HPC

HL-1 cells generally express a similar profile of heat shock protein family members to that of heart tissue; Hsp90 was the highest, followed by Hsp40, and Hsp70 as the lowest expressed (Figure 11A). Preconditioning in HL-1 cells has been reported to be similar to IPC in the heart with regard to the role of extracellular adenosine interacting with the adenosine receptor, triggering the activation of PKCε[225]. Because

IPC and HPC are both induced by brief periods of hypoxia and nutrient withdrawal, and both reduced cardiomyocyte cell death at 24h, we hypothesized that they may have overlapping gene regulatory mechanisms. However, when RNA from HPC HL-1 cells was analyzed by RNA-Seq, we did not observe comparable changes in any of the IPC-regulated genes (see Table 11, p106). Realtime qPCR performed on HL-1 samples 3h after HPC showed very mild increases in HSP levels (Figure 11B). Furthermore, heat shock treatment, which induces the expression of heat shock proteins (Figure 11C), did not significantly decrease cell death from simI/R in either the HL-1 cells (Figure 12) or H9c2 cells (data not shown). The effect of HPC on HSP expression *in vitro* is much less than that of IPC *in vivo*. Because the HSPs were expressed to a similar degree in HL-1 cells and heart tissue, (Figure 11A) we decided to use the HL-1 cell line for testing miRNA regulation of HSP expression with and without heat shock.

Figure 11. Heat Shock Protein Expression in Heart Tissue and HL-1 Cells

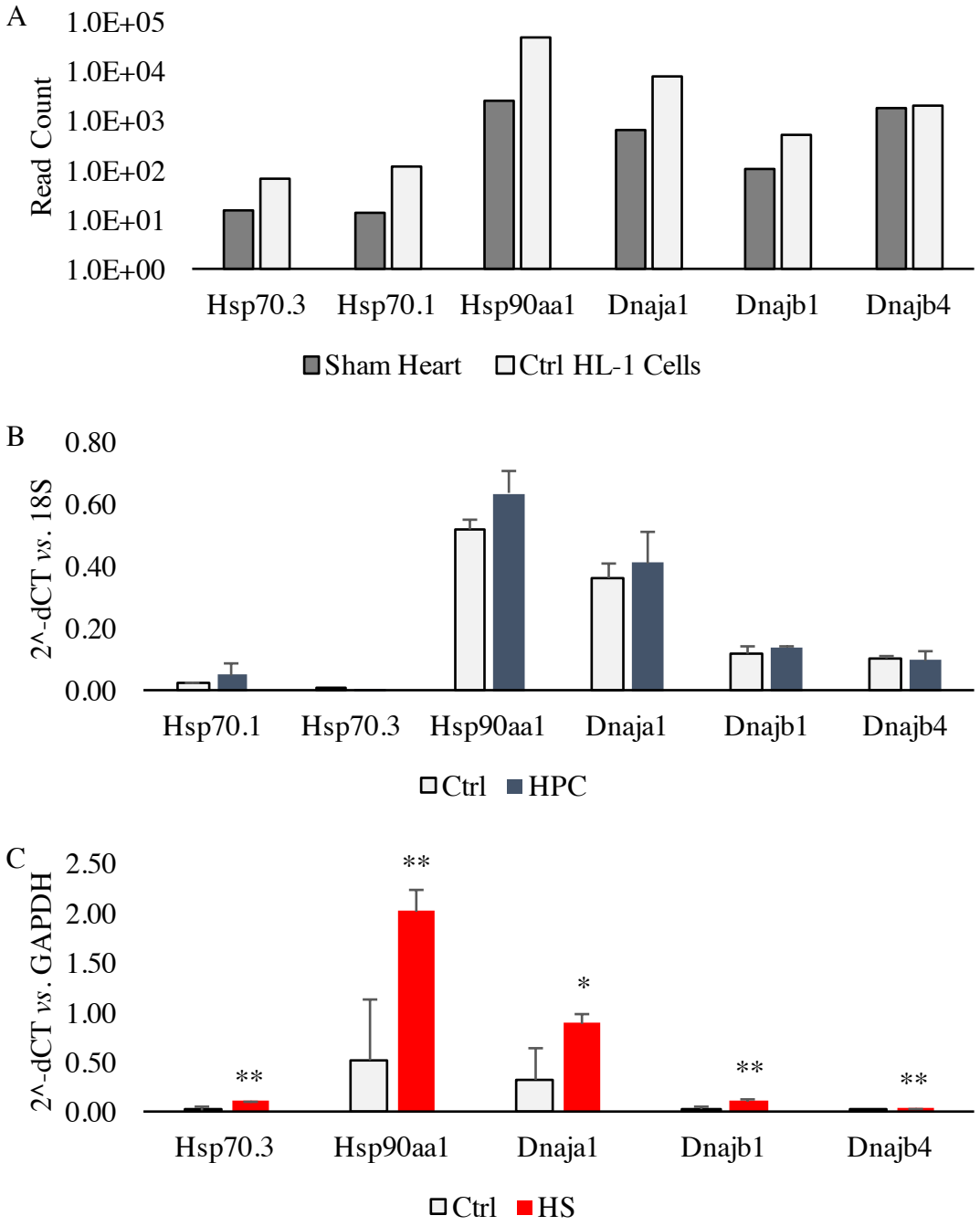

A. Sequencing data showed that Hsp70, Hsp90, and Hsp40 family members are expressed in a similar pattern in control heart tissue and HL-1 cells. B. RNA was extracted from HL-1 cells 3h post-HPC and analyzed by qPCR with 18S as the housekeeping gene (n=3). C. RNA was extracted from HL-1 cells 3h post-heat shock (HS) and analyzed by qPCR with GAPDH as the housekeeping gene (n=3). *P=0.005, ***P*<0.001 *vs.* Ctrl.

Figure 12. Heat Shock Does Not Protect HL-1 Cells from SimI/R

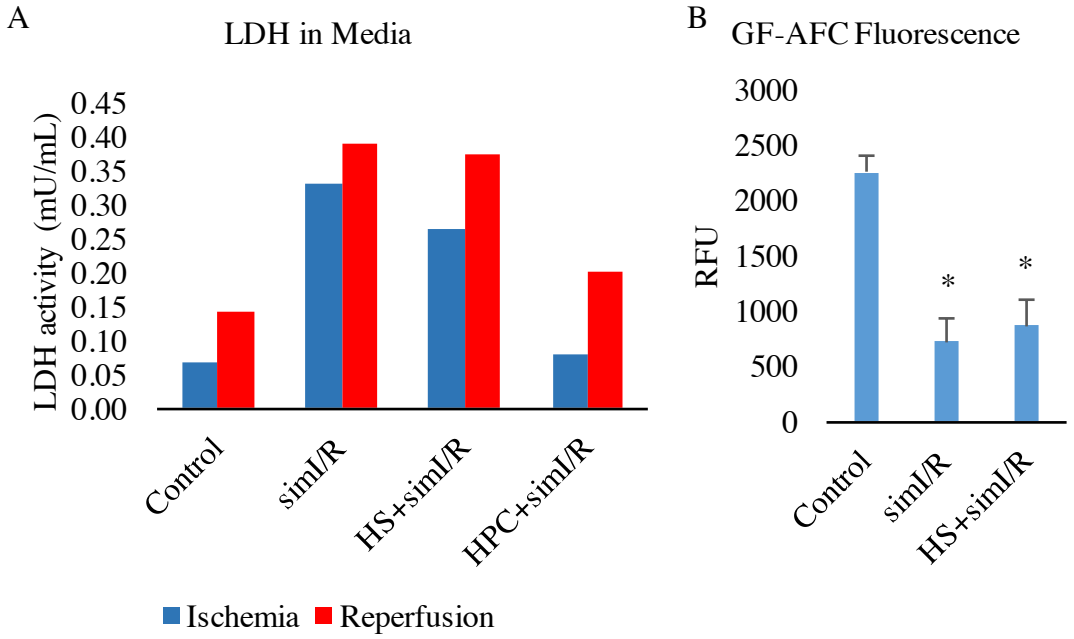

A. HL-1 cells were pre-treated with a 1h heat shock (HS) or 1h HPC and allowed to recover 18h. Then they were subjected to simI/R which consisted of 3h hypoxia and 18h reoxygenation. LDH was assayed in media samples collected after simulated ischemia (blue) and reperfusion (red). B. Cells were treated as in (A) and viability was assayed by measuring GF-AFC cleavage which produces a fluorescent protein, indicative of metabolic activity (n=18). Pairwise comparisons were made of average fluorescence in all conditions by one-way ANOVA with Bonferroni's correction, *P<0.001 *vs*. Control; simI/R *vs*. HS+simI/R, P not significant.

Identification of miRNAs Acting as Nodes in a Network of Heat Shock Protein Expression

Using *in silico* miRNA targeting analysis, we identified all of the miRNAs that are predicted to target each heat shock protein family member with stringent prediction criteria, and eliminated those that target only 1 or 2 of the heat shock protein family members, in order to select for those that are the most interconnected. We then removed those that were expressed below 32 reads, because they are likely to be artifacts or not biologically relevant. Starting with 414 miRNAs, these filtering steps reduced the

number to 15 (Figure 13). Next we looked to the sequencing data and previously performed miRNA PCR array data in order to identify miRNAs which target numerous HSP family members and are decreased in expression by protective stimuli (IPC and/or HPC). Table 8 shows the combination of this data.

The miRNAs selected based on these criteria were miR-148a and b, miR-30b, and let-7a*. The accession numbers and sequences of the miRNAs are shown below.

mmu-miR-148a-3p	MIMAT0000516	UCAGUGCACUACAGAACUUUGU
mmu-miR-148b-3p	MIMAT0000580	UCAGUGCAUCACAGAACUUUGU
mmu-miR-30b-5p	MIMAT0000130	UGUAAACAUCCUACACUCAGCU
mmu-let-7a-1-3p	MIMAT0004620	CUAUACAAUCUACUGUCUUUCC

miR-148a and b were predicted to target both Hsp70's and Dnaja1, miR-30b was predicted to target both Hsp40's and Hsp90, and let-7a* was predicted to target both Hsp40's and Hsp70.1. In order to validate these targeting predictions, we performed luciferase reporter assays as previously described[87].

Figure 13. Generation of miRNA-Heat Shock Protein Targeting Network

A

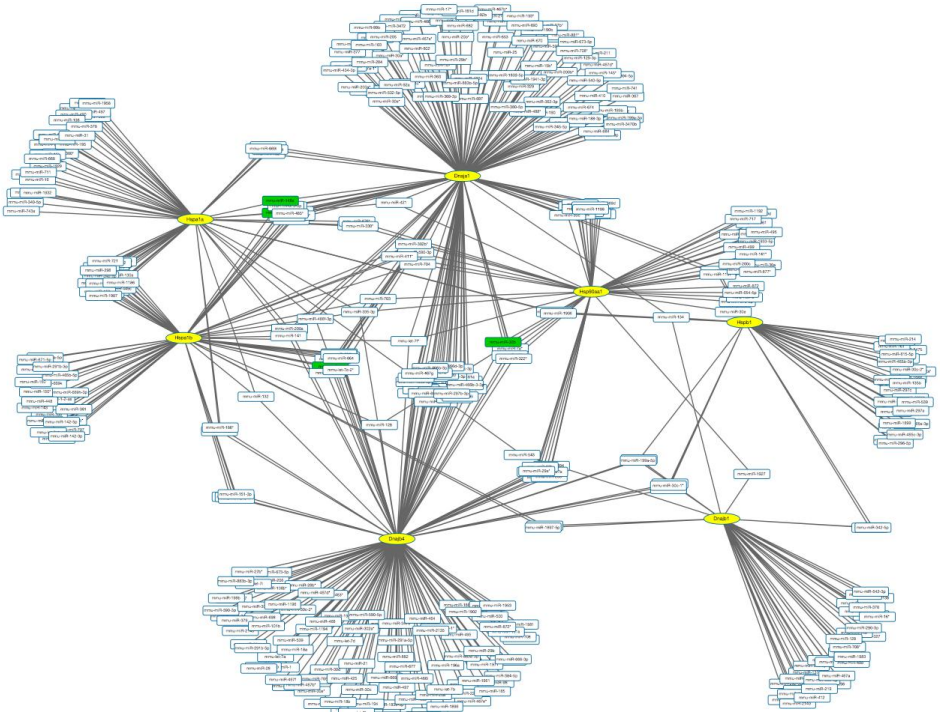

B

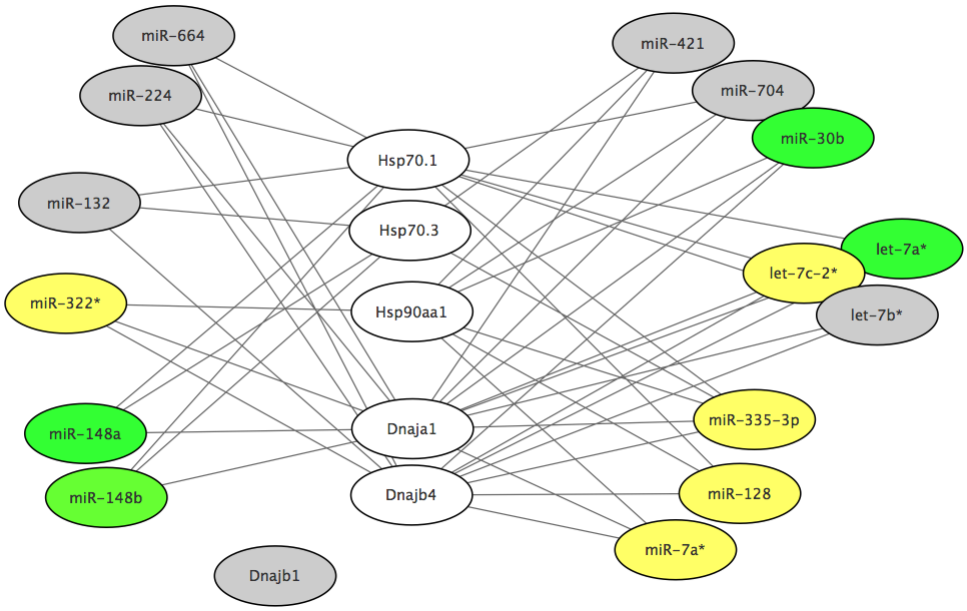

A. All miRNAs targeting Hsp70, Hsp90, and Hsp40 family members are shown. B. miRNAs that targeted only 1 or 2 HSPs (shown in white ovals, middle) were eliminated, resulting in 29 miRNAs remaining. miRNAs were then removed if they had less than 32 reads to remove potential artifacts or very low-expression miRNAs. Gray circles indicate expression of 33 to 100 reads in heart tissue, and yellow color indicates expression greater than 100 reads but no decrease in response to IPC or HPC. Green

represents miRNAs expressed over 400 in the heart and HL-1 cells which do show decreases after IPC and/or HPC. Dnajb1 was removed from the network because there were no miRNAs left that target it once those that targeted only 1 or 2 HSPs were filtered.

Table 8. Expression Data for miRNAs That Target 3 or More Heat Shock Proteins

miR	HSPs targeted	Array fold change in IPC	Counts in heart		Countsl in HL-1	
			Sham	IPC	Ctrl	HPC
let-7a*	Hsp70.1, Dnaja1, Dnajb4	**-1.51**	409	522	**449**	**279**
let-7b*	Hsp70.1, Dnaja1, Dnajb4	1.18	60	68	14300	14300
let-7c-2*	Hsp70.1, Dnaja1, Dnajb4	1.05	126	161	227	155
miR-128a	Hsp70.1, Dnajb4, Hsp90aa1	-1.35	1605	1933	2238	2162
miR-132-3p	Hsp70.1, Dnajb4, Hsp70.3	1.09	44	55	65	90
miR-148a-3p	Hsp70.1, Dnaja1, Hsp70.3	**-1.44**	16000	17000	**18448**	**12732**
miR-148b-3p	Hsp70.1, Dnaja1, Hsp70.3	**-1.17**	**934**	**765**	**4082**	**2246**
miR-199a-5p	Hspb1, Dnajb1, Dnajb4	1.37	1018	985	4	59
miR-224-5p	Hsp70.1, Dnaja1, Dnajb4	-1.03	47	61	25	36
miR-30b-5p	Dnaja1, Dnajb4, Hsp90aa1	**-1.18**	**1484**	**1180**	**3659**	**3070**
miR-322* (322-3p)	Dnaja1, Dnajb4, Hsp90aa1	-1.05	382	401	2978	3703
miR-335-3p	Hsp70.1, Hsp70.3, Dnaja1, Dnajb4, Hsp90aa1	1.04	103	108	41	24
miR-421-3p	Dnaja1, Hsp70.3, Hsp90aa1	-1.06	9	12.5	75	72
miR-664-3p	Hsp70.1, Dnaja1, Dnajb4	?	39	59	31	31
miR-7a*	Dnaja1, Dnajb4, Hsp90aa1	-1.18	355	447	7	13

Data used to select the miRNAs to test came from a combination of previously performed array data and sequencing data, and was based on expression level in the heart. In instances where the protective stimulus caused a decrease detected in either the

array data and the sequencing data from IPC heart tissue or array data and the HPC HL-1 cells, the miRNA was considered for follow-up.

Luciferase Reporter Assays

Hsp70.1 and Hsp70.3 Hsp70.1 (*Hspa1b*) was a predicted target of miR-148a/b and let-7a*. By co-transfecting the Hsp70.1 reporter plasmid along with a dose curve of these miRNAs, we tested whether there was a decrease in luciferase activity 24h later, compared with a non-targeting siRNA control. We found that both miR-148a and b repressed luciferase activity dose dependently to a similar degree, by 53 and 54%, respectively, while let-7a* did not decrease luciferase activity even at the highest dose tested (Figure 14). Because miR-148a and b differ only by the rearrangement of two nucleotides in the out-seed region, they appear to be functionally redundant in binding to the 3'-UTR of Hsp70.1. Similar to Hsp70.1, we tested the Hsp70.3 (*Hspa1a*) 3'-UTR, which was predicted to be targeted by miR-148a/b. We observed a dose-dependent decrease with both miRNAs that was less in magnitude than that of Hsp70.1's 3'-UTR, reaching a maximal inhibition of 31% with 200 nM miR-148a.

Figure 14. Hsp70.1 and Hsp70.3 Regulation by miR-148a, miR-148b, and let-7a*

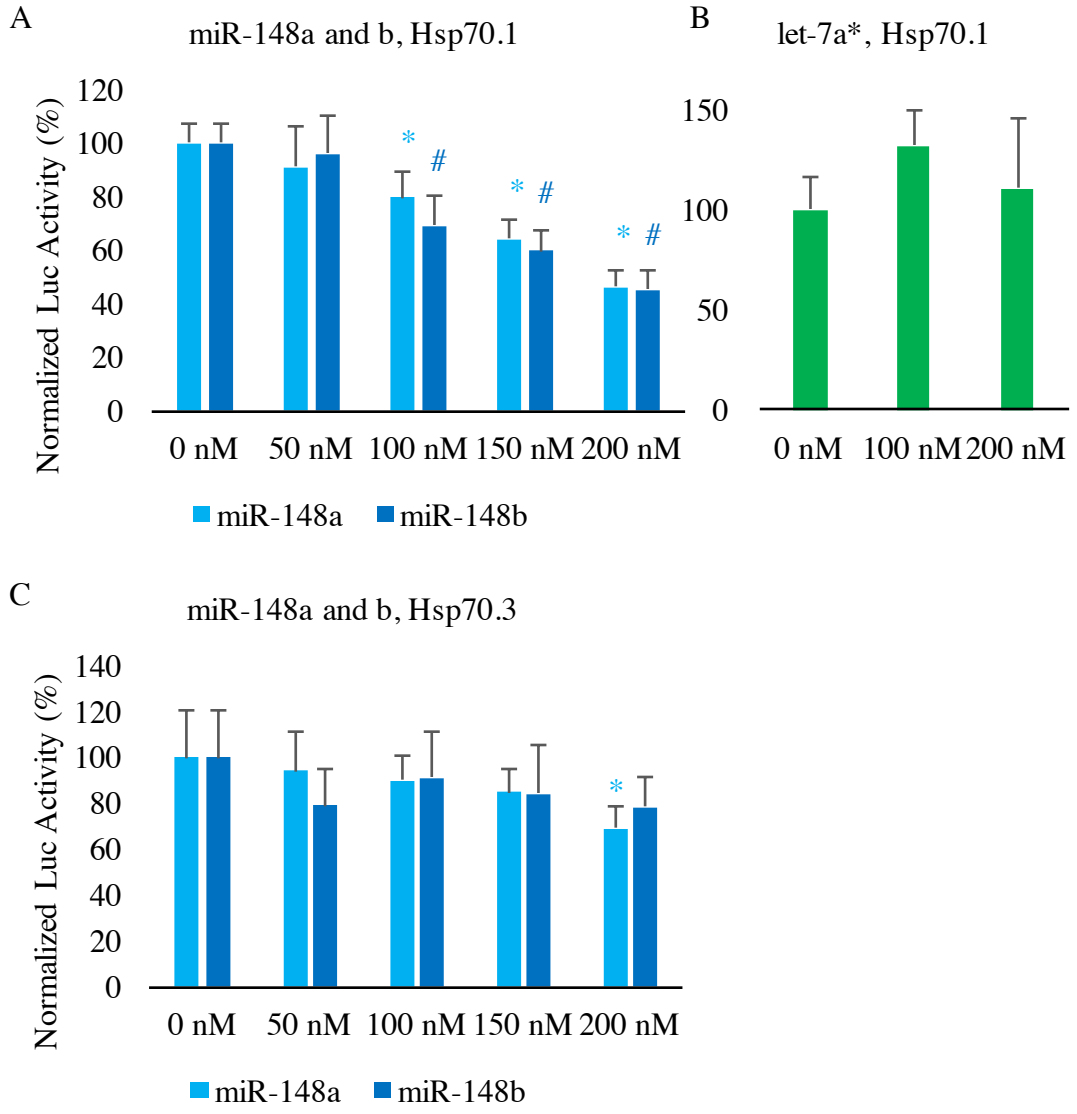

A. H9c2 cells were co-transfected with the Hsp70.1 reporter plasmid (30 ng/well) and a dose curve of miR-148a, 148b, or (B) let-7a*. Non-targeting siRNA served as the negative control (0 nM refers to this control with 0 specific targeting miRNAs, but same concentration of non-targeting siRNA) and was also used to maintain a constant total quantity of RNAi in each condition. Luciferase activity was measured 24h after transfection, normalized to 0 nM miRNA, and expressed as a percentage (n=10). *$P<0.001$ *vs.* 0 nM miR-148a. #$P<0.001$ *vs.* 0 nM miR-148b by one-way ANOVA. C. Cells were treated as in (A) with the Hsp70.3 plasmid (n=10). *$P<0.001$ *vs.* 0 nM miR-148a by one-way ANOVA.

Using luciferase assays, we also tested whether combinations of miRNAs would be more effective at repressing luciferase activity than a similar quantity of only one miRNA. In comparing the effects of miR-148a and miR-148b at the Hsp70.1 3'-UTR, we found that all of the combinations tested from 100% miR-148a to 100% miR-148b repressed luciferase activity to the same extent, which is consistent with both miRNAs targeting the same binding site in the 3'-UTR with equal efficacy (Figure 15A), in agreement with the results of Figure 14A. When we performed this experiment with two different miRNAs, miR-148a and miR-449c, which bind to different sites in Hsp70.1's 3'-UTR, we found that at 200 nM, miR-449c was more efficacious at reducing luciferase activity than 200 nM miR-148a (Figure 15B), reducing the activity to 38.6 *vs*. 58.6%. When the two miRNAs were combined at an equal ratio, we saw a trend towards a reduction in luciferase activity that was greater than either miRNA alone, at 29.8%.

Dnaja1 was the predicted target of all 4 miRNAs. However, at 200 nM of each of them, significant decreases in luciferase activity were not observed (Figure 16).

Dnajb4 was the predicted target of miR-30b and let-7a*. We observed a significant decrease in luciferase activity after transfection with let-7a* but not miR-30b (Figure 17).

Hsp90 (*Hsp90aa1*) was predicted to be targeted by miR-30b, and we did observe a significant decrease in luciferase activity at the highest dose tested (35% decrease *vs*. 0 nM, Figure 18).

Figure 15. Combinations of miRNAs Targeting the 3'-UTR of Hsp70.1

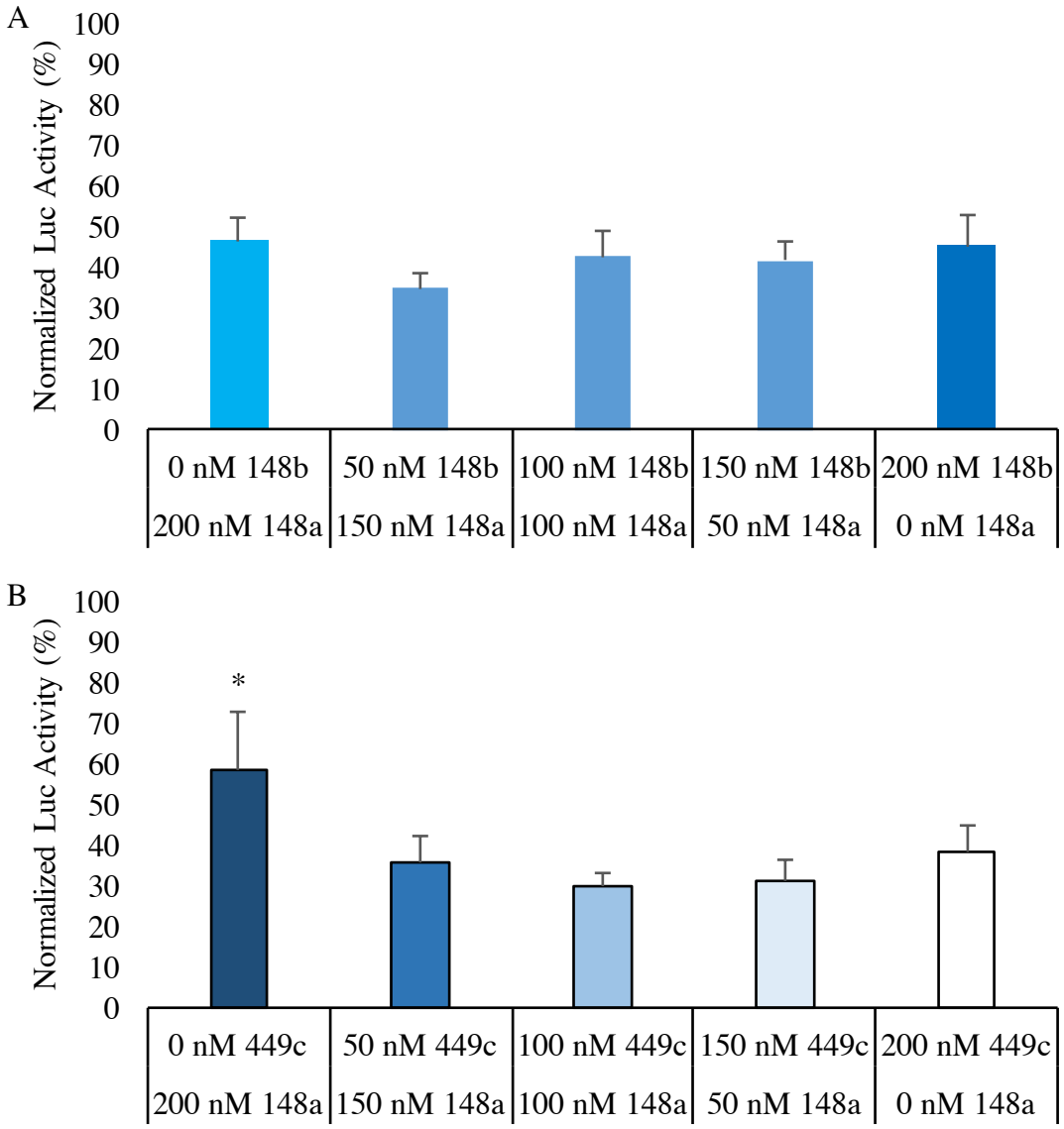

The Hsp70.1 reporter plasmid was transfected along with different ratios of miRNAs. Luc activity was assessed 24h later as in Figure 14. A. The dose of miR-148a and b was varied from 200 nM miR-148a to 200 nM miR-148b, while maintaining a constant level of total miRNA. Pairwise comparisons between all of the values were made using ANOVA with the Bonferroni post hoc test, but there were no significant differences. B. Different ratios of miR-148a and miR-449c were co-transfected, and luc activity values were again compared using ANOVA with the Bonferroni correction for multiple comparisons. The 200 nM miR-148a dose was significantly higher than all other conditions (*P<0.001); there were no other significant differences.

Figure 16. *Dnaja1* Regulation by miR-148a, miR-148b, miR-30b, and let-7a*

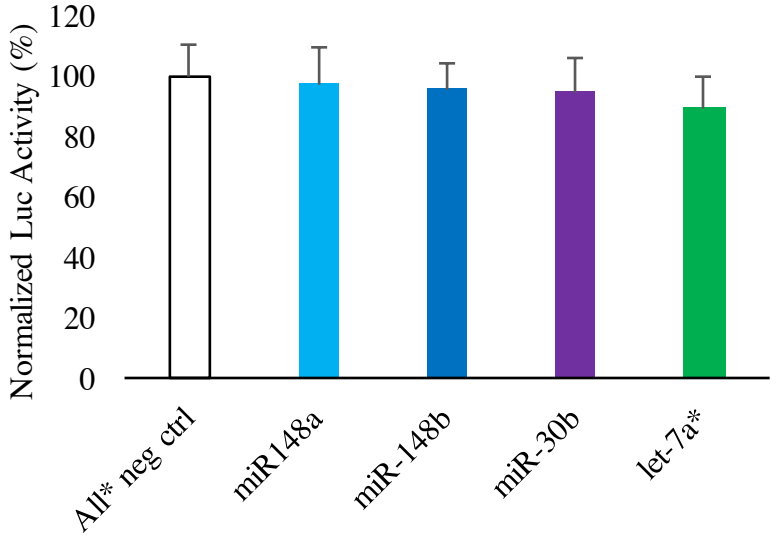

The *Dnaja1* reporter plasmid (30 ng/well) was co-transfected along with a dose curve of miR-148a, 148b, miR-30b, or let-7a*. Non-targeting siRNA served as the negative control (0 nM) and was also used to maintain a constant total quantity of RNAi in each condition. Luciferase activity was measured 24h after transfection, normalized to 0 nM miRNA, and expressed as a percentage (n=10).

Figure 17. *Dnajb4* Regulation by miR-30b and let-7a*

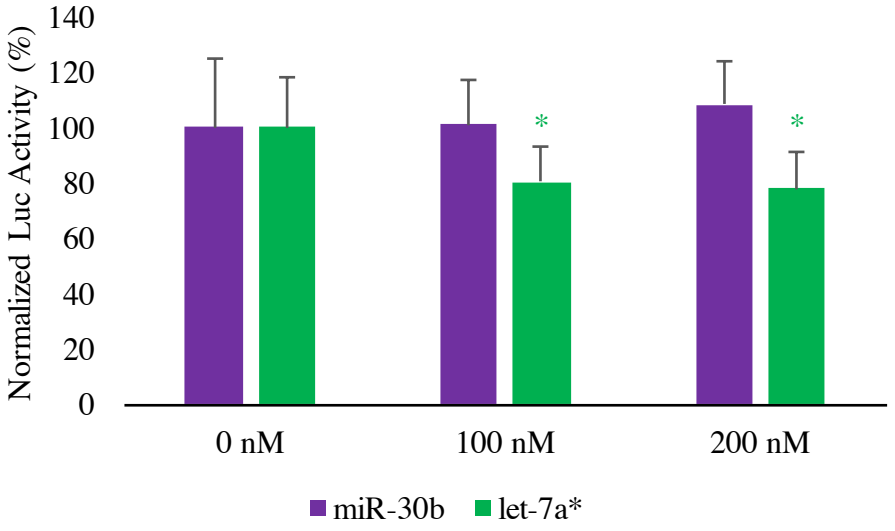

The Dnajb4 reporter plasmid was co-transfected along with a dose curve of miR-30b or let-7a* as described in Figure 14. Luciferase activity was measured 24h after transfection, normalized to 0 nM miRNA, and expressed as a percentage (n=10). *$P<0.05$ *vs*. 0 nM let-7a* by one-way ANOVA.

Figure 18. *Hsp90aa1* Regulation by miR-30b

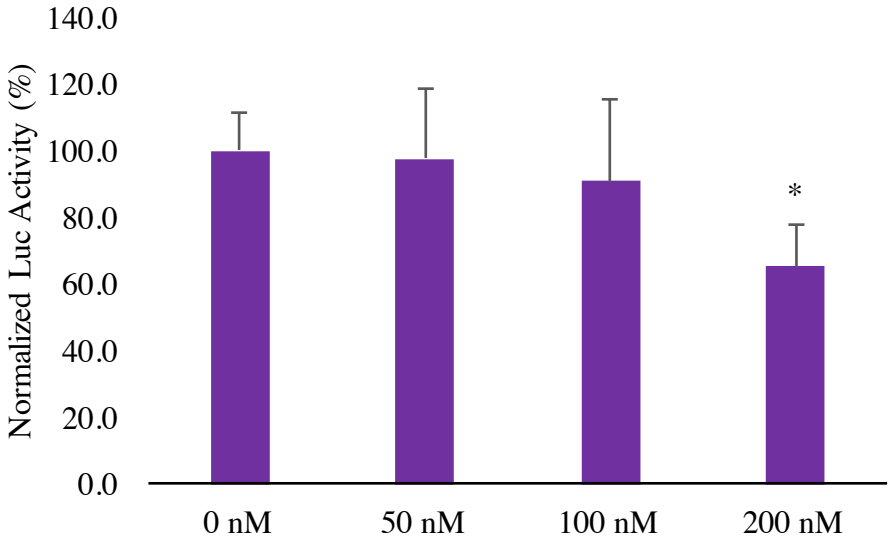

The Hsp90aa1 reporter plasmid was co-transfected along with a dose curve of miR-30b as described in Figure 13. Luciferase activity was measured 24h after transfection, normalized to 0 nM miRNA, and expressed as a percentage (n=16). *P<0.001 *vs.* 0 nM miR-30b by one-way ANOVA.

The next step was to analyze changes in protein levels *in vitro* in response to knockdown and mimic transfection of the miRNAs. We tested the effect of transient transfection of mimics or inhibitors on baseline levels of expression in HL-1 cells as well as H9c2 cells over time (24-72h) as well as after heat shock stimulation.

Knockdown and Mimic Transfection of miRNAs *In Vitro*

miR-148a and b Increasing the level of miR-148a and b by transfection of mimics decreased Hsp70 expression at 24h, which showed a trend towards a continued decrease at 72h, though variability increased at that timepoint (Figure 19A). Knockdown of miR-148a and b with anti-sense inhibitors induced a 1.21-fold increase at 72h. Transfection with 200 nM mimics or inhibitors typically resulted in a ~50-fold increase or decrease, respectively (Figure 19B). Because Hsp70 protein levels are very

low under control conditions, we also tested the effect of the mimics and inhibitors after a 1-hour heat shock (HS), which is known to significantly upregulate this mRNA (Figure 11C and [87]). In so doing, we found a significant decrease in Hsp70 with mimic transfection of miR-148a, miR-148b, or a 50/50 mixture of both. On the other hand, we did not observe a significant increase in Hsp70 protein levels after HS unless both miR-148a and b were inhibited (Figure 19C-D).

Noting that Hsp70 protein levels were increased after HS when miR-148a/b were inhibited, we tested the mRNA levels to determine whether this upregulation occurred at the mRNA level as well. We observed a trend towards an increase when both miR-148a and b were inhibited, though it did not reach statistical significance (Figure 20).

Figure 19. Effect of miR-148a Mimic Transfection or Knockdown on Hsp70

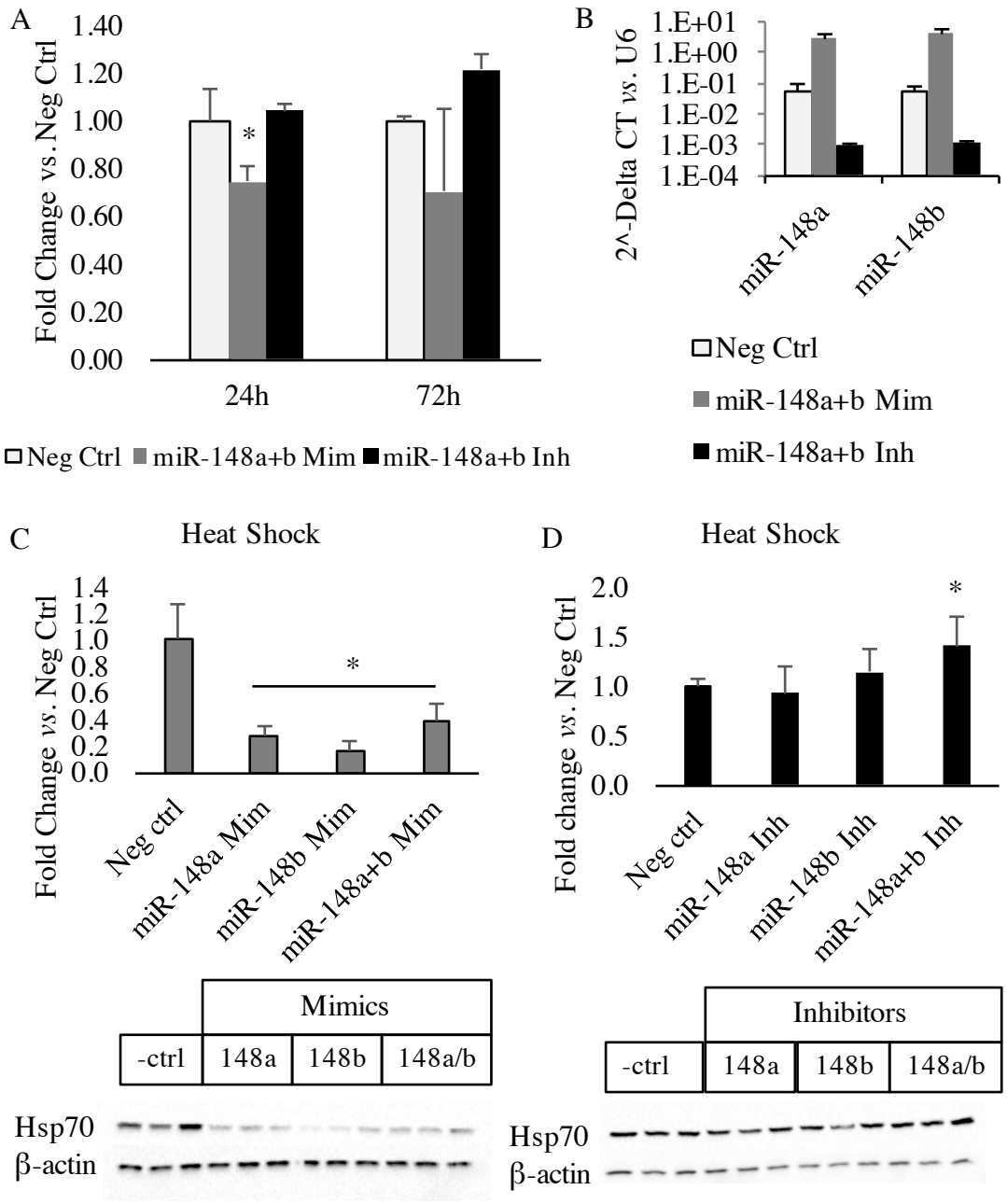

A. HL-1 cells were transfected with 200 nM mimics or inhibitors of miR-148a and b (100 nM each), and Hsp70 protein levels were assessed 24 and 72h later. B. 24h post-transfection, RNA was extracted, and miR-148a and b were assessed by qPCR, n=3. C-D. HL-1 cells were transfected with mimics or inhibitors of miR-148a, miR-148b, or both at an equal ratio. Twenty-four hours later they were heat shocked for 1h and allowed to recover for 6h before protein extraction to assess levels of Hsp70 (n=3). $P<0.05$ *vs.* Neg Ctrl by one-way ANOVA.

Figure 20. mRNA Levels of Hsp70.1 and Hsp70.3 after Transfection and Heat Shock

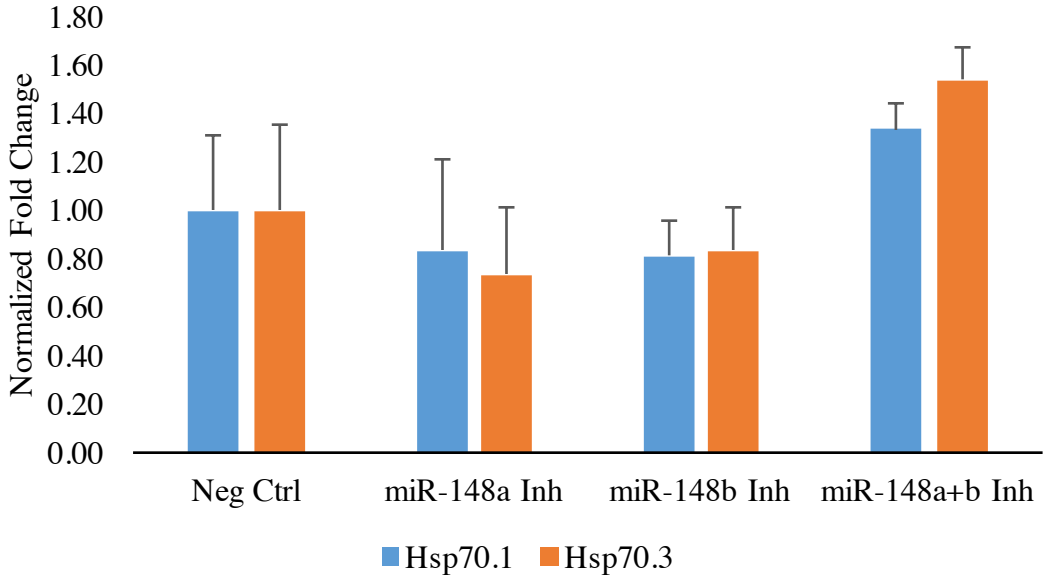

Twenty-four hours after transfection with miR-148a and b inhibitors, HL-1 cells were heat shocked for 1h and allowed to recover 3h before RNA was extracted. Real time qPCR was performed for Hsp70.1 and Hsp70.3. C_T values were normalized to those of GAPDH and expressed as average fold change *vs*. Neg Ctrl.

Dnaja1 was also a predicted target of miR-148a and b. However, luciferase assays did not confirm this. To further evaluate whether miR-148a and b regulated Dnaja1, we tested protein levels after the same conditions we used to test Hsp70, i.e., changes in expression over time in unstimulated cells, and after heat shock. At 24h after transfection with miR-148a and b mimics, we observed a significant decrease in Dnaja1 level, but this was not maintained at 72h. At 72h, there was a trend towards an increase in cells transfected with the miR-148a and b inhibitors (Figure 21A). After heat shock, mimic-treated cells showed a trend towards a decrease and the inhibitor-treated cells showed a trend towards an increase (in miR-148a or miR-148b inhibitor treated cells), though they were not statistically significant (Figure 21B-C). Thus miR-148a and b may weakly or indirectly regulate Dnaja1 expression.

Figure 21. Dnaja1 Protein Level Regulation by miR-148a and b

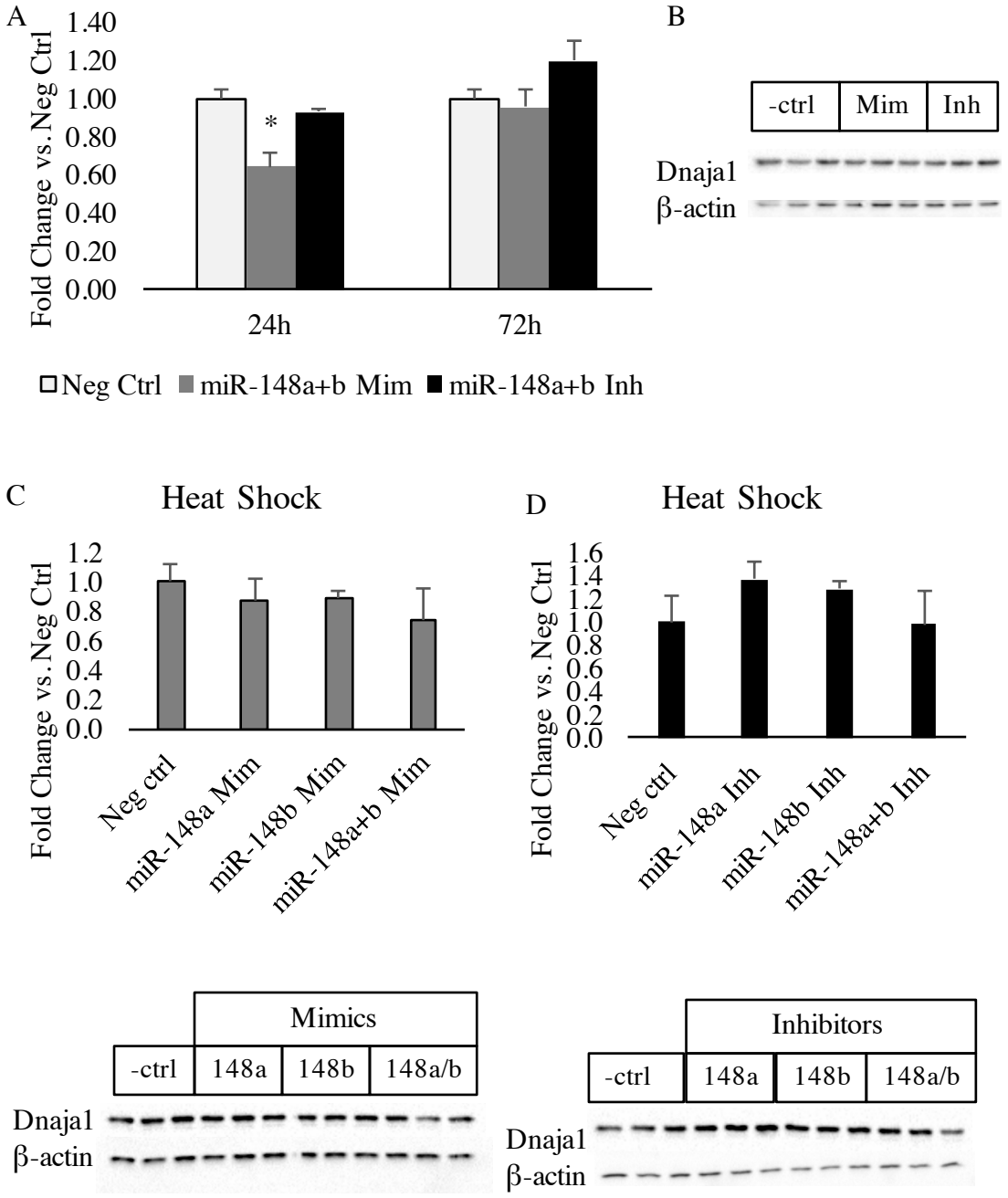

A. HL-1 cells were transfected with mimics and inhibitors of miR-148a and b were 200 nM (100 nM each), and Dnaja1 protein levels were assessed 24 and 72h later by Western blot. $P<0.001$ *vs.* Neg Ctrl at 24h by one-way ANOVA. B. 24h Western blot images. C-D. HL-1 cells were transfected with mimics or inhibitors of miR-148a, miR-148b, or both at an equal ratio. Twenty-four hours later they were heat shocked for 1h and allowed to recover for 6h before protein extraction to assess levels of Hsp70.

miR-30b was predicted to target Dnaja1, Dnajb4, and Hsp90. At 24h, there was a trend towards increased expression in Dnajb4 when miR-30b was inhibited, but this was not maintained at 48h (Figure 22). There were no changes in Dnaja1 in accordance with the negative luciferase data results, or in Hsp90 protein levels.

Figure 22. Dnaja1, Dnajb4, and Hsp90 Regulation by miR-30b

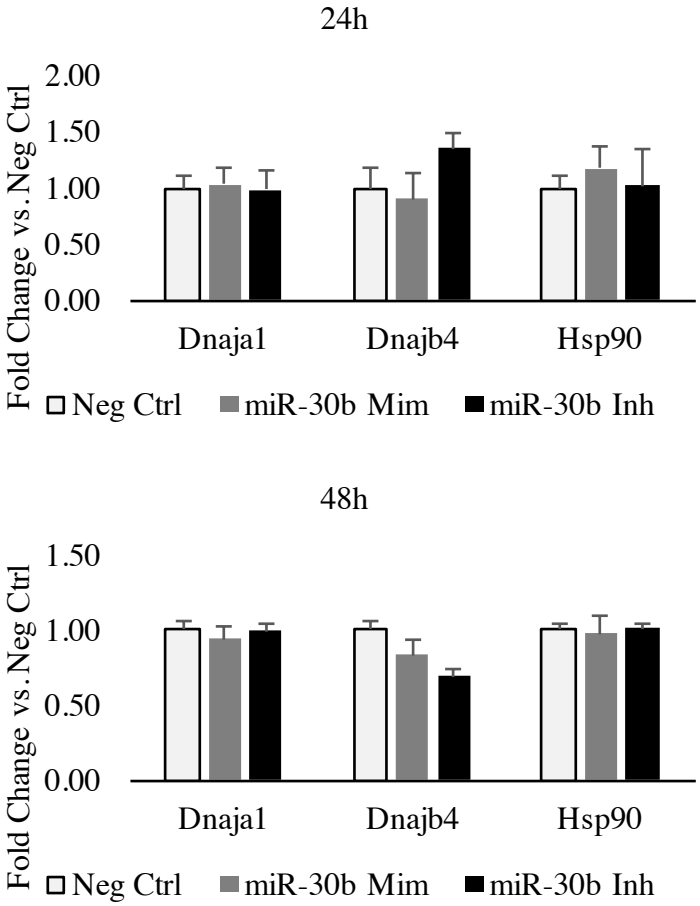

HL-1 cells were transfected with mimics or inhibitors of miR-30b, and Dnaja1, Dnajb4, and Hsp90 protein levels were assessed 24 and 48h later by Western blot (n=3). No significant differences were noted in analysis by one-way ANOVA.

let-7a* was predicted to target Hsp70.1, Dnaja1, and Dnajb4. Consistent with the luciferase data, modulation of let-7a* levels did not affect Hsp70 protein. Aside from a 12% decrease in Dnajb4 occurring at 48h, mimic transfection of let-7a* did not

cause a decrease in expression of its predicted targets, nor did knockdown lead to significant increases (Figure 23).

Figure 23. Effect of let-7a* on Dnaja1, Dnajb4, and Hsp70 Protein Levels

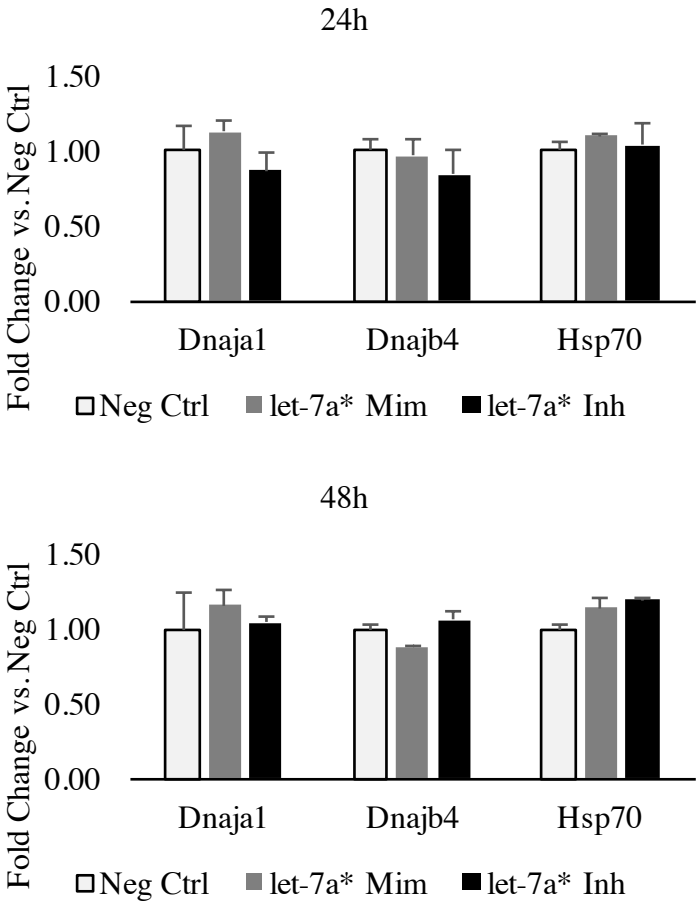

HL-1 cells were transfected with mimics or inhibitors of let-7a*, and Dnaja1, Dnajb4, and Hsp70 protein levels were assessed 24 and 48h later by Western blot (n=3). No significant differences were noted in analysis by one-way ANOVA.

Combinations of miRNAs To expand on the idea of the miRNAs acting together to regulate their targets, we next tested combinations of miRNAs over time and after HS. At 72h, the combination of miR-30b and let-7a* mimics significantly decreased expression of Hsp70, while the inhibitors together increased expression of Dnajb4 at 72h (Figure 24). These effects were stronger than that of the individual

miRNA mimics or inhibitors of miR-30b and let-7a*, which did not induce significant changes in Hsp70 and Dnajb4 on their own (Figures 22-23).

Figure 24. Effect of miR-30b and let-7a* on Protein Levels of Hsp70, Dnaja1, and Dnajb4

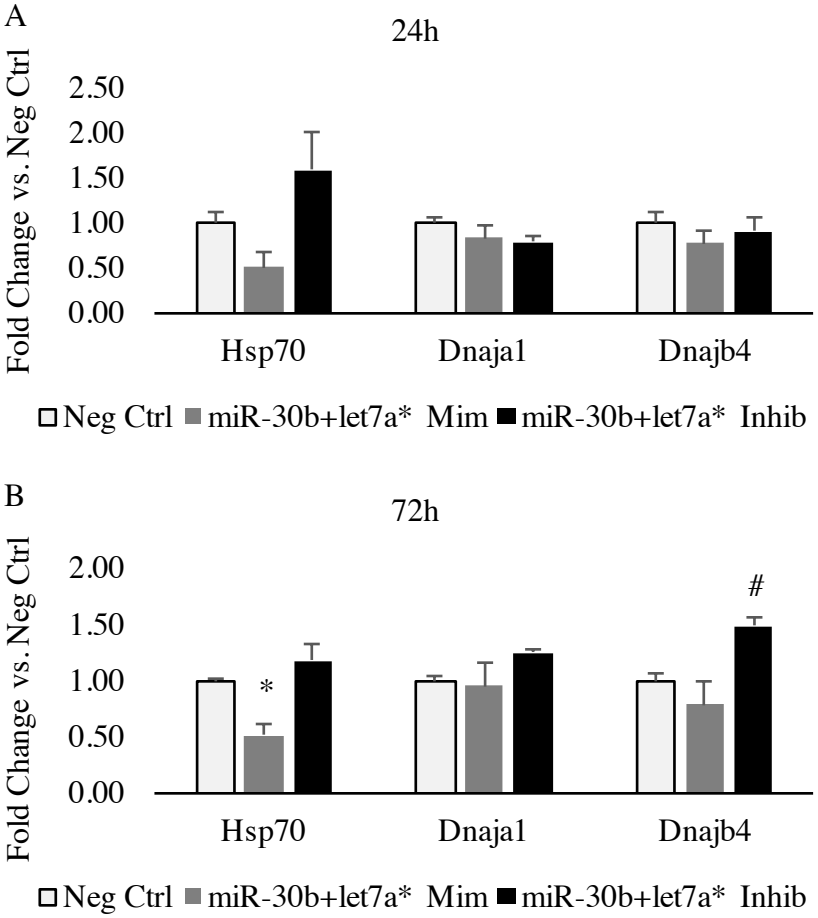

HL-1 cells were transfected with 200 nM RNAi consisting of a 50/50 mixture of miR-30b and let-7a* mimics or inhibitors or an equal quantity of non-targeting control siRNA as the Neg Ctrl. Protein was extracted at 24 and 72h for analysis of protein levels by Western blot (n=3). *P=0.003 *vs*. Neg Ctrl. #P=0.009 *vs*. Neg Ctrl.

The combination of all of the mimics together decreased Hsp70 expression significantly at 72h, and decreased Dnaja1 and Dnajb4 at both 24 and 72h. The combination of all of the inhibitors together significantly increased Hsp70 expression at 24h, and both Hsp70 and Dnajb4 expression at 72h (Figure 25).

The effects of all of the mimics or inhibitors together were stronger than individual ones. Hsp70 showed a trend towards a decrease at 72h when cells were treated with miR-148a/b mimics (Figure 19), while the combination of mimics significantly reduced it to 0.41-fold (Figure 25). Dnaja1 expression was reduced significantly at 24h by miR-148a/b, and also by the combination of all mimics together to a similar extent (Figure 21 and 25); miR-30b and let-7a* did not show this effect singly or in combination (Figures 22-4), supporting a regulatory role only for miR-148a/b. Dnajb4 was the predicted target of miR-30b and let-7a*. Individually, its expression was not significantly affected by their mimics or inhibitors (Figures 22-3). When miR-30b and let-7a* inhibitors were used in combination, expression increased significantly to 1.48-fold at 72h (Figure 24). Interestingly, when miR-148a/b inhibitors were added (i.e., all inhibitors together), expression at 72h further increased to 1.86-fold (Figure 25), though miR-148a/b are not predicted to target Dnajb4. The effects of mimics of miR-30b and let-7a* at 72h were also further enhanced by the addition of miR-148a/b, going from a 0.78-fold to 0.6-fold changes (Figure 24-5).

Figure 25. Effect of Combination of All Mimics or Inhibitors

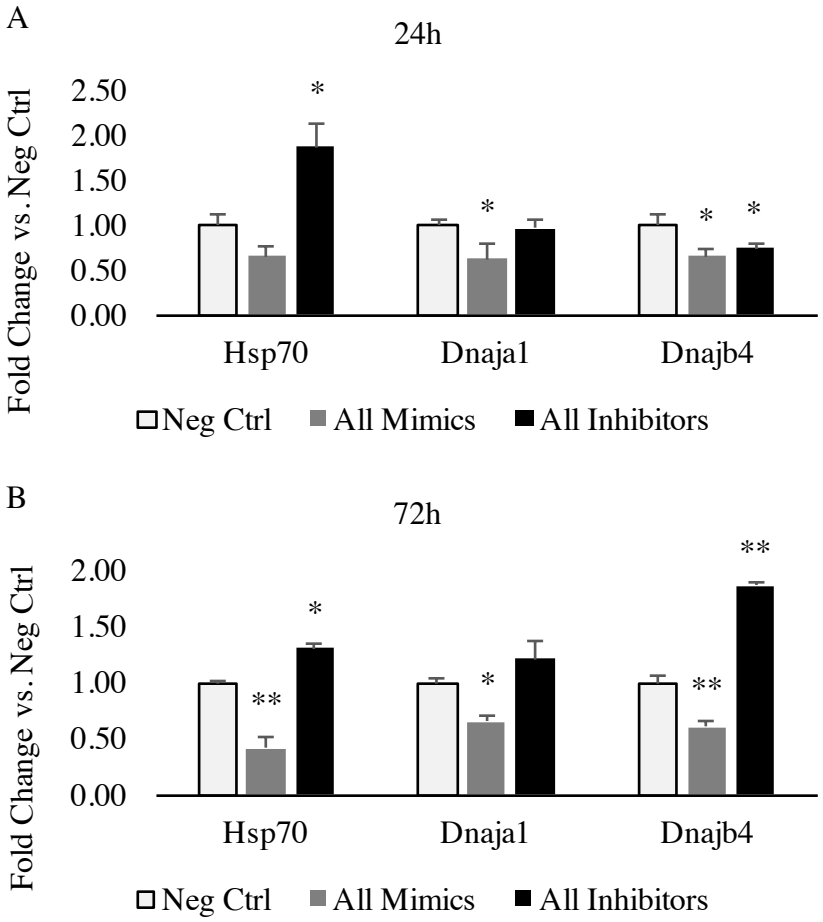

HL-1 cells were transfected with 200 nM RNAi consisting of equal parts miR-148a, miR-148b, miR-30b, and let-7a* mimics or inhibitors or an equal quantity of non-targeting control siRNA as the Neg Ctrl. Protein was extracted at (A) 24h or (B) 72h for analysis of protein levels by Western blot (n=3). *$P<0.05$ *vs*. Neg Ctrl. **$P<0.001$ *vs*. Neg Ctrl by one-way ANOVA.

To confirm our findings in the HL-1 cells, we also tested the combination of all mimics and inhibitors in the H9c2 cell line. Heat shock induced expression of Hsp70 and to a lesser extent, Dnaja1, but not Hsp90 or Dnajb4. The mimics significantly decreased Hsp70 and Dnajb4 expression after HS, but Hsp90 and Dnaja1 were not affected. After treatment with the combination of all inhibitors, Dnaja1 and Dnajb4 increased significantly after heat shock, but Hsp70 and Hsp90 were not changed (Figure 26).

Figure 26. Effect of Combination of All Mimics or Inhibitors in H9c2 Cells

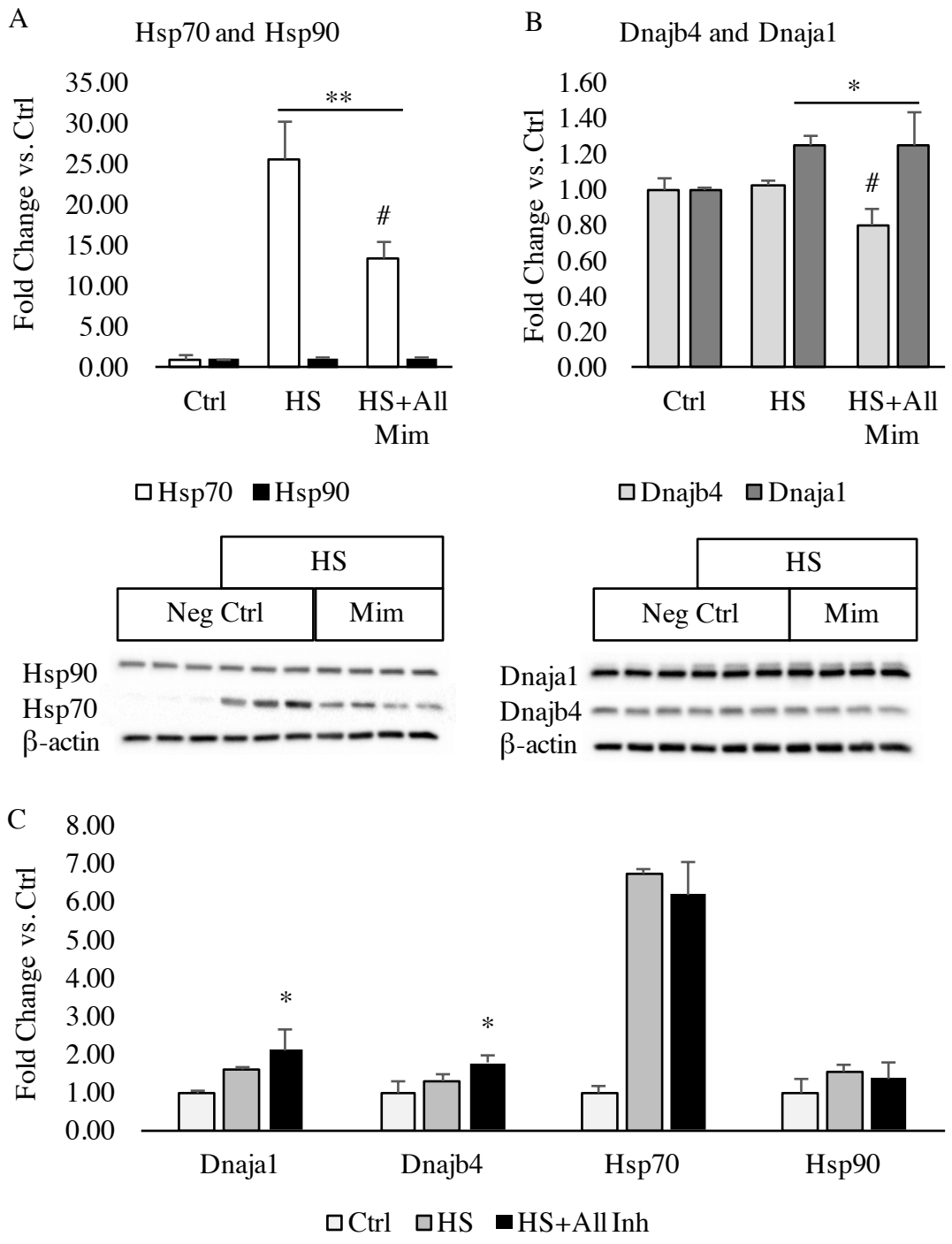

A. H9c2 cells were transfected with Neg Ctrl siRNA or the mimic mix. 24h later, they were heat shocked and allowed to recover for 5h. Hsp70 and Hsp90 levels were assessed by Western blot (n=3-4). For Hsp70, #$P<0.001$ *vs.* HS, **$P<0.001$ *vs*. Ctrl by two-way ANOVA. B. Cells were treated as in (A) and Dnaja1 and Dnajb4 were

analyzed by Western blot (n=3-4). For Dnaja1, *P<0.05 vs. Ctrl. For Dnajb4, #*P*=0.004 *vs*. Neg Ctrl transfected (Ctrl and HS). C. H9c2 cells were treated as in (A) but with inhibitor mix instead of mimic mix (n=3). **P*<0.05 *vs*. Ctrl.

Inhibitor Effects on Viability Upon OGD in HL-1 and H9c2 Cells

We next tested the combination of inhibitors on viability of HL-1 cells and H9c2 cells exposed to hypoxia. In the HL-1 cells, HPC increased viability when performed 24h prior to OGD, as shown in Figure 8 (untransfected cells). Transfection of the inhibitors (Figure 27A) did not increase the viable cell count after OGD only. HPC alone, with or without the inhibitors, did not affect viability. HPC increased viability after OGD (compare with OGD alone) and this was not enhanced by the transfection of inhibitors. Transfection of mimics (Figure 27B) did not negatively affect viability after OGD, with or without HPC.

In H9c2 cells, transfection of inhibitors did increase viability after OGD (Figure 27C). We tested miR-148a/b, miR-30b and let-7a* as well as the combination of all of the inhibitors together at 0, 50, and 200 nM. Cells were transfected 72h prior to OGD challenge, because previous experiments showed that when the miRNAs were inhibited, their target proteins' levels tended to increase over time. With miR-30b, let-7a*, and the combination of all inhibitors, we noted a significant increase compared to 0 nM, and a trend towards an increase over the same dose of miR-148a/b. Though the assay was repeated six times, variability remained high.

Figure 27. Effect of Inhibitors on Viability in H9c2 Cells after OGD

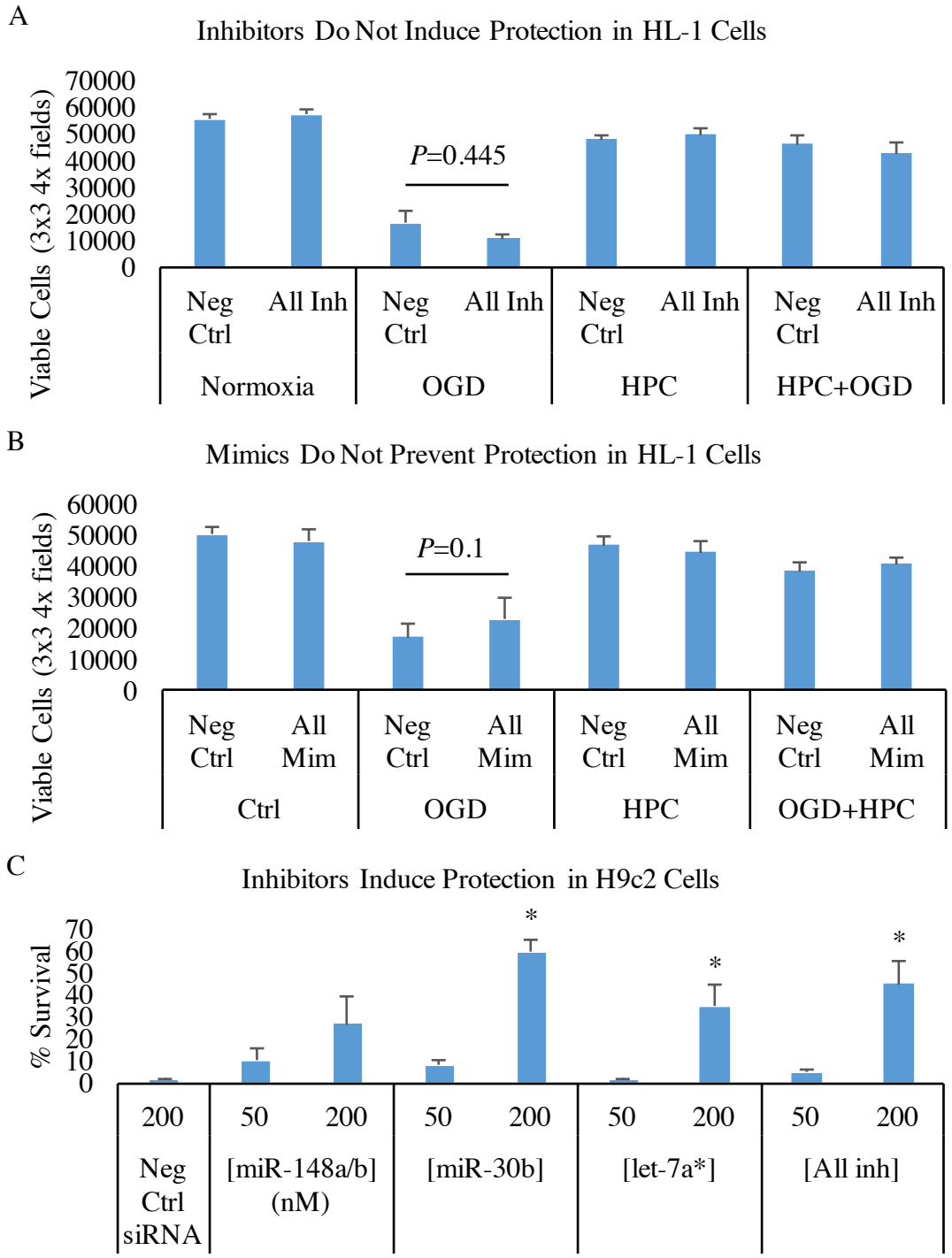

A. HL-1 cells were transfected with 200 nM Neg Ctrl siRNA or a mixture of all of the mimics in equal parts miR-148a/b, miR-30b, and let-7a* (All Mim) in 12-well plates. The next day two plates had HPC and two served as controls. The following day, plates were subjected to simI/R or time-matched normoxic incubation as noted (n=6). Analysis

by three-way ANOVA found significant effects of HPC and simI/R (P<0.001), but no significant effect for transfection (*P*=0.445 for All Mim vs. Neg Ctrl) on viability after HPC, simI/R or both. B. Cells were treated as in (A) except a mixture of all inhibitors was tested, instead of mimics. Analysis by three-way ANOVA showed that inhibitors did not have a significant effect (*P*=0.1 for All Inh *vs.* Neg Ctrl) on viability after HPC, simI/R or both. C. H9c2 cells were transfected with miR-148a/b, miR-30b, let-7a*, or or all inhibitors (equal mix), relative to Neg Ctrl siRNA (i.e., 0 nM is 200 nM Neg Ctrl, 50 nM is 150 nM Neg Ctrl and 50 nM of inhibitors). Seventy-two hours later, cells were counted by labeling all and dead cells with Hoechst and PI, respectively. Then they were subjected to OGD, and all and dead cells were again counted 1h after after reoxygenation, to obtain the % survival for each well. These were averaged for each condition (n=4); error bars represent SEM. P≤0.025 *vs*. Neg Ctrl.

Summary of Findings

Ischemic preconditioning upregulates heat shock proteins in the myocardium. While it was previously established that Hsp70 is significantly increased by IPC at 24h, here we show that at 6h, not only is Hsp70 increased, but also Hsp40 family members and Hsp90 as well. Hypothesizing that changes in expression of miRNAs could contribute to this increased expression, we identified a set of miRNAs that decreased after IPC, which could function to derepress their protective target genes (Figure 28). Luciferase assays confirmed that miR-148a and b directly target Hsp70.1 and Hsp70.3, that miR-30b targets Hsp90, and that let-7a* targets Dnajb4. Through transfection with mimics and inhibitors of the miRNAs, singly and in combination, we established that miR-148a/b can affect Hsp70 and Dnaja1 protein levels, and the combination of miR-30b and let-7a* can affect Hsp70 and Dnajb4 levels. The combination of all of the miRNAs together affected protein levels of Hsp70, Dnaja1, and Dnajb4. No changes in Hsp90 were observed in any of the experiments.

Figure 28. Predicted and Experimentally Validated Targeting

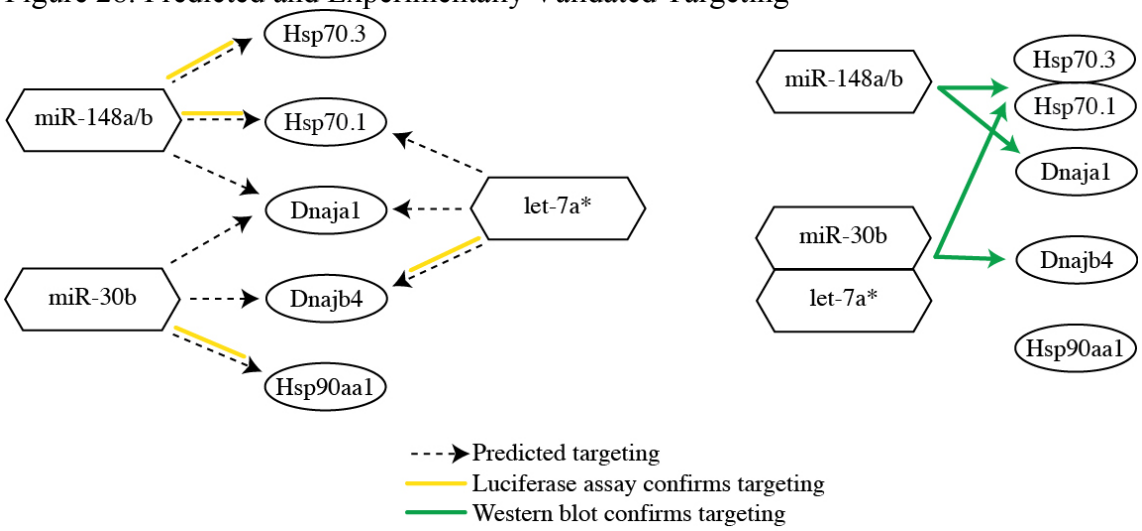

In the heart, IPC strongly induces the expression of heat shock proteins within 6 hours. In the HL-1 cells, heat shock strongly induces their expression, while hypoxic preconditioning as well as transfection of inhibitors of the miRNAs slightly induce their expression. However, both the strong induction after heat shock and the moderate induction that occurs with transfection of inhibitors do not induce cytoprotection from simI/R. Though the miRNAs selected to investigate in this Aim decrease after HPC, preventing this decrease by transfecting the HL-1 cells with mimics does not prevent the protection afforded by HPC. In H9c2 cells, the inhibitors slightly boosted expression of Hsp40 family members, but not Hsp70 or Hsp90. Transfection of the H9c2 cells with inhibitors dose-dependently increased viability in the OGD model.

EXOSOMAL MIRNA AS A PARACRINE MEDIATOR FROM MYOCARDIUM TO TRANSPLANTED MESENCHYMAL STEM CELLS

As shown in the previous section, hypoxic preconditioning (HPC) exerted a strong protective effect on the HL-1 cells (Figure 8). Because of studies showing that MSCs have improved engraftment in preconditioned hearts, which could be mediated by paracrine factors released by cardiac cells[162, 165], we wanted to test whether preconditioning of HL-1's would affect their exosomes' RNA content, and whether protective mRNA or miRNA could be transferred to MSCs, resulting in protection.

Mesenchymal Stem Cells Internalize HL-1 Exosomes

We began by confirming that MSCs internalize HL-1 exosomes, which would be a key first step for RNA transfer. We fluorescently labeled the exosomes using the lipophilic dye PKH26, and exposed the MSCs to the labeled exosomes over a time course of 30 minutes to 18h. Flow cytometry and analysis using the imaging flow cytometer Amnis ImageStream showed that MSCs readily take up HL-1 exosomes, becoming 80% positive after 30 minutes and 98.9% PKH+ after 18h (Figure 29).

Figure 29. MSCs Internalize HL-1 Exosomes

A. Flow Cytometry Histogram Overlay

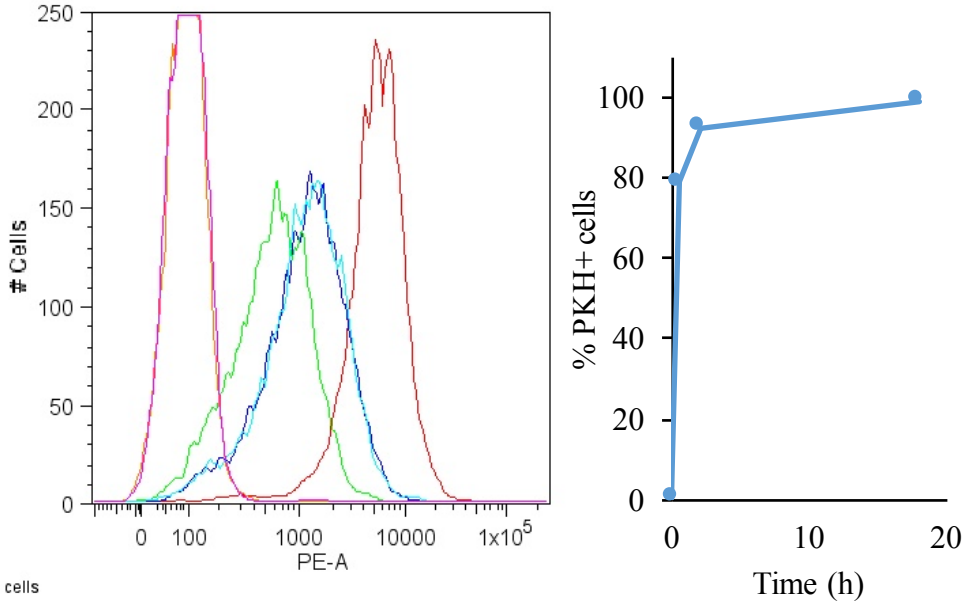

	Sample	%
	KRISTIN150202_UNSTIANED CELLS.fcs	83.8
	KRISTIN150202_MEMBRANE1 HOUR EXO.fcs	82.7
	KRISTIN150202_MEMBRANE STAINING.fcs	79
	KRISTIN150202_MEMBRANE 30 MINS EXO.fcs	78.5
	KRISTIN150202_MEMBRANE 2 HOUR EXO.fcs	82
	KRISTIN150202_MEMBRANE 18 HOUR EXO.fcs	79.8

B. Images from Amnis ImageStream

1 hour

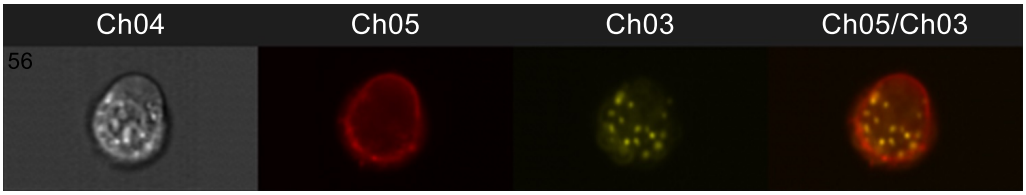

18 hour

HL-1 exosomes were labeled with the fluorescent dye PKH26, and exposed to MSCs over a time course. (A) MSCs rapidly became PKH26+ as shown by an increase in fluorescence intensity in the PE channel. (B) Imaging showed the accumulation of numerous labeled spots (yellow) within the cells. The membranes of the MSCs were labeled with an antibody to CD-44 (red) to confirm exosome internalization.

miRNA-Seq Results

To determine whether the miRNA content of HL-1 exosomes changed after HPC, exosomes were isolated from the following sources: control HL-1 cells, control HL-1 exosomes, HPC HL-1 cells, and HPC HL-1 exosomes. Figure 30 shows the number of total, filtered, and aligned reads for each sample analyzed. Overall alignment averaged 44%.

Figure 30. miRNA-Seq Read Counts

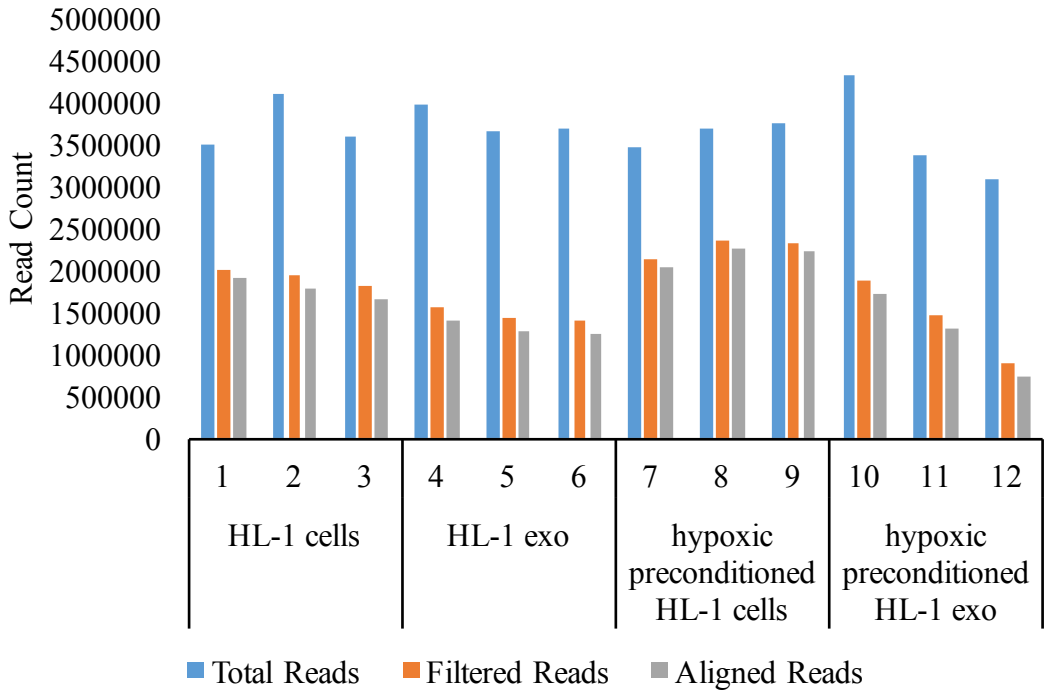

HL-1 cellular and exosomal miRNA was sequenced, and low quality reads were filtered out. The remaining sequences were aligned to the mouse genome for differential expression analysis.

Then we performed differential expression analysis using the DESeq package to compare control *vs*. HPC cells, and control exosomes *vs.* HPC exosomes. Table 9 shows the significant differences in miRNA between the control and HPC cells. According to

the sequencing data, HPC treatment increased the cellular levels of miR-20b and miR-19a/b, with moderate increases in miR-501, 3062, 340, and 465a/c. There were decreases in miR-326, miR-1a*, and miR-184.

Table 9. Differentially Expressed miRNAs Between Control and HPC HL-1 Cells

Gene ID	Name	Reads, Control Cells	Reads, HPC Cells	Fold Change	Adjusted P Value
MIMAT0003187	mmu-miR-20b-5p	21.4	92.4	4.33	0.00005
MIMAT0000559	mmu-miR-326-3p	63.3	19.3	0.31	0.00501
MIMAT0000513	mmu-miR-19b-3p	135.6	502.2	3.70	0.01961
MIMAT0003508	mmu-miR-501-5p	67.4	160.3	2.38	0.03280
MIMAT0016979	mmu-miR-1a-1* mmu-miR-1a-1-5p	27.6	8.0	0.29	0.05544
MIMAT0014830	mmu-miR-3062-5p	18.1	50.0	2.77	0.05544
MIMAT0000213	mmu-miR-184-3p	825.4	398.2	0.48	0.05544
MIMAT0000706	mmu-miR-362-5p	682.1	1355.9	1.99	0.07083
MIMAT0004651	mmu-miR-340-5p	135.3	359.7	2.66	0.07083
MIMAT0004873	mmu-miR-465c-5p	195.6	419.4	2.14	0.07083
MIMAT0002106	mmu-miR-465a-5p	132.0	352.9	2.67	0.07964
MIMAT0000651	mmu-miR-19a-3p	44.3	181.9	4.11	0.09447

Data represent the average of 3 replicates. Intensity of blue color correlates with magnitude of decrease in HPC vs. Control cells. Intensity of red color correlates with magnitude of increase in HPC vs. Control cells.

A comparison of control exosomes *vs.* HPC exosomes revealed that, while changes in the miRNA profile do occur in the parent cells, the miRNA profile in exosomes remains relatively constant, with only two significantly different miRNAs, miR-3535, and miR-208a, both of which decreased independently of significant changes occurring in the parent cells (Table 10).

Table 10. Differentially Expressed miRNAs Between Control and HPC HL-1 Exosomes

Gene ID	Name	Control Exo	HPC Exo	Fold Change	Adjusted P Value
MIMAT0031410	mmu-miR-3535	245.6	68.5	0.28	0.004
MIMAT0000520	mmu-miR-208a-3p	354.6	123.8	0.35	0.004

Data represent the average of 3 replicates.

RNA-Seq Results

Through sequencing the mRNA of control and HPC HL-1 cells, we determined that HPC induces many changes in their gene expression profile (Table 11). Interestingly, this data is substantially different than what occurs in the IPC heart as shown in Section 3.1.2 (Table 6), indicating that HPC and IPC operate by somewhat different cytoprotective mechanisms, despite the common stimuli of oxygen and nutrient deprivation.

Table 11. Differentially Expressed mRNAs Between Control and HPC HL-1 Cells

Symbol	Name	Control Cells	HPC Cells	Fold Change	Adjusted P Value
Kbtbd11	kelch repeat and BTB (POZ) domain containing 11	937.2	163.2	0.17	0.0002
Rora	RAR-related orphan receptor alpha	732.6	190.7	0.26	0.0250
Stc1	stanniocalcin 1	620.6	199.7	0.32	0.0000
Egln3	EGL nine homolog 3 (C. elegans)	1711.8	665.5	0.39	0.0001
Ndnf	neuron-derived neurotrophic factor	1292.8	511.6	0.40	0.0243
Tshr	thyroid stimulating hormone receptor	330.0	133.2	0.40	0.0250
Rnf152	ring finger protein 152	489.0	201.0	0.41	0.0110
Slc2a1	solute carrier family 2 (facilitated glucose transporter), member 1	3545.8	1587.9	0.45	0.0003
Cp	ceruloplasmin	1150.3	515.8	0.45	0.0023
Ppap2b	phosphatidic acid phosphatase type 2B	1640.6	745.9	0.45	0.0034
Slc40a1	solute carrier family 40 (iron-regulated transporter), member 1	1954.5	916.2	0.47	0.0156
Ccng2	cyclin G2	1894.9	897.6	0.47	0.0073
Mylk	myosin, light polypeptide	8634.6	4112.6	0.48	0.0005

	kinase				
Specc1	sperm antigen with calponin homology and coiled-coil domains 1	1280.6	610.7	0.48	0.0156
Mgarp	mitochondria localized glutamic acid rich protein	1355.8	668.2	0.49	0.0181
Hivep2	human immunodeficiency virus type I enhancer binding protein 2	1444.4	729.7	0.51	0.0395
Xbp1	X-box binding protein 1	1438.0	734.2	0.51	0.0230
Slc47a1	solute carrier family 47, member 1	17395.4	9361.1	0.54	0.0230
Ttn	titin	64147.2	34782.6	0.54	0.0156
Pdia6	protein disulfide isomerase associated 6	9037.5	16376.0	1.81	0.0181
Srm	spermidine synthase	566.6	1043.0	1.84	0.0395
Atf5	activating transcription factor 5	587.0	1160.7	1.98	0.0243
Npm3	nucleoplasmin 3	681.6	1382.7	2.03	0.0243
Cd209c	CD209c antigen	572.0	1178.0	2.06	0.0442
Cox6a2	cytochrome c oxidase subunit VIa polypeptide 2	458.9	953.9	2.08	0.0110
Fkbp11	FK506 binding protein 11	715.0	1545.5	2.16	0.0019
Olfr1033	olfactory receptor 1033	428.4	1009.1	2.36	0.0019
Wdr92	WD repeat domain 92	5357.2	13622.4	2.54	0.0000
Bche	butyrylcholinesterase	430.8	1098.2	2.55	0.0201
Cmah	cytidine monophospho-N-acetylneuraminic acid hydroxylase	950.9	2541.6	2.67	0.0025
Krt18	keratin 18	73.2	253.3	3.46	0.0019

Data represent the average of 3 replicates. Intensity of blue color correlates with magnitude of decrease in HPC vs. Control cells. Intensity of red color correlates with magnitude of increase in HPC vs. Control cells.

A comparison of the mRNA in control *vs*. HPC exosomes revealed few differences. Albumin was present to a small degree within the HPC exosomes but not the Control exosomes, and Collagen Type I-α2 was present in Control exosomes but

not HPC exosomes. The low read count of these indicates low abundance of these mRNAs, which could mean that the changes observed may not have an impact on the protectiveness of the HPC HL-1 exosomes (Table 12).

Table 12. Differentially Expressed mRNA in Control and HPC Exosomes

Symbol	**Name**	**Control Exo**	**HPC Exo**	**Fold Change**	**Adjusted P Value**
Alb	albumin	0	46.51	Inf	0.001
Col1a2	collagen, type I, alpha 2	44.36	0.00	0.00	0.021

Data represent the average of 3 replicates.

These data indicate that while the mRNA and miRNA profiles change in HL-1 cells when they undergo HPC, the exosomal contents are not greatly affected by HPC. We had planned to determine how exosomes from HL-1 affected MSC. A limitation to this study was difficulty in establishing an OGD model that induced cell death in the MSCs, which were resistant to even long durations of hypoxia (Figure 31).

Figure 31. MSCs are Resistant to Cell Death from OGD

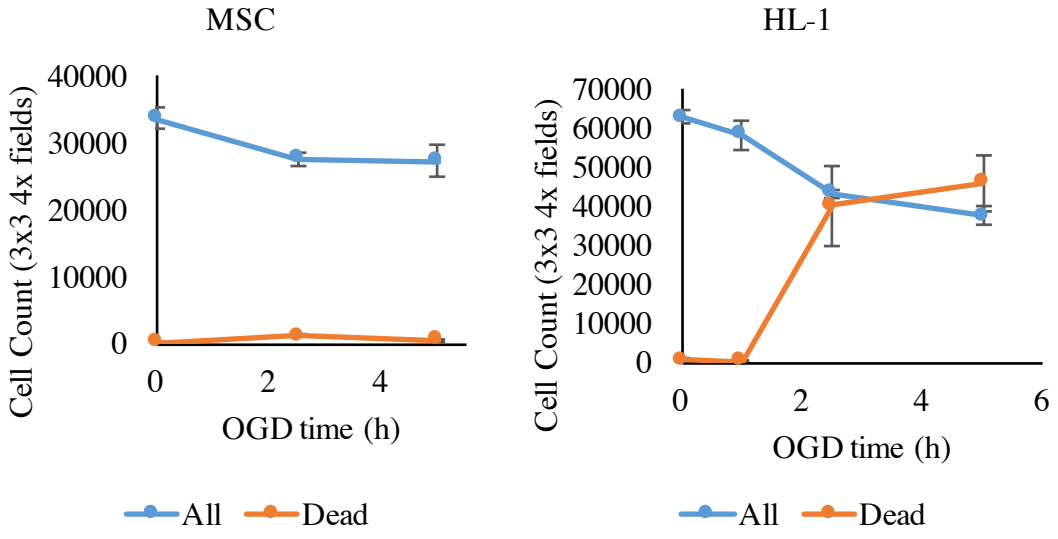

MSCs were plated in 6-well plates and subjected to OGD in serum free glucose free media. Cells were reoxygenated in growth media containing 10% serum, and labeled with Hoechst (all cells, blue line) and PI (dead cells, orange line) for viability analysis 1h later.

miRNA in Stem Cell Mediated Paracrine Effects on the Myocardium

MSC Exosomes Are Protective Against Cell Death Upon OGD Challenge

When H9c2 cells were pre-treated with exosomes (MSC-derived) overnight in doses ranging from 0 to 300 μg/mL exosome protein, a dose dependent increase in viability was observed after OGD (Figure 32A). The percentage of cells surviving increased from 69 to 88%. We also tested the effect of treating H9c2s with microparticles (MP), which are isolated during the exosome isolation procedure. These did not confer protection (Figure 32A). Exosomes were also protective in HL-1 cells (Figure 32B), as evidenced by increased viable cell counts after OGD, and decrease in LDH release. Although the two time points we tested did not induce cell death in NMVMs compared to incubation at normoxia, treatment with exosomes did increase the number of viable cells at 180 min OGD (Figure 32C).

Figure 32. MSC Exosomes Decrease Cell Death from OGD Challenge in Various Cardiac Cell Types

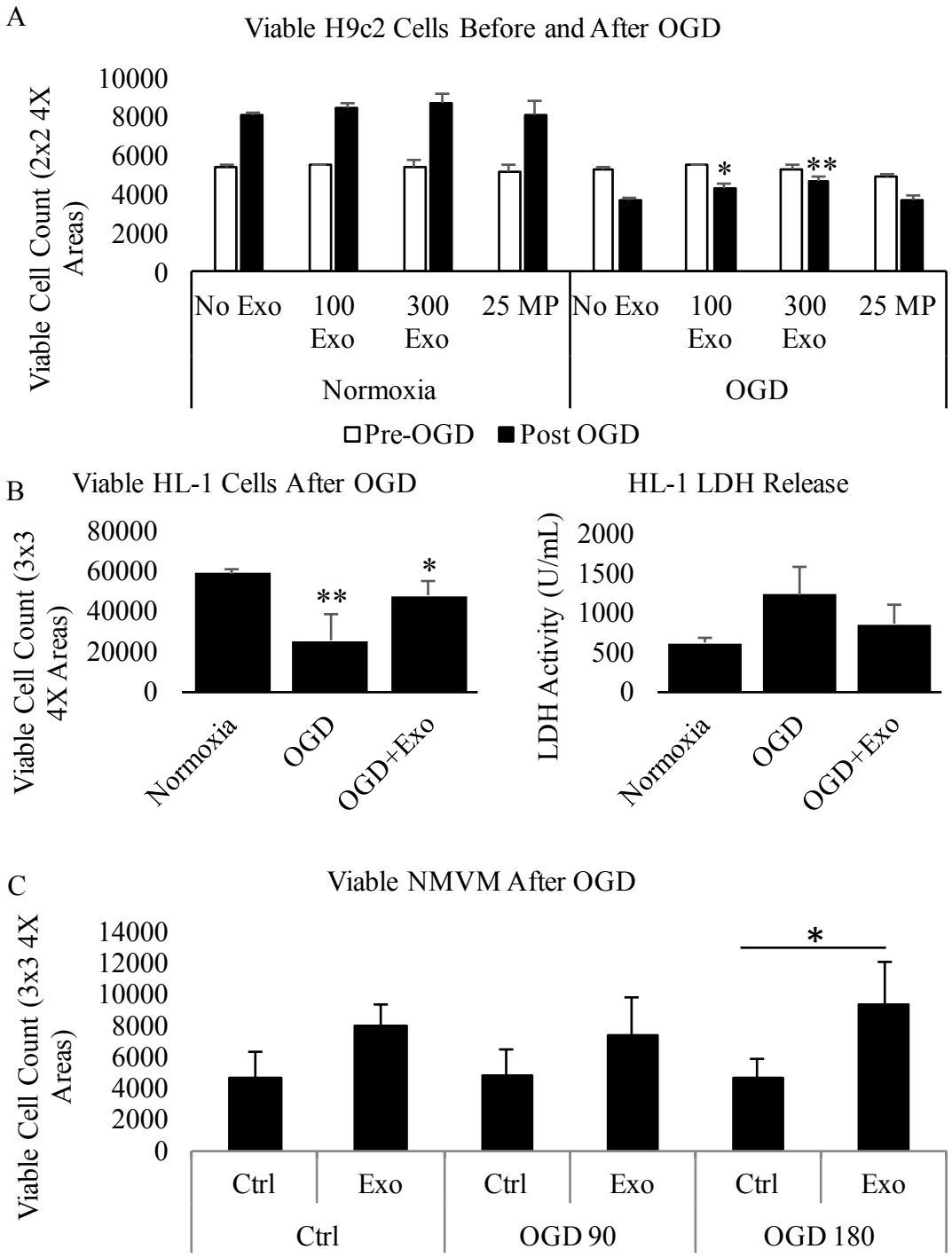

A. H9c2 cells were pre-treated with a dose curve of exosomes (Exo) or one dose of microparticles (MP) overnight and then stained with Hoechst and PI to count all and dead cells, respectively. They were then subjected to OGD challenge, after which they

were reperfused in growth media and counted once more. Data are expressed as viable cell count calculated by subtracting dead/PI+ cells from all cells/Hoechst+ (n=3). *P=0.029, **P=0.004 *vs.* No Exo. B. HL-1 cells were subjected to OGD challenge and treated with 300 μg/mL exosomes overnight. Viable cell count was determined as in A (n=11-12). *P=0.017, **P<0.001 *vs.* Normoxia. C. NMVMs were pre-treated with 300 μg/mL exosomes overnight and subjected to OGD challenge for 90 and 180 min. OGD did not increase the cell death in our hands, but Exo pre-treatment did increase the viable cell count (n=4-8). *P=0.003 *vs.* Ctrl OGD 180 min.

MSC Exosomes Are Internalized by H9c2, HL-1, and NMVM Cells

H9c2, HL-1, and NMVM cells were incubated with PKH26 labeled exosomes and analyzed by flow cytometry and Amnis ImageStream. All three types of cells demonstrated uptake of exosomes, as evidenced by an increase in fluorescence intensity in the phycoerythrin (PE) channel (Figure 33A-C). Furthermore, fluorescently labeled exosomes were visible within the cells imaged by the Amnis (Figure 33D). To determine the concentration of exosomes in media at an exosomal protein concentration of 300 μg/mL before and after cells were treated, an aliquot of media was saved at the beginning and at the end of the 18h treatment and exosomes were counted by Amnis ImageStream. The concentration of exosomes prior to cell uptake was 3.64×10^6/mL while after the 18h treatment, the concentration decreased to 0.07×10^6/mL (about 2% of the exosomes remained in the media).

Figure 33. MSC Exosomes Are Taken Up by H9c2, HL-1, and NMVM Cells.

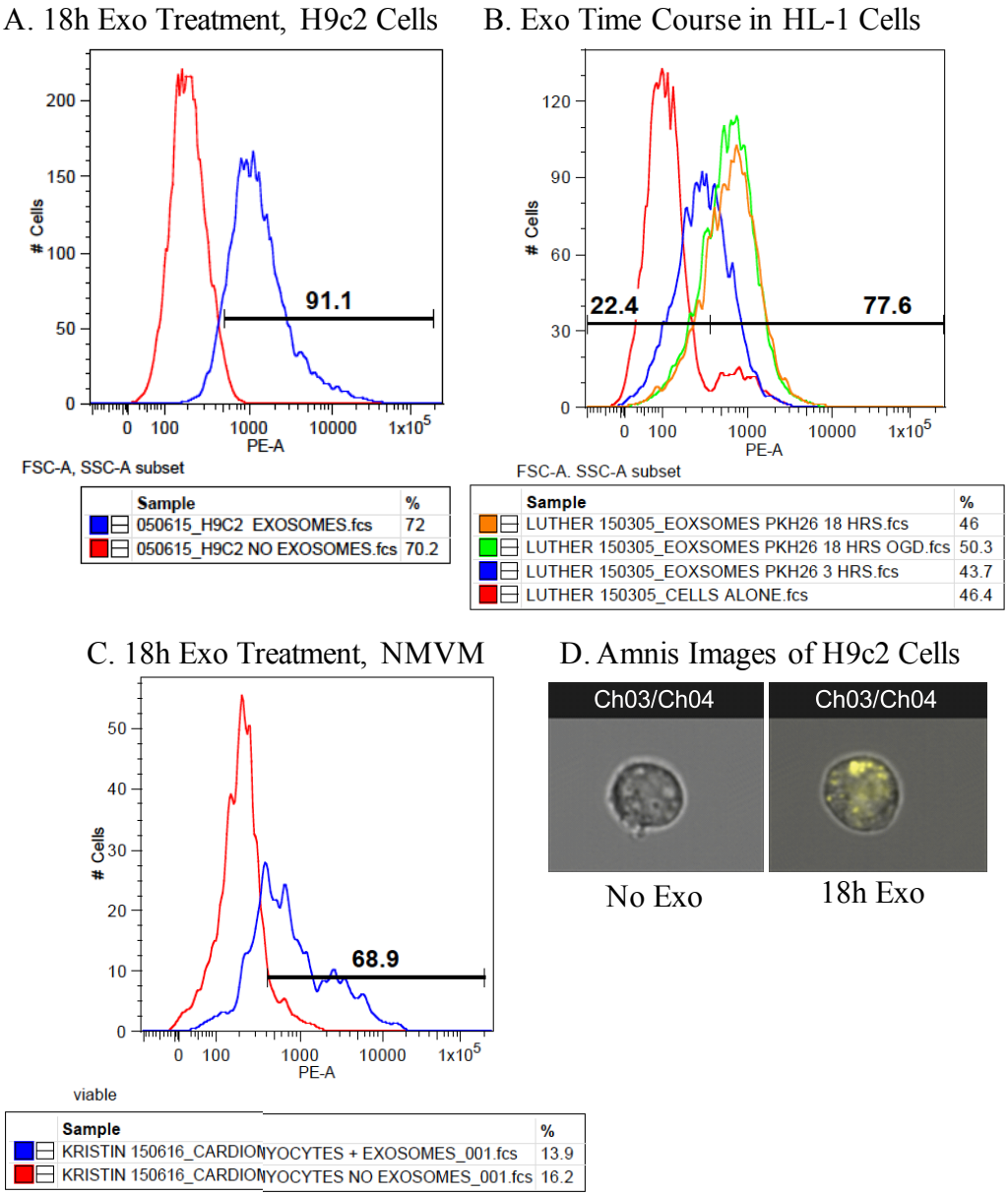

Cells were treated with PKH26-labeled exosomes for 18h (A and C) or a time course (B). They were then analyzed by flow cytometry. (D) H9c2 cells were imaged by Amnis ImageStream, showing labeled exosomes within the cell.

miRNA Seq Results

To determine which miRNAs are highly expressed within MSC exosomes, total RNA was extracted from the MSCs and their exosomes (n=3/group from different passages of MSCs). The profile of miRNAs revealed that the expression pattern was different between the cells and exosomes, as suggested by other published comparisons (Table 13)[195, 197].

Table 13: Significantly Differentially Expressed miRNAs in MSCs and Their Exosomes

Name	MSC Cells	MSC Exosomes	Fold Change	Adjusted P Value
mmu-miR-451	0.844	3959.310	4688.5	0.000000004
mmu-miR-150	0.312	1114.537	3570.8	0.000000005
mmu-miR-223	0	297.663	Inf	0.000000008
mmu-miR-494	0.100	484.685	4830.9	0.000000013
mmu-miR-493*; mmu-miR-493-5p	0	324.916	Inf	0.000009727
mmu-miR-495-3p	0.100	136.769	1363.2	0.000017907
mmu-miR-142-5p	0	255.041	Inf	0.000039516
mmu-miR-144*; mmu-miR-144-5p	0	206.204	Inf	0.000049889
mmu-miR-409-3p	0.401	365.421	910.6	0.000058969
mmu-miR-127-3p	1.394	1355.294	972.6	0.000097942
mmu-miR-144-3p	0	487.572	Inf	0.000305884
mmu-miR-122a	1.854	5308.913	2864.1	0.000377957
mmu-miR-411*; mmu-miR-411-3p	0.201	62.199	310.0	0.000381352
mmu-miR-369-3p	0.106	48.480	457.8	0.000381352
mmu-miR-369-5p;	0	62.441	Inf	0.001097037
mmu-miR-299a-3p	0.201	53.348	265.9	0.001292217
mmu-miR-299b-5p	0.201	53.348	265.9	0.001292217
mmu-miR-6236	1.335	125.464	94.0	0.001292217
mmu-miR-433-3p	0	511.125	Inf	0.001401959
mmu-miR-504-5p	0	86.881	Inf	0.001446907
mmu-miR-451b	0	23.860	Inf	0.001818421

mmu-miR-409-5p	0.100	30.652	305.5	0.003231630
mmu-miR-486-5p	6.352	10715.185	1686.9	0.004490330
mmu-miR-3107*; mmu-miR-3107-3p	6.352	10715.185	1686.9	0.004490330
mmu-miR-381-3p	2.043	349.147	170.9	0.005934268
mu-miR-3107-5p	14.427	28715.119	1990.4	0.007409008
mmu-miR-486*; mmu-miR-486-3p	14.427	28715.119	1990.4	0.007409008
mmu-miR-412-5p	0	19.045	Inf	0.007821526
mmu-miR-142-3p	0	85.318	Inf	0.009487658
mmu-miR-411-5p	2.556	400.806	156.8	0.009772641
mu-miR-370-3p	0.100	58.982	587.9	0.010449075
mmu-miR-126-5p	2.447	172.365	70.4	0.012110825
mmu-miR-434-3p	0.206	28.368	137.6	0.013274568
mmu-miR-382*; mmu-miR-382-3p	0.401	146.574	365.2	0.015102170
mmu-miR-382; mmu-miR-382-5p	0.106	72.811	687.6	0.018437024
mmu-miR-6240	2.021	83.180	41.2	0.020513287
mmu-miR-200b-3p	0.131	22.976	175.3	0.023077551
mmu-miR-134-5p	0.100	19.640	195.8	0.023792018
mmu-miR-2137	0.237	20.269	85.5	0.026085925
mmu-miR-126-3p	50.245	2799.285	55.7	0.030018186
mmu-miR-299*; mmu-miR-299-5p	0	11.607	Inf	0.032574692
mmu-miR-299b-3p	0	11.607	Inf	0.032574692

Data represent the average of 3 replicates. Intensity of red color correlates with magnitude of increase in exosomes vs. cells. Inf, infinite.

To determine whether miRNA within MSC exosomes could mediate their cardioprotective effects, we also determined which miRNAs were highly expressed within the MSC exosomes, with read counts higher than 1024, and performed a literature search to determine whether any of these are known to be cardioprotective (Table 14). The rationale for using 1024 reads as a cutoff was based on histogram analysis of the $\log_2$ of the frequency of the number of reads for each miRNA in each

sample, in order to focus on those miRNAs within the top ~50% most highly expressed (see Figure 34).

Table 14. Highly Expressed miRNAs in MSC Exosomes

Gene ID	Name	Read Count	Refs (if known cardioprotective)
MIMAT0000530	mmu-miR-21a-5p	45255.27	[81-85, 226-228]
MIMAT0014943	mmu-miR-486b-5p	28715.12	
MIMAT0017206	mmu-miR-486a-3p	28715.12	
MIMAT0000247	mmu-miR-143-3p	11931.92	
MIMAT0000539	mmu-miR-92a-3p	11286.39	
MIMAT0003130	mmu-miR-486a-5p	10715.18	
MIMAT0014944	mmu-miR-486b-3p	10715.18	
MIMAT0000531	mmu-miR-22-3p	9674.50	[203]
MIMAT0000221	mmu-miR-191-5p	8571.52	
MIMAT0000521	mmu-let-7a-5p	8505.54	
MIMAT0000522	mmu-let-7b-5p	8193.79	[229]
MIMAT0000152	mmu-miR-140* mmu-miR-140-3p	6268.33	
MIMAT0000136	mmu-miR-125b-5p	5680.82	
MIMAT0000533	mmu-miR-26a-5p	5528.38	
MIMAT0000655	mmu-miR-100-5p	5450.84	
MIMAT0000132	mmu-miR-99b-5p	5443.74	
MIMAT0000121	mmu-let-7g-5p	5392.06	
MIMAT0000515	mmu-miR-30d-5p	5351.18	
MIMAT0000246	mmu-miR-122-5p	5308.91	
MIMAT0000523	mmu-let-7c-5p	5290.96	
MIMAT0000131	mmu-miR-99a-5p	5158.83	
MIMAT0000383	mmu-let-7d-5p	5156.14	
MIMAT0000122	mmu-let-7i-5p	4875.94	
MIMAT0000532	mmu-miR-23a-3p	4536.37	
MIMAT0003454	mmu-miR-423-3p	4332.23	
MIMAT0004825	mmu-miR-423-5p	4156.89	
MIMAT0000666	mmu-miR-320-3p	4127.96	
MIMAT0001632	mmu-miR-451a	3959.31	[80]
MIMAT0000525	mmu-let-7f-5p	3927.54	
MIMAT0000652	mmu-miR-25-3p	3785.08	
MIMAT0000516	mmu-miR-148a-3p	3433.13	
MIMAT0000135	mmu-miR-125a-5p	3246.42	
MIMAT0000138	mmu-miR-126-3p	2799.29	[230]
MIMAT0000230	mmu-miR-199a* mmu-miR-199a-3p	2449.21	

MIMAT0004667	mmu-miR-199b-3p	2445.06	
MIMAT0000524	mmu-let-7e-5p	2310.92	
MIMAT0000125	mmu-miR-23b-3p	2223.53	
MIMAT0000661	mmu-miR-214-3p	2200.85	[231, 232]
MIMAT0000669	mmu-miR-221-3p	2079.00	
MIMAT0000126	mmu-miR-27b-3p	1690.11	
MIMAT0000648	mmu-miR-10a-5p	1600.75	
MIMAT0000140	mmu-miR-128-3p	1504.61	
MIMAT0000208	mmu-miR-10b-5p	1463.62	
MIMAT0000219	mmu-miR-24-3p	1445.74	[233-237]
MIMAT0014856	mmu-miR-3074-5p	1445.74	
MIMAT0000139	mmu-miR-127-3p	1355.29	
MIMAT0000384	mmu-let-7d* mmu-let-7d-3p	1272.16	
MIMAT0000229	mmu-miR-199a-5p	1259.88	
MIMAT0000670	mmu-miR-222-3p	1259.57	
MIMAT0000514	mmu-miR-30c-5p	1223.28	
MIMAT0000535	mmu-miR-29a-3p	1126.91	
MIMAT0000160	mmu-miR-150-5p	1114.54	
MIMAT0000534	mmu-miR-26b-5p	1076.65	

Data represent the average of 3 replicates. Yellow highlight indicates published reports which support that the miRNA is cardioprotective.

Figure 34: miRNA Expression Histograms

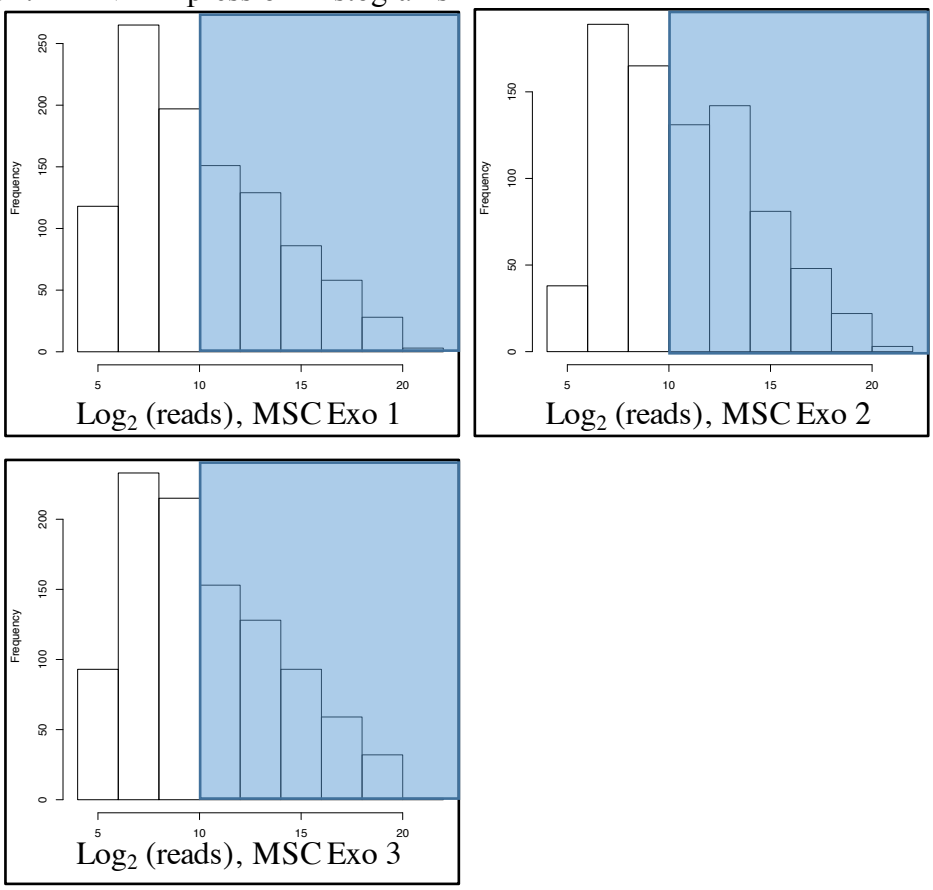

The frequency of the read count for each exosomal sample was plotted *vs*. the log2 of the reads. Counts below 32 (i.e., $\log_2(5)$, to the left on the x axis) were considered to be "noise" and were not plotted. The blue highlight covers the area of reads expressed at a level of 1024 or higher which corresponds to ~$\log_2(10)$.

The most abundant miRNA in MSC exosomes was mmu-miR-21a-5p. This miRNA is well known to be cardioprotective, as it increases in IPC, post-conditioning, and anesthetic-mediated cardioprotection[81-85, 226-228, 238]. We thus chose to follow up on this miRNA, and validated its presence in MSC exosomes through qPCR, compared against a standard curve of commercially available miR-21 mimic (Figure 35). Based on the molecular weight of miR-21 and the molarity as determined by its C_T, this correlates with 3.04×10^{12} copies per μg RNA in the exosomes.

Figure 35. miR-21 is Present in MSC Exosomes

Initial quantity (pmol)	Log (initial quantity)	CT	Slope	E*
200	2.301	13.39	-3.3135	2.00
20	1.301	16.93		100%
2	0.301	19.82		
0.2	-0.699	23.28		
0.02	-1.699	26.78		

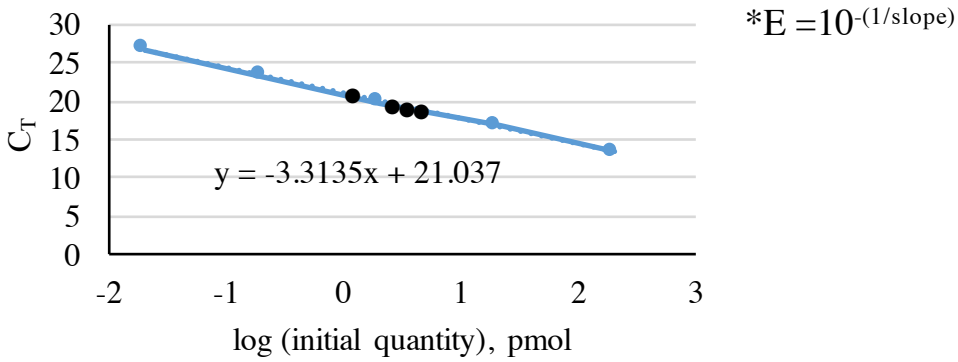

<u>Calculation of molarity and miR-21 copy number</u>
Average CT of 4 exosomal RNA samples = 19.7
(19.7-21.037)/-3.3135 = 0.404, the log of the initial quantity
Initial quantity = 10^0.404 = 2.53 pmol in 500 ng total RNA input
2.53 pmol * Avogadro's number = 1.52×10^{12} molecules
3.04×10^{12} molecules per μg exosomal RNA

Total RNA was extracted from 4 preparations of MSC exosomes and 500 ng of RNA were reverse transcribed. Realtime PCR was performed and the C_T was plotted (black circles) along with those of a standard curve of miR-21 mimic (blue circles). Primer efficiency was determined by plotting the CT *vs.* the log of the initial starting quantity (stock of known molarity from Qiagen). The slope of this line was used to calculate E as shown. The efficiency was 100%. The trendline equation was then used to calculate the log of the initial quantity of miR-21 in pmol. Then the quantity in pmol was converted to number of miR-21 molecules using Avogadro's number.

Tarbase 7.0 is a manually curated database of experimentally validated miRNA targets[239]. In order to identify potential miR-21 target genes, we searched this database and filtered for results that were validated by normal throughput methods including qPCR and Western blot. This returned 11 candidates, of which several are known to

play an injurious role in the context of I/R injury (Figure 36). The genes that we chose for follow up were Fas ligand (FasL), phosphatase and tensin homologue (PTEN), pellino 1 (Peli1), and programmed cell death 4 (PDCD4), based on literature which supports that they contribute to apoptosis after I/R injury and that reducing their levels is protective[6, 7, 81, 83, 205, 226, 240].

Figure 36. A Screenshot Showing the Search Results from Tarbase7 for Mir-21 Targets

mmu-miR-21-5p

Gene name	miRNA name	Methods	Pred.Score
Fasl (mmu)	mmu-miR-21-5p	RA WB	0.877
Pten (mmu)	mmu-miR-21-5p	WB	-
Pten (mmu)	mmu-miR-21-5p	qP	-
Gata3 (mmu)	mmu-miR-21-5p	qP	-
Peli1 (mmu)	mmu-miR-21-5p	RA qP	0.999
Btg2 (mmu)	mmu-miR-21-5p	IP qP	0.793
Spry2 (mmu)	mmu-miR-21-5p	RA WB	0.975
Pdcd4 (mmu)	mmu-miR-21-5p	WB	0.621
Pdcd4 (mmu)	mmu-miR-21-5p	qP IP	-
Spry4 (mmu)	mmu-miR-21-5p	WB	-
Smad7 (mmu)	mmu-miR-21-5p	qP	0.986
Il12a (mmu)	mmu-miR-21-5p	qP	0.822
Spry1 (mmu)	mmu-miR-21-5p	IP MA qP	0.989
Spry1 (mmu)	mmu-miR-21-5p	WB	-

The search results were filtered by Method Type to include normal throughput results. RA, reporter assay; WB, Western blot; qP, real time PCR; IP, immunoprecipitation; MA, microarray. Green indicates a positive result, red indicates a negative result.

mRNA Seq Results

The mRNA profile of MSCs and their exosomes was also determined through RNA-Seq. As with the miRNA profile, many mRNAs were differentially expressed (see Appendix B). We also determined the most highly expressed mRNAs in the MSC

exosomes with reads higher than 2000 counts (Appendix C). Some of these may have cardioprotective roles, which will be the subject of future studies.

miR-21 Knockout Exosomes Are Less Cardioprotective Than Wildtype Exosomes *In Vitro*

Conventional full-body miR-21a knockout mice[241] were obtained from Jackson Labs and their MSCs (KO MSCs) were isolated using the same procedure as for the wild-type (WT) mice. Their MSCs grew normally and released exosomes just like the WT MSCs. The KO MSCs still expressed a small level of miR-21, likely from other miR-21 family member genes which include miR-21b, and miR-21c. miRNAs are grouped into families based on the sequence of the mature miRNA or sequence/structure of the (precursor) pre-miRNA. Families of miRNAs share a conserved seed sequence, and thus might bind overlapping targets. The sequences of miR-21a, b, and c are shown in Figure 36. The miR-21 present in the KO MSCs was 0.2% of that of WT MSCs (Figure 37).

Figure 37. miR-21 Knockout MSCs Express miR-21 at Very Low Levels

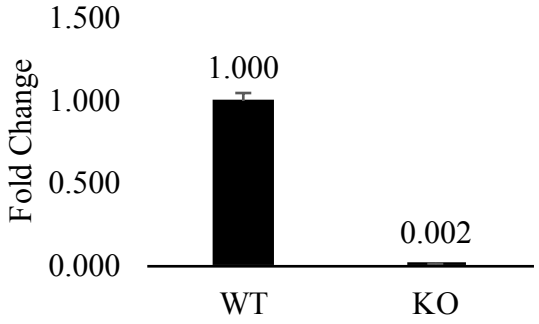

mmu-miR-21a	MIMAT0000530	U**AGCUUAU**CAGACUGAUGUUGA
mmu-miR-21b	MIMAT0025121	U**AGUUUAU**CAGACUGAUAUUUCC
mmu-miR-21c	MIMAT0025148	U**AGCUUAU**CAGACUGGUACAA

Total RNA was isolated from WT and KO MSCs, reverse transcribed, and analyzed by qPCR for miR-21 and U6. Data are shown as normalized fold change from WT control

MSCs (n=3). The sequences of miR-21a, b, and c are shown. The seed sequence is in bold, and differences in miR-21b and miR-21c from miR-21a are in red.

We next compared the ability of exosomes isolated from cultured KO MSCs and WT MSCs to reduce cell death from OGD. We isolated exosomes from equivalent volumes of conditioned media from both cell types, assayed their protein, and adjusted the treatments so that the amounts of exosomes used for pre-treatment were equal. We found that while the WT exosomes were significantly more protective than the KO exosomes, improving survival from 48±4.5% to 60±5.1%, the KO exosomes were still more protective than no exosome treatment, increasing the survival to 56±4.5% (Figure 38). Furthermore, the WT exosomes were noted at times (including in the experiment below) to exert a significant proliferative effect on the H9c2 cells after the overnight pre-treatment (black bars) which the KO exosomes did not demonstrate, indicating that miR-21 triggered cell division.

Figure 38. KO Exosomes Are Less Protective Than WT Exosomes

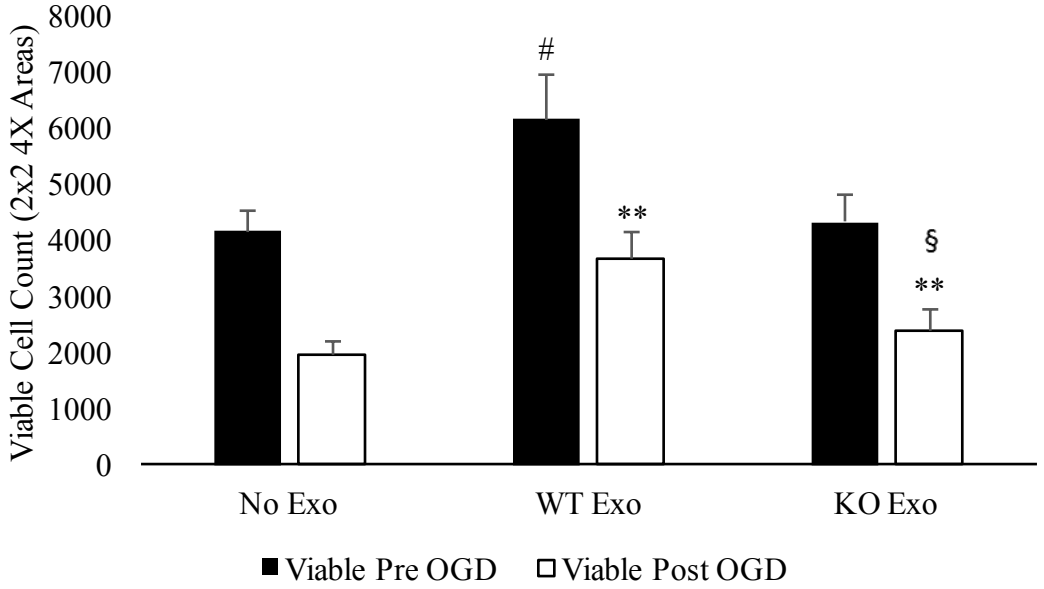

H9c2 cells were pre-treated with equal concentrations of WT and KO exosomes overnight, and then labeled with Hoechst and PI to determine viable cell counts before (black bars) and after OGD (white bars) (n=20). #$P \leq 0.001$ *vs.* Pre-OGD No Exo **$P \leq 0.001$ *vs.* Post-OGD No Exo, §$P=0.001$ *vs.* Post-OGD WT Exo.

To determine whether other time points than 24h pre-treatment would be protective, we performed (1) a short pre-treatment of one hour or (2) "per-conditioning" with exosomes present during the entire 18h OGD (Figure 39). We found that a 1-hour pre-treatment with either type of exosomes was not protective, and did not result in proliferation, while per-conditioning with either type of exosomes increased survival, from 34±7.0% to 63±8.6% (WT) or 57±4.6% (KO). The percent viability did not differ significantly between the WT and KO exosomes, indicating that the protection observed during per-conditioning does not require miR-21.

Figure 39. Preconditioning for 1 Hour Does Not Protect, While Per-Conditioning with Either WT or KO Exosomes Is Protective

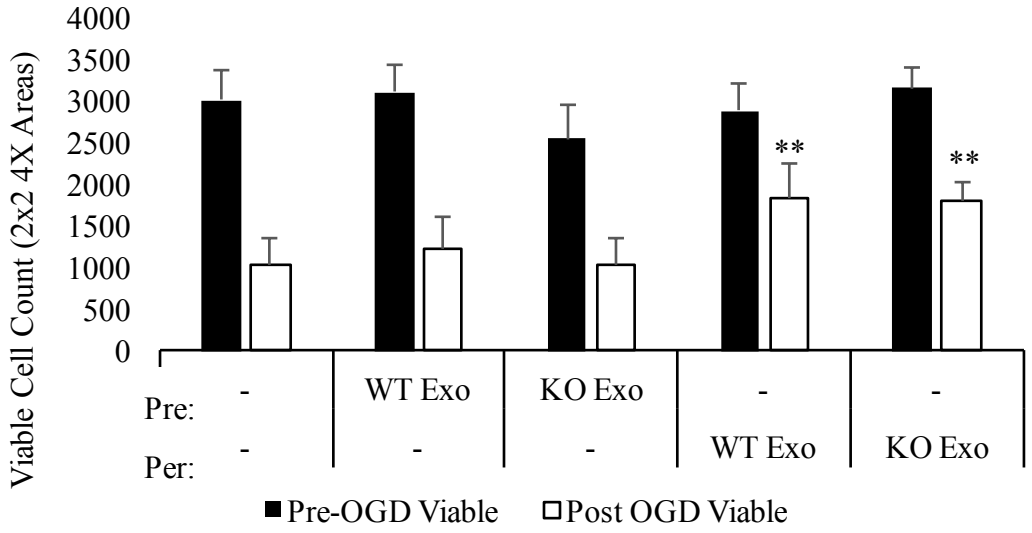

H9c2 cells were pretreated with exosomes in their growth media for 1 hour before OGD, or per-conditioned with exosomes in the ischemia mimetic solution during OGD. Viable cells were quantified before and after OGD by staining with Hoechst and PI and subtracting dead cell count from total cells (n=20). Error bars represent SD. **P<0.001 *vs.* Post-OGD No Exo. Pre-OGD viable counts did not show any statistically significant difference.

Reporter Assays for PDCD4 and FasL

In order to test whether miR-21 regulates its predicted target genes *PDCD4* and *FasL* through interactions with their 3'-UTR, luciferase reporter assays were performed. We co-transfected H9c2 cells with the reporter plasmid and a dose curve of miR-21 mimic, and noted significant decreases in the luciferase activity (Figure 40). We also transfected the H9c2 cells with either reporter plasmid, and then treated them with WT or KO exosomes to determine whether exosomal miR-21 could repress the luciferase activity. Both types of exosome could decrease luciferase activity, but the miR-21 KO exosomes showed a trend towards less effective repression. Taken together these data show that miR-21 represses *PDCD4* and *FasL* through specific interaction with their 3'-

UTR. However, based upon the fact that the KO exosomes will exhibit some repression, we conclude that miR-21 is not the only exosomal factor that can downregulate these genes.

Figure 40. miR-21 Reduces Luciferase Activity of PDCD4 and FasL 3'-UTR Reporters

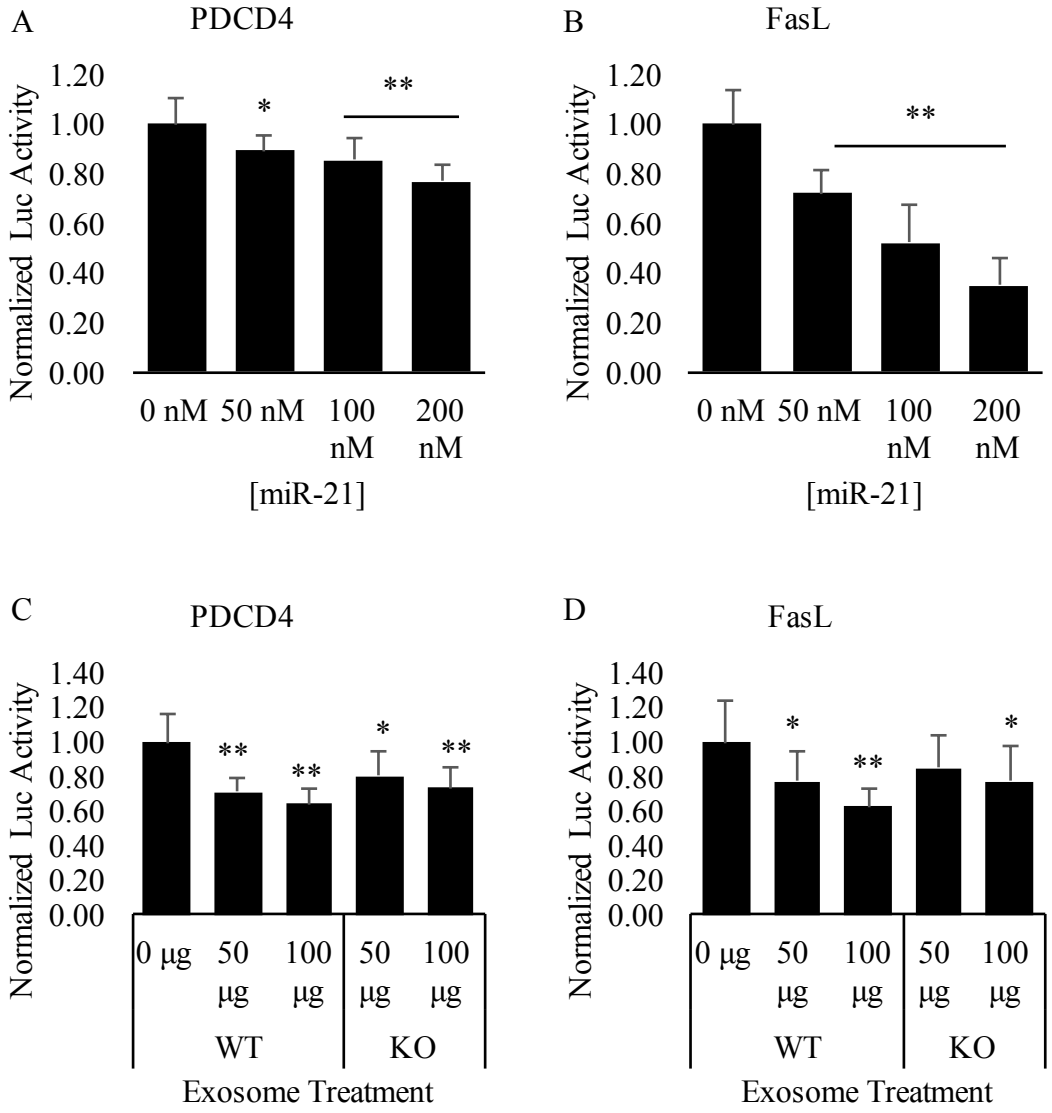

H9c2 cells were transfected with (A) PDCD4 or (B) FasL reporter plasmids and a dose curve of miR-21 mimic. (C-D) Cells were transfected with PDCD4 or FasL reporter plasmids and two doses of exosomes. After 18h, cells were stained with Hoechst and PI to quantify viable cells, and then luciferase activity was measured. Data are presented as

the raw luminescence values per viable cell, normalized to 0nM miR-21, with error bars representing SD (n=8-10). *$P \leq 0.05$, **$P \leq 0.001$ *vs.* 0 nM miR-21 or 0 μg exosomes.

***PDCD4* 3'-UTR Variants**

A search of the NCBI database indicated that in mice and rats, *PDCD4* has predicted alternative splicing. As shown in Figure 41E, splice variants 1 and 2 differ in the 5' region of the coding sequence but have the same 3'-UTR, while variant 3 has the same coding sequence as variant 2, but a large portion of the middle of the 3'-UTR is alternatively spliced, resulting in removal of the miR-21 binding site. To determine which variant predominates in rat H9c2 cells, mouse HL-1 cells, neonatal mouse ventricular myocytes (NMVM), and mouse heart, we designed primers to amplify both the full-length and spliced RNA by traditional and real time PCR. We found that the predominant form of the 3'-UTR was the spliced form in heart and cell samples according to real time qPCR and traditional PCR with product size analysis on an agarose gel. The sizes of the bands correspond to the predicted sizes of the full length (F) and spliced (S) products in mouse and rat cells. In HL-1 cells, only the spliced product is visible. In mouse heart tissue and neonatal cardiomyocytes, there is a strong band at the predicted size of the spliced product, and the full length product is faintly visible. Its intensity does not seem to change with the treatment (control vs. MSC exosomes). In H9c2 cells, the full length product is again visible, though far less intense than the spliced product. Interestingly, the intensity of the full length product appears to decrease remarkably with the transfection of miR-21 mimic, supporting that miR-21 mediates degradation of variant 3 mRNA.

Figure 41. The Predominant Splice Variant of *PDCD4* in Cells and Mouse Heart Lacks the Portion of the 3'-UTR Containing a Predicted miR-21 Binding Site

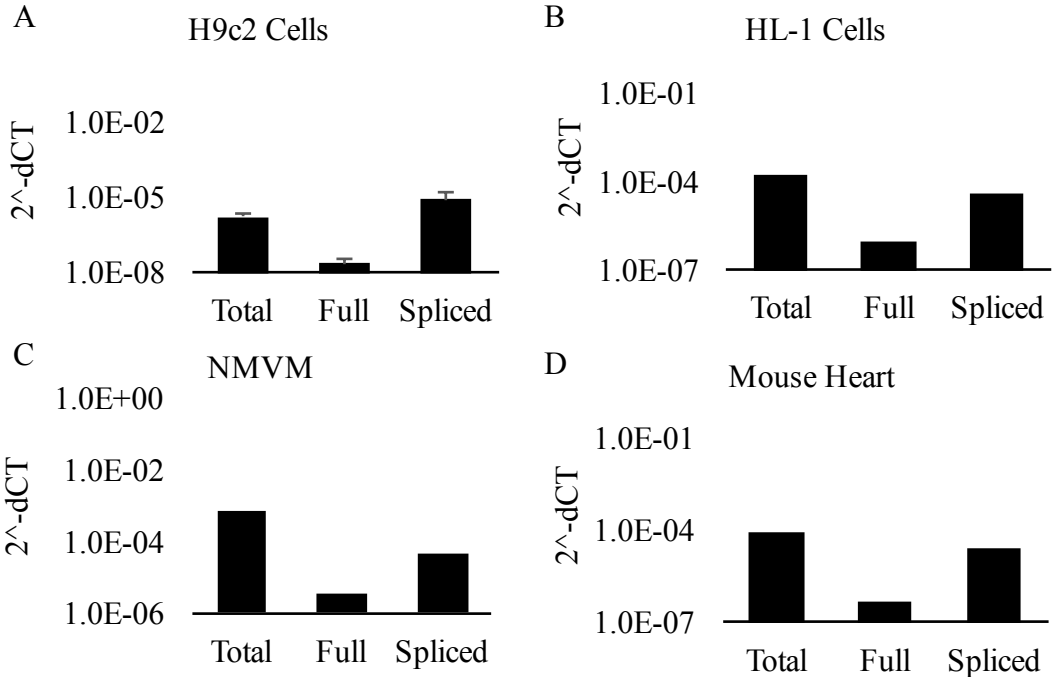

E. Primer Design Strategy for 3'-UTR Variants

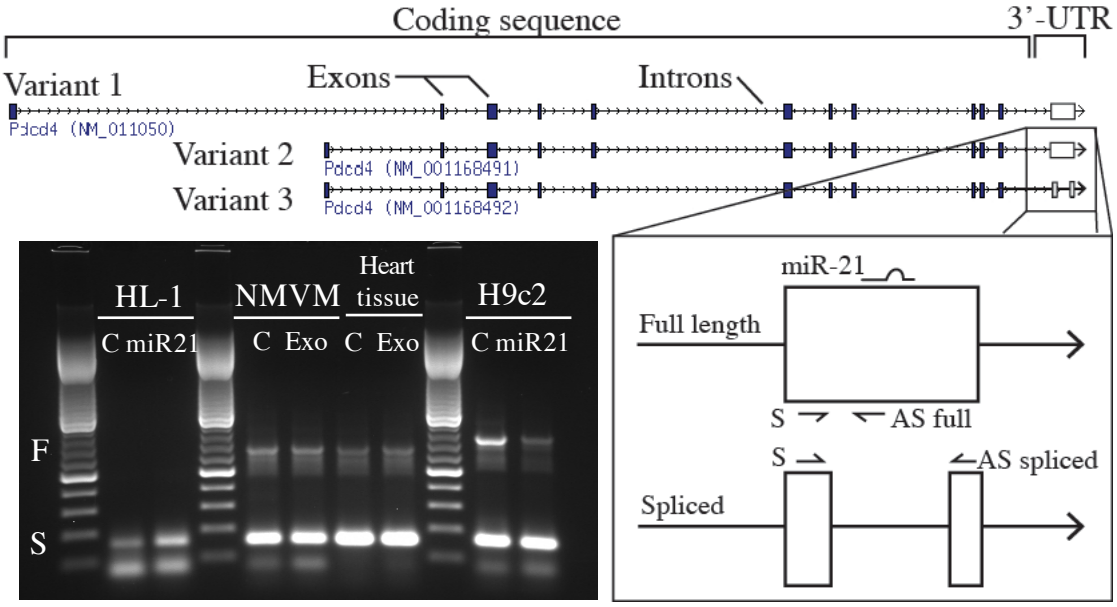

(A-D) RNA was isolated and reverse transcribed. Then real time PCR was performed to amplify the total, full length, and spliced 3'-UTR variants. Expression was normalized to 18S and bars represent the 2^-dCT values (n=1-2/condition). (E) A schematic of the structure of *PDCD4* variants 1, 2, and 3. The locations of the primers within the 3'-UTR

of *PDCD4* are shown. The total *PDCD4* primers are not shown but are located in the coding region. The PCR products from HL-1 cells, NMVMs, heart tissue, and H9c2 cells were run on an agarose gel. The cell lines were transfected with Neg Ctrl siRNA(C), or miR-21 mimic (miR21), and NMVMs and heart tissue were treated with saline (C) or MSC exosomes (Exo). F=full length product, expected size 681 bases in mouse cells and 777 in rat cells. S=spliced product, 157 bases.

Despite the apparent preponderance of the mRNA lacking the miR-21 binding site in the 3'-UTR, miR-21 robustly downregulates PDCD4 protein (Figure 43), indicating that there must be other binding sites, perhaps within the coding sequence. A search of the DIANA microT-CDS database[242] revealed two binding sites within the coding sequence of *PDCD4* which may mediate miR-21's effects (Figure 42). All of the human splice variants express the full 3'-UTR, according to NCBI.

Figure 42. A Screenshot from DIANA MicroT-CDS Shows Two Binding Sites Within the Mouse *PDCD4* Coding Region

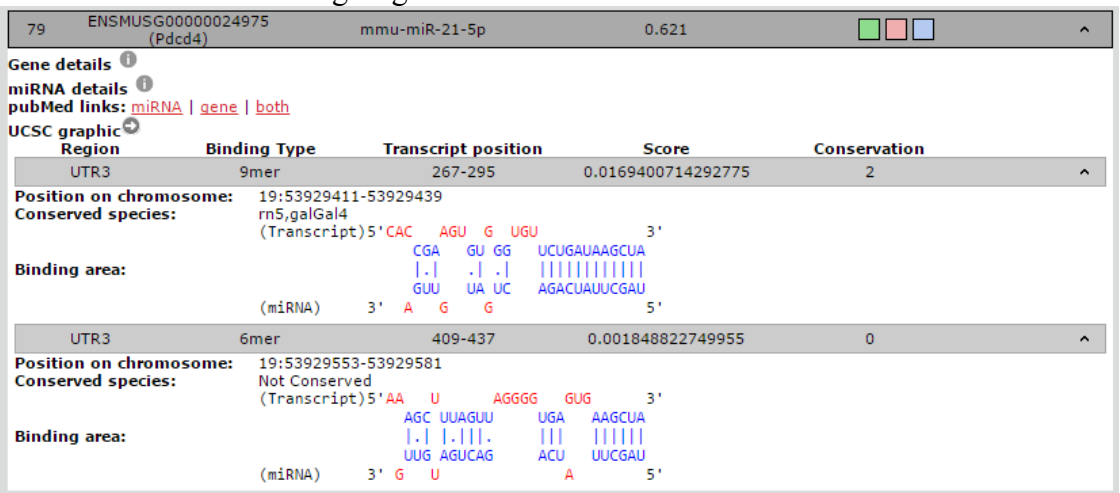

Protein and RNA Levels of Predicted miR-21 Target Genes After miR-21 Transfection and Treatment of Cells with Exosomes

Transfection of H9c2 cells with miR-21 resulted in significant downregulation of FasL, PDCD4, and PTEN *vs.* treatment with negative control siRNA, with trends towards decreased protein levels of Peli1 at 24 and 48h which were not always significant (Figure 43).

In general, miRNA may or may not mediate degradation of its mRNA targets (depending on the extent of base pairing outside the seed region). To test whether miR-21 decreases the mRNA level of its target genes, we performed real time PCR 24h after miR-21 transfection, and found that total *PDCD4* decreased significantly, while spliced *PDCD4* showed a trend towards a decrease that did not reach statistical significance. Interestingly, *PTEN* increased significantly and *FasL* also showed a trend towards an increase, while *Peli1* did not change (Figure 44).

When cells were treated with WT exosomes, a similar effect was observed to that of transfection of miR-21, with significant downregulation of PDCD4 and FasL. However, when cells were treated with KO exosomes, these changes were not observed, which further supports a role for miR-21 within exosomes (Figure 45).

Figure 43. Transfection with miR-21 Mimic Reduced Steady State Protein Levels of Predicted miR-21 Target Genes *in vitro*

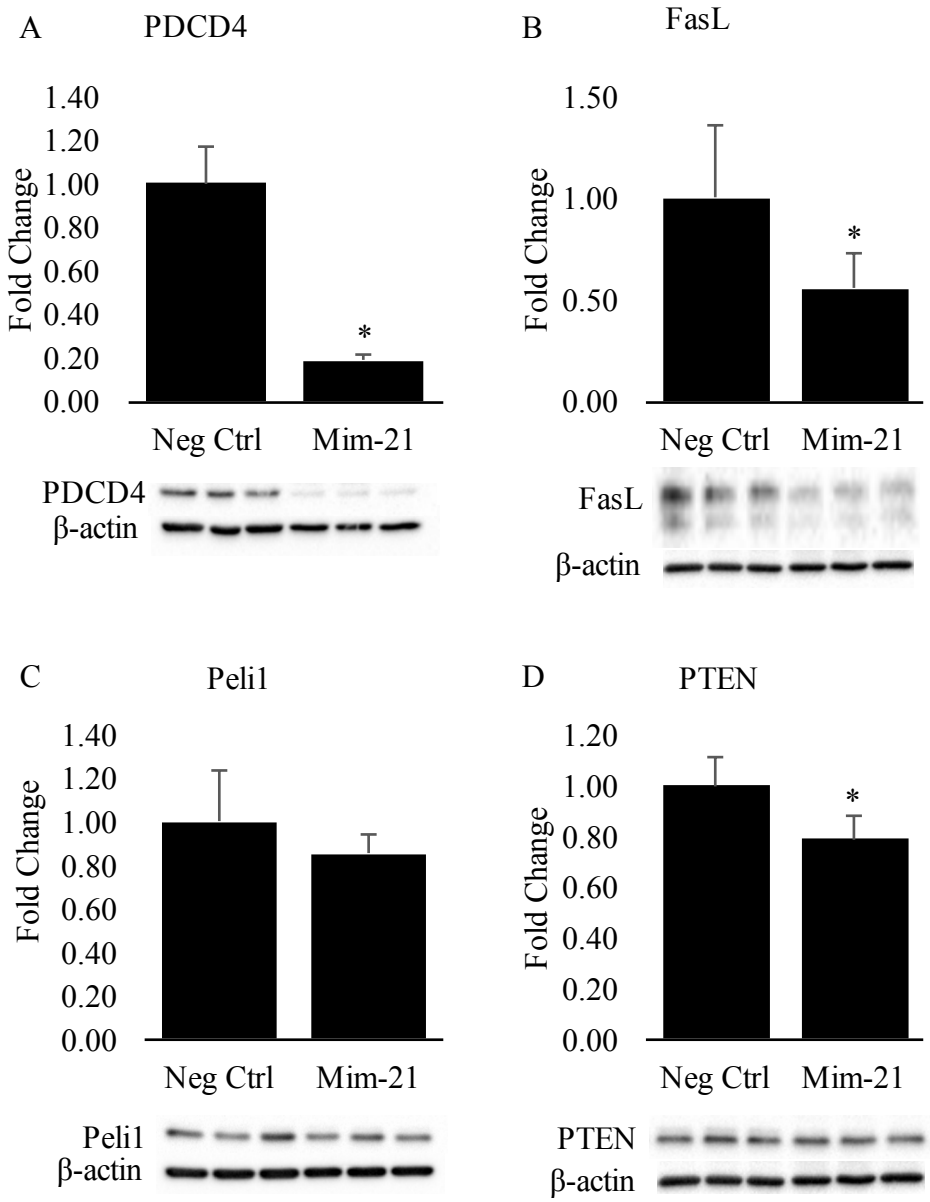

H9c2 cells were transfected with 200 nM Neg Ctrl siRNA (Neg Ctrl) or miR-21 using Lipofectamine 2000. Total protein was extracted using RIPA buffer 24 to 48h later, and 5-10 μg of protein were analyzed by Western blot (n=3-6). Band intensities were normalized to β-actin, error bars represent SD. *$P<0.05$ *vs.* Neg Ctrl.

Figure 44. RNA Levels of miR-21 Target Genes 24h after miR-21 Transfection

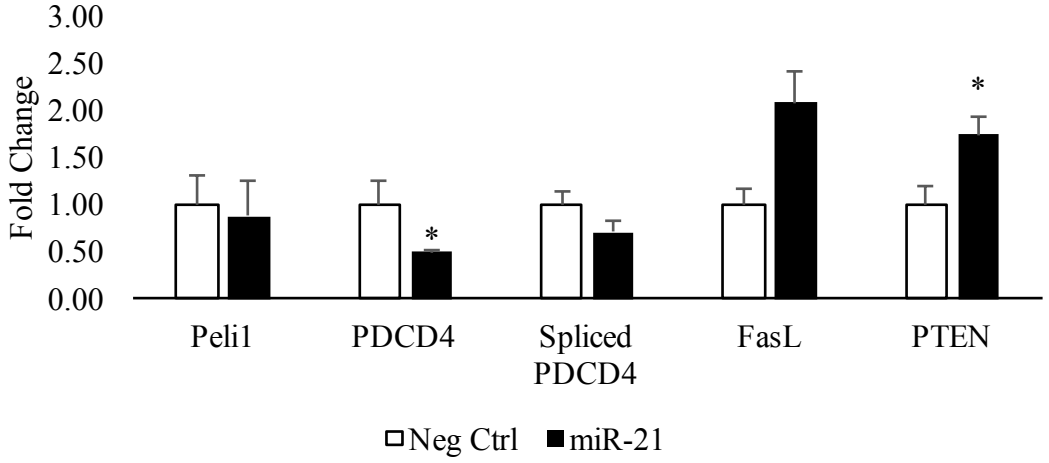

H9c2 cells were transfected with 200 nM Neg Ctrl siRNA or miR-21. RNA was extracted from the cells 24h later and reverse transcribed for analysis by real time PCR. CTs were normalized to 18S and expressed as fold change *vs.* Neg Ctrl (n=3). Error bars represent SD. *P<0.05 *vs.* Neg Ctrl.

Figure 45. Treatment of Cells with WT Exosomes Reduces Expression of PDCD4 and FasL

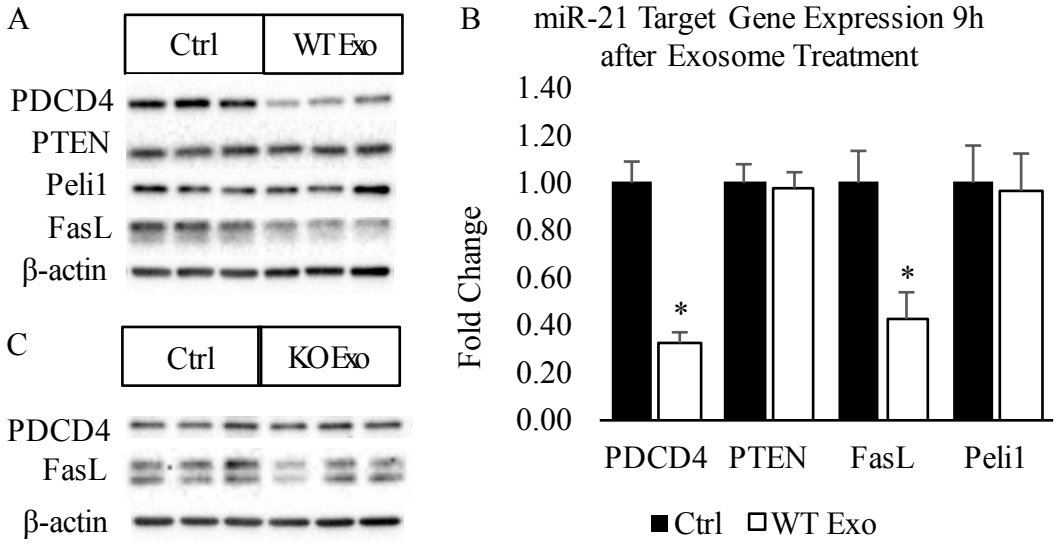

A. H9c2 cells were treated with WT exosomes for 9h, followed by protein extraction and Western blot. B. Quantification of band intensities normalized to β-actin and expressed as fold change *vs.* Ctrl (n=6). *P<0.001. C. H9c2 cells were treated as before, but with KO Exo (n=6). Error bars represent SD.

Pericardial Sac Injection of WT and KO Exosomes

Because the *in vitro* data supported that exosome uptake has protective effects in cells, and that miR-21 mediates these effects at least in part through downregulation of PDCD4 and FasL, we next tested whether WT and KO exosomes were protective when injected into the pericardial sac of mice 24h prior to I/R injury. We determined infarct size as a percentage of the area at risk 24h after I/R injury, and found a significant 68% decrease in infarct size after WT exosome injection (Figure 46). The KO exosomes also caused a trend towards a decrease, which was not significantly different from the saline control group (P=0.22).

Figure 46. Injection of WT Exosomes Reduces Infarct Size in Mice

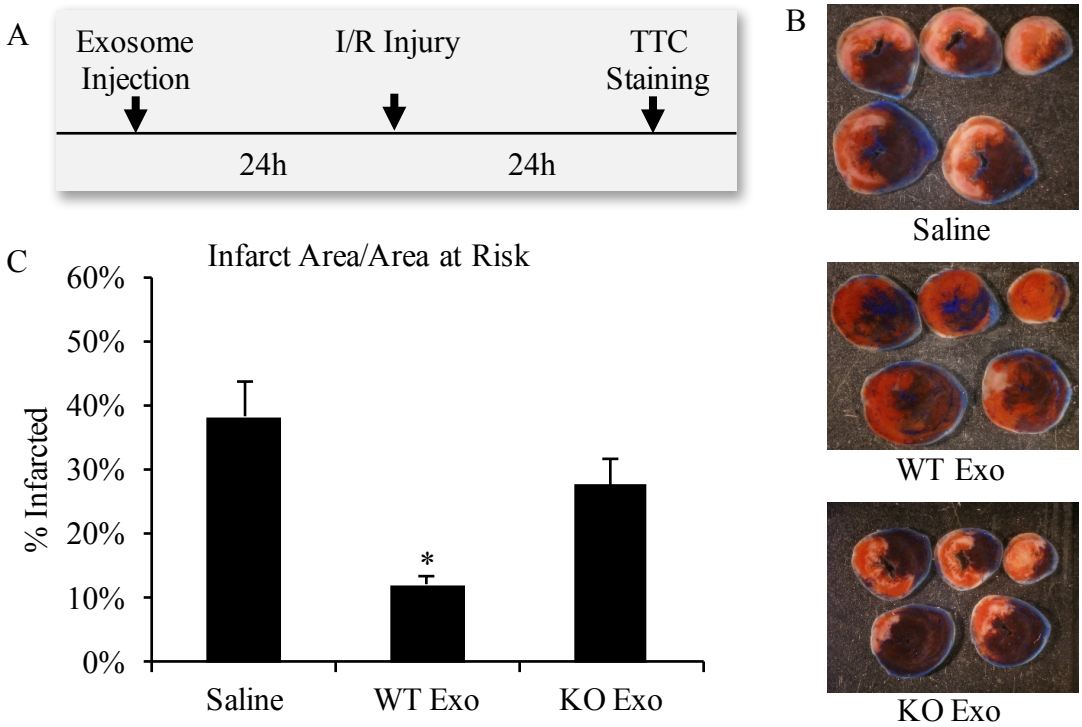

A. Experimental timeline: on Day 0, mice received an injection of exosomes or saline to the pericardial sac and were allowed to recover overnight. They then underwent I/R injury, and the next day hearts were stained with TTC, frozen, and sectioned for infarct analysis. B. Representative hearts from each group. C. Quantification presented as the

average infarcted percent of the risk region, error bars represent SE (n=8). *P<0.001 *vs.* saline.

Expression of miR-21 Target Genes 24h After Exosome Injection and 6h after I/R Injury

To determine whether the protective effect we observed *in vivo* was due to downregulation of miR-21's pro-apoptotic target genes, we next tested the expression of PDCD4, PTEN, Peli1, and FasL 24h after exosome injection. We did not observe a significant decrease in protein levels of these genes, though there was a trend towards a decrease in FasL (18% decrease *vs.* saline), and interestingly, a trend towards increased expression of PDCD4 (Figure 47A-B). This led us to question whether the miR-21 being taken up was having a priming effect such that it bound its target mRNAs, but changes in target protein levels would only be apparent after a relevant stimulus such as I/R injury. Real time PCR analysis showed no significant changes at 24h after exosome injection other than a 51% decrease in PDCD4 full length mRNA with WT exosome injection (Figure 47C). This is in agreement with PCR data from the miR-21 transfected H9c2 cells, which only showed significant decreases in PDCD4 levels but not other target genes. We therefor tested the levels of these proteins after exosome injection followed 24h later by I/R injury, and we then observed significant decreases in all four of these proteins 6h after I/R (Figure 48).

Figure 47. Expression of PDCD4, Peli1, and FasL 24h after Injection of WT or KO Exosomes

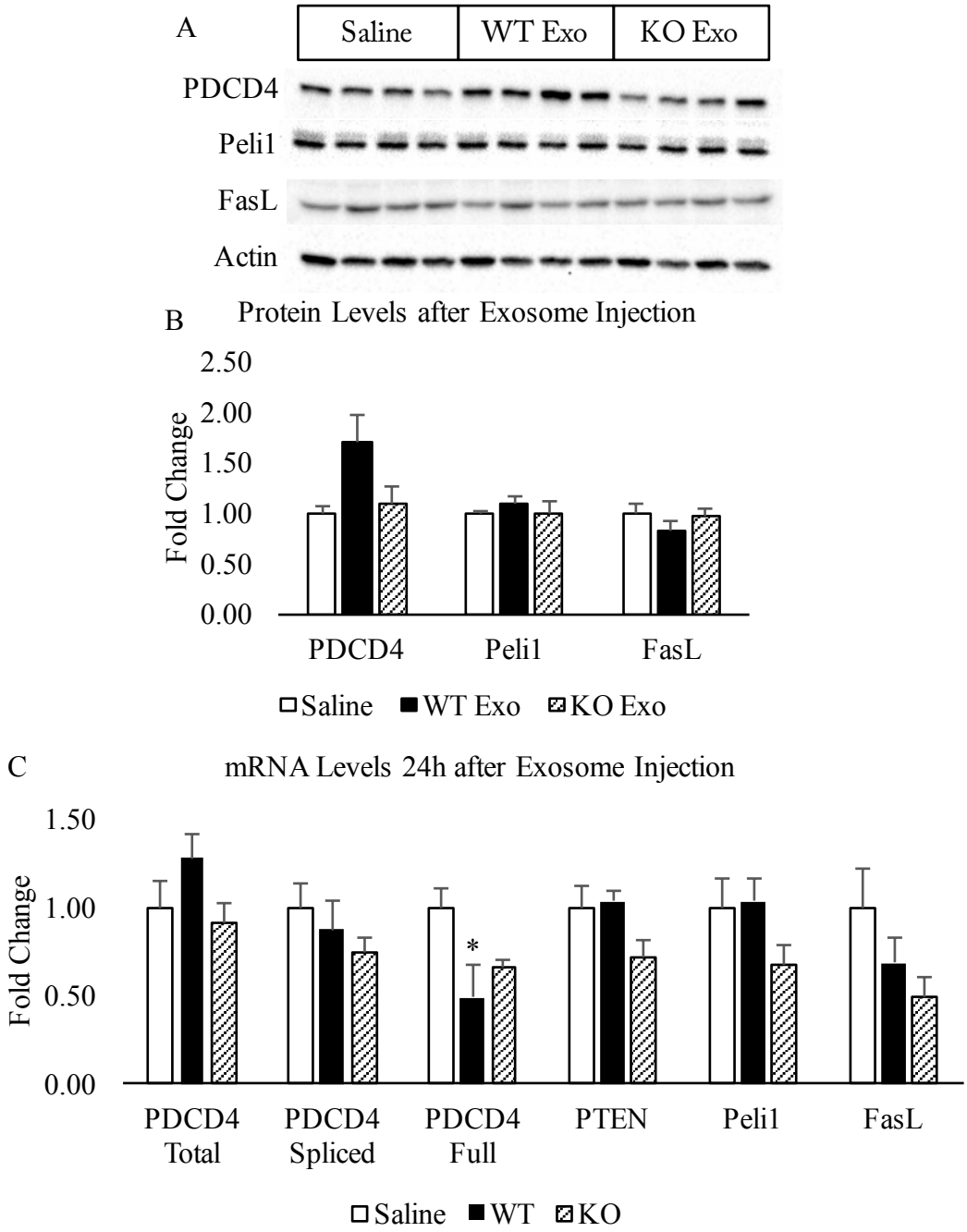

WT and KO exosomes were injected into the pericardial sac of mice, and hearts were removed 24h later. (A) Total protein was extracted and analyzed by Western blot (n=4). (B) Quantification of band intensities normalized to actin and displayed as fold change vs. Saline. (C) RNA was extracted and reverse transcribed for real time PCR analysis.

Data were normalized to 18S and are shown as the average fold change *vs.* Saline (n=4). Error bars represent SEM. *P=0.038 *vs.* Saline.

Figure 48. WT Exosomes Decrease Expression of PDCD4, PTEN, FasL, and Peli1 6 Hours after I/R Injury

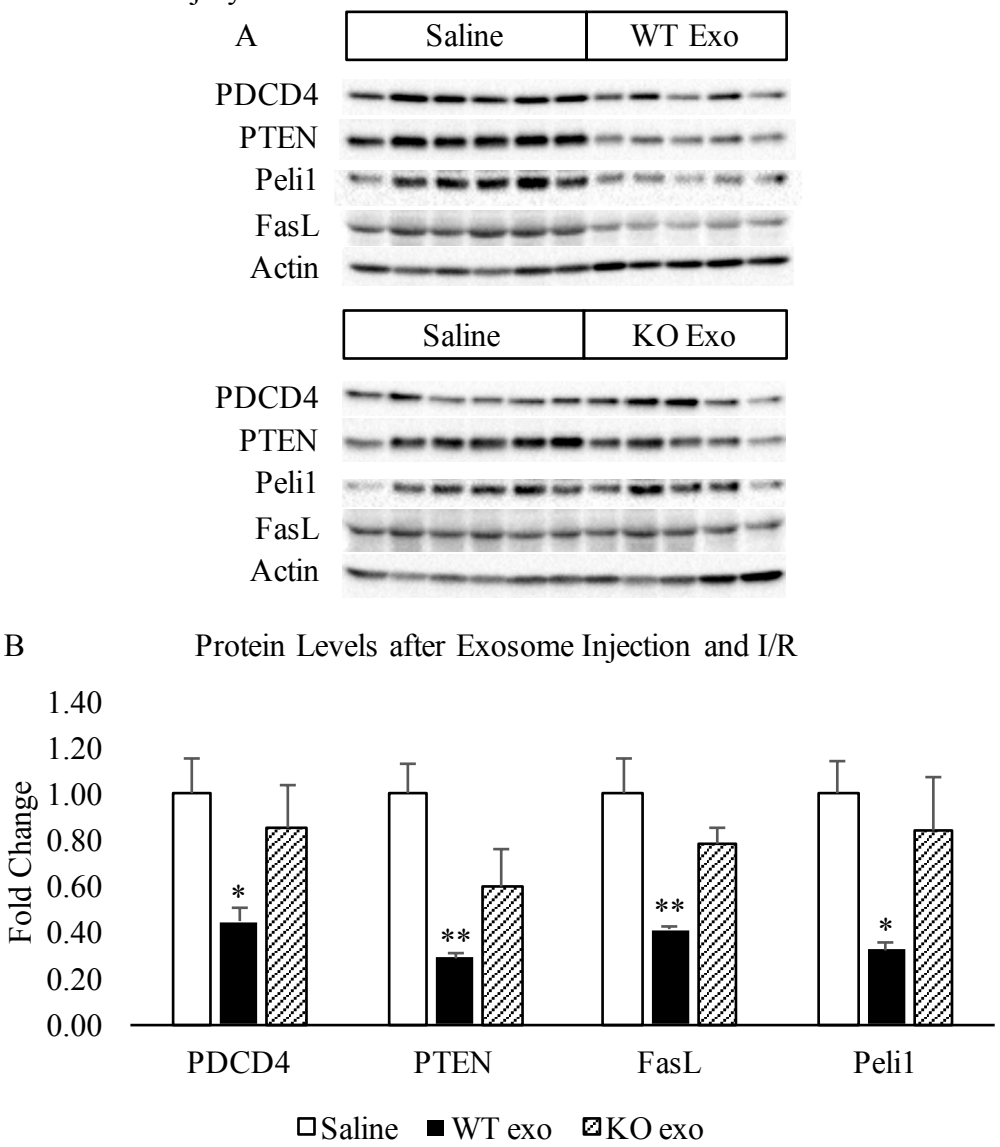

Saline, WT exo, or KO exo were injected into the pericardial sac of mice (n=5-6) 24h prior to I/R injury. Mice were sacrificed 6h later and protein was isolated from the infarct zone of the heart for Western blot analysis. (B) Band intensities were quantified and data were normalized to Actin. Bars represent the normalized average fold change vs. Saline controls with error bars representing SEM. *P<0.05; **P<0.005 *vs.* Saline.

CHAPTER 4

DISCUSSION

SUMMARY OF HYPOTHESES AND RESULTS

This section briefly summarizes the central hypotheses of each research aim, and the results of the experiments undertaken to test them, which have contributed to our understanding of how miRNA is involved in cardioprotection from IPC and stem cell paracrine effects.

Hypothesis 1

We hypothesized that a network of miRNAs and heat shock proteins are regulated in response to preconditioning. Because each miRNA has many potential mRNA targets, and most mRNAs have many potential miRNA binding sites in their 3'-UTRs, we were interested in finding miRNAs that co-regulated targets with a common function, which could be a powerful way to induce gene-expression mediated cardioprotection, such as that which occurs during IPC. To investigate this hypothesis, we selected a set of heat shock proteins which two preliminary datasets (array and sequencing data) suggested were increased by IPC, including Hsp40/Dnaj proteins, inducible Hsp70 family members, and Hsp90. We confirmed that indeed the mRNA levels of *Hsp70 (Hspa1a* and *Hspa1b), Hsp90aa1, Dnaja1* and *Dnajb4* increased 3 hours after IPC, leading to significant protein increases 6 hours after. We then selected a handful of miRNAs which were predicted to regulate them, including miR-148a/b, miR-

30b, and let-7a*, and tested whether this regulation actually occurs at the protein level. We confirmed that the miRNAs act synergistically to regulate the heat shock proteins of interest in two cardiomyocyte cell lines.

Hypothesis 2

We hypothesized that preconditioning of cardiomyocytes leads to increased exosomal loading of protective miRNA, which exerts pro-survival effects on transplanted MSC. Because cardioprotection from postconditioning[162] or electro-acupuncture[165] have been shown to enhance the engraftment of transplanted stem cells through changes in the myocardial microenvironment[162], we wanted to test the role of exosomes, which are an important mediator of paracrine communication that have never been studied in this context. Preconditioning the HL-1 cells by HPC induced the expression of several miRNAs with known pro-survival or regenerative effects, including miR-19 and 20[243, 244]. HPC also upregulated several protective mRNAs. However, RNA-Seq did not detect corresponding increases in these RNAs in the exosomes produced by the HL-1 cells, and thus did not support Hypothesis 2. This does not rule out the possibility that exosomes from the preconditioned intact heart do act in this manner to enhance stem cell engraftment in the harsh environment of the post-I/R heart.

Hypothesis 3

We hypothesized that MSC exosome-mediated cardioprotective effects are mediated through transfer of protective mRNA and/or miRNA. Having found that MSC exosomes could decrease cell death in H9c2 cells after OGD after an 18h pre-treatment, a time point that is consistent with regulation of protein levels in response to the

exosomes, we sequenced their RNA content to reveal their profile of miRNA and mRNA. We determined that miR-21 was the highest expressed miRNA in the exosomes. Because miR-21 is a well-known cardioprotective miRNA, we fine-tuned the hypothesis to investigate the role of miR-21 in exosome-mediated cardioprotection. Experiments yielded the following major results. First, miR-21 and wildtype MSC exosomes regulated the expression of known miR-21 target genes in vitro and in vivo, while miR-21 knockout exosomes did not. Second, pre-treatment of H9c2 cells or pericardial sac injection with wildtype MSC exosomes *in vivo* was protective, while miR-21 knockout exosomes were not. Taken together, these data support the hypothesis that miR-21 is a key mediator of cardioprotection from MSC exosomes.

THE ROLE OF MICRORNA IN ISCHEMIC PRECONDITIONING

The goals of Aim 1 were to (1) build upon previous work performed in the lab and further characterize the gene expression response of the heart to IPC; (2) to identify miRNAs that could be manipulated experimentally to induce a key aspect of this gene expression response by acting as nodes in a network; (3) to establish whether these miRNAs interact with the 3'-UTR of the genes of interest; and (4) to determine whether overexpression or knockdown of these miRNAs results in changes in the expression of these genes consistent with preconditioning.

Gene Expression after IPC and HPC

The IPC microarray dataset was originally published in 2010 and detected 1376 significant differences between wildtype sham and IPC mice. The RNA-Seq experiment was performed in 2013, and detected 292 significant differences. These two datasets overlapped by 61 genes. In most cases, the array data and the sequencing data were in

agreement with regard to the direction of the change (up or downregulated), with the exception of growth arrest and DNA-damage-inducible 45 beta (Gadd45b) and potassium voltage gated channel, Shab-related subfamily, member 1 (Kcnb1). Nearly all of the genes increased after IPC, with only 6 genes that decreased in both datasets. Comparing these two datasets allowed us to select genes of interest for follow-up more confidently. We chose to focus on the heat shock proteins because there were several that were upregulated strongly by IPC, all of which were NF-κB dependent, and we validated these by real time qPCR. Additionally, we evaluated expression of Hsp70.3, which was not included in the microarray dataset, but which we know is required for in IPC from previous work in the lab[38, 87].

Knowing that Hsp70 was upregulated at 24h after IPC[87], we tested whether Hsp90 or the Hsp40 family members were also increased at that time, and found that they were not. We then tested an earlier time point, 6h, and found that they were elevated then. Hsp70.1 and Hsp70.3 exhibited the greatest fold increases at the mRNA level at 3 hours after IPC, perhaps this is why Hsp70 is the only protein that is still elevated the next day.

It is known that late IPC requires new protein synthesis[245], but it is unclear whether early IPC also requires new protein synthesis. Rizvi *et al.*[245] showed that 2 hours after IPC, protein synthesis nearly doubled as measured by the incorporation of ^{3}H leucine. Rowland and colleagues also found that in the isolated perfused rat heart, IPC increased myocardial protein content, and blocking translation with cycloheximide blocked the protection from early IPC[35], a finding that was verified in the isolated rabbit heart[34]. Conversely, another group[246] found that early IPC was not blocked by

cycloheximide in an intact rabbit model. Our data are consistent with the observed increase in protein synthesis in the hours after IPC. Synthesis of Dnaja1, Dnajb4, and Hsp70 and Hsp90 likely function to assist with the enhanced production of other cardioprotective late phase mediator proteins such as iNOS and COX2, in addition to helping to refold proteins damaged by oxidative stress in the instance of subsequent I/R injury.

Studies using Hsp70.1/.3 knockout mice have shown that Hsp70 is required for late IPC[38] but it is unknown whether the increases in Hsp40 levels that occur during early IPC are required, for either early or late IPC. A Dnaja1 knockout mouse was made but is currently unavailable for purchase (embryonic stem cells are held in the Knockout Mouse Phenotyping Project repository).

In order to test miRNAs that are protective in the context of myocardial I/R injury, we established *in vitro* models of hypoxic preconditioning and simulated I/R injury. The HPC protocol remarkably reduced cell death upon subsequent simI/R. However, expression of heat shock proteins did not seem to constitute an important aspect of this protection, as they were not strongly upregulated after HPC, and their forced expression by heat shock did not protect HL-1 cells from simI/R. For a discussion of the genes that were regulated by HPC, see Section 4.3.2. While heat shock has not been established in HL-1 cells as a protective stimulus against hypoxia or simulated ischemia, Brundel *et al*.[247] showed that it protected them from tachypacing-induced myolysis in their *in vitro* atrial fibrillation model. By contrast, a few publications have reported that overexpression of heat shock proteins mediated by heat shock or gene transfer is protective in H9c2 cells upon subsequent hypoxic challenge[248-250]. Our

experiments with heat shock of HL-1 cells and H9c2 cells did not reproduce these findings.

Noting that the HSPs of interest in the murine heart are induced by heat shock in HL-1 cells, and that they express them similarly to the pattern observed in the heart, we decided that the HL-1 cells would be an acceptable model for testing the effects of different miRNAs on heat shock protein expression under control and heat shock conditions.

miRNA/HSP Network

We then set out to identify miRNAs that could be manipulated experimentally in order to affect the expression of Hsp70, Hsp90 and Hsp40 family members. Based on the concept of miRNAs as nodes in a network, we identified miRNAs predicted to target 3 or more of the genes by creating a Cytoscape network from a database including every miRNA predicted (with stringent criteria) to target each heat shock protein of interest. By cross-referencing all of the available datasets within the lab describing miRNA in cardioprotection, including a PCR array, miRNA-Seq on IPC heart tissue, and miRNA-Seq on HPC HL-1 cells, we selected 4 miRNAs for follow-up. miR-148a, which was predicted to target Hsp70 and Dnaja1, was of interest because its expression is very high in both the heart tissue and HL-1 cells, and in HL-1 cells it decreases with HPC. miR-148b showed moderate expression, but decreases with IPC/HPC in both datasets. The array data also showed that miR-148a and b decrease after IPC. The genes for miR-148a and b are located within the introns of other genes, and their expression is regulated by methylation state of their promoters[251]. Two recent studies have identified miR-148a as a regulator of NF-κB signaling through regulation of RelA[252] (Bao 2014), and IκB kinase-

β (IKK-β, [253]). Thus a reduction in miR-148a would support enhanced NF-κB signaling, the activation of which is known to be protective in the context of IPC.

miR-30b was predicted to target Dnaja1, Dnajb4 and Hsp90aa1. All three datasets showed a decrease in miR-30b expression after IPC, which has also been observed by others[83]. MiR-30b has an intergenic location on chromosome 15, and its expression is regulated by NF-κB[254]. Inhibition of miR-30b has been shown to be cardioprotective through de-repression of its target gene cystathione γ-lyase [255], which produces the protective mediator H_2S. Furthermore, it has been confirmed to target the important anti-apoptotic protein Bcl-2[254], so decreases in miR-30b would be expected to be cardioprotective. On the other hand, it has also been reported to target Cyclophilin D, a component of the mitochondrial permeability transition pore, and thereby to be protective in a cardiac-specific overexpression mouse model [256]. Mimic transfection of miR-30b in H9c2 cells was also shown to decrease apoptosis in a model of hypoxia-reoxygenation[257].

Lastly, let-7a-1-3p (let-7a*) was predicted to target Hsp70.1, Dnaja1, and Dnajb4. Let-7a* is the passenger strand of the let-7a transcript, which has an intergenic position on chromosome 13 in the mouse. In HEK and HeLa cells, overexpression of Argonaute3 (Ago3) but not other Argonaute family members 1, 2, or 4, was shown to increase the expression of let-7a* over its relatively low baseline expression. This effect appears to be selective for the passenger strand of let-7a*, because overexpression of Ago3 did not increase expression of 33 other miRNA passenger strands tested[258]. Ago2 is the canonical active enzyme in RISC complexes, but Ago3 has an intact catalytic motif[259], and let-7a* was shown to be a functional miRNA in that it repressed luciferase

activity and downregulated a target gene, Rab10[258]. Little is known about its role in the heart.

Reporter Assays in Support of 3'-UTR Targeting

The next step was to confirm whether the predicted targets were *bona fide* targets of each miRNA by using luciferase 3'-UTR reporter assays. miR-148a/b was confirmed to target Hsp70.1 and Hsp70.3, miR-30b targeted Hsp90aa1, and let-7a* targeted Dnajb4. A key aspect of our hypothesis is that miRNAs act synergistically to regulate expression of their target genes. We tested this idea through use of luciferase assays in which we compared the decrease in luciferase activity observed with two different miRNAs with different efficacies at reducing luc activity. Transfection of 200 nM of miR-449c reduced activity to about 40%, while the same dose of 148a reduced it to about 60%. If no synergy occurred, when cells were transfected with a 50/50 mix (100 nM of both) we would expect the reduction in luc activity to be intermediate between the two, about 50%. However, what we observed was repression that was greater than either mimic alone, down to 29.8%. This suggests that two or more miRNAs can act additively to repress protein levels in the heart as has been reported, for example, miR-451 and miR-144, which synergistically target CUGBP2[260].

Luciferase 3'-UTR reporter assays have some limitations (see Chapter 2 p64). They are useful for determining whether a miRNA can interact with a predicted binding site in a given 3'-UTR, but ultimately effects on protein levels must be determined experimentally.

Knockdown and Mimic Transfection of miRNAs: Effect on HSP Levels

We next tested the effect of transfection of mimics and inhibitors on protein levels. Based on the luciferase data, we expected to find that Hsp70 would be regulated by miR-148a and b, and this was the case. While mimic transfection of either miRNA was sufficient to reduce Hsp70 protein levels after heat shock, inhibition of both miRNAs led to a significant increase in Hsp70 expression. This, together with the luciferase data from the Hsp70.1 reporter assay, supports that miR-148a and b are functionally redundant (they will therefore be referred to as miR-148a/b hereafter). It should also be noted that while the 3'-UTR of Hsp70.3 is known to be alternatively polyadenylated in response to heat shock[87], the miR-148a/b binding site is retained.

The luciferase data did not indicate that Hsp70 was a *bona fide* target of let-7a*, and indeed the Western blots did not show that Hsp70 protein levels changed when let-7a* was overexpressed or inhibited. However, to our surprise, Hsp70 protein levels did change in response to the combination of miR-30b and let-7a*, though miR-30b wasn't predicted to target either Hsp70.1 or Hsp70.3. The mimics downregulated Hsp70 at 24 and 72h, while the inhibitors showed a trend towards increasing its expression. With the addition of inhibitors of miR-148a/b, this increase became significant at both 24 and 72h. Hsp70 protein levels were not assayed after transfection of miR-30b mimics or inhibitors alone, because it was not a predicted target of miR-30b. This would be an interesting future study, in light of recent publications showing miR-30b to regulate other cardioprotective genes and signaling cascades[254-257, 261].

Because expression of miR-148a and b at baseline was high in HL-1 cells (18,500 and 4000 reads respectively), we expected to find that knocking it down would

increase the protein level of Dnaja1, which also had significant expression at baseline (compare to very low baseline levels of Hsp70). Dnaja1 did decrease slightly in response to miR-148a/b mimics, but contrary to our expectation, inhibition of these miRNAs did not induce upregulation at the protein level. This is consistent with the lack of interaction observed in the reporter assay. If the miRNAs do not bind to the 3'-UTR, they don't repress expression of the protein, and their removal would not lessen such repression. It is possible that downregulation observed in response to miR-148a/b mimic was indirect.

Dnaja1 was not affected by mimic transfection or knockdown of miR-30b or let-7a* individually or together. However, Figure 25 shows that the addition of miR-148a/b mimics to miR-30b and let-7a* does induce significant downregulation. There was a trend towards upregulation of Dnaja1 at 72h in both Figure 24 and 25, which did not reach statistical significance.

Luciferase data supported that Dnajb4 would be regulated (perhaps weakly) by let-7a* but not miR-30b. Figures 22 and 23 show that individually, neither affects Dnajb4 levels, but as shown in Figure 24, when the let-7a* and miR-30b inhibitors are combined, Dnajb4 was significantly upregulated 3 days after transfection, by 1.48-fold. With the addition of miR-148a/b inhibitors, this increased to 1.86-fold (Figure 25). Thus there is evidence of synergistic regulation of the Hsp40 family members as well as Hsp70.

Hsp90 was expected to be regulated by miR-30b, but this did not turn out to be the case. In fact, none of the combinations of miRNAs regulated its expression, which was very high at baseline in HL-1 and H9c2 cells (i.e., Western blot membranes required very short exposure times during ECL).

Viability Assays

Despite the observation that the miRNAs decreased after HPC in HL-1 cells, this decrease was not a key aspect of cytoprotection in this model, as shown in Figure 28A and B. Inducing this decrease by transfecting the inhibitors, which successfully diminished the levels of the miRNAs, did not increase viability after OGD, nor did it enhance the effect of HPC. This makes sense in light of the fact that the mechanism by which the inhibitors would have protected is upregulation of heat shock proteins. Heat shock, which strongly upregulates Hsp70, also failed to induce protection in HL-1 cells and H9c2 cells in our hands, so it is not surprising that upregulation of heat shock proteins through inhibitor transfection likewise did not protect them.

In line with this, transfection of mimics, which maintained the miRNAs at high levels, and which we confirmed to downregulate heat shock protein expression, did not prevent the protection from HPC (Figure 28B). This further emphasizes that other mechanisms than HSP expression likely underlie the protection from simI/R in this model. Other mRNAs showed significant regulation in the RNA-Seq data as discussed in Section 4.3; these may play a role or the effect may be regulated by non-gene regulatory changes in HL-1 physiology, such as bioenergetic state or protective signaling cascade activation.

Different conditions were employed for hypoxic challenges in the HL-1 and H9c2 cells. The HL-1 cells required relatively brief periods of 1.5 to 3 hours of hypoxia along with glucose and serum withdrawal to demonstrate 50%-60% cell death, whereas H9c2 cells did not show significant numbers of dead cells with this treatment. Instead they required an overnight period of hypoxia in ischemia mimetic solution to achieve

this degree of cell death (hence the two different names for these procedures, simI/R and OGD). The HL-1 cells may need a shorter time because they grow much more densely than the H9c2 cells, and use up energy stores more rapidly because they contract (see Figure 5). Perhaps owing to differences in the hypoxia time or other differences in the two cell lines, transfection of the inhibitors did increase viability in the H9c2 cells after OGD. It is unclear whether these increases in viability were dependent on enhanced heat shock protein expression though, because while the combination of mimics did downregulate Hsp70, the inhibitors did not induce upregulation of Hsp70 even after heat shock. The inhibitors did however boost expression of Dnaja1 and Dnajb4 after heat shock, so perhaps a similar effect contributed to protection from OGD.

Conclusions: Interactions of miRNAs and Transcription Factors During IPC

Transcription factors and miRNAs work together during IPC to regulate gene expression and protein levels such that protective proteins are upregulated and pro-apoptotic proteins are downregulated, which enhances cell survival of I/R injury. Signaling cascades triggered by IPC result in the activation of transcription factors such as Hif-1α[262, 263] and NF-κB[37, 38], which upregulate expression of protective genes including HSPs, as well as miRNAs, which in turn downregulate injurious genes (Figure 49A). For example, NF-κB and Hif-1α have both been shown to be transcription factors for miR-21[264, 265], which protects the heart through downregulation of PDCD4[83], FasL[85], and PTEN[84] (for in-depth discussion of this see page 156-161). Hif-1α is also a transcription factor for miR-107[266] and miR-210[266, 267], which increase after preconditioning and downregulate the pro-apoptotic genes PDCD10 and Casp8ap, respectively, resulting in cytoprotection in MSCs.

Another facet of miRNA/transcription factor interaction during IPC is that the expression of other miRNAs is reduced, which can indirectly enhance the actions of transcription factors such as NF-κB by simply removing an impediment to the expression of the genes they upregulate (Figure 49A). This is the case for miR-711 and miR-378*, which were previously shown by Tranter *et al*.[87] to downregulate expression of the NF-κB-dependent gene Hsp70.3; these miRNAs decrease in the heart after IPC. Furthermore, the decrease in miR-711 appears to be mediated by NF-κB, because this decrease did not occur in an NF-κB dominant negative mouse strain (2M)[87].

Likewise, the results presented herein support a repressive role for miR-148a/b, miR-30b, and let-7a* in expression of Hsp70 and Hsp40 family members. While miR-148a/b was sufficient on its own to downregulate Hsp70, synergistic actions of miR-30b and let-7a* mimics were also observed, because transfection of the combination of mimics resulted in the greatest reduction of Hsp70, Dnaja1, and Dnajb4 expression (Figure 49B). Similarly, blocking miR-148a/b significantly enhanced Hsp70 protein levels after HS compared with negative control siRNA transfection, but inhibition of the combination of miRNAs produced the greatest increase in expression of Hsp70 and Dnajb4. Increases in Dnaja1 expression were not noted in HL-1 cells, but it did increase after HS in H9c2 cells transfected with the combination of inhibitors.

miRNAs have also been shown to interact directly with transcription factors by regulating their expression or the expression of their upstream activators in IPC (Figure 49A). For example, miR-199 targets and inhibits the translation of Hif-1α, and is decreased by HPC, which allows for increased levels and activity of Hif-1α. Furthermore miR-199 downregulates Sirtuin1, which is an element of a pathway

involved in the constitutive degradation of Hif-1α protein during normoxia, so decreased miR-199 expression by HPC contributes to increased Hif-1α by increasing its translation and preventing its degradation[86]. miR-148a has been shown to reduce NF-κB signaling by downregulating the expression of one of the NF-κB subunits, RelA[252], as well as a subunit of the activating upstream kinase required for degradation of inhibitor of κB (IκBα), known as inhibitor of κB kinase β (IKKβ)[253]. Whether reductions in miR-148a/b by IPC are necessary or sufficient for enhanced NF-κB activation during IPC has not been investigated and would be an interesting future study.

Regardless of the outcome of the *in vitro* viability assays, which did not show protection in HL-1 cells, we believe that treatment with the inhibitors *in vivo* would be cardioprotective through increased HSP expression. The combination of inhibitors synergistically induced increases in expression of HSPs in the HL-1 cell line, which expressed a similar profile of HSPs and miRNAs as is found in heart tissue. Thus inhibition of the miRNAs *in vivo* would likely also lead to increased HSP expression. Elevated HSP expression through a variety of means other than IPC, including whole body heat shock[63, 248, 268], transgenic overexpression[64, 269-272], and adenoviral delivery[273-275] have all been shown to be cardioprotective. Thus we anticipate that if the miRNA inhibitors allow the HSPs to become upregulated in the heart as expected, that infarct size would be reduced upon subsequent I/R injury.

Figure 49. IPC Regulation of Gene Expression by Transcription Factors and miRNA

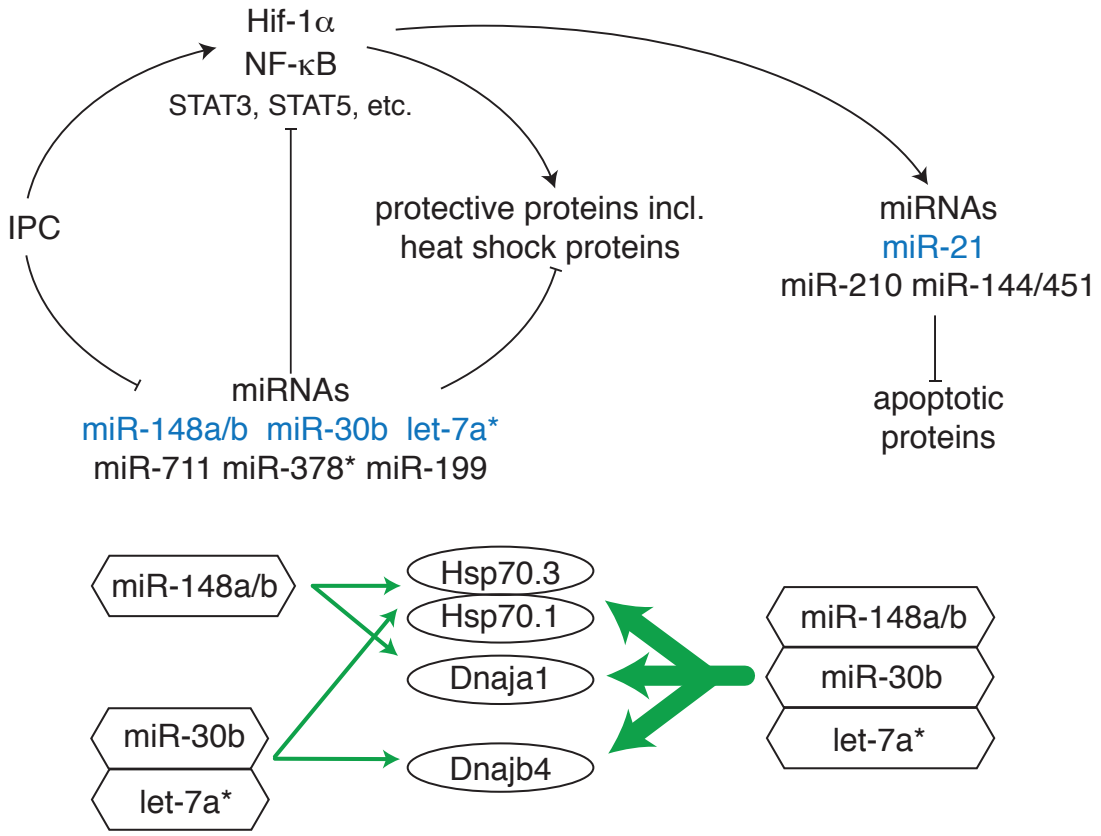

A. IPC activates transcription factors including Hif-1α and NF-κB, which transcribe protective proteins and miRNAs that downregulate proteins favoring cell death. IPC also reduces the expression of another set of miRNAs which leads to enhanced expression of their targets, which can include protective proteins and the transcription factors for them. miRNAs shown in blue are the subject of this dissertation, while those in black are examples from other publications. B. The network of miRNA/mRNA interactions is depicted. The arrows represent the effect of the miRNA(s) on protein levels, with the thicker lines representing the strongest effect of modulating the combination of all 3 miRNAs.

Exosomal miRNA as a Paracrine Mediator from Myocardium to Transplanted Mesenchymal Stem Cells

Hypoxic Preconditioning Regulates HL-1 miRNA

We confirmed that MSCs could take up exosomes produced by HL-1 cells. If HPC were to increase the abundance of a cytoprotective miRNA or mRNA within the

parent cells, we hypothesized that this RNA would also increase in the exosomes, which would allow it to be transferred to the MSCs and potentially enhance their viability. The sequencing analysis showed changes in the mRNA and miRNA profiles of the HL-1 cells, which may have resulted in their protection from OGD. For instance, miR-19, part of the miR17-92 cluster, has been shown to be protective in the context of I/R injury by reducing expression of the pro-apoptotic protein PTEN, and to induce proliferation of cardiomyocytes even in the adult myocardium[243]. MiR-20, another component of this cluster, is also significantly upregulated, though its target mRNAs within the heart have not been described. Little is known about the other miRNAs that increased. Despite increases within the HL-1 cells, these miRNAs did not increase in the exosomes. The only significant changes in miRNA expression in the HPC exosomes were downregulations of miR-3535 and miR-208a.

We observed a decrease in miR-184, which has been reported to target the anti-apoptotic genes Bcl-xL and Bcl-W[276], so one would expect that a decrease in miR-184 would be cardioprotective. However, we did not detect an increase in the expression of Bcl-xL in previous experiments with HPC HL-1 cells (Jones lab, unpublished observations).

Hypoxic Preconditioning Regulates HL-1 mRNA

HPC induced numerous significant changes in mRNA levels. These changes overlapped very little with those seen in the mouse IPC heart, suggesting that the gene regulatory mechanisms contributing to the protective effects from these two stimuli are very different. Keratin 18 (Krt18) and Activating Transcription Factor 5 (ATF5) increased 3.5- and 2-fold respectively; gene ontology analysis revealed that they are anti-

apoptotic genes. Furthermore, there were increases in two proteins, FK506 binding protein (FKBP11) and protein disulfide isomerase associated 6 (Pdia6), which are isomerases that assist with protein folding. Pdia6 has been shown to be induced by the ER stress response in the heart and cultured cells, and to be protective when overexpressed in cells exposed to simI/R[277]. Lastly, there was upregulation of the enzymes cytidine monophospho-N-acetylneuraminic acid hydroxylase, butyrylcholinesterase, cytochrome c oxidase subunit VIa polypeptide 2, and spermidine synthase, which could boost cellular metabolism. However, the only mRNA that increased in the exosomes was albumin, which has no known cytoprotective effects.

Several mRNAs that decreased after HPC are known to be regulated by hypoxia and/or hypoxia inducible factor 1α (HIF-1α), including stanniocalcin 1 (Stc-1), EGL nine homolog 3, solute carrier family 2 (facilitated glucose transporter) member 1, myosin light polypeptide kinase, ceruloplasmin, cyclin G2, and RAR-related orphan receptor-α. This downregulation may serve to decrease the cells' responsiveness to hypoxia upon a subsequent prolonged hypoxic stimulus, which could constitute a protective mechanism. Furthermore, Stc-1, slc40a1, and cyclin G2 are targets of the miR-17/92 cluster. The aforementioned upregulation of this cluster may have mediated the decreases in these genes, though this has not been experimentally validated.

Stc-1 is a secreted homodimeric glycoprotein that was shown by Zhang *et al.* to be protective against calcium overload and hypoxia in neurons[278]. Recently the same group reported that in hypoxia-preconditioned HL-1 cells, Stc-1 is remarkably upregulated (>50-fold increase vs. normoxia), which is in contrast to the decrease that we observed. However, their model of hypoxic preconditioning and time point of testing

Stc-1 expression were different from ours. Whereas we preconditioned the HL-1 cells with 1 hour at 0.5% O_2 in ischemia mimetic solution, and measured RNA levels 18h later, this group treated their cells for 6 hours at 2% O_2 and measured RNA levels immediately after this period. They also measured Stc-1 expression at 17 and 41 hours later, and found that its level had returned to baseline at both time points. Thus had we measured Stc-1 expression at a time point closer to the end of the HPC period, we may have noted an increase also. It should be noted that this publication does not show data that indicate that their HPC protocol actually induced cytoprotection (i.e., decreased cell death upon more prolonged hypoxic challenge).

Conclusions

Taken together these results led us to reject the hypothesis that HL-1 exosomes are modified by HPC to contain increased levels of anti-apoptotic miRNA and mRNA, reflecting protective changes in the transcriptome of the HL-1s. Our findings support the conclusions of Villaroya-Beltri *et al.,* who found in T cells that changes in the miRNA profiles of parent cells are not reflected in the exosomes they produce[195]. This is in contrast to the findings of Genneback *et al*., who showed that the contents of HL-1 exosomes were modified after the cells were exposed to the growth factors TGF-β2 or PDGF-BB[170]. Quite possibly the HPC stimulus invoked fewer or less profound changes in gene expression than these stimuli, and thus didn't result in many exosomal changes. It should be noted that this *in vitro* study does not rule out the possibility that IPC or other preconditioning stimuli in the heart could enhance exosome-mediated paracrine effects, due to differences in the stimuli and between HL-1 cells and primary cardiomyocytes.

miRNA in Stem Cell Mediated Paracrine Effects on the Myocardium

MSC Exosome Mediated Preconditioning

Exosomes of various sources have been shown to induce cardioprotection in two different but interconnected ways: induction of pro-survival signaling, and changes in gene expression (i.e., transfer of mRNA and miRNA). Our data support that MSC exosomes act through changes in gene expression, and raise the possibility of induction of pro-survival signaling. Figure 32 shows that pre-treatment with exosomes overnight, a time point that corresponded to substantial uptake, induces protection while Figure 39 shows that a 1-hour pre-treatment is ineffective. The need for overnight timing suggests a gene-regulatory mechanism. However, Figure 39 also shows that when either WT or miR-21 KO exosomes are present during OGD, cell death is decreased, which may indicate the rapid activation of pro-survival signaling pathways, which don't require miR-21. However, changes in gene expression over the time course of the OGD treatment cannot be ruled out, because the hypoxic period is 18h, which is long enough for gene expression changes to occur.

Pre-treatment with MSC microparticles (MP) did not show a protective effect (Figure 32A). This suggests that MSC exosomes are the more important type of extracellular vesicle released by MSCs for paracrine communication of cardioprotection in this model, though a full dose curve of MP was not performed, nor was PKH26 uptake analysis.

Sequencing revealed that many miRNAs are enriched in the exosomes compared with the parent cell population, and even some which were read exclusively in the exosomes but not the MSCs (Table 13). Notably, miR-451 was the most enriched in the

exosomes compared with the cells, which is in agreement with other published studies[195, 197]. Looking for highly expressed miRNAs within MSC exosomes (regardless of parent cell expression) revealed numerous ones with known cardioprotective roles (Table 14). The most highly expressed of these was miR-21, with nearly twice as many reads as the next most abundant miRNA. After validating its presence through real time PCR (Figure 35), we chose to investigate this miRNA and determine whether its presence in MSC exosomes contributes significantly to their cardioprotective effects.

We employed a loss-of-function approach using a commercially available KO mouse. This is a conventional full-body knockout in which miR-21a-5p was deleted from its locus within the 3'-UTR of the gene TMEM49. The expression of TMEM49 was not affected by the deletion of miR-21a-5p[241]. Other than miR-21a, there are also miR-21b and miR-21c family members. These are found in other locations of the genome, and how the knockout of miR-21a affects their expression is not known (*i.e.,* if they undergo compensatory upregulation). However, real time PCR showed very low levels of miR-21 are present in the cells of miR-21 KO mice (Figure 37). A feature of the most recent version of the miRBase database (the primary microRNA sequence repository, v21, June 2014) is the inclusion of "confidence" criteria for each miRNA. While miR-21b and miR-21c are included in the database, they do not meet the criteria for confidence that they are real miRNAs. The criteria are based on the number of deep sequencing reads from the mined datasets that map to each arm (-3p and -5p) of the stem-loop precursor. Specifically, to be "high confidence" a miRNA must have 10 reads that map to each arm, or at least 5 reads that map to each arm with 100 reads total[279]. Thus the low abundance of miR-21b and c reflected in this study are confirmed in the

data from many other deep sequencing studies that comprise the miRBase dataset. Furthermore, there are no published studies regarding cardioprotective effects of miR-21b or c. Thus we acknowledged their presence but proceeded with experiments to compare WT to miR-21a KO exosomes based on the assumption that their expression is too low to impact the results.

In vitro and *in vivo*, we found that the WT exosomes were highly cardioprotective, decreasing cell death upon OGD and infarct size upon I/R injury *in vivo*, while the miR-21 KO exosomes were less so (Figures 38 and 46). In the H9c2 model, the KO exosomes were still significantly more protective than the control treatment (no exosomes), but in the mouse heart, there was only a non-significant trend towards a decrease in infarct size with the miR-21 KO exosomes compared to saline controls. Had we performed this procedure on a larger group of mice, we may have found that this decrease was also significant, but the inherent variability of the procedure would have necessitated the use of approximately 30 more mice per group to establish this, based on power analysis. However, together with the sequencing data, the residual protection observed in cells suggests that other miRNAs or mRNAs could be assisting miR-21 in beneficially regulating gene expression. These will be the subject of future studies.

miR-21 Target Genes

Having established that miR-21 is a critical component of MSC exosome mediated preconditioning, we sought to determine the mechanism by identifying pro-apoptotic target genes that miR-21 downregulates. Search of the literature and online databases identified *FasL, PTEN, Peli1,* and *PDCD4* as validated miR-21 target genes in

the heart and other tissues, and for each of these genes, there were also publications showing that their downregulation (by miR-21 or otherwise) was cardioprotective in the context of I/R injury, which strongly suggested that this was the mechanism of our observed preconditioning.

Transfection of miR-21 mimic into H9c2 cells resulted in the downregulation of PDCD4 and FasL (Figure 43A-B). PDCD4 exhibited reductions in both mRNA and protein levels but FasL and PTEN mRNA levels were increased at 24h (Figure 44). This could represent feedback regulation of transcription in response to decreases in protein levels, to maintain homeostasis at under normal growth conditions. Luciferase reporter assays supported that downregulation of PDCD4 and FasL was mediated through the 3'-UTR of these genes (Figure 40A-B). There was minimal change in expression of PTEN or Peli1 in the H9c2 cells, so reporter assays for these genes were not performed. In cells treated with exosomes, Western blot also showed downregulation of protein levels of PDCD4 and FasL (Figure 45) as well as decreased luciferase reporter activity (Figure 40C-D), indicative of the transfer of functional miR-21.

Because most of the 3'-UTR of *PDCD4*, including the binding site for miR-21, is spliced out in the cells and mouse heart (Figure 41), this effect on protein levels might be mediated through miR-21 binding sites within the coding sequence or 5'-UTR. We identified two sites within the coding sequence *in silico* using the DIANA MicroT-CDS software (Figure 42). Future work will be needed to demonstrate the necessity and sufficiency of each site for miR-21 repression.

The reporter assays also revealed that while WT exosomes exerted a dose-dependent decrease in luciferase activity, miR-21 KO exosomes also decreased reporter

activity to only a slightly lesser extent, which supports that other miRNAs or factors within the exosomes can target these 3'-UTRs. Indeed, the next most abundant miRNA after miR-21 in Table 14, miR-486b-5p, is predicted by microRNA.org to target *PDCD4*. Furthermore, the highly expressed miR-24, miR-92, and the let-7 family members a, c, d, f, g, and i are all predicted to target *FasL*. It seems that MSC exosomes may carry a cocktail of selective anti-apoptotic miRNAs for the purpose of paracrine downregulation of specific target genes, perhaps as part of their biological role in the bone marrow and other tissues.

Having noted decreases in PDCD4 and FasL after exosome treatment *in vitro*, we next asked whether these genes are decreased by exosome treatment in the heart. Twenty-four hours after exosomes were injected into the pericardial sac, a time point at which the infarct size was decreased, we did not observe significant downregulation of PDCD4, Peli1, or FasL (Figure 47A-B). At the RNA level, we did observe a significant decrease in the PDCD4 splice variant with the full length 3'-UTR, which is consistent with the presence of a functional miR-21 binding site being retained (Figure 47C). However, given the relatively low contribution of this variant to the total amount of PDCD4 mRNA present, it is not surprising that the protein did not decrease as a result of this change.

We next asked whether the levels of the proteins were changed at a relevant time point after the I/R injury. Western blots on protein extracted from the ischemic zone 6h after I/R injury showed significant downregulation of PDCD4, PTEN, FasL and Peli1 (Figure 48). From this we concluded that miR-21 acted to prime the transcriptome of the cells such that expression of these genes was blunted after I/R injury.

Literature supports that increases in miR-21 level reduce infarct size. Increases in miR-21 occur endogenously in response to cardioprotective stimuli such as IPC (3.5-fold increase *vs.* sham 6 hours after IPC[83]), ischemic postconditioning (IPost, 3-fold increase *vs.* I/R alone at 3h reperfusion[84]) and anesthetic-mediated preconditioning (2.5-fold increase *vs.* control after 30 minutes[81]). Highlighting the role of miR-21, several studies have shown that overexpression, mediated by viral vectors[226, 227] or a cardiac-specific overexpressing genetic mouse model[85], can reduce infarct size to a similar degree as these maneuvers. Consistent with this, knockdown of miR-21 by administration of an antagomir[83] or use of a miR-21 KO mouse[81] abrogates the reduction of infarct size from IPC or anesthetic-mediated preconditioning, respectively.

Regarding the mechanism by which miR-21 reduces infarct size, the data support that it decreases apoptosis through downregulation of *PDCD4, PTEN,* and *FasL*. The Zhang group noted that in cultured NRVMs, transfection of pre-mir-21 decreased PDCD4 protein levels by ~45%, and importantly through adenoviral overexpression and siRNA mediated knockdown, they confirmed a role for PDCD4 in apoptosis (as measured by TUNEL staining) from hypoxia/reoxygenation[226]. Likewise, Olson *et al*. showed that miR-21 downregulated PDCD4 by 18% in NRVMs treated with isofluorane, but no effect on expression of PTEN was observed. However, evidence that miR-21 regulates PTEN in the mouse heart is supported by other studies. For example, cardiac-specific overexpression of miR-21 in the mouse heart downregulated PTEN as well as FasL in a mouse model of permanent occlusion[85]. FasL has been shown to increase in the hours after I/R injury in mice[280], in the isolated perfused heart, and in NRVMs[281]. Activation of Fas by FasL induces apoptosis, and this is been shown to

contribute significantly to infarct size in mice[6-8]. Thus, treatments that increase the level of miR-21 would be expected to decrease apoptosis in the heart after MI by blunting the expression of FasL, as supported by Sayed *et al*.[85]. Downregulation of these was associated with increased p-Akt and decreased caspase 6, consistent with decreased apoptosis. Additionally, knockdown of miR-21 using an antagomir prevented miR-21 from increasing in response to IPost, and prevented IPost from reducing PTEN expression[84]. In this study, downregulation of PTEN increased p-Akt levels which coincided with increased Bcl-2, decreased Bax, and decreased cleaved caspase-3, leading to decreased apoptosis as measured by TUNEL staining in heart slices. That miR-21 contributes to a decrease in apoptosis after MI was further supported by a recent study in which lentiviral miR-21 was delivered to the myocardium, preventing miR-21 expression from decreasing over from 1-2 weeks after MI. This resulted in decreased TUNEL staining, increased Bcl-2/Bax ratio and decreased caspase-3[227].

Our data are consistent with these reports which identify PTEN and FasL as target genes of miR-21 in the heart, which mediate pro-apoptotic signaling in response to I/R injury. Our data also extend the findings of the Zhang group which identified PDCD4 as a pro-apoptotic miR-21 target *in vitro,* by supporting that exosome-mediated increases in miR-21 modulate PDCD4 protein levels *in vivo*. An effect of miR-21 on Peli1 expression in the heart has not been demonstrated before. However, knockdown of Peli1 by adenoviral siRNA delivery was associated with reduced scar size and improved heart function in a mouse model of permanent occlusion[205]. Thus if exosomal miR-21 acts in a similar fashion to the adenovirally delivered siRNA, to downregulate Peli1, this would be consistent with the protection that we observed.

Interconnected Regulation of miR-21 and Its Targets

Akt is a kinase known to stimulate cellular metabolism, protein synthesis, proliferation, and survival. It is activated in response to a variety of receptor mediated stimuli, including adhesion, growth factors, cytokines, and hormones. Binding of these ligands leads to activation of phosphatidylinositide-3 kinase (PI3K), which phosphorylates the membrane lipid phosphatidylinositol to produce phosphatidylinositol 3-phosphate (PIP3). Enriched regions of PIP3 in the membrane recruit Akt via its pleckstrin homology (PH) domain, which is then phosphorylated by phosphoinositide dependent kinase-1 (PDK-1). Akt is then active and carries out its pro-survival and metabolic signaling. Akt is inactivated by PTEN through dephosphorylation of PIP3, for example in response to growth factor withdrawal.

There is a regulatory loop that exists between Akt and miR-21. Akt drives the expression of miR-21[85, 282], and miR-21 downregulates PTEN, enhancing Akt activity. Perhaps because of this, miR-21 appears to be required for cardioprotection that is driven by Akt signaling. For instance, isofluorane-mediated cardioprotection strongly induces expression of miR-21, and also activates Akt, as evidenced by increased phosphorylation. In miR-21 KO mice, Qiao *et al.* found that infarct size reduction by isofluorane was completely abrogated, as was AKT activation[82].

Akt and miR-21 also act together to block PDCD4. Akt directly phosphorylates PDCD4, which leads to its inactivation and translocation to the nucleus[283], while miR-21 acts to reduce its expression. These effects result in enhanced AP-1 signaling (which is blocked by PDCD4) and removes PDCD4's inhibition of protein synthesis, furthering Akt's role of enhancement of protein synthesis. Furthermore, PDCD4 has been shown to

downregulate the anti-apoptotic protein FLIP (Flice Inhibitory Protein, also known as Caspase 8 and FADD like Apoptosis Regulator, CFLAR) in some types of cancer cells[284]. FLIP blocks the extrinsic apoptosis pathway by displacing Caspase 8 from the Fas Associated Death Domain (FADD) complex. When FLIP is silenced in cardiomyocytes using shRNA, apoptosis is enhanced both at baseline as well as upon simI/R[285], indicative of its protective role within the heart. By downregulating both FasL and PDCD4 (and possibly thereby increasing FLIP expression), miR-21 may block extrinsic apoptosis in at least two ways.

Akt's induction of miR-21 expression has been shown to require the transcription factors CBP/p300, CREB, and NF-κB[282]. Another target of miR-21, Peli1, is a ubiquitin ligase that acts upstream of NF-κB activation. In the regenerating liver, NF-κB is initially activated and miR-21 levels increase. This results in downregulation of Peli1, and thereby subsequent reduction of NF-κB activity[286]. By downregulating Peli1 in the heart, miR-21 could reduce NF-κB activity, and thereby blunt the feed-forward loop of Akt activity and its own expression. However, whether Akt's activation of miR-21 transcription requires Peli1 is not known. It has been shown that blocking the expression of Peli1 using siRNA or Cre-LoxP-mediated conditional deletion in the heart is beneficial in the context of post-I/R injury remodeling[205].

Figure 50. miR-21 Targets and Signaling Pathways

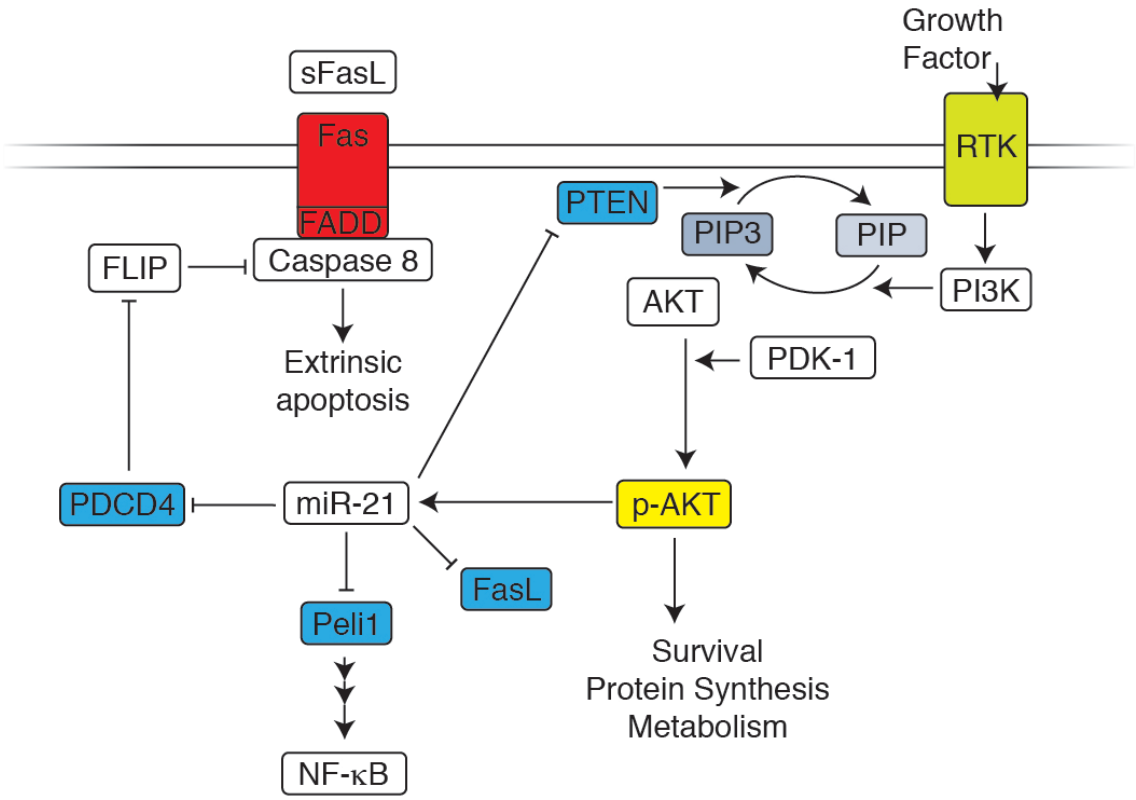

Akt is recruited to enriched regions of PIP3 in the membrane and phosphorylated by PDK-1. This results in upregulation of miR-21, which reduces the expression of PTEN, FasL, Peli1, and PDCD4. This may result in decreased infarct size by further increasing AKT activity, decreasing activation of Fas, and decreasing NF-κB signaling. Abbreviations: RTK, receptor tyrosine kinase. PI3K, phosphoinositide 3-kinase. PIP, phosphatidylinositol. PIP3, phosphatidylinositol 3-phosphate. PTEN, phosphatase and tensin homologue. p-AKT, phosphorylated AKT. PDK-1, phosphoinositide dependent kinase-1. PDCD4, programmed cell death 4. Peli1, pellino 1. FasL, Fas ligand. sFasL, soluble Fas ligand. FLIP, Flice Inhibitory Protein. FADD, Fas associated death domain.

Conclusions

These interactions between Akt, miR-21, and the miR-21 target genes PTEN, PDCD4, FasL, and Peli1 enable the understanding of how the delivery of miR-21 from MSCs to cardiomyocytes could act to reduce infarct size after myocardial infarction. These data support a key role of miR-21 within MSC exosomes in their paracrine effects.

The results presented herein suggest a number of questions which could be addressed by future studies. First, while expression of PTEN was found to be decreased by transfer of exosomal miR-21, Akt activation was not investigated. We would expect this activation to increase, which is consistent with the pro-survival effect that we observed. Furthermore, studies in which miR-21 is administered *in vivo* were not performed, but we would expect miR-21 to recapitulate many of the effects of the exosomes with regard to both gene expression and infarct size.

While the exosomes were shown to be cardioprotective in a preconditioning model, these studies did not address their potential regenerative or angiogenic effects, which would require a longer time course, and for the effects on initial infarct size to be controlled for. Lastly, it will be important for a follow-up study to sequence the miRNA content of the WT and miR-21 KO exosomes to ensure that miR-21 is the only major difference. The loss of miR-21 could affect the expression of mRNAs in the MSCs, such as transcription factors, resulting in changes to the overall profile of miRNAs present, in which case the lack of protective effect could not be attributed to miR-21 alone.

Potential Significance (Basic and Medical)

The cardioprotective properties of stem cell exosomes, including MSC exosomes, have recently begun to be explored[155, 157, 183, 199, 200, 287-289]. In particular, the importance of transfer of exosomal miRNA from stem cells has been recognized; our findings are in support of this. For example, transfer of miR-146a and miR-22 have been shown to be important for paracrine effects from CDCs[199] and MSCs[203], respectively. miR-21 was also observed to be enriched in these types of exosomes, but until now has not been directly investigated. Whether miR-21 is an important component of

therapeutic benefits in other types of stem cell exosomes or the exosomes of human MSCs is not known.

Using the miR-21 mimic *in vitro*, we confirmed that PDCD4, FasL, and PTEN are targets of miR-21 as suggested by others[83-85]. Treatment of the mouse heart with the exosomes resulted in the downregulation of these proteins as well as Peli1, which strongly suggests that Peli1 is a target of miR-21 in the mouse heart. To prove this conclusively, experiments in which miR-21 is administered *in vivo* would have to be undertaken, because in theory another component of the exosomes could be responsible for the downregulation of Peli1 observed.

If miR-21 were confirmed to target Peli1 in the heart, this would represent another layer of regulation of NF-κB driven gene expression. This implies that miR-21 could affect the expression of NF-κB-dependent genes, including the heat shock proteins. One scenario is if miR-21 increases after IPC as shown in a number of publications[83, 85], it would downregulate Peli1, which would reign in NF-κB activity. Because miR-21 expression peaks at 6h after IPC, while NF-κB-dependent genes begin to show regulation by 3 hours after IPC, perhaps this represents a homeostatic mechanism to return NF-κB activity to baseline. After prolonged hypoxia such as during I/R injury, miR-21 decreases[85], which could allow Peli1 to increase, hypothetically increasing NF-κB activation, which could contribute to increased infarct size and expression of inflammatory cytokines[205]. In support of this, our previously published array data show HSP expression is higher after I/R than after IPC, though this has not been experimentally validated.

The results presented herein have potential translational ramifications. The effectiveness of stem cell exosomes in activating cardioprotection suggests a way to circumvent some of the limitations of cell therapy for myocardial infarction. One such limitation is the timing of administration of cells relative to the MI. It takes weeks to expand purified cultures of autologous MSCs from bone marrow biopsies to have enough cells for transplantation, by which time the infarcted area is replaced by scar tissue. Exosomes could be produced by allogeneic MSCs or other stem cell populations, and stored for use as needed. Of course, stem cell populations have already been investigated that do not require culture-expansion, such as BM-MNCs[110] and adipose derived regenerative cells[143]. Data from one clinical trial (POSEIDON, as shown in[144]) support that allogeneic mesenchymal stem cells are equally effective to autologous, which would circumvent this limitation. But exosomes may have the additional benefit of being easier to preserve for later use because viability after storage is not a concern.

If the beneficial factor(s) that transplanted stem cells secrete could be isolated, it/they could be used instead of or in addition to the cells themselves. Because exosomes have been shown to recapitulate many of the benefits of their parent stem cells, they could represent one such factor. Taking this reductionist approach even further, our findings support the importance of miR-21 within the exosomes as a key factor of their mechanism of action. Thus if miR-21 could be administered after MI and recapitulate the effects of the exosomes and the cells, this would circumvent the need for them, potentially saving time and money.

A limitation to these reductionist approaches is that stem cells release many factors in addition to exosomes, including HGF and VEGF[146, 149, 152]; use of exosomes

alone would eliminate the exposure of the heart to these, potentially preventing the antifibrotic and angiogenic benefits of MSCs themselves. Likewise, administering miR-21 alone would prevent the heart from being exposed to the other protective miRNAs, as well as mRNAs and proteins found in exosomes[154-156]. In support of this, while miR-146a was found to be a key component of CDC exosome regenerative effects, its administration in the absence of exosomes did not reproduce all of their benefits. It increased viable mass, but failed to improve global function or decrease scar mass. Exosomes from cells depleted of miR-146a could still suppress apoptosis, though to a lesser extent. Thus the authors concluded that other miRNAs may be needed to reproduce the full repertoire of the exosomes' effects, and that exosomal miRNAs may act synergistically[199]. Our sequencing data showed the presence of other miRNAs which share pro-apoptotic targets with miR-21, with expression levels that were also quite high, which suggests the potential for synergy with miR-21. Thus we believe exosomes would be more therapeutically efficacious than individual miRNAs alone. Potentially, a cocktail of the most enriched miRNAs could recapitulate exosomes' effects. Future studies are needed to compare the benefits of stem cells, their exosomes, and the bioactive miRNAs within the exosomes.

APPENDIX A

RNA-SEQ DATA: GENES WITH DIFFERENTIAL EXPRESSION BETWEEN SHAM AND IPC MOUSE HEART TISSUE

Symbol	Name	Sham	IPC	Fold	P
Slc5a3	solute carrier family 5 (inositol transporters), member 3	93.4	494.5	5.3	8.49E-11
Nr4a3	nuclear receptor subfamily 4, group A, member 3	9.4	107.1	11.5	1.10E-10
Hsph1	heat shock 105kDa/110kDa protein 1	860.0	3534.4	4.1	2.22E-10
Ch25h	cholesterol 25-hydroxylase	68.4	324.1	4.7	1.22E-06
Ucp3	uncoupling protein 3 (mitochondrial, proton carrier)	692.6	183.8	0.3	1.41E-06
Hspa1b	heat shock protein 1B	14.6	10090.6	690.7	1.52E-06
Akap12	A kinase (PRKA) anchor protein (gravin) 12	311.9	957.7	3.1	1.52E-06
Hsp90aa1	heat shock protein 90, alpha (cytosolic), class A member 1	2664.0	24336.4	9.1	4.08E-06
Adamts4	a disintegrin-like and metallopeptidase (reprolysin type) with thrombospondin type 1 motif, 4	17.5	94.3	5.4	8.94E-06
Dnaja1	DnaJ (Hsp40) homolog, subfamily A, member 1	642.8	4557.1	7.1	1.23E-05
Peg10	paternally expressed 10	13.6	95.6	7.0	1.44E-05
Icam1	intercellular adhesion molecule 1	86.0	309.9	3.6	1.65E-05
Hspa1a	heat shock protein 1A	16.1	8741.7	541.6	3.54E-05
S100a8	S100 calcium binding protein A8 (calgranulin A)	26.3	115.7	4.4	6.08E-05
Sele	selectin, endothelial cell	24.2	99.9	4.1	1.06E-04
Dnaja4	DnaJ (Hsp40) homolog, subfamily A, member 4	1745.7	4055.4	2.3	1.14E-04
Il6	interleukin 6	23.2	88.9	3.8	2.02E-04
Rell1	RELT-like 1	113.5	300.2	2.6	3.28E-04
Nuak1	NUAK family, SNF1-like kinase, 1	229.4	667.3	2.9	3.85E-04
Tiparp	TCDD-inducible poly(ADP-ribose) polymerase	634.0	1431.6	2.3	4.01E-04
Bhlhe41	basic helix-loop-helix family, member e41	254.9	714.9	2.8	5.49E-04
Lhfpl2	lipoma HMGIC fusion	16.2	65.5	4.0	5.68E-04

	partner-like 2				
Csf2rb2	colony stimulating factor 2 receptor, beta 2, low-affinity (granulocyte-macrophage)	37.2	131.1	3.5	7.74E-04
Casp4	caspase 4, apoptosis-related cysteine peptidase	74.4	209.9	2.8	8.74E-04
Gcnt2	glucosaminyl (N-acetyl) transferase 2, I-branching enzyme	216.3	491.0	2.3	0.001
Spry4	sprouty homolog 4 (Drosophila)	147.0	334.6	2.3	0.001
P4ha1	procollagen-proline, 2-oxoglutarate 4-dioxygenase (proline 4-hydroxylase), alpha 1 polypeptide	396.1	1183.2	3.0	0.001
Slfn4	schlafen 4	34.9	103.7	3.0	0.001
Retnlg	resistin like gamma	2.0	23.3	11.6	0.001
Pim1	proviral integration site 1	93.9	223.1	2.4	0.001
Atp2c1	ATPase, Ca++-sequestering	844.9	1730.4	2.0	0.001
Ankrd33b	ankyrin repeat domain 33B	335.8	759.0	2.3	0.001
Dnajb4	DnaJ (Hsp40) homolog, subfamily B, member 4	1840.1	6440.2	3.5	0.001
Csf2rb	colony stimulating factor 2 receptor, beta, low-affinity (granulocyte-macrophage)	27.5	91.2	3.3	0.002
Map3k8	mitogen-activated protein kinase kinase kinase 8	92.4	204.8	2.2	0.002
Txnrd1	thioredoxin reductase 1	911.7	1830.4	2.0	0.002
Tmem173	transmembrane protein 173	49.9	136.0	2.7	0.002
Hspa8	heat shock protein 8	8147.0	18962.1	2.3	0.002
Hmox1	heme oxygenase (decycling) 1	152.8	471.5	3.1	0.003
S100a9	S100 calcium binding protein A9 (calgranulin B)	14.5	58.8	4.1	0.003
Sema6c	sema domain, transmembrane domain (TM), and cytoplasmic domain, (semaphorin) 6C	71.5	21.6	0.3	0.003
Rgs16	regulator of G-protein signaling 16	3.6	26.1	7.2	0.003
Icosl	icos ligand	76.6	178.8	2.3	0.003
Cnksr3	Cnksr family member 3	201.8	402.1	2.0	0.003

Sat1	spermidine/spermine N1-acetyl transferase 1	319.8	617.5	1.9	0.003
Lima1	LIM domain and actin binding 1	104.5	242.8	2.3	0.004
Selp	selectin, platelet	43.6	141.8	3.3	0.004
Zkscan8	zinc finger with KRAB and SCAN domains 8	368.5	162.7	0.4	0.004
Gem	GTP binding protein (gene overexpressed in skeletal muscle)	37.2	92.2	2.5	0.004
Fnip2	folliculin interacting protein 2	308.9	741.5	2.4	0.004
Il4ra	interleukin 4 receptor, alpha	314.4	641.9	2.0	0.004
Litaf	LPS-induced TN factor	154.7	326.9	2.1	0.004
Akap2	A kinase (PRKA) anchor protein 2	1977.2	3800.5	1.9	0.004
Bbs10	Bardet-Biedl syndrome 10 (human)	37.7	7.7	0.2	0.004
Clec4e	C-type lectin domain family 4, member e	10.6	45.8	4.3	0.004
Osmr	oncostatin M receptor	503.8	1644.8	3.3	0.004
Smad1	SMAD family member 1	330.2	612.2	1.9	0.004
Eif1a	eukaryotic translation initiation factor 1A	378.8	719.3	1.9	0.004
Gm4070	predicted gene 4070	2933.2	5854.6	2.0	0.004
Gvin1	GTPase, very large interferon inducible 1	2933.2	5854.6	2.0	0.004
Lnx2	ligand of numb-protein X 2	114.3	246.9	2.2	0.004
Atp8b1	ATPase, class I, type 8B, member 1	131.9	284.3	2.2	0.005
Dnajb5	DnaJ (Hsp40) homolog, subfamily B, member 5	257.4	541.6	2.1	0.005
Plac9b	placenta specific 9b	141.6	64.5	0.5	0.005
Stx11	syntaxin 11	19.3	58.0	3.0	0.005
Ppp1r18	protein phosphatase 1, regulatory subunit 18	95.1	203.2	2.1	0.005
Banp	BTG3 associated nuclear protein	12.4	45.4	3.7	0.006
Gprc5a	G protein-coupled receptor, family C, group 5, member A	9.0	36.4	4.1	0.006

Plekho2	pleckstrin homology domain containing, family O member 2	63.1	147.9	2.3	0.006
Rassf1	Ras association (RalGDS/AF-6) domain family member 1	122.0	291.6	2.4	0.006
Spred1	sprouty protein with EVH-1 domain 1, related sequence	752.4	1348.8	1.8	0.006
Thbd	thrombomodulin	588.0	1169.5	2.0	0.006
Nfil3	nuclear factor, interleukin 3, regulated	121.8	244.1	2.0	0.006
Esm1	endothelial cell-specific molecule 1	4.2	23.0	5.4	0.007
Serpina3f	serine (or cysteine) peptidase inhibitor, clade A, member 3F	26.9	104.2	3.9	0.007
Ptgs2	prostaglandin-endoperoxide synthase 2	48.4	112.6	2.3	0.007
Sdc4	syndecan 4	274.8	686.2	2.5	0.007
Sema6d	sema domain, transmembrane domain (TM), and cytoplasmic domain, (semaphorin) 6D	388.0	737.4	1.9	0.007
Jmjd1c	jumonji domain containing 1C	702.8	1357.6	1.9	0.007
Tfpi2	tissue factor pathway inhibitor 2	26.3	68.4	2.6	0.007
Serpinh1	serine (or cysteine) peptidase inhibitor, clade H, member 1	410.5	1915.1	4.7	0.007
Zfp568	zinc finger protein 568	179.7	508.3	2.8	0.007
Art4	ADP-ribosyltransferase 4	168.4	78.2	0.5	0.008
Gm8989	very large inducible GTPase 1 pseudogene	235.7	556.7	2.4	0.008
Ttc30a2	tetratricopeptide repeat domain 30A2	104.2	40.0	0.4	0.008
Nfkbiz	nuclear factor of kappa light polypeptide gene enhancer in B cells inhibitor, zeta	73.2	143.0	2.0	0.008
Kazn	kazrin, periplakin interacting protein	35.8	88.1	2.5	0.009
Car13	carbonic anhydrase 13	10.8	32.5	3.0	0.009
Slco5a1	solute carrier organic anion transporter family, member	290.1	543.6	1.9	0.009

	5A1				
Cxcl1	chemokine (C-X-C motif) ligand 1	66.6	186.3	2.8	0.009
Tmem2	transmembrane protein 2	206.1	393.0	1.9	0.009
Map3k1	mitogen-activated protein kinase kinase kinase 1	358.8	658.6	1.8	0.009
Slc23a2	solute carrier family 23 (nucleobase transporters), member 2	419.8	750.7	1.8	0.010
Ets2	E26 avian leukemia oncogene 2, 3' domain	748.3	1433.4	1.9	0.010
Zfp697	zinc finger protein 697	125.8	528.9	4.2	0.010
Fam26e	family with sequence similarity 26, member E	21.5	55.5	2.6	0.010
Tnfaip3	tumor necrosis factor, alpha-induced protein 3	43.2	101.0	2.3	0.010
Tmem88b	transmembrane protein 88B	24.4	96.6	4.0	0.010
Socs3	suppressor of cytokine signaling 3	169.1	393.5	2.3	0.010
Mmp8	matrix metallopeptidase 8	5.4	28.6	5.3	0.010
Tmem254a	transmembrane protein 254a	203.6	93.1	0.5	0.010
Rel	reticuloendotheliosis oncogene	127.8	241.8	1.9	0.010
Ell	elongation factor RNA polymerase II	39.6	111.4	2.8	0.011
Gpr176	G protein-coupled receptor 176	0.0	9.4	Inf	0.011
Cxcl2	chemokine (C-X-C motif) ligand 2	12.9	57.4	4.5	0.012
Maff	v-maf musculoaponeurotic fibrosarcoma oncogene family, protein F (avian)	124.2	373.1	3.0	0.012
Smim5	small integral membrane protein 5	94.2	38.2	0.4	0.012
Mgat5	mannoside acetylglucosaminyltransferase 5	39.8	97.4	2.4	0.012
Mir24-1	microRNA 24-1	0.0	9.1	Inf	0.012
Mir3074-1	microRNA 3074-1	0.0	9.1	Inf	0.012
Egr1	early growth response 1	254.0	616.3	2.4	0.012
Fgl2	fibrinogen-like protein 2	1719.5	5952.5	3.5	0.012

Frmd6	FERM domain containing 6	322.5	789.5	2.4	0.012
Kank1	KN motif and ankyrin repeat domains 1	409.1	742.6	1.8	0.013
Kdm6b	KDM1 lysine (K)-specific demethylase 6B	202.5	372.4	1.8	0.013
Rps6ka5	ribosomal protein S6 kinase, polypeptide 5	281.9	136.2	0.5	0.013
Tpm3	tropomyosin 3, gamma	366.5	660.0	1.8	0.013
Fam189a2	family with sequence similarity 189, member A2	421.0	728.4	1.7	0.014
Dusp16	dual specificity phosphatase 16	271.2	521.9	1.9	0.014
Unc45b	unc-45 homolog B (C. elegans)	1163.8	2972.8	2.6	0.014
Il17ra	interleukin 17 receptor A	70.2	149.5	2.1	0.014
Tsku	tsukushi	16.5	47.2	2.9	0.014
Odc1	ornithine decarboxylase, structural 1	501.9	925.2	1.8	0.014
Trim16	tripartite motif-containing 16	45.9	113.0	2.5	0.015
Sbno2	strawberry notch homolog 2 (Drosophila)	100.2	390.3	3.9	0.016
Alkbh1	alkB, alkylation repair homolog 1 (E. coli)	87.7	171.3	2.0	0.016
Akap13	A kinase (PRKA) anchor protein 13	1350.9	2322.6	1.7	0.016
Tmem254b	transmembrane protein 254b	198.4	89.9	0.5	0.017
Tmem254c	transmembrane protein 254c	198.4	89.9	0.5	0.017
Kcnj3	potassium inwardly-rectifying channel, subfamily J, member 3	575.8	304.1	0.5	0.017
Igsf9b	immunoglobulin superfamily, member 9B	1.9	15.0	7.9	0.017
Irf8	interferon regulatory factor 8	31.5	73.2	2.3	0.018
Thbs1	thrombospondin 1	321.1	3253.6	10.1	0.018
Ptpn21	protein tyrosine phosphatase, non-receptor type 21	223.6	480.5	2.1	0.018
Slc20a1	solute carrier family 20, member 1	239.7	402.8	1.7	0.018
Gin1	gypsy retrotransposon integrase 1	213.6	105.0	0.5	0.018
Pgm1	phosphoglucomutase 1	66.9	141.1	2.1	0.018
Casp8	caspase 8	61.6	126.0	2.0	0.018

Atp7a	ATPase, Cu++ transporting, alpha polypeptide	306.9	544.7	1.8	0.018
Ugdh	UDP-glucose dehydrogenase	200.1	392.6	2.0	0.019
Ccl19	chemokine (C-C motif) ligand 19	13.0	37.7	2.9	0.019
Slc25a25	solute carrier family 25 (mitochondrial carrier, phosphate carrier), member 25	89.9	161.2	1.8	0.019
Jak2	Janus kinase 2	386.0	698.5	1.8	0.019
Arrdc4	arrestin domain containing 4	104.8	186.1	1.8	0.020
AI507597	expressed sequence AI507597	31.0	9.4	0.3	0.020
Ttc30b	tetratricopeptide repeat domain 30B	364.8	138.6	0.4	0.020
Il1r2	interleukin 1 receptor, type II	7.8	28.6	3.7	0.020
Arid5b	AT rich interactive domain 5B (MRF1-like)	143.2	369.5	2.6	0.021
Fam110b	family with sequence similarity 110, member B	18.7	48.9	2.6	0.021
Ky	kyphoscoliosis peptidase	73.9	30.8	0.4	0.022
Cacybp	calcyclin binding protein	601.6	1032.8	1.7	0.022
Lonrf1	LON peptidase N-terminal domain and ring finger 1	108.7	217.5	2.0	0.022
Kcne4	potassium voltage-gated channel, Isk-related subfamily, gene 4	51.3	101.9	2.0	0.022
Bag3	BCL2-associated athanogene 3	532.9	2181.5	4.1	0.022
Adamts1	a disintegrin-like and metallopeptidase (reprolysin type) with thrombospondin type 1 motif, 1	459.5	1883.6	4.1	0.023
Sh2d5	SH2 domain containing 5	1.2	12.1	10.5	0.023
Olfr56	olfactory receptor 56	1.2	11.6	10.0	0.023
Gp49a	glycoprotein 49 A	118.6	223.2	1.9	0.023
Aebp1	AE binding protein 1	29.3	72.4	2.5	0.024
Nts	neurotensin	20.5	51.8	2.5	0.024
Zfp516	zinc finger protein 516	96.8	177.3	1.8	0.024
Nudt18	nudix (nucleoside diphosphate linked moiety X)-type motif 18	66.3	131.7	2.0	0.024

Samsn1	SAM domain, SH3 domain and nuclear localization signals, 1	10.9	35.2	3.2	0.025
Prrg3	proline rich Gla (G-carboxyglutamic acid) 3 (transmembrane)	185.0	92.6	0.5	0.025
Cxcr5	chemokine (C-X-C motif) receptor 5	12.0	1.3	0.1	0.025
Cyp1b1	cytochrome P450, family 1, subfamily b, polypeptide 1	167.0	323.9	1.9	0.025
Emp1	epithelial membrane protein 1	576.5	1264.1	2.2	0.025
Nek6	NIMA (never in mitosis gene a)-related expressed kinase 6	36.1	84.7	2.3	0.025
Ppara	peroxisome proliferator activated receptor alpha	1466.8	840.4	0.6	0.025
Urb1	URB1 ribosome biogenesis 1 homolog (S. cerevisiae)	85.6	187.8	2.2	0.026
Dab2	disabled 2, mitogen-responsive phosphoprotein	483.7	889.5	1.8	0.026
Entpd5	ectonucleoside triphosphate diphosphohydrolase 5	2380.5	1367.8	0.6	0.026
Rbm18	RNA binding motif protein 18	637.7	1038.8	1.6	0.026
Lilrb4	leukocyte immunoglobulin-like receptor, subfamily B, member 4	134.3	272.7	2.0	0.026
AI593442	expressed sequence AI593442	60.3	16.8	0.3	0.026
Zfp420	zinc finger protein 420	72.0	34.0	0.5	0.026
Ptx3	pentraxin related gene	77.2	438.5	5.7	0.026
Sh3rf2	SH3 domain containing ring finger 2	241.1	130.8	0.5	0.027
NA	NA	18.0	45.8	2.5	0.027
Prodh	proline dehydrogenase	94.8	48.0	0.5	0.027
Zfp948	zinc finger protein 948	100.6	276.8	2.8	0.027
Map3k5	mitogen-activated protein kinase kinase kinase 5	633.9	1623.6	2.6	0.028
Cytip	cytohesin 1 interacting protein	19.1	45.7	2.4	0.028
Ccr1	chemokine (C-C motif) receptor 1	58.6	121.2	2.1	0.028

Hspd1	heat shock protein 1 (chaperonin)	3284.7	5474.3	1.7	0.028
Zkscan7	zinc finger with KRAB and SCAN domains 7	31.3	9.9	0.3	0.029
Sgms2	sphingomyelin synthase 2	34.1	107.1	3.1	0.029
Dnajb1	DnaJ (Hsp40) homolog, subfamily B, member 1	112.1	939.4	8.4	0.029
Dapk2	death-associated protein kinase 2	38.0	13.1	0.3	0.029
Ptpn12	protein tyrosine phosphatase, non-receptor type 12	509.6	1113.3	2.2	0.029
Nle1	notchless homolog 1 (Drosophila)	11.3	50.6	4.5	0.029
Pde4b	phosphodiesterase 4B, cAMP specific	517.2	1157.0	2.2	0.029
Nr5a2	nuclear receptor subfamily 5, group A, member 2	4.6	19.7	4.3	0.030
Ripk1	receptor (TNFRSF)-interacting serine-threonine kinase 1	150.7	256.8	1.7	0.030
Kit	kit oncogene	33.7	73.5	2.2	0.030
Tmem120a	transmembrane protein 120A	62.8	123.7	2.0	0.030
Gadd45b	growth arrest and DNA-damage-inducible 45 beta	45.7	95.8	2.1	0.030
Ctso	cathepsin O	416.2	231.4	0.6	0.030
Swap70	SWA-70 protein	131.1	240.2	1.8	0.030
Klf6	Kruppel-like factor 6	1375.1	2668.2	1.9	0.031
Map3k14	mitogen-activated protein kinase kinase kinase 14	23.3	55.2	2.4	0.031
Arid5a	AT rich interactive domain 5A (MRF1-like)	43.8	124.5	2.8	0.031
Sh3pxd2b	SH3 and PX domains 2B	95.4	202.7	2.1	0.032
Ccdc14	coiled-coil domain containing 14	71.8	30.8	0.4	0.032
Stip1	stress-induced phosphoprotein 1	274.7	769.1	2.8	0.032
Epb4.1l5	erythrocyte protein band 4.1-like 5	137.1	67.9	0.5	0.032
Nt5e	5' nucleotidase, ecto	520.2	1328.0	2.6	0.033
Ect2	ect2 oncogene	24.3	8.1	0.3	0.033
Rasgef1b	RasGEF domain family, member 1B	134.1	253.1	1.9	0.034

Eid2b	EP300 interacting inhibitor of differentiation 2B	135.2	68.4	0.5	0.034
Acvrl1	activin A receptor, type II-like 1	124.3	233.1	1.9	0.034
Cyb5r2	cytochrome b5 reductase 2	36.5	13.3	0.4	0.034
Gda	guanine deaminase	464.2	1075.4	2.3	0.034
Fjx1	four jointed box 1 (Drosophila)	1.7	14.1	8.3	0.035
Ccng2	cyclin G2	633.2	360.9	0.6	0.035
Apol10b	apolipoprotein L 10B	19.7	50.1	2.5	0.036
Tec	tec protein tyrosine kinase	55.9	149.6	2.7	0.036
Aloxe3	arachidonate lipoxygenase 3	0.0	7.1	Inf	0.036
Runx1	runt related transcription factor 1	55.5	110.3	2.0	0.036
Nol10	nucleolar protein 10	108.1	193.1	1.8	0.036
Errfi1	ERBB receptor feedback inhibitor 1	307.9	565.9	1.8	0.036
Zfp606	zinc finger protein 606	215.4	118.9	0.6	0.037
Tmem41b	transmembrane protein 41B	671.4	1121.5	1.7	0.037
Mum1l1	melanoma associated antigen (mutated) 1-like 1	27.4	162.0	5.9	0.037
Nedd9	neural precursor cell expressed, developmentally down-regulated gene 9	245.1	401.9	1.6	0.038
Atf3	activating transcription factor 3	65.8	1124.3	17.1	0.038
Vcam1	vascular cell adhesion molecule 1	207.1	354.5	1.7	0.038
Fam46a	family with sequence similarity 46, member A	858.3	1316.8	1.5	0.038
Sema6b	sema domain, transmembrane domain (TM), and cytoplasmic domain, (semaphorin) 6B	161.6	276.9	1.7	0.038
Bcl9l	B cell CLL/lymphoma 9-like	155.5	85.2	0.5	0.038
Ell2	elongation factor RNA polymerase II 2	256.9	974.6	3.8	0.039
Cd83	CD83 antigen	39.8	77.8	2.0	0.039
Bambi	BMP and activin membrane-bound inhibitor	83.1	160.1	1.9	0.039
Pddc1	Parkinson disease 7 domain containing 1	90.0	45.9	0.5	0.039

Kcnb1	potassium voltage gated channel, Shab-related subfamily, member 1	792.5	438.7	0.6	0.039
Dhrs3	dehydrogenase/reductase (SDR family) member 3	1059.5	625.6	0.6	0.039
Fbxo30	F-box protein 30	518.1	903.6	1.7	0.039
Palm2	paralemmin 2	38.5	73.5	1.9	0.039
Paqr7	progestin and adipoQ receptor family member VII	81.3	40.0	0.5	0.039
Etv6	ets variant gene 6 (TEL oncogene)	176.8	286.1	1.6	0.040
Ctps	cytidine 5'-triphosphate synthase	434.1	757.9	1.7	0.040
Capn12	calpain 12	66.9	120.5	1.8	0.041
Il1r1	interleukin 1 receptor, type I	758.5	1275.9	1.7	0.041
Fam210b	family with sequence similarity 210, member B	106.1	52.9	0.5	0.041
Zfp266	zinc finger protein 266	667.3	394.5	0.6	0.041
Has2	hyaluronan synthase 2	8.0	23.5	2.9	0.041
Map3k13	mitogen-activated protein kinase kinase kinase 13	39.7	13.7	0.3	0.041
Elovl6	ELOVL family member 6, elongation of long chain fatty acids (yeast)	32.9	71.9	2.2	0.041
Slco2a1	solute carrier organic anion transporter family, member 2a1	20.2	49.1	2.4	0.042
Fzd1	frizzled homolog 1 (Drosophila)	45.6	92.0	2.0	0.042
Capn5	calpain 5	14.6	2.7	0.2	0.043
Cnksr1	connector enhancer of kinase suppressor of Ras 1	63.5	178.8	2.8	0.043
Kif18a	kinesin family member 18A	28.3	10.3	0.4	0.043
Kcnn2	potassium intermediate/small conductance calcium-activated channel, subfamily N, member 2	126.6	65.1	0.5	0.043
Inip	INTS3 and NABP interacting protein	108.6	196.5	1.8	0.043
Cpt1a	carnitine palmitoyltransferase 1a, liver	539.5	272.1	0.5	0.044
Klf7	Kruppel-like factor 7 (ubiquitous)	18.3	46.0	2.5	0.044

Srbd1	S1 RNA binding domain 1	63.1	28.7	0.5	0.044
Phf19	PHD finger protein 19	8.5	0.7	0.1	0.044
Itga3	integrin alpha 3	53.2	108.0	2.0	0.044
Frat2	frequently rearranged in advanced T cell lymphomas 2	20.1	104.8	5.2	0.044
Ska2	spindle and kinetochore associated complex subunit 2	112.1	61.0	0.5	0.044
Slc35b2	solute carrier family 35, member B2	103.5	56.2	0.5	0.044
Ankrd2	ankyrin repeat domain 2 (stretch responsive muscle)	0.4	8.7	20.3	0.044
Ccl11	chemokine (C-C motif) ligand 11	24.9	70.4	2.8	0.045
Cnst	consortin, connexin sorting protein	824.7	489.0	0.6	0.045
Kcnq1	potassium voltage-gated channel, subfamily Q, member 1	229.2	132.9	0.6	0.045
Senp7	SUMO1/sentrin specific peptidase 7	302.9	167.7	0.6	0.045
Tube1	epsilon-tubulin 1	16.3	3.4	0.2	0.045
Map2k3	mitogen-activated protein kinase kinase 3	386.8	872.0	2.3	0.045
Adora2b	adenosine A2b receptor	35.4	75.9	2.1	0.046
Ttc30a1	tetratricopeptide repeat domain 30A1	190.4	74.6	0.4	0.046
Srrm4	serine/arginine repetitive matrix 4	89.9	29.6	0.3	0.046
Plec	plectin	1082.3	1976.2	1.8	0.046
Rad51d	RAD51 homolog D	121.2	62.9	0.5	0.046
Klhl6	kelch-like 6	41.9	94.4	2.3	0.046
Tcta	T cell leukemia translocation altered gene	274.1	164.3	0.6	0.046
Sphk1	sphingosine kinase 1	13.4	167.6	12.5	0.046
Zfp273	zinc finger protein 273	38.0	16.1	0.4	0.047
Swt1	SWT1 RNA endoribonuclease homolog (S. cerevisiae)	142.1	468.2	3.3	0.047
Ssfa2	sperm specific antigen 2	434.3	653.6	1.5	0.047
Cd53	CD53 antigen	123.2	220.5	1.8	0.047

Sdr42e1	short chain dehydrogenase/reductase family 42E, member 1	23.4	7.7	0.3	0.047
Phlda1	pleckstrin homology-like domain, family A, member 1	115.2	709.7	6.2	0.048
Zc4h2	zinc finger, C4H2 domain containing	35.5	10.7	0.3	0.048
Kcnd3	potassium voltage-gated channel, Shal-related family, member 3	286.2	160.7	0.6	0.048
Nme1	NME/NM23 nucleoside diphosphate kinase 1	77.0	137.9	1.8	0.048
C3ar1	complement component 3a receptor 1	36.3	79.1	2.2	0.048
Dcbld1	discoidin, CUB and LCCL domain containing 1	65.7	115.2	1.8	0.048
Zfp944	zinc finger protein 944	150.9	79.9	0.5	0.049
Bicd1	bicaudal D homolog 1 (Drosophila)	179.9	92.5	0.5	0.049
Dpy19l1	dpy-19-like 1 (C. elegans)	178.1	101.5	0.6	0.049
Tnfaip6	tumor necrosis factor alpha induced protein 6	52.5	96.2	1.8	0.049
Hif3a	hypoxia inducible factor 3, alpha subunit	134.4	57.3	0.4	0.049
Setdb2	SET domain, bifurcated 2	493.6	261.1	0.5	0.049
Kctd6	potassium channel tetramerisation domain containing 6	148.5	407.5	2.7	0.049
Cc2d2a	coiled-coil and C2 domain containing 2A	109.5	56.6	0.5	0.050

APPENDIX B

RNA-SEQ DATA: GENES WITH DIFFERENTIAL EXPRESSION BETWEEN MESECHYMAL STEM CELLS AND THEIR EXOSOMES

Symbol	Name	MSC	Exo	Fold	P
Rn45s	45S pre-ribosomal RNA	38894.6	56755301	1459.207	8.55E-11
Rpph1	ribonuclease P RNA component H1	1.1	2988.4	2708.797	8.55E-11
Dnm3os	dynamin 3, opposite strand	1044.7	0	0	2.75E-10
Tm4sf1	transmembrane 4 superfamily member 1	977.8	0	0	8.56E-10
Ogn	osteoglycin	4118.7	195.7	0.048	9.25E-10
Ugcg	UDP-glucose ceramide glucosyltransferase	890.9	0	0	3.96E-09
Sdc2	syndecan 2	1944.7	67.2	0.035	5.50E-09
Col6a1	collagen, type VI, alpha 1	3857.1	211.7	0.055	1.33E-08
Fstl1	follistatin-like 1	4188.7	186.8	0.045	1.38E-08
Dag1	dystroglycan 1	885.0	2.2	0.003	2.35E-08
Itgav	integrin alpha V	1940.6	62.5	0.032	5.10E-08
Ogt	O-linked N-acetylglucosamine (GlcNAc) transferase	2003.1	67.0	0.033	5.10E-08
Tmem59	transmembrane protein 59	1711.7	46.9	0.027	5.10E-08
Aspn	asporin	723.3	0	0	9.55E-08
Col4a5	collagen, type IV, alpha 5	713.9	0	0	1.11E-07
M6pr	mannose-6-phosphate receptor, cation dependent	711.7	0	0	1.11E-07
Rprl3	ribonuclease P RNA-like 3	0.2	2467.0	10083.803	1.11E-07
Lamp2	lysosomal-associated membrane protein 2	1846.9	92.3	0.050	3.44E-07
Cdh2	cadherin 2	1433.9	70.2	0.049	3.44E-07
Tmed10	transmembrane emp24-like trafficking protein 10 (yeast)	730.8	3.9	0.005	4.08E-07
Alpl	alkaline phosphatase, liver/bone/kidney	2259.8	120.5	0.053	9.30E-07
Aplp2	amyloid beta (A4) precursor-like protein 2	1284.1	35.7	0.028	9.58E-07
Vcan	versican	1401.8	46.9	0.033	1.25E-06
Adam9	a disintegrin and metallopeptidase domain 9 (meltrin gamma)	602.9	0	0	1.25E-06
Hmgcr	3-hydroxy-3-	787.8	6.7	0.009	1.25E-06

	methylglutaryl-Coenzyme A reductase				
Adam10	a disintegrin and metallopeptidase domain 10	672.9	2.2	0.003	1.27E-06
Atp6ap2	ATPase, H+ transporting, lysosomal accessory protein 2	783.4	6.7	0.009	1.27E-06
Col1a2	collagen, type I, alpha 2	33716.3	2792.9	0.083	1.27E-06
Sema3a	sema domain, immunoglobulin domain (Ig), short basic domain, secreted, (semaphorin) 3A	596.2	0.0	0.000	1.27E-06
Postn	periostin, osteoblast specific factor	6227.1	464.9	0.075	1.28E-06
Ncstn	nicastrin	666.6	2.2	0.003	1.31E-06
Fbln5	fibulin 5	582.2	0	0	1.70E-06
Dkk3	dickkopf homolog 3 (Xenopus laevis)	729.6	0	0	2.01E-06
Tmx1	thioredoxin-related transmembrane protein 1	572.8	0	0	2.08E-06
Serinc1	serine incorporator 1	1207.8	60.5	0.050	2.93E-06
Col5a2	collagen, type V, alpha 2	8519.6	933.6	0.110	2.93E-06
Fbn2	fibrillin 2	551.7	0	0	3.39E-06
Derl1	Der1-like domain family, member 1	551.5	0	0	3.39E-06
Tcf4	transcription factor 4	2834.5	279.2	0.098	5.21E-06
Pcdh18	protocadherin 18	528.7	0	0	6.18E-06
Plod2	procollagen lysine, 2-oxoglutarate 5-dioxygenase 2	528.0	0	0	6.18E-06
Ssr3	signal sequence receptor, gamma	3382.1	394.3	0.117	8.42E-06
Hspa13	heat shock protein 70 family, member 13	515.6	0	0	8.42E-06
Serinc3	serine incorporator 3	952.7	23.6	0.025	8.67E-06
Zmpste24	zinc metallopeptidase, STE24	512.3	0	0	8.88E-06
B3gat2	beta-1,3-glucuronyltransferase 2 (glucuronosyltransferase S)	511.1	0	0	9.00E-06
Nptn	neuroplastin	940.4	24.6	0.026	9.90E-06
Cpe	carboxypeptidase E	3730.2	320.7	0.086	1.02E-05

Cpd	carboxypeptidase D	800.6	27.5	0.034	1.07E-05
Cst3	cystatin C	501.6	0	0	1.07E-05
Mat2a	methionine adenosyltransferase II, alpha	1350.7	78.3	0.058	1.07E-05
Npnt	nephronectin	501.1	0	0	1.07E-05
Cacna2d1	calcium channel, voltage-dependent, alpha2/delta subunit 1	497.6	0	0	1.15E-05
Sned1	sushi, nidogen and EGF-like domains 1	497.4	0	0	1.15E-05
Serpinf1	serine (or cysteine) peptidase inhibitor, clade F, member 1	2277.6	233.4	0.102	1.56E-05
Col8a1	collagen, type VIII, alpha 1	478.1	0	0	1.92E-05
Arsb	arylsulfatase B	477.9	0	0	1.92E-05
Pdia3	protein disulfide isomerase associated 3	2333.5	273.3	0.117	1.92E-05
Edem3	ER degradation enhancer, mannosidase alpha-like 3	470.1	0	0	2.36E-05
Tmtc3	transmembrane and tetratricopeptide repeat containing 3	466.8	0	0	2.57E-05
Ikbip	IKBKB interacting protein	465.6	0	0	2.62E-05
Bmpr2	bone morphogenetic protein receptor, type II (serine/threonine kinase)	1188.5	55.8	0.047	2.84E-05
Spcs3	signal peptidase complex subunit 3 homolog (S. cerevisiae)	951.0	47.0	0.049	2.88E-05
Abca5	ATP-binding cassette, sub-family A (ABC1), member 5	454.1	0	0	3.53E-05
Ccnl2	cyclin L2	740.3	15.6	0.021	3.53E-05
Ltbp2	latent transforming growth factor beta binding protein 2	450.5	0	0	3.83E-05
Abcc5	ATP-binding cassette, sub-family C (CFTR/MRP), member 5	448.9	0	0	3.96E-05
Kif1c	kinesin family member 1C	452.9	15529.0	34.291	4.02E-05
P4ha1	procollagen-proline, 2-oxoglutarate 4-dioxygenase	801.1	30.8	0.038	4.45E-05

	(proline 4-hydroxylase), alpha 1 polypeptide				
Insig1	insulin induced gene 1	431.4	0	0	6.45E-05
Pdia4	protein disulfide isomerase associated 4	537.8	3.5	0.006	6.45E-05
Alg10b	asparagine-linked glycosylation 10B (alpha-1,2-glucosyltransferase)	425.4	0	0	7.57E-05
Yipf5	Yip1 domain family, member 5	521.8	7.8	0.015	8.53E-05
Tmed5	transmembrane emp24 protein transport domain containing 5	686.1	15.6	0.023	9.62E-05
Vasn	vasorin	415.6	0	0	9.88E-05
Slc12a2	solute carrier family 12, member 2	412.2	0	0	0.0001
Sc4mol	sterol-C4-methyl oxidase-like	410.6	0	0	0.0001
Rprl2	ribonuclease P RNA-like 2	0.1	1034.8	7049.679	0.0001
Tspan3	tetraspanin 3	409.4	0	0	0.0001
Omd	osteomodulin	1296.1	144.0	0.111	0.0001
Lbr	lamin B receptor	402.6	0	0	0.0001
Slc7a6	solute carrier family 7 (cationic amino acid transporter, y+ system), member 6	400.6	0	0	0.0001
Pam	peptidylglycine alpha-amidating monooxygenase	1357.9	160.8	0.118	0.0002
Slc38a2	solute carrier family 38, member 2	2069.1	282.5	0.137	0.0002
Col4a3bp	collagen, type IV, alpha 3 (Goodpasture antigen) binding protein	391.9	0	0	0.0002
Dnajc3	DnaJ (Hsp40) homolog, subfamily C, member 3	491.3	3.5	0.007	0.0002
Tpbg	trophoblast glycoprotein	390.3	0	0	0.0002
Tm9sf2	transmembrane 9 superfamily member 2	882.8	72.9	0.083	0.0002
Zc2hc1a	zinc finger, C2HC-type containing 1A	388.1	0	0	0.0002
Zmym2	zinc finger, MYM-type 2	384.2	0	0	0.0002
Tm9sf1	transmembrane 9 superfamily member 1	383.6	0	0	0.0002

Pmp22	peripheral myelin protein 22	415.7	0	0	0.0003
Timp2	tissue inhibitor of metalloproteinase 2	2705.5	313.4	0.116	0.0003
Mmp14	matrix metallopeptidase 14 (membrane-inserted)	2107.3	243.5	0.116	0.0003
Bmpr1a	bone morphogenetic protein receptor, type 1A	817.4	18.7	0.023	0.0003
Pdzd8	PDZ domain containing 8	373.4	0	0	0.0003
Sgpl1	sphingosine phosphate lyase 1	567.4	11.2	0.020	0.0003
Vldlr	very low density lipoprotein receptor	371.3	0	0	0.0003
Hiatl1	hippocampus abundant transcript-like 1	584.4	13.4	0.023	0.0004
Mkln1	muskelin 1, intracellular mediator containing kelch motifs	415.7	3.9	0.009	0.0004
Elovl5	ELOVL family member 5, elongation of long chain fatty acids (yeast)	363.5	0	0	0.0004
Hist3h2ba	histone cluster 3, H2ba	0.0	364.0	Inf	0.0004
Zkscan3	zinc finger with KRAB and SCAN domains 3	359.3	0	0	0.0004
Ptprs	protein tyrosine phosphatase, receptor type, S	2088.5	155.4	0.074	0.0004
Degs1	degenerative spermatocyte homolog 1 (Drosophila)	356.1	0	0	0.0005
Camk2d	calcium/calmodulin-dependent protein kinase II, delta	354.4	0	0	0.0005
Hs2st1	heparan sulfate 2-O-sulfotransferase 1	351.9	0	0	0.0005
Rtn4	reticulon 4	2043.5	311.9	0.153	0.0006
Azi2	5-azacytidine induced gene 2	348.2	0	0	0.0006
Ibsp	integrin binding sialoprotein	503.4	0	0	0.0006
Lars2	leucyl-tRNA synthetase, mitochondrial	10357.3	4473632.4	431.932	0.0007
Ltbp3	latent transforming growth factor beta binding protein 3	390.8	3.9	0.010	0.0007

Tfrc	transferrin receptor	538.1	23.5	0.044	0.0007
Mbnl1	muscleblind-like 1 (Drosophila)	2590.4	347.5	0.134	0.0007
Emilin2	elastin microfibril interfacer 2	337.8	0	0	0.0008
Ppap2a	phosphatidic acid phosphatase type 2A	337.4	0	0	0.0008
Hsp90b1	heat shock protein 90, beta (Grp94), member 1	3479.4	622.8	0.179	0.0008
Cyb5r3	cytochrome b5 reductase 3	499.2	12797.1	25.634	0.0008
Thbs1	thrombospondin 1	33026.4	2375.4	0.072	0.0008
Itpr1	inositol 1,4,5-trisphosphate receptor 1	384.5	2.2	0.006	0.0008
Col5a1	collagen, type V, alpha 1	2971.7	436.3	0.147	0.0009
Alb	albumin	0.0	213.2	4356.990	0.0009
Rnf145	ring finger protein 145	330.8	0	0	0.0009
Srsf10	serine/arginine-rich splicing factor 10	1112.4	88.3	0.079	0.0009
Pdia6	protein disulfide isomerase associated 6	1370.1	141.4	0.103	0.0009
Mir3064	microRNA 3064	328.9	0	0	0.0009
Sypl	synaptophysin-like protein	328.8	0	0	0.0009
Satb2	special AT-rich sequence binding protein 2	326.5	0	0	0.0010
Slc41a2	solute carrier family 41, member 2	325.1	0	0	0.0010
Clk1	CDC-like kinase 1	891.6	91.3	0.102	0.0011
Man2a1	mannosidase 2, alpha 1	806.4	46.9	0.058	0.0012
St3gal5	ST3 beta-galactoside alpha-2,3-sialyltransferase 5	321.1	0	0	0.0012
Acp2	acid phosphatase 2, lysosomal	321.0	0	0	0.0012
Col12a1	collagen, type XII, alpha 1	10271.0	494.7	0.048	0.0012
Tia1	cytotoxic granule-associated RNA binding protein 1	579.2	20.1	0.035	0.0014
Hspa5	heat shock protein 5	2652.4	340.5	0.128	0.0014
Atp6ap1	ATPase, H+ transporting, lysosomal accessory protein 1	315.0	0	0	0.0014
Ssr1	signal sequence receptor, alpha	1244.7	152.1	0.122	0.0014

Epm2aip1	EPM2A (laforin) interacting protein 1	771.6	44.6	0.058	0.0015
Heatr5a	HEAT repeat containing 5A	529.7	15.6	0.030	0.0015
Btbd7	BTB (POZ) domain containing 7	311.2	0.0	0.000	0.0015
Slc35b4	solute carrier family 35, member B4	310.2	0.0	0.000	0.0016
Lrrcc1	leucine rich repeat and coiled-coil domain containing 1	946.0	118.7	0.126	0.0016
Ubn2	ubinuclein 2	857.5	91.3	0.106	0.0016
Fam3c	family with sequence similarity 3, member C	308.5	0	0	0.0016
Ece1	endothelin converting enzyme 1	307.9	0	0	0.0016
Mgea5	meningioma expressed antigen 5 (hyaluronidase)	585.6	22.3	0.038	0.0017
Ift80	intraflagellar transport 80	305.4	0	0	0.0018
Pgrmc1	progesterone receptor membrane component 1	960.3	75.6	0.079	0.0018
Otud4	OTU domain containing 4	823.3	78.3	0.095	0.0018
Ndnf	neuron-derived neurotrophic factor	302.7	0.0	0.000	0.0019
Zfp36l1	zinc finger protein 36, C3H type-like 1	1023.5	110.8	0.108	0.0020
Adamts9	a disintegrin-like and metallopeptidase (reprolysin type) with thrombospondin type 1 motif, 9	301.1	0	0	0.0020
Hsd17b12	hydroxysteroid (17-beta) dehydrogenase 12	300.8	0	0	0.0020
Dnajc10	DnaJ (Hsp40) homolog, subfamily C, member 10	1049.2	93.8	0.089	0.0021
Tmx3	thioredoxin-related transmembrane protein 3	662.3	33.5	0.051	0.0021
Itgb1	integrin beta 1 (fibronectin receptor beta)	4483.4	557.1	0.124	0.0021
Bmp1	bone morphogenetic protein 1	642.5	31.3	0.049	0.0021
Insig2	insulin induced gene 2	343.6	2.2	0.006	0.0022
Tmem2	transmembrane protein 2	705.3	78.5	0.111	0.0022
Rcn2	reticulocalbin 2	605.4	26.8	0.044	0.0022

Cd44	CD44 antigen	1509.0	130.7	0.087	0.0022
Morf4l1	mortality factor 4 like 1	3209.2	810.9	0.253	0.0022
Asah1	N-acylsphingosine amidohydrolase 1	407.3	6.7	0.016	0.0022
Heatr1	HEAT repeat containing 1	294.6	0.0	0.000	0.0023
Gas1	growth arrest specific 1	741.5	71.1	0.096	0.0023
Man1a2	mannosidase, alpha, class 1A, member 2	822.0	57.1	0.069	0.0023
Cnst	consortin, connexin sorting protein	292.9	0	0	0.0024
Rab11a	RAB11a, member RAS oncogene family	292.5	0	0	0.0024
Gja1	gap junction protein, alpha 1	649.7	33.5	0.052	0.0024
Tmem30a	transmembrane protein 30A	1503.9	94.7	0.063	0.0024
Map3k2	mitogen-activated protein kinase kinase kinase 2	694.8	78.5	0.113	0.0024
Ids	iduronate 2-sulfatase	881.8	104.1	0.118	0.0024
Sdc3	syndecan 3	1050.3	114.0	0.109	0.0024
Hmgcs1	3-hydroxy-3-methylglutaryl-Coenzyme A synthase 1	999.2	134.9	0.135	0.0025
Slc30a7	solute carrier family 30 (zinc transporter), member 7	399.2	9.1	0.023	0.0025
Aebp2	AE binding protein 2	917.4	75.9	0.083	0.0026
Cav2	caveolin 2	535.8	20.1	0.037	0.0026
Cd164	CD164 antigen	1300.9	121.9	0.094	0.0026
Ptx3	pentraxin related gene	700.3	13.4	0.019	0.0026
Xiap	X-linked inhibitor of apoptosis	674.0	38.0	0.056	0.0026
Fads3	fatty acid desaturase 3	284.3	0.0	0.000	0.0030
Slc35f5	solute carrier family 35, member F5	284.1	0.0	0.000	0.0030
Pcdh19	protocadherin 19	538.1	30.8	0.057	0.0030
Ap4e1	adaptor-related protein complex AP-4, epsilon 1	283.5	0.0	0.000	0.0030
Hist1h2bn	histone cluster 1, H2bn	20.7	1199.5	57.977	0.0030
Calu	calumenin	4266.0	900.4	0.211	0.0031
Ltbp1	latent transforming growth factor beta binding protein	1928.3	224.3	0.116	0.0032

	1				
Tmem106b	transmembrane protein 106B	1089.0	57.3	0.053	0.0032
Itm2a	integral membrane protein 2A	688.7	42.4	0.062	0.0033
Papd5	PAP associated domain containing 5	279.7	0	0	0.0033
Fmod	fibromodulin	279.7	0	0	0.0033
Serpinh1	serine (or cysteine) peptidase inhibitor, clade H, member 1	1558.3	185.2	0.119	0.0033
Sh3bp4	SH3-domain binding protein 4	278.7	0	0	0.0034
Plxna2	plexin A2	277.8	0	0	0.0035
Lmbrd1	LMBR1 domain containing 1	354.1	4.5	0.013	0.0037
A730098P 11Rik	mortality factor 4 like 1 pseudogene	2809.8	733.1	0.261	0.0037
Wnt10b	wingless related MMTV integration site 10b	274.9	0	0	0.0038
Cpne3	copine III	351.7	4.5	0.013	0.0039
Fkbp10	FK506 binding protein 10	951.4	89.3	0.094	0.0039
Gfra2	glial cell line derived neurotrophic factor family receptor alpha 2	271.6	0	0	0.0042
Prosc	proline synthetase co-transcribed	269.4	0	0	0.0045
Rab2a	RAB2A, member RAS oncogene family	1189.9	133.5	0.112	0.0046
Atp2b1	ATPase, Ca++ transporting, plasma membrane 1	773.1	60.3	0.078	0.0047
Timp3	tissue inhibitor of metalloproteinase 3	2185.4	359.1	0.164	0.0049
Csgalnact 2	chondroitin sulfate N-acetylgalactosaminyltransf erase 2	265.2	0	0	0.0051
Runx2	runt related transcription factor 2	1111.0	188.6	0.170	0.0051
Mme	membrane metallo endopeptidase	1096.1	122.8	0.112	0.0051
Ptgs2	prostaglandin-endoperoxide synthase 2	264.4	0.0	0.000	0.0052

Ddx17	DEAD (Asp-Glu-Ala-Asp) box polypeptide 17	2290.9	391.6	0.171	0.0052
Hist1h2bg	histone cluster 1, H2bg	33.3	1521.6	45.678	0.0053
Prpf39	PRP39 pre-mRNA processing factor 39 homolog (yeast)	722.3	53.6	0.074	0.0053
Ssr2	signal sequence receptor, beta	456.0	15.6	0.034	0.0054
Smurf2	SMAD specific E3 ubiquitin protein ligase 2	413.3	11.2	0.027	0.0055
Arl6ip5	ADP-ribosylation factor-like 6 interacting protein 5	453.7	15.6	0.034	0.0056
Ankle2	ankyrin repeat and LEM domain containing 2	260.9	0	0	0.0056
Tnfrsf11b	tumor necrosis factor receptor superfamily, member 11b (osteoprotegerin)	260.8	0	0	0.0056
Npc1	Niemann Pick type C1	260.5	0	0	0.0057
Zfyve16	zinc finger, FYVE domain containing 16	260.1	0	0	0.0057
Lman1	lectin, mannose-binding, 1	1058.9	194.3	0.184	0.0059
Tm2d1	TM2 domain containing 1	450.7	15.6	0.035	0.0059
Larp4	La ribonucleoprotein domain family, member 4	850.3	78.1	0.092	0.0059
Man2a2	mannosidase 2, alpha 2	258.8	0	0	0.0059
Fam134a	family with sequence similarity 134, member A	257.6	0	0	0.0061
Sppl2a	signal peptide peptidase like 2A	655.5	44.6	0.068	0.0061
Map4k3	mitogen-activated protein kinase kinase kinase kinase 3	406.0	11.2	0.027	0.0063
Hist1h2bj	histone cluster 1, H2bj	13.9	821.4	59.233	0.0063
Yipf4	Yip1 domain family, member 4	706.5	53.6	0.076	0.0063
Kdelr3	KDEL (Lys-Asp-Glu-Leu) endoplasmic reticulum protein retention receptor 3	255.9	0.0	0.000	0.0064
Sh3pxd2a	SH3 and PX domains 2A	881.3	9843.8	11.170	0.0065
15-Sep	selenoprotein	828.0	75.9	0.092	0.0065
Itm2c	integral membrane protein 2C	689.4	51.3	0.074	0.0066

Ptgfrn	prostaglandin F2 receptor negative regulator	253.6	0.0	0.000	0.0068
Hspg2	perlecan (heparan sulfate proteoglycan 2)	3331.4	521.8	0.157	0.0070
Prelp	proline arginine-rich end leucine-rich repeat	252.5	0	0	0.0070
Col15a1	collagen, type XV, alpha 1	251.5	0	0	0.0072
Fnbp4	formin binding protein 4	251.2	0	0	0.0072
Med12	mediator of RNA polymerase II transcription, subunit 12 homolog (yeast)	324.5	4.5	0.014	0.0072
Nipbl	Nipped-B homolog (Drosophila)	935.9	146.1	0.156	0.0073
Cers6	ceramide synthase 6	250.7	0	0	0.0073
Nedd9	neural precursor cell expressed, developmentally down-regulated gene 9	250.4	0	0	0.0073
Slc4a7	solute carrier family 4, sodium bicarbonate cotransporter, member 7	473.7	39.2	0.083	0.0074
Tmem57	transmembrane protein 57	249.2	0.0	0.000	0.0075
Snx14	sorting nexin 14	249.0	0.0	0.000	0.0076
Rad21	RAD21 homolog (S. pombe)	1815.4	283.4	0.156	0.0078
Stt3b	STT3, subunit of the oligosaccharyltransferase complex, homolog B (S. cerevisiae)	908.1	96.0	0.106	0.0081
Txndc16	thioredoxin domain containing 16	246.3	0.0	0.000	0.0082
Gabbr1	gamma-aminobutyric acid (GABA) B receptor, 1	246.2	0.0	0.000	0.0082
Anapc1	anaphase promoting complex subunit 1	1185.3	156.3	0.132	0.0083
Enpp2	ectonucleotide pyrophosphatase/phosphodiesterase 2	375.3	3.9	0.010	0.0083
Plat	plasminogen activator, tissue	245.4	0.0	0.000	0.0084
Ptprd	protein tyrosine phosphatase, receptor type, D	621.8	83.7	0.135	0.0084
Colec12	collectin sub-family	1312.4	297.4	0.227	0.0087

	member 12				
Myadm	myeloid-associated differentiation marker	591.6	48.6	0.082	0.0087
Zdhhc20	zinc finger, DHHC domain containing 20	480.8	40.5	0.084	0.0087
Laptm4a	lysosomal-associated protein transmembrane 4A	1423.3	216.0	0.152	0.0089
Hip1	huntingtin interacting protein 1	478.1	22.3	0.047	0.0090
Ddhd2	DDHD domain containing 2	241.6	0.0	0.000	0.0093
Nrp2	neuropilin 2	2332.4	118.3	0.051	0.0094
Gns	glucosamine (N-acetyl)-6-sulfatase	739.8	86.1	0.116	0.0094
Pigs	phosphatidylinositol glycan anchor biosynthesis, class S	240.6	0.0	0.000	0.0096
Gclc	glutamate-cysteine ligase, catalytic subunit	356.3	14.0	0.039	0.0097
Itga1	integrin alpha 1	239.9	0.0	0.000	0.0097
Mtdh	metadherin	1931.4	261.1	0.135	0.0099
Lgmn	legumain	472.4	22.3	0.047	0.0099
Mfsd1	major facilitator superfamily domain containing 1	547.7	66.7	0.122	0.0099
Lnp	limb and neural patterns	238.9	0.0	0.000	0.0099
Rassf3	Ras association (RalGDS/AF-6) domain family member 3	89.3	1933.9	21.664	0.0099
Lats1	large tumor suppressor	471.7	22.3	0.047	0.0099
Ttc14	tetratricopeptide repeat domain 14	703.5	60.3	0.086	0.0099
Cenpb	centromere protein B	302.5	6595.3	21.801	0.0099
Tmem127	transmembrane protein 127	238.5	0.0	0.000	0.0099
Mmp16	matrix metallopeptidase 16	238.5	0.0	0.000	0.0099
Tgfbr2	transforming growth factor, beta receptor II	567.9	44.7	0.079	0.0099
Cln5	ceroid-lipofuscinosis, neuronal 5	237.8	0.0	0.000	0.0100
Pdgfrb	platelet derived growth factor receptor, beta polypeptide	966.8	149.3	0.154	0.0100
Alcam	activated leukocyte cell	237.7	0.0	0.000	0.0100

	adhesion molecule				
Ep400	E1A binding protein p400	485.5	24.6	0.051	0.0100
Fbxo33	F-box protein 33	237.5	0.0	0.000	0.0100
Dlx5	distal-less homeobox 5	237.3	0.0	0.000	0.0100
Antxr1	anthrax toxin receptor 1	1148.8	116.3	0.101	0.0100
Slc35e1	solute carrier family 35, member E1	236.9	0.0	0.000	0.0101
Hist1h2bh	histone cluster 1, H2bh	20.3	919.1	45.229	0.0103
Ano6	anoctamin 6	563.5	58.8	0.104	0.0107
6720401G 13Rik	RIKEN cDNA 6720401G13 gene	234.5	0.0	0.000	0.0109
Csnk2a2	casein kinase 2, alpha prime polypeptide	234.5	0.0	0.000	0.0109
Ccnt2	cyclin T2	234.4	0.0	0.000	0.0109
Zbtb7a	zinc finger and BTB domain containing 7a	233.9	0.0	0.000	0.0110
Laptm4b	lysosomal-associated protein transmembrane 4B	496.1	54.9	0.111	0.0119
Gpc6	glypican 6	678.5	44.6	0.066	0.0119
Rbbp6	retinoblastoma binding protein 6	468.0	13.4	0.029	0.0119
Marcks	myristoylated alanine rich protein kinase C substrate	4577.6	1038.1	0.227	0.0119
Man1b1	mannosidase, alpha, class 1B, member 1	230.2	0.0	0.000	0.0124
Gpc4	glypican 4	472.5	24.6	0.052	0.0124
Hiat1	hippocampus abundant gene transcript 1	229.5	0.0	0.000	0.0126
Dhx33	DEAH (Asp-Glu-Ala-His) box polypeptide 33	339.8	15.7	0.046	0.0127
Cnot8	CCR4-NOT transcription complex, subunit 8	228.4	0.0	0.000	0.0131
Rpn1	ribophorin I	831.3	104.6	0.126	0.0131
Soat1	sterol O-acyltransferase 1	403.3	15.6	0.039	0.0132
Cdk2	cyclin-dependent kinase 2	227.0	0.0	0.000	0.0136
Cyth3	cytohesin 3	226.9	0.0	0.000	0.0136
Derl2	Der1-like domain family, member 2	226.0	0.0	0.000	0.0140
Dcaf8	DDB1 and CUL4 associated factor 8	449.7	22.3	0.050	0.0140
Cdh11	cadherin 11	1321.5	147.1	0.111	0.0140

Sec61a1	Sec61 alpha 1 subunit (S. cerevisiae)	925.9	113.9	0.123	0.0140
Olfml2b	olfactomedin-like 2B	595.6	66.0	0.111	0.0140
Zbed6	zinc finger, BED domain containing 6	912.0	125.7	0.138	0.0142
Vcl	vinculin	2535.0	489.8	0.193	0.0142
Hist1h2be	histone cluster 1, H2be	35.7	1478.3	41.414	0.0147
Syvn1	synovial apoptosis inhibitor 1, synoviolin	223.8	0.0	0.000	0.0148
Tmco1	transmembrane and coiled-coil domains 1	316.4	6.7	0.021	0.0149
Ccne2	cyclin E2	223.1	0.0	0.000	0.0151
Hist1h2bb	histone cluster 1, H2bb	12.6	786.5	62.499	0.0156
Nrp1	neuropilin 1	534.6	58.8	0.110	0.0159
Fmnl2	formin-like 2	221.0	0.0	0.000	0.0160
Fn1	fibronectin 1	23220.2	4837.4	0.208	0.0160
Tlr2	toll-like receptor 2	220.8	0.0	0.000	0.0160
Mpc2	mitochondrial pyruvate carrier 2	220.5	0.0	0.000	0.0162
Tmem19	transmembrane protein 19	220.3	0.0	0.000	0.0162
Vaultrc5	vault RNA component 5	0.0	358.4	Inf	0.0164
Ubr3	ubiquitin protein ligase E3 component n-recognin 3	777.5	83.8	0.108	0.0164
Fam160b1	family with sequence similarity 160, member B1	219.7	0.0	0.000	0.0164
Sun1	Sad1 and UNC84 domain containing 1	423.6	20.1	0.047	0.0164
Rmnd5a	required for meiotic nuclear division 5 homolog A (S. cerevisiae)	584.0	91.5	0.157	0.0167
B3galtl	beta 1,3-galactosyltransferase-like	218.9	0.0	0.000	0.0167
Piezo1	piezo-type mechanosensitive ion channel component 1	632.6	55.8	0.088	0.0167
Cd109	CD109 antigen	452.8	24.6	0.054	0.0167
Eif4enif1	eukaryotic translation initiation factor 4E nuclear import factor 1	218.7	0.0	0.000	0.0167
Fnip1	folliculin interacting protein 1	650.8	77.7	0.119	0.0167
Dlg1	discs, large homolog 1 (Drosophila)	590.1	70.0	0.119	0.0167

Hexa	hexosaminidase A	218.5	0.0	0.000	0.0167
Zfx	zinc finger protein X-linked	770.5	84.8	0.110	0.0171
Mbnl2	muscleblind-like 2	1271.9	257.6	0.203	0.0175
Nfib	nuclear factor I/B	1102.7	184.3	0.167	0.0175
Ecm1	extracellular matrix protein 1	216.3	0.0	0.000	0.0179
Dzip3	DAZ interacting protein 3, zinc finger	466.6	54.9	0.118	0.0181
Arf2	ADP-ribosylation factor 2	215.8	0.0	0.000	0.0181
Gpr176	G protein-coupled receptor 176	253.3	2.2	0.009	0.0181
Casd1	CAS1 domain containing 1	215.5	0.0	0.000	0.0182
Rsbn1	rosbin, round spermatid basic protein 1	215.4	0.0	0.000	0.0183
Ttyh3	tweety homolog 3 (Drosophila)	215.3	0.0	0.000	0.0183
Zc3h11a	zinc finger CCCH type containing 11A	1124.1	121.3	0.108	0.0183
Ppib	peptidylprolyl isomerase B	651.9	94.0	0.144	0.0184
Zdhhc17	zinc finger, DHHC domain containing 17	214.7	0.0	0.000	0.0184
Hexb	hexosaminidase B	214.7	0.0	0.000	0.0184
Adnp	activity-dependent neuroprotective protein	473.8	29.0	0.061	0.0184
Col6a3	collagen, type VI, alpha 3	2169.4	228.2	0.105	0.0184
Dsel	dermatan sulfate epimerase-like	214.3	0.0	0.000	0.0186
Angptl4	angiopoietin-like 4	251.7	1.2	0.005	0.0192
Hist1h2bk	histone cluster 1, H2bk	23.0	1346.0	58.588	0.0194
Nup155	nucleoporin 155	715.1	75.9	0.106	0.0196
Lgr4	leucine-rich repeat-containing G protein-coupled receptor 4	212.0	0.0	0.000	0.0199
Gxylt2	glucoside xylosyltransferase 2	211.8	0.0	0.000	0.0200
Prrx1	paired related homeobox 1	3175.9	633.5	0.199	0.0200
Naa25	N(alpha)-acetyltransferase 25, NatB auxiliary subunit	211.6	0.0	0.000	0.0201
Kdelc1	KDEL (Lys-Asp-Glu-Leu) containing 1	211.5	0.0	0.000	0.0201

Trpm7	transient receptor potential cation channel, subfamily M, member 7	742.7	82.6	0.111	0.0201
Qsox1	quiescin Q6 sulfhydryl oxidase 1	575.2	68.3	0.119	0.0202
Slc35a1	solute carrier family 35 (CMP-sialic acid transporter), member 1	211.1	0.0	0.000	0.0202
C1s	complement component 1, s subcomponent	300.6	6.7	0.022	0.0202
Pcolce	procollagen C-endopeptidase enhancer protein	775.5	146.1	0.188	0.0202
Sgms1	sphingomyelin synthase 1	210.5	0.0	0.000	0.0206
Senp7	SUMO1/sentrin specific peptidase 7	210.2	0.0	0.000	0.0207
Tiparp	TCDD-inducible poly(ADP-ribose) polymerase	209.2	0.0	0.000	0.0214
Klf3	Kruppel-like factor 3 (basic)	208.9	0.0	0.000	0.0216
Col11a1	collagen, type XI, alpha 1	208.6	0.0	0.000	0.0218
Tor1aip2	torsin A interacting protein 2	893.1	147.0	0.165	0.0220
Cd47	CD47 antigen (Rh-related antigen, integrin-associated signal transducer)	317.5	8.9	0.028	0.0222
Tmem245	transmembrane protein 245	321.1	5.0	0.016	0.0224
Ski	ski sarcoma viral oncogene homolog (avian)	505.0	45.1	0.089	0.0225
Lamc1	laminin, gamma 1	849.0	70.7	0.083	0.0228
Dedd	death effector domain-containing	271.0	4.5	0.016	0.0230
Mylip	myosin regulatory light chain interacting protein	206.4	0.0	0.000	0.0231
Eya4	eyes absent 4 homolog (Drosophila)	430.6	24.6	0.057	0.0233
Cers5	ceramide synthase 5	205.7	0.0	0.000	0.0236
Mark3	MAP/microtubule affinity-regulating kinase 3	325.5	19.6	0.060	0.0236
Ext2	exostoses (multiple) 2	205.5	0.0	0.000	0.0236
Sparc	secreted acidic cysteine rich glycoprotein	12720.9	3340.4	0.263	0.0236

Hs6st2	heparan sulfate 6-O-sulfotransferase 2	333.5	11.2	0.033	0.0236
Smap1	stromal membrane-associated protein 1	611.4	58.0	0.095	0.0236
Ergic1	endoplasmic reticulum-golgi intermediate compartment (ERGIC) 1	507.6	38.0	0.075	0.0236
Tcea1	transcription elongation factor A (SII) 1	1704.9	448.7	0.263	0.0240
Prpf40a	PRP40 pre-mRNA processing factor 40 homolog A (yeast)	1265.1	278.0	0.220	0.0241
Tmem50a	transmembrane protein 50A	368.7	31.4	0.085	0.0245
Prdx4	peroxiredoxin 4	631.4	60.5	0.096	0.0245
Plxna3	plexin A3	203.7	0.0	0.000	0.0245
Clcn7	chloride channel 7	203.7	0.0	0.000	0.0245
Sun2	Sad1 and UNC84 domain containing 2	585.2	53.6	0.092	0.0246
Rbm12b2	RNA binding motif protein 12 B2	202.7	0.0	0.000	0.0252
Sfrp2	secreted frizzled-related protein 2	16768.7	309.5	0.018	0.0252
Rprd1a	regulation of nuclear pre-mRNA domain containing 1A	266.3	4.5	0.017	0.0252
Ahr	aryl-hydrocarbon receptor	201.9	0.0	0.000	0.0258
Tmem168	transmembrane protein 168	201.7	0.0	0.000	0.0260
Erp44	endoplasmic reticulum protein 44	310.0	7.9	0.026	0.0260
Igf2bp3	insulin-like growth factor 2 mRNA binding protein 3	201.3	0.0	0.000	0.0262
Hist1h3e	histone cluster 1, H3e	3.6	841.7	234.947	0.0264
Dhx36	DEAH (Asp-Glu-Ala-His) box polypeptide 36	637.3	84.4	0.132	0.0267
Pros1	protein S (alpha)	528.2	63.8	0.121	0.0267
Pappa2	pappalysin 2	424.9	51.0	0.120	0.0272
Lpin2	lipin 2	199.8	0.0	0.000	0.0273
Ppp3cb	protein phosphatase 3, catalytic subunit, beta isoform	446.3	29.0	0.065	0.0273
Zfp281	zinc finger protein 281	263.5	3.5	0.013	0.0274
Lifr	leukemia inhibitory factor	1265.4	253.0	0.200	0.0274

	receptor				
Ccl7	chemokine (C-C motif) ligand 7	258.3	0.0	0.000	0.0278
Pole	polymerase (DNA directed), epsilon	199.0	0.0	0.000	0.0278
Spcs2	signal peptidase complex subunit 2 homolog (S. cerevisiae)	198.9	0.0	0.000	0.0278
Nxf1	nuclear RNA export factor 1	430.2	26.8	0.062	0.0285
Slc30a5	solute carrier family 30 (zinc transporter), member 5	415.9	24.6	0.059	0.0288
Emc1	ER membrane protein complex subunit 1	432.0	54.9	0.127	0.0288
Nov	nephroblastoma overexpressed gene	362.2	0.0	0.000	0.0294
Ccdc88a	coiled coil domain containing 88A	972.3	192.3	0.198	0.0294
Tbk1	TANK-binding kinase 1	355.0	15.6	0.044	0.0297
Fam114a1	family with sequence similarity 114, member A1	513.1	42.4	0.083	0.0300
Rtf1	Rtf1, Paf1/RNA polymerase II complex component, homolog (S. cerevisiae)	408.8	44.4	0.109	0.0303
Sp7	Sp7 transcription factor 7	195.9	0.0	0.000	0.0304
Dpy19l4	dpy-19-like 4 (C. elegans)	195.3	0.0	0.000	0.0310
Iars2	isoleucine-tRNA synthetase 2, mitochondrial	450.1	31.3	0.069	0.0313
Zfp948	zinc finger protein 948	194.9	0.0	0.000	0.0314
Gpc1	glypican 1	724.3	88.3	0.122	0.0317
Mzt1	mitotic spindle organizing protein 1	391.2	43.2	0.110	0.0318
Zfp955a	zinc finger protein 955A	194.0	0.0	0.000	0.0321
Atp13a1	ATPase type 13A1	193.5	0.0	0.000	0.0326
Preb	prolactin regulatory element binding	193.4	0.0	0.000	0.0326
Eml4	echinoderm microtubule associated protein like 4	394.1	22.3	0.057	0.0327
Cd63	CD63 antigen	972.9	154.0	0.158	0.0329
Mid2	midline 2	191.2	0.0	0.000	0.0351
Serinc5	serine incorporator 5	191.1	0.0	0.000	0.0352

Kdm6a	lysine (K)-specific demethylase 6A	191.0	0.0	0.000	0.0353
Pdgfa	platelet derived growth factor, alpha	190.5	0.0	0.000	0.0359
Fzd1	frizzled homolog 1 (Drosophila)	216.8	0.0	0.000	0.0360
Tomm22	translocase of outer mitochondrial membrane 22 homolog (yeast)	477.0	38.0	0.080	0.0360
Ppp1cb	protein phosphatase 1, catalytic subunit, beta isoform	3189.7	903.2	0.283	0.0368
Afg3l2	AFG3(ATPase family gene 3)-like 2 (yeast)	189.4	0.0	0.000	0.0371
Slc7a2	solute carrier family 7 (cationic amino acid transporter, y+ system), member 2	270.5	8.4	0.031	0.0374
Fubp1	far upstream element (FUSE) binding protein 1	600.8	114.3	0.190	0.0376
Rer1	RER1 retention in endoplasmic reticulum 1 homolog (S. cerevisiae)	431.6	38.0	0.088	0.0376
Crim1	cysteine rich transmembrane BMP regulator 1 (chordin like)	309.1	11.2	0.036	0.0382
Pdp1	pyruvate dehyrogenase phosphatase catalytic subunit 1	188.3	0.0	0.000	0.0382
Tfb2m	transcription factor B2, mitochondrial	188.2	0.0	0.000	0.0382
Ubtd2	ubiquitin domain containing 2	371.4	20.1	0.054	0.0382
Dnaja1	DnaJ (Hsp40) homolog, subfamily A, member 1	1027.1	204.2	0.199	0.0382
Nisch	nischarin	1655.6	300.6	0.182	0.0382
Sp1	trans-acting transcription factor 1	664.6	82.3	0.124	0.0385
Erlin1	ER lipid raft associated 1	187.5	0.0	0.000	0.0388
Lox	lysyl oxidase	12316.7	1966.6	0.160	0.0389
Hist1h2bq	histone cluster 1, H2bq	68.0	2861.1	42.075	0.0389
Hist1h2br	histone cluster 1 H2br	68.0	2861.1	42.075	0.0389
Arhgap29	Rho GTPase activating protein 29	191.3	0.0	0.000	0.0389

BC016423	cDNA sequence BC016423	488.1	74.0	0.151	0.0389
Ccnh	cyclin H	186.4	0.0	0.000	0.0398
Neto2	neuropilin (NRP) and tolloid (TLL)-like 2	186.1	0.0	0.000	0.0402
Hist1h3a	histone cluster 1, H3a	4.1	677.8	166.280	0.0410
Zdhhc8	zinc finger, DHHC domain containing 8	185.5	0.0	0.000	0.0410
Tmed2	transmembrane emp24 domain trafficking protein 2	1256.9	378.5	0.301	0.0410
Edem1	ER degradation enhancer, mannosidase alpha-like 1	476.4	68.3	0.143	0.0412
Usp10	ubiquitin specific peptidase 10	185.1	0.0	0.000	0.0412
Dock5	dedicator of cytokinesis 5	276.2	0.0	0.000	0.0413
Csf1	colony stimulating factor 1 (macrophage)	1142.6	134.0	0.117	0.0413
Vps37a	vacuolar protein sorting 37A (yeast)	320.6	13.4	0.042	0.0413
Galnt13	UDP-N-acetyl-alpha-D-galactosamine:polypeptide N-acetylgalactosaminyltransferase 13	320.5	13.4	0.042	0.0413
Fth1	ferritin heavy chain 1	1570.2	11992.4	7.637	0.0413
Sp8	trans-acting transcription factor 8	184.6	0.0	0.000	0.0413
Snrk	SNF related kinase	184.6	0.0	0.000	0.0413
Ifnar1	interferon (alpha and beta) receptor 1	245.4	3.5	0.014	0.0413
Thbs2	thrombospondin 2	4566.0	470.4	0.103	0.0413
Tmem184b	transmembrane protein 184b	184.4	0.0	0.000	0.0415
Angptl2	angiopoietin-like 2	441.6	33.5	0.076	0.0415
Fzd5	frizzled homolog 5 (Drosophila)	496.8	58.7	0.118	0.0416
Hist1h2bf	histone cluster 1, H2bf	18.0	871.8	48.557	0.0418
Naa15	N(alpha)-acetyltransferase 15, NatA auxiliary subunit	1219.0	252.4	0.207	0.0418
Met	met proto-oncogene	183.6	0.0	0.000	0.0423
Ufl1	UFM1 specific ligase 1	183.4	0.0	0.000	0.0426

Kctd10	potassium channel tetramerisation domain containing 10	968.9	10082.6	10.407	0.0428
Smad7	SMAD family member 7	183.1	0.0	0.000	0.0429
Tm9sf4	transmembrane 9 superfamily protein member 4	183.0	0.0	0.000	0.0430
Phf20l1	PHD finger protein 20-like 1	400.9	26.8	0.067	0.0441
BC030336	cDNA sequence BC030336	182.2	0.0	0.000	0.0441
Lphn2	latrophilin 2	413.1	29.0	0.070	0.0442
Tmem18	transmembrane protein 18	182.0	0.0	0.000	0.0442
B4galt6	UDP-Gal:betaGlcNAc beta 1,4-galactosyltransferase, polypeptide 6	181.8	0.0	0.000	0.0445
Col4a2	collagen, type IV, alpha 2	181.7	0.0	0.000	0.0445
Gtf3a	general transcription factor III A	181.6	0.0	0.000	0.0445
Sepp1	selenoprotein P, plasma, 1	384.9	41.0	0.107	0.0453
Maf	avian musculoaponeurotic fibrosarcoma (v-maf) AS42 oncogene homolog	502.1	44.6	0.089	0.0453
Inpp5b	inositol polyphosphate-5-phosphatase B	181.0	0.0	0.000	0.0453
D4Wsu53e	DNA segment, Chr 4, Wayne State University 53, expressed	599.8	69.2	0.115	0.0460
Crtap	cartilage associated protein	561.7	95.7	0.170	0.0460
AU040320	expressed sequence AU040320	180.5	0.0	0.000	0.0460
AW549877	expressed sequence AW549877	700.6	136.5	0.195	0.0461
Zfp277	zinc finger protein 277	180.1	0.0	0.000	0.0465
Tmed9	transmembrane emp24 protein transport domain containing 9	260.1	6.7	0.026	0.0467
Rab13	RAB13, member RAS oncogene family	28.9	892.4	30.840	0.0467
Papd7	PAP associated domain containing 7	179.2	0.0	0.000	0.0479
Zmym6	zinc finger, MYM-type 6	179.0	0.0	0.000	0.0479
Mrc2	mannose receptor, C type 2	755.3	130.8	0.173	0.0479

G2e3	G2/M-phase specific E3 ubiquitin ligase	382.0	24.6	0.064	0.0482
Prtg	protogenin homolog (Gallus gallus)	178.6	0.0	0.000	0.0486
Rnf149	ring finger protein 149	276.5	8.9	0.032	0.0498
Masp2	mannan-binding lectin serine peptidase 2	177.8	0.0	0.000	0.0498

APPENDIX C

RNA-SEQ DATA: HIGHLY EXPRESSED GENES IN MSC EXOSOMES

Symbol	Gene Name	Read Count
Rn45s	45S pre-ribosomal RNA	56755301
Lars2	leucyl-tRNA synthetase, mitochondrial	4473632
Eef1a1	eukaryotic translation elongation factor 1 alpha 1	65146
Rps2	ribosomal protein S2	25272
Ncl	nucleolin	24177
Ftl1	ferritin light chain 1	21388
Actb	actin, beta	18815
Eef2	eukaryotic translation elongation factor 2	18021
Wdr92	WD repeat domain 92	15788
Kif1c	kinesin family member 1C	15529
Rplp0	ribosomal protein, large, P0	14565
Cyb5r3	cytochrome b5 reductase 3	12797
Fth1	ferritin heavy chain 1	11992
Rpsa	ribosomal protein SA	11464
Gm6548	eukaryotic translation elongation factor 1 alpha 1 pseudogene	10779
Rpl41	ribosomal protein L41	10733
Ccnd2	cyclin D2	10624
Npm1	nucleophosmin 1	10281
Kctd10	potassium channel tetramerisation domain containing 10	10083
Anp32b	acidic (leucine-rich) nuclear phosphoprotein 32 family, member B	10060
Sh3pxd2a	SH3 and PX domains 2A	9844
Vim	vimentin	9770
Actg1	actin, gamma, cytoplasmic 1	9672
Pabpc1	poly(A) binding protein, cytoplasmic 1	9401
Dst	dystonin	9341
Hsp90ab1	heat shock protein 90 alpha (cytosolic), class B member 1	9086
Ddr2	discoidin domain receptor family, member 2	8866
Eif3a	eukaryotic translation initiation factor 3, subunit A	8815
Gapdh	glyceraldehyde-3-phosphate dehydrogenase	8778
Ahnak	AHNAK nucleoprotein (desmoyokin)	8325

Naa50	N(alpha)-acetyltransferase 50, NatE catalytic subunit	7804
Gm12070	glyceraldehyde-3-phosphate dehydrogenase pseudogene	7466
Ubc	ubiquitin C	7440
Tpt1	tumor protein, translationally-controlled 1	7340
Hspa8	heat shock protein 8	7221
Ubb	ubiquitin B	7083
Gnb2l1	guanine nucleotide binding protein (G protein), beta polypeptide 2 like 1	6840
Trak2	trafficking protein, kinesin binding 2	6712
Cenpb	centromere protein B	6595
Ppia	peptidylprolyl isomerase A	6544
Tmem38b	transmembrane protein 38B	6158
Rps27a	ribosomal protein S27A	6120
Rpl3	ribosomal protein L3	5783
Rpl5	ribosomal protein L5	5739
Myo10	myosin X	5739
Ybx1	Y box protein 1	5667
Net1	neuroepithelial cell transforming gene 1	5646
S100a6	S100 calcium binding protein A6 (calcyclin)	5465
Cald1	caldesmon 1	5465
Plec	plectin	5315
Rps6	ribosomal protein S6	5285
Rps3a1	ribosomal protein S3A1	5170
Nedd4	neural precursor cell expressed, developmentally down-regulated 4	5035
Huwe1	HECT, UBA and WWE domain containing 1	4998
Dynll2	dynein light chain LC8-type 2	4895
Fn1	fibronectin 1	4837
Acta2	actin, alpha 2, smooth muscle, aorta	4835
Malat1	metastasis associated lung adenocarcinoma transcript 1 (non-coding RNA)	4823
Rps14	ribosomal protein S14	4800
Rps12	ribosomal protein S12	4759
Rpl4	ribosomal protein L4	4759
Bgn	biglycan	4735
Tuba1b	tubulin, alpha 1B	4690

Myh9	myosin, heavy polypeptide 9, non-muscle	4668
Rps18	ribosomal protein S18	4636
Gm5643	heterogeneous nuclear ribonucleoprotein A1 pseudogene	4600
Pkm	pyruvate kinase, muscle	4587
Rpl12	ribosomal protein L12	4359
Tpm4	tropomyosin 4	4238
Lgals1	lectin, galactose binding, soluble 1	4191
Palld	palladin, cytoskeletal associated protein	4150
Set	SET nuclear oncogene	4135
Gnas	GNAS (guanine nucleotide binding protein, alpha stimulating) complex locus	4102
Csde1	cold shock domain containing E1, RNA binding	4076
Arhgap11a	Rho GTPase activating protein 11A	4045
Rpl8	ribosomal protein L8	3912
Wnk1	WNK lysine deficient protein kinase 1	3910
Hsp90aa1	heat shock protein 90, alpha (cytosolic), class A member 1	3902
Tuba1c	tubulin, alpha 1C	3885
Rps24	ribosomal protein S24	3821
Calr	calreticulin	3779
Map4	microtubule-associated protein 4	3675
Tpm1	tropomyosin 1, alpha	3659
Hdlbp	high density lipoprotein (HDL) binding protein	3641
Hnrnpa3	heterogeneous nuclear ribonucleoprotein A3	3591
Eif5a	eukaryotic translation initiation factor 5A	3561
Tmsb4x	thymosin, beta 4, X chromosome	3475
Trp53inp2	transformation related protein 53 inducible nuclear protein 2	3435
Myo1h	myosin 1H	3423
Sparc	secreted acidic cysteine rich glycoprotein	3340
Sptbn1	spectrin beta, non-erythrocytic 1	3278
Pkp4	plakophilin 4	3276
Rps8	ribosomal protein S8	3260
Tuba1a	tubulin, alpha 1A	3250
Rpl23a	ribosomal protein L23A	3226
Rps23	ribosomal protein S23	3210
Gm15772	ribosomal protein L26 pseudogene	3190

Rpl26	ribosomal protein L26	3190
Rpl38	ribosomal protein L38	3153
Rps4x	ribosomal protein S4, X-linked	3135
Ccng1	cyclin G1	3110
Hspa9	heat shock protein 9	3104
Hnrnpa1	heterogeneous nuclear ribonucleoprotein A1	3045
Rpl10	ribosomal protein L10	3026
Rplp1	ribosomal protein, large, P1	3018
Ptma	prothymosin alpha	3007
Rpl31	ribosomal protein L31	3005
Scd1	stearoyl-Coenzyme A desaturase 1	2999
Ywhae	tyrosine 3-monooxygenase/tryptophan 5-monooxygenase activation protein, epsilon polypeptide	2988
Rpph1	ribonuclease P RNA component H1	2988
Eif4b	eukaryotic translation initiation factor 4B	2967
Cfl1	cofilin 1, non-muscle	2930
Rpl27a	ribosomal protein L27A	2893
Pcbp2	poly(rC) binding protein 2	2876
Hist1h2bq	histone cluster 1, H2bq	2861
Hist1h2br	histone cluster 1 H2br	2861
Rps29	ribosomal protein S29	2824
Myl6	myosin, light polypeptide 6, alkali, smooth muscle and non-muscle	2816
Eno1	enolase 1, alpha non-neuron	2816
Tmsb10	thymosin, beta 10	2804
Col1a2	collagen, type I, alpha 2	2793
Rpl23	ribosomal protein L23	2781
Serbp1	serpine1 mRNA binding protein 1	2777
Rpl18a	ribosomal protein L18A	2757
Rpl7	ribosomal protein L7	2731
Rbm3	RNA binding motif protein 3	2716
Eif1	eukaryotic translation initiation factor 1	2710
Uba52	ubiquitin A-52 residue ribosomal protein fusion product 1	2701
Rpl13	ribosomal protein L13	2697
Kpnb1	karyopherin (importin) beta 1	2670
Tubb5	tubulin, beta 5 class I	2660

Nrd1	nardilysin, N-arginine dibasic convertase, NRD convertase 1	2625
Fat1	FAT tumor suppressor homolog 1 (Drosophila)	2603
Pgk1	phosphoglycerate kinase 1	2584
Zc3h13	zinc finger CCCH type containing 13	2583
Htatsf1	HIV TAT specific factor 1	2570
Rpl17	ribosomal protein L17	2545
Fgd3	FYVE, RhoGEF and PH domain containing 3	2533
Flna	filamin, alpha	2490
Rprl3	ribonuclease P RNA-like 3	2467
Rps26	ribosomal protein S26	2460
Rps5	ribosomal protein S5	2397
Hnrnpa2b1	heterogeneous nuclear ribonucleoprotein A2/B1	2377
Thbs1	thrombospondin 1	2375
Rps20	ribosomal protein S20	2323
Atp5b	ATP synthase, H+ transporting mitochondrial F1 complex, beta subunit	2316
Tagln	transgelin	2311
Map4k4	mitogen-activated protein kinase kinase kinase kinase 4	2303
Cdv3	carnitine deficiency-associated gene expressed in ventricle 3	2298
Rpl9	ribosomal protein L9	2279
Map2k7	mitogen-activated protein kinase kinase 7	2271
Rps3	ribosomal protein S3	2260
Cnn2	calponin 2	2225
Lrrc58	leucine rich repeat containing 58	2211
Rpl13a	ribosomal protein L13A	2190
Rpl37a	ribosomal protein L37a	2184
Eef1g	eukaryotic translation elongation factor 1 gamma	2167
Zeb1	zinc finger E-box binding homeobox 1	2162
Ctnnb1	catenin (cadherin associated protein), beta 1	2151
Rpl10a	ribosomal protein L10A	2138
Cltc	clathrin, heavy polypeptide (Hc)	2136
Ptpn11	protein tyrosine phosphatase, non-receptor type 11	2105

Hnrnpab	heterogeneous nuclear ribonucleoprotein A/B	2097
Rps9	ribosomal protein S9	2091
Gm6682	tubulin, alpha 1C pseudogene	2087
Macf1	microtubule-actin crosslinking factor 1	2072
Samd4	sterile alpha motif domain containing 4	2068
Rps19	ribosomal protein S19	2065
Rpl11	ribosomal protein L11	2060
Utrn	utrophin	2038
Hist1h2ap	histone cluster 1, H2ap	2028
Hist1h2ao	histone cluster 1, H2ao	2028
Rpl15	ribosomal protein L15	2004
Eif4a1	eukaryotic translation initiation factor 4A1	2003

Data represent the average of 3 samples collected from different passages of MSCs and their exosomes.

REFERENCE LIST

1. Mozaffarian D, Benjamin EJ, Go AS, Arnett DK, Blaha MJ, Cushman M, de Ferranti S, Despres JP, Fullerton HJ, Howard VJ, Huffman MD, Judd SE, Kissela BM, Lackland DT, Lichtman JH, Lisabeth LD, Liu S, Mackey RH, Matchar DB, McGuire DK, Mohler ER, 3rd, Moy CS, Muntner P, Mussolino ME, Nasir K, Neumar RW, Nichol G, Palaniappan L, Pandey DK, Reeves MJ, Rodriguez CJ, Sorlie PD, Stein J, Towfighi A, Turan TN, Virani SS, Willey JZ, Woo D, Yeh RW and Turner MB. Heart disease and stroke statistics--2015 update: a report from the American Heart Association. *Circulation*. 2015;131:e29-322.

2. Heusch G. Treatment of Myocardial Ischemia/Reperfusion Injury by Ischemic and Pharmacological Postconditioning. *Compr Physiol*. 2015;5:1123-45.

3. Yellon DM and Hausenloy DJ. Myocardial reperfusion injury. *N Engl J Med*. 2007;357:1121-35.

4. Factor SM and Bache RJ. Pathophysiology of Myocardial Ischemia. In: R. W. Alexander, R. C. Schlant and V. Fuster, eds. *Hurst's The Heart, Arteries, and Veins*. 9 ed. New York: McGraw-Hill; 1998.

5. Movassagh M and Foo RS. Simplified apoptotic cascades. *Heart Fail Rev*. 2008;13:111-9.

6. Jeremias I, Kupatt C, Martin-Villalba A, Habazettl H, Schenkel J, Boekstegers P and Debatin KM. Involvement of CD95/Apo1/Fas in cell death after myocardial ischemia. *Circulation*. 2000;102:915-20.

7. Lee P, Sata M, Lefer DJ, Factor SM, Walsh K and Kitsis RN. Fas pathway is a critical mediator of cardiac myocyte death and MI during ischemia-reperfusion in vivo. *Am J Physiol Heart Circ Physiol*. 2003;284:H456-63.

8. Li Y, Takemura G, Kosai K, Takahashi T, Okada H, Miyata S, Yuge K, Nagano S, Esaki M, Khai NC, Goto K, Mikami A, Maruyama R, Minatoguchi S, Fujiwara T and Fujiwara H. Critical roles for the Fas/Fas ligand system in postinfarction ventricular remodeling and heart failure. *Circulation research*. 2004;95:627-36.

9. Glembotski CC. The role of the unfolded protein response in the heart. *Journal of molecular and cellular cardiology*. 2008;44:453-9.

10. Szegezdi E, Duffy A, O'Mahoney ME, Logue SE, Mylotte LA, O'Brien T and Samali A. ER stress contributes to ischemia-induced cardiomyocyte apoptosis. *Biochem Biophys Res Commun*. 2006;349:1406-11.

11. Thuerauf DJ, Marcinko M, Gude N, Rubio M, Sussman MA and Glembotski CC. Activation of the unfolded protein response in infarcted mouse heart and hypoxic cultured cardiac myocytes. *Circulation research*. 2006;99:275-82.

12. Toth A, Nickson P, Mandl A, Bannister ML, Toth K and Erhardt P. Endoplasmic reticulum stress as a novel therapeutic target in heart diseases. *Cardiovasc Hematol Disord Drug Targets*. 2007;7:205-18.

13. Wang J, Hu X and Jiang H. ER stress-induced apoptosis: a novel therapeutic target in heart failure. *Int J Cardiol*. 2014;177:564-5.

14. Morishima N, Nakanishi K, Takenouchi H, Shibata T and Yasuhiko Y. An endoplasmic reticulum stress-specific caspase cascade in apoptosis. Cytochrome c-independent activation of caspase-9 by caspase-12. *The Journal of biological chemistry*. 2002;277:34287-94.

15. Murry CE, Jennings RB and Reimer KA. Preconditioning with ischemia: a delay of lethal cell injury in ischemic myocardium. *Circulation*. 1986;74:1124-36.

16. Sumeray MS and Yellon DM. Ischaemic preconditioning reduces infarct size following global ischaemia in the murine myocardium. *Basic research in cardiology*. 1998;93:384-90.

17. Yellon DM, Alkhulaifi AM, Browne EE and Pugsley WB. Ischaemic preconditioning limits infarct size in the rat heart. *Cardiovascular research*. 1992;26:983-7.

18. Cohen MV, Liu GS and Downey JM. Preconditioning causes improved wall motion as well as smaller infarcts after transient coronary occlusion in rabbits. *Circulation*. 1991;84:341-9.

19. Schott RJ, Rohmann S, Braun ER and Schaper W. Ischemic preconditioning reduces infarct size in swine myocardium. *Circulation research*. 1990;66:1133-42.

20. Heusch G. Cardioprotection: chances and challenges of its translation to the clinic. *The Lancet*. 2013;381:166-175.

21. Zhao ZQ, Corvera JS, Halkos ME, Kerendi F, Wang NP, Guyton RA and Vinten-Johansen J. Inhibition of myocardial injury by ischemic postconditioning during reperfusion: comparison with ischemic preconditioning. *Am J Physiol Heart Circ Physiol*. 2003;285:H579-88.

22. Kin H, Zhao ZQ, Sun HY, Wang NP, Corvera JS, Halkos ME, Kerendi F, Guyton RA and Vinten-Johansen J. Postconditioning attenuates myocardial ischemia-reperfusion injury by inhibiting events in the early minutes of reperfusion. *Cardiovascular research*. 2004;62:74-85.

23. Khan AR, Binabdulhak AA, Alastal Y, Khan S, Faricy-Beredo BM, Luni FK, Lee WM, Khuder S and Tinkel J. Cardioprotective role of ischemic postconditioning in acute myocardial infarction: a systematic review and meta-analysis. *Am Heart J*. 2014;168:512-521.e4.

24. Przyklenk K, Bauer B, Ovize M, Kloner RA and Whittaker P. Regional ischemic 'preconditioning' protects remote virgin myocardium from subsequent sustained coronary occlusion. *Circulation*. 1993;87:893-9.

25. Heusch G, Botker HE, Przyklenk K, Redington A and Yellon D. Remote ischemic conditioning. *Journal of the American College of Cardiology*. 2015;65:177-95.

26. Guo Y, Wu WJ, Qiu Y, Tang XL, Yang Z and Bolli R. Demonstration of an early and a late phase of ischemic preconditioning in mice. *The American journal of physiology*. 1998;275:H1375-87.

27. Bolli R. The late phase of preconditioning. *Circulation research*. 2000;87:972-83.

28. Hausenloy DJ, Tsang A, Mocanu MM and Yellon DM. Ischemic preconditioning protects by activating prosurvival kinases at reperfusion. *Am J Physiol Heart Circ Physiol*. 2005;288:H971-6.

29. Hamacher-Brady A, Brady NR and Gottlieb RA. Enhancing macroautophagy protects against ischemia/reperfusion injury in cardiac myocytes. *The Journal of biological chemistry*. 2006;281:29776-87.

30. Huang C, Andres AM, Ratliff EP, Hernandez G, Lee P and Gottlieb RA. Preconditioning involves selective mitophagy mediated by Parkin and p62/SQSTM1. *PLoS One*. 2011;6:e20975.

31. Huang C, Yitzhaki S, Perry CN, Liu W, Giricz Z, Mentzer RM, Jr. and Gottlieb RA. Autophagy induced by ischemic preconditioning is essential for cardioprotection. *Journal of cardiovascular translational research*. 2010;3:365-73.

32. Gurusamy N, Lekli I, Gorbunov NV, Gherghiceanu M, Popescu LM and Das DK. Cardioprotection by adaptation to ischaemia augments autophagy in association with BAG-1 protein. *Journal of cellular and molecular medicine*. 2009;13:373-87.

33. Murry CE, Jennings RB and Reimer KA. New insights into potential mechanisms of ischemic preconditioning. *Circulation*. 1991;84:442-5.

34. Matsuyama N, Leavens JE, McKinnon D, Gaudette GR, Aksehirli TO and Krukenkamp IB. Ischemic but not pharmacological preconditioning requires protein synthesis. *Circulation*. 2000;102:Iii312-8.

35. Rowland RT, Meng X, Cleveland JC, Meldrum DR, Harken AH and Brown JM. Cardioadaptation induced by cyclic ischemic preconditioning is mediated by translational regulation of de novo protein synthesis. *The Journal of surgical research*. 1997;71:155-60.

36. Takashi E, Wang Y and Ashraf M. Activation of Mitochondrial KATP Channel Elicits Late Preconditioning Against Myocardial Infarction via Protein Kinase C Signaling Pathway. *Circulation research*. 1999;85:1146-1153.

37. Xuan YT, Tang XL, Banerjee S, Takano H, Li RC, Han H, Qiu Y, Li JJ and Bolli R. Nuclear factor-kappaB plays an essential role in the late phase of ischemic preconditioning in conscious rabbits. *Circulation research*. 1999;84:1095-109.

38. Tranter M, Ren X, Forde T, Wilhide ME, Chen J, Sartor MA, Medvedovic M and Jones WK. NF-kappaB driven cardioprotective gene programs; Hsp70.3 and cardioprotection after late ischemic preconditioning. *Journal of molecular and cellular cardiology*. 2010;49:664-72.

39. Shohet RV and Garcia JA. Keeping the engine primed: HIF factors as key regulators of cardiac metabolism and angiogenesis during ischemia. *J Mol Med (Berl)*. 2007;85:1309-15.

40. Heusch G, Musiolik J, Gedik N and Skyschally A. Mitochondrial STAT3 activation and cardioprotection by ischemic postconditioning in pigs with regional myocardial ischemia/reperfusion. *Circulation research*. 2011;109:1302-8.

41. Heusch G, Musiolik J, Kottenberg E, Peters J, Jakob H and Thielmann M. STAT5 activation and cardioprotection by remote ischemic preconditioning in humans: short communication. *Circulation research*. 2012;110:111-5.

42. Kim HK, Thu VT, Heo HJ, Kim N and Han J. Cardiac proteomic responses to ischemia-reperfusion injury and ischemic preconditioning. *Expert Rev Proteomics*. 2011;8:241-61.

43. Das DK and Maulik N. Cardiac genomic response following preconditioning stimulus. *Cardiovascular research*. 2006;70:254-63.

44. Eisenhardt BD. Small heat shock proteins: recent developments. *Biomol Concepts*. 2013;4:583-95.

45. Haslbeck M, Franzmann T, Weinfurtner D and Buchner J. Some like it hot: the structure and function of small heat-shock proteins. *Nat Struct Mol Biol*. 2005;12:842-6.

46. Fan GC, Chu G and Kranias EG. Hsp20 and its cardioprotection. *Trends Cardiovasc Med*. 2005;15:138-41.

47. Fan GC, Chu G, Mitton B, Song Q, Yuan Q and Kranias EG. Small heat-shock protein Hsp20 phosphorylation inhibits beta-agonist-induced cardiac apoptosis. *Circulation research*. 2004;94:1474-82.

48. Fan GC, Ren X, Qian J, Yuan Q, Nicolaou P, Wang Y, Jones WK, Chu G and Kranias EG. Novel cardioprotective role of a small heat-shock protein, Hsp20, against ischemia/reperfusion injury. *Circulation*. 2005;111:1792-9.

49. Qian J, Ren X, Wang X, Zhang P, Jones WK, Molkentin JD, Fan GC and Kranias EG. Blockade of Hsp20 phosphorylation exacerbates cardiac ischemia/reperfusion injury by suppressed autophagy and increased cell death. *Circulation research*. 2009;105:1223-31.

50. Krishnamoorthy V, Donofrio AJ and Martin JL. O-GlcNAcylation of alphaB-crystallin regulates its stress-induced translocation and cytoprotection. *Molecular and cellular biochemistry*. 2013;379:59-68.

51. Lu XY, Chen L, Cai XL and Yang HT. Overexpression of heat shock protein 27 protects against ischaemia/reperfusion-induced cardiac dysfunction via stabilization of troponin I and T. *Cardiovascular research*. 2008;79:500-8.

52. Weber NC, Toma O, Wolter JI, Wirthle NM, Schlack W and Preckel B. Mechanisms of xenon- and isoflurane-induced preconditioning - a potential link to the cytoskeleton via the MAPKAPK-2/HSP27 pathway. *British journal of pharmacology*. 2005;146:445-55.

53. Efthymiou CA, Mocanu MM, de Belleroche J, Wells DJ, Latchmann DS and Yellon DM. Heat shock protein 27 protects the heart against myocardial infarction. *Basic research in cardiology*. 2004;99:392-4.

54. Maloyan A, Sanbe A, Osinska H, Westfall M, Robinson D, Imahashi K, Murphy E and Robbins J. Mitochondrial dysfunction and apoptosis underlie the pathogenic process in alpha-B-crystallin desmin-related cardiomyopathy. *Circulation*. 2005;112:3451-61.

55. Pattison JS, Osinska H and Robbins J. Atg7 induces basal autophagy and rescues autophagic deficiency in CryABR120G cardiomyocytes. *Circulation research*. 2011;109:151-60.

56. Sanbe A, Osinska H, Saffitz JE, Glabe CG, Kayed R, Maloyan A and Robbins J. Desmin-related cardiomyopathy in transgenic mice: a cardiac amyloidosis. *Proceedings of the National Academy of Sciences of the United States of America*. 2004;101:10132-6.

57. Qiu XB, Shao YM, Miao S and Wang L. The diversity of the DnaJ/Hsp40 family, the crucial partners for Hsp70 chaperones. *Cell Mol Life Sci*. 2006;63:2560-70.

58. Kampinga HH and Craig EA. The HSP70 chaperone machinery: J proteins as drivers of functional specificity. *Nature reviews Molecular cell biology*. 2010;11:579-92.

59. Cheetham ME and Caplan AJ. Structure, function and evolution of DnaJ: conservation and adaptation of chaperone function. *Cell stress & chaperones*. 1998;3:28-36.

60. Abdul KM, Terada K, Gotoh T, Hafizur RM and Mori M. Characterization and functional analysis of a heart-enriched DnaJ/ Hsp40 homolog dj4/DjA4. *Cell stress & chaperones*. 2002;7:156-66.

61. Depre C, Wang L, Tomlinson JE, Gaussin V, Abdellatif M, Topper JN and Vatner SF. Characterization of pDJA1, a cardiac-specific chaperone found by genomic profiling of the post-ischemic swine heart. *Cardiovascular research*. 2003;58:126-35.

62. Tanaka S, Kitagawa K, Ohtsuki T, Yagita Y, Takasawa K, Hori M and Matsumoto M. Synergistic induction of HSP40 and HSC70 in the mouse hippocampal neurons after cerebral ischemia and ischemic tolerance in gerbil hippocampus. *J Neurosci Res*. 2002;67:37-47.

63. Marber MS, Latchman DS, Walker JM and Yellon DM. Cardiac stress protein elevation 24 hours after brief ischemia or heat stress is associated with resistance to myocardial infarction. *Circulation*. 1993;88:1264-72.

64. Marber MS, Mestril R, Chi SH, Sayen MR, Yellon DM and Dillmann WH. Overexpression of the rat inducible 70-kD heat stress protein in a transgenic mouse increases the resistance of the heart to ischemic injury. *The Journal of clinical investigation*. 1995;95:1446-56.

65. Hampton CR, Shimamoto A, Rothnie CL, Griscavage-Ennis J, Chong A, Dix DJ, Verrier ED and Pohlman TH. HSP70.1 and -70.3 are required for late-phase protection induced by ischemic preconditioning of mouse hearts. *Am J Physiol Heart Circ Physiol*. 2003;285:H866-74.

66. Wilhide ME, Tranter M, Ren X, Chen J, Sartor MA, Medvedovic M and Jones WK. Identification of a NF-kappaB cardioprotective gene program: NF-kappaB regulation of Hsp70.1 contributes to cardioprotection after permanent coronary occlusion. *Journal of molecular and cellular cardiology*. 2011;51:82-9.

67. Nayeem MA, Hess ML, Qian YZ, Loesser KE and Kukreja RC. Delayed preconditioning of cultured adult rat cardiac myocytes: role of 70- and 90-kDa heat stress proteins. *The American journal of physiology*. 1997;273:H861-8.

68. Jiang B, Xiao W, Shi Y, Liu M and Xiao X. Heat shock pretreatment inhibited the release of Smac/DIABLO from mitochondria and apoptosis induced by hydrogen peroxide in cardiomyocytes and C2C12 myogenic cells. *Cell stress & chaperones*. 2005;10:252-62.

69. Jiao JD, Garg V, Yang B and Hu K. Novel functional role of heat shock protein 90 in ATP-sensitive K+ channel-mediated hypoxic preconditioning. *Cardiovascular research*. 2008;77:126-33.

70. Amour J, Brzezinska AK, Weihrauch D, Billstrom AR, Zielonka J, Krolikowski JG, Bienengraeber MW, Warltier DC, Pratt PF, Jr. and Kersten JR. Role of heat shock protein 90 and endothelial nitric oxide synthase during early anesthetic and ischemic preconditioning. *Anesthesiology*. 2009;110:317-25.

71. Lee RC, Feinbaum RL and Ambros V. The C. elegans heterochronic gene lin-4 encodes small RNAs with antisense complementarity to lin-14. *Cell*. 1993;75:843-54.

72. Bartel DP. MicroRNAs: target recognition and regulatory functions. *Cell*. 2009;136:215-33.

73. Ha M and Kim VN. Regulation of microRNA biogenesis. *Nature reviews Molecular cell biology*. 2014;15:509-24.

74. Betel D, Wilson M, Gabow A, Marks DS and Sander C. The microRNA.org resource: targets and expression. *Nucleic Acids Res*. 2008;36:D149-53.

75. Pratt AJ and MacRae IJ. The RNA-induced silencing complex: a versatile gene-silencing machine. *The Journal of biological chemistry*. 2009;284:17897-901.

76. Gaidatzis D, van Nimwegen E, Hausser J and Zavolan M. Inference of miRNA targets using evolutionary conservation and pathway analysis. *BMC Bioinformatics*. 2007;8:69.

77. Tsang JS, Ebert MS and van Oudenaarden A. Genome-wide dissection of microRNA functions and cotargeting networks using gene set signatures. *Molecular cell*. 2010;38:140-53.

78. Pisano F, Altomare C, Cervio E, Barile L, Rocchetti M, Ciuffreda MC, Malpasso G, Copes F, Mura M, Danieli P, Viarengo G, Zaza A and Gnecchi M. Combination of miRNA499 and miRNA133 exerts a synergic effect on cardiac differentiation. *Stem cells (Dayton, Ohio)*. 2015;33:1187-99.

79. Zhu W, Zhao Y, Xu Y, Sun Y, Wang Z, Yuan W and Du Z. Dissection of protein interactomics highlights microRNA synergy. *PLoS One*. 2013;8:e63342.

80. Wang X, Zhu H, Zhang X, Liu Y, Chen J, Medvedovic M, Li H, Weiss MJ, Ren X and Fan GC. Loss of the miR-144/451 cluster impairs ischaemic preconditioning-mediated cardioprotection by targeting Rac-1. *Cardiovascular research*. 2012;94:379-90.

81. Olson JM, Yan Y, Bai X, Ge ZD, Liang M, Kriegel AJ, Twaroski DM and Bosnjak ZJ. Up-regulation of microRNA-21 mediates isoflurane-induced protection of cardiomyocytes. *Anesthesiology*. 2015;122:795-805.

82. Qiao S, Olson JM, Paterson M, Yan Y, Zaja I, Liu Y, Riess ML, Kersten JR, Liang M, Warltier DC, Bosnjak ZJ and Ge ZD. MicroRNA-21 Mediates Isoflurane-induced Cardioprotection against Ischemia-Reperfusion Injury via Akt/Nitric Oxide Synthase/Mitochondrial Permeability Transition Pore Pathway. *Anesthesiology*. 2015;123:786-98.

83. Cheng Y, Zhu P, Yang J, Liu X, Dong S, Wang X, Chun B, Zhuang J and Zhang C. Ischaemic preconditioning-regulated miR-21 protects heart against ischaemia/reperfusion injury via anti-apoptosis through its target PDCD4. *Cardiovascular research*. 2010;87:431-9.

84. Tu Y, Wan L, Fan Y, Wang K, Bu L, Huang T, Cheng Z and Shen B. Ischemic postconditioning-mediated miRNA-21 protects against cardiac ischemia/reperfusion injury via PTEN/Akt pathway. *PLoS One*. 2013;8:e75872.

85. Sayed D, He M, Hong C, Gao S, Rane S, Yang Z and Abdellatif M. MicroRNA-21 is a downstream effector of AKT that mediates its antiapoptotic effects via suppression of Fas ligand. *The Journal of biological chemistry*. 2010;285:20281-90.

86. Rane S, He M, Sayed D, Vashistha H, Malhotra A, Sadoshima J, Vatner DE, Vatner SF and Abdellatif M. Downregulation of miR-199a derepresses hypoxia-inducible factor-1alpha and Sirtuin 1 and recapitulates hypoxia preconditioning in cardiac myocytes. *Circulation research*. 2009;104:879-86.

87. Tranter M, Helsley RN, Paulding WR, McGuinness M, Brokamp C, Haar L, Liu Y, Ren X and Jones WK. Coordinated post-transcriptional regulation of Hsp70.3 gene expression by microRNA and alternative polyadenylation. *The Journal of biological chemistry*. 2011;286:29828-37.

88. Cluzeaut F and Maurer-Schultze B. Proliferation of cardiomyocytes and interstitial cells in the cardiac muscle of the mouse during pre- and postnatal development. *Cell Tissue Kinet*. 1986;19:267-74.

89. Porrello ER, Mahmoud AI, Simpson E, Hill JA, Richardson JA, Olson EN and Sadek HA. Transient regenerative potential of the neonatal mouse heart. *Science (New York, NY)*. 2011;331:1078-80.

90. Laflamme MA and Murry CE. Heart regeneration. *Nature*. 2011;473:326-35.

91. Li F, Wang X, Capasso JM and Gerdes AM. Rapid transition of cardiac myocytes from hyperplasia to hypertrophy during postnatal development. *Journal of molecular and cellular cardiology*. 1996;28:1737-46.

92. Adler CP. Relationship between deoxyribonucleic acid content and nucleoli in human heart muscle cells and estimation of cell number during cardiac growth and hyperfunction. *Recent advances in studies on cardiac structure and metabolism*. 1975;8:373-86.

93. Adler CP and Costabel U. Cell number in human heart in atrophy, hypertrophy, and under the influence of cytostatics. *Recent advances in studies on cardiac structure and metabolism*. 1975;6:343-55.

94. Olivetti G, Cigola E, Maestri R, Corradi D, Lagrasta C, Gambert SR and Anversa P. Aging, cardiac hypertrophy and ischemic cardiomyopathy do not affect the proportion of mononucleated and multinucleated myocytes in the human heart. *Journal of molecular and cellular cardiology*. 1996;28:1463-77.

95. Adler CP and Friedburg H. Myocardial DNA content, ploidy level and cell number in geriatric hearts: post-mortem examinations of human myocardium in old age. *Journal of molecular and cellular cardiology*. 1986;18:39-53.

96. Soonpaa MH, Rubart M and Field LJ. Challenges measuring cardiomyocyte renewal. *Biochim Biophys Acta*. 2013;1833:799-803.

97. Soonpaa MH and Field LJ. Assessment of cardiomyocyte DNA synthesis in normal and injured adult mouse hearts. *The American journal of physiology*. 1997;272:H220-6.

98. Hsieh PC, Segers VF, Davis ME, MacGillivray C, Gannon J, Molkentin JD, Robbins J and Lee RT. Evidence from a genetic fate-mapping study that stem cells refresh adult mammalian cardiomyocytes after injury. *Nat Med*. 2007;13:970-4.

99. de Weger RA, Verbrugge I, Bruggink AH, van Oosterhout MM, de Souza Y, van Wichen DF, Gmelig-Meyling FH, de Jonge N and Verdonck LF. Stem cell-derived cardiomyocytes after bone marrow and heart transplantation. *Bone Marrow Transplant*. 2008;41:563-9.

100. Bayes-Genis A, Salido M, Sole Ristol F, Puig M, Brossa V, Camprecios M, Corominas JM, Marinoso ML, Baro T, Vela MC, Serrano S, Padro JM, Bayes de Luna A and Cinca J. Host cell-derived cardiomyocytes in sex-mismatch cardiac allografts. *Cardiovascular research*. 2002;56:404-10.

101. Bergmann O, Bhardwaj RD, Bernard S, Zdunek S, Barnabe-Heider F, Walsh S, Zupicich J, Alkass K, Buchholz BA, Druid H, Jovinge S and Frisen J. Evidence for cardiomyocyte renewal in humans. *Science (New York, NY)*. 2009;324:98-102.

102. Marelli D, Desrosiers C, el-Alfy M, Kao RL and Chiu RC. Cell transplantation for myocardial repair: an experimental approach. *Cell Transplant*. 1992;1:383-90.

103. Reinecke H and Murry CE. Transmural replacement of myocardium after skeletal myoblast grafting into the heart. Too much of a good thing? *Cardiovasc Pathol*. 2000;9:337-44.

104. Menasche P, Hagege AA, Vilquin JT, Desnos M, Abergel E, Pouzet B, Bel A, Sarateanu S, Scorsin M, Schwartz K, Bruneval P, Benbunan M, Marolleau JP and Duboc D. Autologous

skeletal myoblast transplantation for severe postinfarction left ventricular dysfunction. *Journal of the American College of Cardiology*. 2003;41:1078-83.

105. Veltman CE, Soliman OI, Geleijnse ML, Vletter WB, Smits PC, ten Cate FJ, Jordaens LJ, Balk AH, Serruys PW, Boersma E, van Domburg RT and van der Giessen WJ. Four-year follow-up of treatment with intramyocardial skeletal myoblasts injection in patients with ischaemic cardiomyopathy. *Eur Heart J*. 2008;29:1386-96.

106. Orlic D, Kajstura J, Chimenti S, Jakoniuk I, Anderson SM, Li B, Pickel J, McKay R, Nadal-Ginard B, Bodine DM, Leri A and Anversa P. Bone marrow cells regenerate infarcted myocardium. *Nature*. 2001;410:701-5.

107. Fernandez-Aviles F, San Roman JA, Garcia-Frade J, Fernandez ME, Penarrubia MJ, de la Fuente L, Gomez-Bueno M, Cantalapiedra A, Fernandez J, Gutierrez O, Sanchez PL, Hernandez C, Sanz R, Garcia-Sancho J and Sanchez A. Experimental and clinical regenerative capability of human bone marrow cells after myocardial infarction. *Circulation research*. 2004;95:742-8.

108. Kamihata H, Matsubara H, Nishiue T, Fujiyama S, Tsutsumi Y, Ozono R, Masaki H, Mori Y, Iba O, Tateishi E, Kosaki A, Shintani S, Murohara T, Imaizumi T and Iwasaka T. Implantation of bone marrow mononuclear cells into ischemic myocardium enhances collateral perfusion and regional function via side supply of angioblasts, angiogenic ligands, and cytokines. *Circulation*. 2001;104:1046-52.

109. Kocher AA, Schuster MD, Szabolcs MJ, Takuma S, Burkhoff D, Wang J, Homma S, Edwards NM and Itescu S. Neovascularization of ischemic myocardium by human bone-marrow-derived angioblasts prevents cardiomyocyte apoptosis, reduces remodeling and improves cardiac function. *Nat Med*. 2001;7:430-6.

110. Jeevanantham V, Butler M, Saad A, Abdel-Latif A, Zuba-Surma EK and Dawn B. Adult bone marrow cell therapy improves survival and induces long-term improvement in cardiac parameters: a systematic review and meta-analysis. *Circulation*. 2012;126:551-68.

111. Scherschel JA, Soonpaa MH, Srour EF, Field LJ and Rubart M. Adult bone marrow-derived cells do not acquire functional attributes of cardiomyocytes when transplanted into peri-infarct myocardium. *Molecular therapy : the journal of the American Society of Gene Therapy*. 2008;16:1129-37.

112. Nygren JM, Jovinge S, Breitbach M, Sawen P, Roll W, Hescheler J, Taneera J, Fleischmann BK and Jacobsen SE. Bone marrow-derived hematopoietic cells generate cardiomyocytes at a low frequency through cell fusion, but not transdifferentiation. *Nat Med*. 2004;10:494-501.

113. Balsam LB, Wagers AJ, Christensen JL, Kofidis T, Weissman IL and Robbins RC. Haematopoietic stem cells adopt mature haematopoietic fates in ischaemic myocardium. *Nature*. 2004;428:668-73.

114. Murry CE, Soonpaa MH, Reinecke H, Nakajima H, Nakajima HO, Rubart M, Pasumarthi KB, Virag JI, Bartelmez SH, Poppa V, Bradford G, Dowell JD, Williams DA and

Field LJ. Haematopoietic stem cells do not transdifferentiate into cardiac myocytes in myocardial infarcts. *Nature*. 2004;428:664-8.

115. Limbourg FP, Ringes-Lichtenberg S, Schaefer A, Jacoby C, Mehraein Y, Jager MD, Limbourg A, Fuchs M, Klein G, Ballmaier M, Schlitt HJ, Schrader J, Hilfiker-Kleiner D and Drexler H. Haematopoietic stem cells improve cardiac function after infarction without permanent cardiac engraftment. *Eur J Heart Fail*. 2005;7:722-9.

116. Gnecchi M, Zhang Z, Ni A and Dzau VJ. Paracrine mechanisms in adult stem cell signaling and therapy. *Circulation research*. 2008;103:1204-19.

117. Hierlihy AM, Seale P, Lobe CG, Rudnicki MA and Megeney LA. The post-natal heart contains a myocardial stem cell population. *FEBS letters*. 2002;530:239-43.

118. Beltrami AP, Barlucchi L, Torella D, Baker M, Limana F, Chimenti S, Kasahara H, Rota M, Musso E, Urbanek K, Leri A, Kajstura J, Nadal-Ginard B and Anversa P. Adult cardiac stem cells are multipotent and support myocardial regeneration. *Cell*. 2003;114:763-76.

119. Messina E, De Angelis L, Frati G, Morrone S, Chimenti S, Fiordaliso F, Salio M, Battaglia M, Latronico MV, Coletta M, Vivarelli E, Frati L, Cossu G and Giacomello A. Isolation and expansion of adult cardiac stem cells from human and murine heart. *Circulation research*. 2004;95:911-21.

120. Makkar RR, Smith RR, Cheng K, Malliaras K, Thomson LE, Berman D, Czer LS, Marban L, Mendizabal A, Johnston PV, Russell SD, Schuleri KH, Lardo AC, Gerstenblith G and Marban E. Intracoronary cardiosphere-derived cells for heart regeneration after myocardial infarction (CADUCEUS): a prospective, randomised phase 1 trial. *Lancet*. 2012;379:895-904.

121. Malliaras K, Makkar RR, Smith RR, Cheng K, Wu E, Bonow RO, Marban L, Mendizabal A, Cingolani E, Johnston PV, Gerstenblith G, Schuleri KH, Lardo AC and Marban E. Intracoronary cardiosphere-derived cells after myocardial infarction: evidence of therapeutic regeneration in the final 1-year results of the CADUCEUS trial (CArdiosphere-Derived aUtologous stem CElls to reverse ventricUlar dySfunction). *Journal of the American College of Cardiology*. 2014;63:110-22.

122. Chimenti I, Smith RR, Li TS, Gerstenblith G, Messina E, Giacomello A and Marban E. Relative roles of direct regeneration versus paracrine effects of human cardiosphere-derived cells transplanted into infarcted mice. *Circulation research*. 2010;106:971-80.

123. Malliaras K, Li TS, Luthringer D, Terrovitis J, Cheng K, Chakravarty T, Galang G, Zhang Y, Schoenhoff F, Van Eyk J, Marban L and Marban E. Safety and efficacy of allogeneic cell therapy in infarcted rats transplanted with mismatched cardiosphere-derived cells. *Circulation*. 2012;125:100-12.

124. Malliaras K, Zhang Y, Seinfeld J, Galang G, Tseliou E, Cheng K, Sun B, Aminzadeh M and Marban E. Cardiomyocyte proliferation and progenitor cell recruitment underlie therapeutic regeneration after myocardial infarction in the adult mouse heart. *EMBO Mol Med*. 2013;5:191-209.

125. Nombela-Arrieta C, Ritz J and Silberstein LE. The elusive nature and function of mesenchymal stem cells. *Nature reviews Molecular cell biology*. 2011;12:126-31.

126. Zhang Y, Sivakumaran P, Newcomb AE, Hernandez D, Harris N, Khanabdali R, Liu GS, Kelly DJ, Pebay A, Hewitt AW, Boyle A, Harvey R, Morrison WA, Elliott DA, Dusting GJ and Lim SY. Cardiac Repair With a Novel Population of Mesenchymal Stem Cells Resident in the Human Heart. *Stem cells (Dayton, Ohio)*. 2015;33:3100-13.

127. Friedenstein AJ, Chailakhjan RK and Lalykina KS. The development of fibroblast colonies in monolayer cultures of guinea-pig bone marrow and spleen cells. *Cell Tissue Kinet*. 1970;3:393-403.

128. Peister A, Mellad JA, Larson BL, Hall BM, Gibson LF and Prockop DJ. Adult stem cells from bone marrow (MSCs) isolated from different strains of inbred mice vary in surface epitopes, rates of proliferation, and differentiation potential. *Blood*. 2004;103:1662-8.

129. Soleimani M and Nadri S. A protocol for isolation and culture of mesenchymal stem cells from mouse bone marrow. *Nat Protoc*. 2009;4:102-6.

130. Zhu H, Guo ZK, Jiang XX, Li H, Wang XY, Yao HY, Zhang Y and Mao N. A protocol for isolation and culture of mesenchymal stem cells from mouse compact bone. *Nat Protoc*. 2010;5:550-60.

131. Gnecchi M and Melo LG. Bone marrow-derived mesenchymal stem cells: isolation, expansion, characterization, viral transduction, and production of conditioned medium. *Methods Mol Biol*. 2009;482:281-94.

132. Wang JS, Shum-Tim D, Galipeau J, Chedrawy E, Eliopoulos N and Chiu RC. Marrow stromal cells for cellular cardiomyoplasty: feasibility and potential clinical advantages. *J Thorac Cardiovasc Surg*. 2000;120:999-1005.

133. Makino S, Fukuda K, Miyoshi S, Konishi F, Kodama H, Pan J, Sano M, Takahashi T, Hori S, Abe H, Hata J, Umezawa A and Ogawa S. Cardiomyocytes can be generated from marrow stromal cells in vitro. *The Journal of clinical investigation*. 1999;103:697-705.

134. Toma C, Pittenger MF, Cahill KS, Byrne BJ and Kessler PD. Human mesenchymal stem cells differentiate to a cardiomyocyte phenotype in the adult murine heart. *Circulation*. 2002;105:93-8.

135. Shake JG, Gruber PJ, Baumgartner WA, Senechal G, Meyers J, Redmond JM, Pittenger MF and Martin BJ. Mesenchymal stem cell implantation in a swine myocardial infarct model: engraftment and functional effects. *Ann Thorac Surg*. 2002;73:1919-25; discussion 1926.

136. Tang YL, Zhao Q, Zhang YC, Cheng L, Liu M, Shi J, Yang YZ, Pan C, Ge J and Phillips MI. Autologous mesenchymal stem cell transplantation induce VEGF and neovascularization in ischemic myocardium. *Regul Pept*. 2004;117:3-10.

137. Kinnaird T, Stabile E, Burnett MS, Lee CW, Barr S, Fuchs S and Epstein SE. Marrow-derived stromal cells express genes encoding a broad spectrum of arteriogenic cytokines and

promote in vitro and in vivo arteriogenesis through paracrine mechanisms. *Circulation research*. 2004;94:678-85.

138. Davani S, Marandin A, Mersin N, Royer B, Kantelip B, Herve P, Etievent JP and Kantelip JP. Mesenchymal progenitor cells differentiate into an endothelial phenotype, enhance vascular density, and improve heart function in a rat cellular cardiomyoplasty model. *Circulation*. 2003;108 Suppl 1:Ii253-8.

139. Dai W, Hale SL, Martin BJ, Kuang JQ, Dow JS, Wold LE and Kloner RA. Allogeneic mesenchymal stem cell transplantation in postinfarcted rat myocardium: short- and long-term effects. *Circulation*. 2005;112:214-23.

140. Tang J, Xie Q, Pan G, Wang J and Wang M. Mesenchymal stem cells participate in angiogenesis and improve heart function in rat model of myocardial ischemia with reperfusion. *European journal of cardio-thoracic surgery : official journal of the European Association for Cardio-thoracic Surgery*. 2006;30:353-61.

141. Chen SL, Fang WW, Ye F, Liu YH, Qian J, Shan SJ, Zhang JJ, Chunhua RZ, Liao LM, Lin S and Sun JP. Effect on left ventricular function of intracoronary transplantation of autologous bone marrow mesenchymal stem cell in patients with acute myocardial infarction. *Am J Cardiol*. 2004;94:92-5.

142. Hare JM, Traverse JH, Henry TD, Dib N, Strumpf RK, Schulman SP, Gerstenblith G, DeMaria AN, Denktas AE, Gammon RS, Hermiller JB, Jr., Reisman MA, Schaer GL and Sherman W. A randomized, double-blind, placebo-controlled, dose-escalation study of intravenous adult human mesenchymal stem cells (prochymal) after acute myocardial infarction. *Journal of the American College of Cardiology*. 2009;54:2277-86.

143. Houtgraaf JH, den Dekker WK, van Dalen BM, Springeling T, de Jong R, van Geuns RJ, Geleijnse ML, Fernandez-Aviles F, Zijlsta F, Serruys PW and Duckers HJ. First experience in humans using adipose tissue-derived regenerative cells in the treatment of patients with ST-segment elevation myocardial infarction. *Journal of the American College of Cardiology*. 2012;59:539-40.

144. Karantalis V and Hare JM. Use of mesenchymal stem cells for therapy of cardiac disease. *Circulation research*. 2015;116:1413-30.

145. Hu X, Yu SP, Fraser JL, Lu Z, Ogle ME, Wang JA and Wei L. Transplantation of hypoxia-preconditioned mesenchymal stem cells improves infarcted heart function via enhanced survival of implanted cells and angiogenesis. *J Thorac Cardiovasc Surg*. 2008;135:799-808.

146. Li L, Zhang Y, Li Y, Yu B, Xu Y, Zhao S and Guan Z. Mesenchymal stem cell transplantation attenuates cardiac fibrosis associated with isoproterenol-induced global heart failure. *Transpl Int*. 2008;21:1181-9.

147. Li L, Zhang S, Zhang Y, Yu B, Xu Y and Guan Z. Paracrine action mediate the antifibrotic effect of transplanted mesenchymal stem cells in a rat model of global heart failure. *Mol Biol Rep*. 2009;36:725-31.

148. Mias C, Lairez O, Trouche E, Roncalli J, Calise D, Seguelas MH, Ordener C, Piercecchi-Marti MD, Auge N, Salvayre AN, Bourin P, Parini A and Cussac D. Mesenchymal stem cells promote matrix metalloproteinase secretion by cardiac fibroblasts and reduce cardiac ventricular fibrosis after myocardial infarction. *Stem cells (Dayton, Ohio)*. 2009;27:2734-43.

149. Lu F, Zhao X, Wu J, Cui Y, Mao Y, Chen K, Yuan Y, Gong D, Xu Z and Huang S. MSCs transfected with hepatocyte growth factor or vascular endothelial growth factor improve cardiac function in the infarcted porcine heart by increasing angiogenesis and reducing fibrosis. *Int J Cardiol*. 2013;167:2524-32.

150. Hatzistergos KE, Quevedo H, Oskouei BN, Hu Q, Feigenbaum GS, Margitich IS, Mazhari R, Boyle AJ, Zambrano JP, Rodriguez JE, Dulce R, Pattany PM, Valdes D, Revilla C, Heldman AW, McNiece I and Hare JM. Bone marrow mesenchymal stem cells stimulate cardiac stem cell proliferation and differentiation. *Circulation research*. 2010;107:913-22.

151. Williams AR, Hatzistergos KE, Addicott B, McCall F, Carvalho D, Suncion V, Morales AR, Da Silva J, Sussman MA, Heldman AW and Hare JM. Enhanced effect of combining human cardiac stem cells and bone marrow mesenchymal stem cells to reduce infarct size and to restore cardiac function after myocardial infarction. *Circulation*. 2013;127:213-23.

152. Gnecchi M, He H, Noiseux N, Liang OD, Zhang L, Morello F, Mu H, Melo LG, Pratt RE, Ingwall JS and Dzau VJ. Evidence supporting paracrine hypothesis for Akt-modified mesenchymal stem cell-mediated cardiac protection and functional improvement. *FASEB journal : official publication of the Federation of American Societies for Experimental Biology*. 2006;20:661-9.

153. Timmers L, Lim SK, Arslan F, Armstrong JS, Hoefer IE, Doevendans PA, Piek JJ, El Oakley RM, Choo A, Lee CN, Pasterkamp G and de Kleijn DP. Reduction of myocardial infarct size by human mesenchymal stem cell conditioned medium. *Stem Cell Res*. 2007;1:129-37.

154. Lai RC, Arslan F, Lee MM, Sze NS, Choo A, Chen TS, Salto-Tellez M, Timmers L, Lee CN, El Oakley RM, Pasterkamp G, de Kleijn DP and Lim SK. Exosome secreted by MSC reduces myocardial ischemia/reperfusion injury. *Stem Cell Res*. 2010;4:214-22.

155. Arslan F, Lai RC, Smeets MB, Akeroyd L, Choo A, Aguor EN, Timmers L, van Rijen HV, Doevendans PA, Pasterkamp G, Lim SK and de Kleijn DP. Mesenchymal stem cell-derived exosomes increase ATP levels, decrease oxidative stress and activate PI3K/Akt pathway to enhance myocardial viability and prevent adverse remodeling after myocardial ischemia/reperfusion injury. *Stem Cell Res*. 2013;10:301-12.

156. Tomasoni S, Longaretti L, Rota C, Morigi M, Conti S, Gotti E, Capelli C, Introna M, Remuzzi G and Benigni A. Transfer of growth factor receptor mRNA via exosomes unravels the regenerative effect of mesenchymal stem cells. *Stem Cells Dev*. 2013;22:772-80.

157. Bian S, Zhang L, Duan L, Wang X, Min Y and Yu H. Extracellular vesicles derived from human bone marrow mesenchymal stem cells promote angiogenesis in a rat myocardial infarction model. *J Mol Med (Berl)*. 2014;92:387-97.

158. Afzal MR, Haider H, Idris NM, Jiang S, Ahmed RP and Ashraf M. Preconditioning promotes survival and angiomyogenic potential of mesenchymal stem cells in the infarcted heart via NF-kappaB signaling. *Antioxid Redox Signal*. 2010;12:693-702.

159. Suzuki Y, Kim HW, Ashraf M and Haider H. Diazoxide potentiates mesenchymal stem cell survival via NF-kappaB-dependent miR-146a expression by targeting Fas. *Am J Physiol Heart Circ Physiol*. 2010;299:H1077-82.

160. Hu S, Huang M, Nguyen PK, Gong Y, Li Z, Jia F, Lan F, Liu J, Nag D, Robbins RC and Wu JC. Novel microRNA prosurvival cocktail for improving engraftment and function of cardiac progenitor cell transplantation. *Circulation*. 2011;124:S27-34.

161. Zhang Q, Yang YJ, Wang H, Dong QT, Wang TJ, Qian HY and Xu H. Autophagy activation: a novel mechanism of atorvastatin to protect mesenchymal stem cells from hypoxia and serum deprivation via AMP-activated protein kinase/mammalian target of rapamycin pathway. *Stem Cells Dev*. 2012;21:1321-32.

162. Fang J, Chen L, Fan L, Wu L, Chen X, Li W, Lin Y and Wang W. Enhanced therapeutic effects of mesenchymal stem cells on myocardial infarction by ischemic postconditioning through paracrine mechanisms in rats. *Journal of molecular and cellular cardiology*. 2011;51:839-47.

163. Tsou MT, Huang CH and Chiu JH. Electroacupuncture on PC6 (Neiguan) attenuates ischemia/reperfusion injury in rat hearts. *Am J Chin Med*. 2004;32:951-65.

164. Redington KL, Disenhouse T, Li J, Wei C, Dai X, Gladstone R, Manlhiot C and Redington AN. Electroacupuncture reduces myocardial infarct size and improves post-ischemic recovery by invoking release of humoral, dialyzable, cardioprotective factors. *J Physiol Sci*. 2013;63:219-23.

165. Zhang J, Jia XH, Xu ZW, Ding FP, Zhou X, Fu H, Liu Y, Ou LL, Li ZJ and Kong DL. Improved mesenchymal stem cell survival in ischemic heart through electroacupuncture. *Chin J Integr Med*. 2013;19:573-81.

166. Dickson EW, Lorbar M, Porcaro WA, Fenton RA, Reinhardt CP, Gysembergh A and Przyklenk K. Rabbit heart can be "preconditioned" via transfer of coronary effluent. *The American journal of physiology*. 1999;277:H2451-7.

167. Kamota T, Li TS, Morikage N, Murakami M, Ohshima M, Kubo M, Kobayashi T, Mikamo A, Ikeda Y, Matsuzaki M and Hamano K. Ischemic pre-conditioning enhances the mobilization and recruitment of bone marrow stem cells to protect against ischemia/reperfusion injury in the late phase. *Journal of the American College of Cardiology*. 2009;53:1814-22.

168. Gupta S and Knowlton AA. HSP60 trafficking in adult cardiac myocytes: role of the exosomal pathway. *Am J Physiol Heart Circ Physiol*. 2007;292:H3052-6.

169. Waldenstrom A, Genneback N, Hellman U and Ronquist G. Cardiomyocyte microvesicles contain DNA/RNA and convey biological messages to target cells. *PLoS One*. 2012;7:e34653.

170. Genneback N, Hellman U, Malm L, Larsson G, Ronquist G, Waldenstrom A and Morner S. Growth factor stimulation of cardiomyocytes induces changes in the transcriptional contents of secreted exosomes. *J Extracell Vesicles*. 2013;2.

171. Boon RA and Vickers KC. Intercellular transport of microRNAs. *Arteriosclerosis, thrombosis, and vascular biology*. 2013;33:186-92.

172. Colombo M, Moita C, van Niel G, Kowal J, Vigneron J, Benaroch P, Manel N, Moita LF, Thery C and Raposo G. Analysis of ESCRT functions in exosome biogenesis, composition and secretion highlights the heterogeneity of extracellular vesicles. *J Cell Sci*. 2013;126:5553-65.

173. Baietti MF, Zhang Z, Mortier E, Melchior A, Degeest G, Geeraerts A, Ivarsson Y, Depoortere F, Coomans C, Vermeiren E, Zimmermann P and David G. Syndecan-syntenin-ALIX regulates the biogenesis of exosomes. *Nature cell biology*. 2012;14:677-85.

174. Tan SS, Yin Y, Lee T, Lai RC, Yeo RW, Zhang B, Choo A and Lim SK. Therapeutic MSC exosomes are derived from lipid raft microdomains in the plasma membrane. *J Extracell Vesicles*. 2013;2.

175. Bobrie A, Colombo M, Raposo G and Thery C. Exosome secretion: molecular mechanisms and roles in immune responses. *Traffic*. 2011;12:1659-68.

176. Pant S, Hilton H and Burczynski ME. The multifaceted exosome: biogenesis, role in normal and aberrant cellular function, and frontiers for pharmacological and biomarker opportunities. *Biochem Pharmacol*. 2012;83:1484-94.

177. Colombo M, Raposo G and Thery C. Biogenesis, secretion, and intercellular interactions of exosomes and other extracellular vesicles. *Annu Rev Cell Dev Biol*. 2014;30:255-89.

178. Alvarez-Erviti L, Seow Y, Yin H, Betts C, Lakhal S and Wood MJ. Delivery of siRNA to the mouse brain by systemic injection of targeted exosomes. *Nature biotechnology*. 2011;29:341-5.

179. Tian T, Zhu YL, Zhou YY, Liang GF, Wang YY, Hu FH and Xiao ZD. Exosome uptake through clathrin-mediated endocytosis and macropinocytosis and mediating miR-21 delivery. *The Journal of biological chemistry*. 2014;289:22258-67.

180. Feng D, Zhao WL, Ye YY, Bai XC, Liu RQ, Chang LF, Zhou Q and Sui SF. Cellular internalization of exosomes occurs through phagocytosis. *Traffic*. 2010;11:675-87.

181. Villarroya-Beltri C, Baixauli F, Gutierrez-Vazquez C, Sanchez-Madrid F and Mittelbrunn M. Sorting it out: regulation of exosome loading. *Seminars in cancer biology*. 2014;28:3-13.

182. Montecalvo A, Larregina AT, Shufesky WJ, Stolz DB, Sullivan ML, Karlsson JM, Baty CJ, Gibson GA, Erdos G, Wang Z, Milosevic J, Tkacheva OA, Divito SJ, Jordan R, Lyons-Weiler J, Watkins SC and Morelli AE. Mechanism of transfer of functional microRNAs between mouse dendritic cells via exosomes. *Blood*. 2012;119:756-66.

183. Vicencio JM, Yellon DM, Sivaraman V, Das D, Boi-Doku C, Arjun S, Zheng Y, Riquelme JA, Kearney J, Sharma V, Multhoff G, Hall AR and Davidson SM. Plasma exosomes protect the myocardium from ischemia-reperfusion injury. *Journal of the American College of Cardiology*. 2015;65:1525-36.

184. Keerthikumar S, Chisanga D, Ariyaratne D, Al Saffar H, Anand S, Zhao K, Samuel M, Pathan M, Jois M, Chilamkurti N, Gangoda L and Mathivanan S. ExoCarta: A Web-Based Compendium of Exosomal Cargo. *Journal of molecular biology*. 2015.

185. Sahu R, Kaushik S, Clement CC, Cannizzo ES, Scharf B, Follenzi A, Potolicchio I, Nieves E, Cuervo AM and Santambrogio L. Microautophagy of cytosolic proteins by late endosomes. *Developmental cell*. 2011;20:131-9.

186. Perez-Hernandez D, Gutierrez-Vazquez C, Jorge I, Lopez-Martin S, Ursa A, Sanchez-Madrid F, Vazquez J and Yanez-Mo M. The intracellular interactome of tetraspanin-enriched microdomains reveals their function as sorting machineries toward exosomes. *The Journal of biological chemistry*. 2013;288:11649-61.

187. Mazurov D, Barbashova L and Filatov A. Tetraspanin protein CD9 interacts with metalloprotease CD10 and enhances its release via exosomes. *The FEBS journal*. 2013;280:1200-13.

188. Verweij FJ, van Eijndhoven MA, Hopmans ES, Vendrig T, Wurdinger T, Cahir-McFarland E, Kieff E, Geerts D, van der Kant R, Neefjes J, Middeldorp JM and Pegtel DM. LMP1 association with CD63 in endosomes and secretion via exosomes limits constitutive NF-kappaB activation. *The EMBO journal*. 2011;30:2115-29.

189. Li X, Arslan F, Ren Y, Adav SS, Poh KK, Sorokin V, Lee CN, de Kleijn D, Lim SK and Sze SK. Metabolic adaptation to a disruption in oxygen supply during myocardial ischemia and reperfusion is underpinned by temporal and quantitative changes in the cardiac proteome. *Journal of proteome research*. 2012;11:2331-46.

190. Valadi H, Ekstrom K, Bossios A, Sjostrand M, Lee JJ and Lotvall JO. Exosome-mediated transfer of mRNAs and microRNAs is a novel mechanism of genetic exchange between cells. *Nature cell biology*. 2007;9:654-9.

191. Jansen RP. mRNA localization: message on the move. *Nature reviews Molecular cell biology*. 2001;2:247-56.

192. Kislauskis EH and Singer RH. Determinants of mRNA localization. *Current opinion in cell biology*. 1992;4:975-8.

193. Martin KC and Ephrussi A. mRNA localization: gene expression in the spatial dimension. *Cell*. 2009;136:719-30.

194. Bolukbasi MF, Mizrak A, Ozdener GB, Madlener S, Strobel T, Erkan EP, Fan JB, Breakefield XO and Saydam O. miR-1289 and "Zipcode"-like Sequence Enrich mRNAs in Microvesicles. *Mol Ther Nucleic Acids*. 2012;1:e10.

195. Villarroya-Beltri C, Gutierrez-Vazquez C, Sanchez-Cabo F, Perez-Hernandez D, Vazquez J, Martin-Cofreces N, Martinez-Herrera DJ, Pascual-Montano A, Mittelbrunn M and Sanchez-Madrid F. Sumoylated hnRNPA2B1 controls the sorting of miRNAs into exosomes through binding to specific motifs. *Nature communications*. 2013;4:2980.

196. Squadrito ML, Baer C, Burdet F, Maderna C, Gilfillan GD, Lyle R, Ibberson M and De Palma M. Endogenous RNAs modulate microRNA sorting to exosomes and transfer to acceptor cells. *Cell reports*. 2014;8:1432-46.

197. Guduric-Fuchs J, O'Connor A, Camp B, O'Neill CL, Medina RJ and Simpson DA. Selective extracellular vesicle-mediated export of an overlapping set of microRNAs from multiple cell types. *BMC genomics*. 2012;13:357.

198. Gibbings DJ, Ciaudo C, Erhardt M and Voinnet O. Multivesicular bodies associate with components of miRNA effector complexes and modulate miRNA activity. *Nature cell biology*. 2009;11:1143-9.

199. Ibrahim AG, Cheng K and Marban E. Exosomes as critical agents of cardiac regeneration triggered by cell therapy. *Stem Cell Reports*. 2014;2:606-19.

200. Barile L, Lionetti V, Cervio E, Matteucci M, Gherghiceanu M, Popescu LM, Torre T, Siclari F, Moccetti T and Vassalli G. Extracellular vesicles from human cardiac progenitor cells inhibit cardiomyocyte apoptosis and improve cardiac function after myocardial infarction. *Cardiovascular research*. 2014;103:530-41.

201. Sahoo S, Klychko E, Thorne T, Misener S, Schultz KM, Millay M, Ito A, Liu T, Kamide C, Agrawal H, Perlman H, Qin G, Kishore R and Losordo DW. Exosomes from human CD34(+) stem cells mediate their proangiogenic paracrine activity. *Circulation research*. 2011;109:724-8.

202. Wang Y, Zhang L, Li Y, Chen L, Wang X, Guo W, Zhang X, Qin G, He SH, Zimmerman A, Liu Y, Kim IM, Weintraub NL and Tang Y. Exosomes/microvesicles from induced pluripotent stem cells deliver cardioprotective miRNAs and prevent cardiomyocyte apoptosis in the ischemic myocardium. *Int J Cardiol*. 2015;192:61-9.

203. Feng Y, Huang W, Wani M, Yu X and Ashraf M. Ischemic preconditioning potentiates the protective effect of stem cells through secretion of exosomes by targeting Mecp2 via miR-22. *PLoS One*. 2014;9:e88685.

204. Yu B, Kim HW, Gong M, Wang J, Millard RW, Wang Y, Ashraf M and Xu M. Exosomes secreted from GATA-4 overexpressing mesenchymal stem cells serve as a reservoir of anti-apoptotic microRNAs for cardioprotection. *Int J Cardiol*. 2015;182:349-60.

205. Wu W, Hu Y, Li J, Zhu W, Ha T, Que L, Liu L, Zhu Q, Chen Q, Xu Y, Li C and Li Y. Silencing of Pellino1 improves post-infarct cardiac dysfunction and attenuates left ventricular remodelling in mice. *Cardiovascular research*. 2014;102:46-55.

206. Ren X, Wang Y and Jones WK. TNF-alpha is required for late ischemic preconditioning but not for remote preconditioning of trauma. *The Journal of surgical research*. 2004;121:120-9.

207. Fishbein MC, Meerbaum S, Rit J, Lando U, Kanmatsuse K, Mercier JC, Corday E and Ganz W. Early phase acute myocardial infarct size quantification: validation of the triphenyl tetrazolium chloride tissue enzyme staining technique. *Am Heart J*. 1981;101:593-600.

208. Tranter M, Liu Y, He S, Gulick J, Ren X, Robbins J, Jones WK and Reineke TM. In vivo delivery of nucleic acids via glycopolymer vehicles affords therapeutic infarct size reduction in vivo. *Molecular therapy : the journal of the American Society of Gene Therapy*. 2012;20:601-8.

209. White SM, Constantin PE and Claycomb WC. Cardiac physiology at the cellular level: use of cultured HL-1 cardiomyocytes for studies of cardiac muscle cell structure and function. *Am J Physiol Heart Circ Physiol*. 2004;286:H823-9.

210. Kimes BW and Brandt BL. Properties of a clonal muscle cell line from rat heart. *Experimental cell research*. 1976;98:367-81.

211. Ehler E, Moore-Morris T and Lange S. Isolation and Culture of Neonatal Mouse Cardiomyocytes. 2013:e50154.

212. Thery C, Amigorena S, Raposo G and Clayton A. Isolation and characterization of exosomes from cell culture supernatants and biological fluids *Curr Protoc Cell Biol*. 2008/01/30 ed.: John Wiley & Sons, Inc; 2006: 1-29.

213. Taylor DD and Shah S. Methods of isolating extracellular vesicles impact down-stream analyses of their cargoes. *Methods*. 2015;87:3-10.

214. Livak KJ and Schmittgen TD. Analysis of relative gene expression data using real-time quantitative PCR and the 2(-Delta Delta C(T)) Method. *Methods*. 2001;25:402-8.

215. Trapnell C, Pachter L and Salzberg SL. TopHat: discovering splice junctions with RNA-Seq. *Bioinformatics (Oxford, England)*. 2009;25:1105-11.

216. Anders S and Huber W. Differential expression analysis for sequence count data. *Genome biology*. 2010;11:R106.

217. Enright AJ, John B, Gaul U, Tuschl T, Sander C and Marks DS. MicroRNA targets in Drosophila. *Genome biology*. 2003;5:R1.

218. Betel D, Koppal A, Agius P, Sander C and Leslie C. Comprehensive modeling of microRNA targets predicts functional non-conserved and non-canonical sites. *Genome biology*. 2010;11:R90.

219. Ren XP, Wu J, Wang X, Sartor MA, Qian J, Jones K, Nicolaou P, Pritchard TJ and Fan GC. MicroRNA-320 is involved in the regulation of cardiac ischemia/reperfusion injury by targeting heat-shock protein 20. *Circulation*. 2009;119:2357-66.

220. van Rooij E, Sutherland LB, Thatcher JE, DiMaio JM, Naseem RH, Marshall WS, Hill JA and Olson EN. Dysregulation of microRNAs after myocardial infarction reveals a role of miR-29 in cardiac fibrosis. *Proceedings of the National Academy of Sciences of the United States of America*. 2008;105:13027-32.

221. Latchman DS. Heat shock proteins and cardiac protection. *Cardiovascular research*. 2001;51:637-46.

222. Brown M, McGuinness M, Wright T, Ren X, Wang Y, Boivin GP, Hahn H, Feldman AM and Jones WK. Cardiac-specific blockade of NF-kappaB in cardiac pathophysiology: differences between acute and chronic stimuli in vivo. *Am J Physiol Heart Circ Physiol*. 2005;289:H466-76.

223. Downey JM, Davis AM and Cohen MV. Signaling pathways in ischemic preconditioning. *Heart Fail Rev*. 2007;12:181-8.

224. Jones WK, Flaherty MP, Tang XL, Takano H, Qiu Y, Banerjee S, Smith T and Bolli R. Ischemic preconditioning increases iNOS transcript levels in conscious rabbits via a nitric oxide-dependent mechanism. *Journal of molecular and cellular cardiology*. 1999;31:1469-81.

225. Chaudary N, Naydenova Z, Shuralyova I and Coe IR. The adenosine transporter, mENT1, is a target for adenosine receptor signaling and protein kinase Cepsilon in hypoxic and pharmacological preconditioning in the mouse cardiomyocyte cell line, HL-1. *The Journal of pharmacology and experimental therapeutics*. 2004;310:1190-8.

226. Dong S, Cheng Y, Yang J, Li J, Liu X, Wang X, Wang D, Krall TJ, Delphin ES and Zhang C. MicroRNA expression signature and the role of microRNA-21 in the early phase of acute myocardial infarction. *The Journal of biological chemistry*. 2009;284:29514-25.

227. Gu GL, Xu XL, Sun XT, Zhang J, Guo CF, Wang CS, Sun B, Guo GL, Ma K, Huang YY, Sun LQ and Wang YQ. Cardioprotective Effect of MicroRNA-21 in Murine Myocardial Infarction. *Cardiovasc Ther*. 2015;33:109-17.

228. Tong Z, Jiang B, Wu Y, Liu Y, Li Y, Gao M, Jiang Y, Lv Q and Xiao X. MiR-21 Protected Cardiomyocytes against Doxorubicin-Induced Apoptosis by Targeting BTG2. *International journal of molecular sciences*. 2015;16:14511-25.

229. Varga ZV, Zvara A, Farago N, Kocsis GF, Pipicz M, Gaspar R, Bencsik P, Gorbe A, Csonka C, Puskas LG, Thum T, Csont T and Ferdinandy P. MicroRNAs associated with ischemia-reperfusion injury and cardioprotection by ischemic pre- and postconditioning: protectomiRs. *Am J Physiol Heart Circ Physiol*. 2014;307:H216-27.

230. Wang S, Aurora AB, Johnson BA, Qi X, McAnally J, Hill JA, Richardson JA, Bassel-Duby R and Olson EN. The endothelial-specific microRNA miR-126 governs vascular integrity and angiogenesis. *Developmental cell*. 2008;15:261-71.

231. Lv G, Shao S, Dong H, Bian X, Yang X and Dong S. MicroRNA-214 protects cardiac myocytes against H2O2-induced injury. *Journal of cellular biochemistry*. 2014;115:93-101.

232. Yang X, Qin Y, Shao S, Yu Y, Zhang C, Dong H, Lv G and Dong S. MicroRNA-214 Inhibits Left Ventricular Remodeling in an Acute Myocardial Infarction Rat Model by Suppressing Cellular Apoptosis via the Phosphatase and Tensin Homolog (PTEN). *International heart journal*. 2016;57:247-50.

233. Fiedler J, Jazbutyte V, Kirchmaier BC, Gupta SK, Lorenzen J, Hartmann D, Galuppo P, Kneitz S, Pena JT, Sohn-Lee C, Loyer X, Soutschek J, Brand T, Tuschl T, Heineke J, Martin U, Schulte-Merker S, Ertl G, Engelhardt S, Bauersachs J and Thum T. MicroRNA-24 regulates vascularity after myocardial infarction. *Circulation*. 2011;124:720-30.

234. Guo C, Deng Y, Liu J and Qian L. Cardiomyocyte-specific role of miR-24 in promoting cell survival. *Journal of cellular and molecular medicine*. 2015;19:103-12.

235. Meloni M, Marchetti M, Garner K, Littlejohns B, Sala-Newby G, Xenophontos N, Floris I, Suleiman MS, Madeddu P, Caporali A and Emanueli C. Local inhibition of microRNA-24 improves reparative angiogenesis and left ventricle remodeling and function in mice with myocardial infarction. *Molecular therapy : the journal of the American Society of Gene Therapy*. 2013;21:1390-402.

236. Qian L, Van Laake LW, Huang Y, Liu S, Wendland MF and Srivastava D. miR-24 inhibits apoptosis and represses Bim in mouse cardiomyocytes. *The Journal of experimental medicine*. 2011;208:549-60.

237. Wang J, Huang W, Xu R, Nie Y, Cao X, Meng J, Xu X, Hu S and Zheng Z. MicroRNA-24 regulates cardiac fibrosis after myocardial infarction. *Journal of cellular and molecular medicine*. 2012;16:2150-60.

238. Cheng Y, Liu X, Zhang S, Lin Y, Yang J and Zhang C. MicroRNA-21 protects against the H(2)O(2)-induced injury on cardiac myocytes via its target gene PDCD4. *Journal of molecular and cellular cardiology*. 2009;47:5-14.

239. Vlachos IS, Paraskevopoulou MD, Karagkouni D, Georgakilas G, Vergoulis T, Kanellos I, Anastasopoulos IL, Maniou S, Karathanou K, Kalfakakou D, Fevgas A, Dalamagas T and Hatzigeorgiou AG. DIANA-TarBase v7.0: indexing more than half a million experimentally supported miRNA:mRNA interactions. *Nucleic Acids Res*. 2015;43:D153-9.

240. Keyes KT, Xu J, Long B, Zhang C, Hu Z and Ye Y. Pharmacological inhibition of PTEN limits myocardial infarct size and improves left ventricular function postinfarction. *Am J Physiol Heart Circ Physiol*. 2010;298:H1198-208.

241. Ma X, Kumar M, Choudhury SN, Becker Buscaglia LE, Barker JR, Kanakamedala K, Liu MF and Li Y. Loss of the miR-21 allele elevates the expression of its target genes and reduces tumorigenesis. *Proceedings of the National Academy of Sciences of the United States of America*. 2011;108:10144-9.

242. Reczko M, Maragkakis M, Alexiou P, Grosse I and Hatzigeorgiou AG. Functional microRNA targets in protein coding sequences. *Bioinformatics (Oxford, England)*. 2012;28:771-6.

243. Chen J, Huang ZP, Seok HY, Ding J, Kataoka M, Zhang Z, Hu X, Wang G, Lin Z, Wang S, Pu WT, Liao R and Wang DZ. mir-17-92 cluster is required for and sufficient to induce cardiomyocyte proliferation in postnatal and adult hearts. *Circulation research*. 2013;112:1557-66.

244. Zhou M, Cai J, Tang Y and Zhao Q. MiR-17-92 cluster is a novel regulatory gene of cardiac ischemic/reperfusion injury. *Medical hypotheses*. 2013;81:108-10.

245. Rizvi A, Tang XL, Qiu Y, Xuan YT, Takano H, Jadoon AK and Bolli R. Increased protein synthesis is necessary for the development of late preconditioning against myocardial stunning. *The American journal of physiology*. 1999;277:H874-84.

246. Thornton J, Striplin S, Liu GS, Swafford A, Stanley AW, Van Winkle DM and Downey JM. Inhibition of protein synthesis does not block myocardial protection afforded by preconditioning. *The American journal of physiology*. 1990;259:H1822-5.

247. Brundel BJ, Henning RH, Ke L, van Gelder IC, Crijns HJ and Kampinga HH. Heat shock protein upregulation protects against pacing-induced myolysis in HL-1 atrial myocytes and in human atrial fibrillation. *Journal of molecular and cellular cardiology*. 2006;41:555-62.

248. Mestril R, Chi SH, Sayen MR, O'Reilly K and Dillmann WH. Expression of inducible stress protein 70 in rat heart myogenic cells confers protection against simulated ischemia-induced injury. *The Journal of clinical investigation*. 1994;93:759-67.

249. Heads RJ, Yellon DM and Latchman DS. Differential cytoprotection against heat stress or hypoxia following expression of specific stress protein genes in myogenic cells. *Journal of molecular and cellular cardiology*. 1995;27:1669-78.

250. Mestril R, Giordano FJ, Conde AG and Dillmann WH. Adenovirus-mediated gene transfer of a heat shock protein 70 (hsp 70i) protects against simulated ischemia. *Journal of molecular and cellular cardiology*. 1996;28:2351-8.

251. Chen Y, Song YX and Wang ZN. The microRNA-148/152 family: multi-faceted players. *Mol Cancer*. 2013;12:43.

252. Bao JL and Lin L. MiR-155 and miR-148a reduce cardiac injury by inhibiting NF-kappaB pathway during acute viral myocarditis. *European review for medical and pharmacological sciences*. 2014;18:2349-56.

253. Patel V, Carrion K, Hollands A, Hinton A, Gallegos T, Dyo J, Sasik R, Leire E, Hardiman G, Mohamed SA, Nigam S, King CC, Nizet V and Nigam V. The stretch responsive microRNA miR-148a-3p is a novel repressor of IKBKB, NF-kappaB signaling, and inflammatory gene expression in human aortic valve cells. *FASEB journal : official publication of the Federation of American Societies for Experimental Biology*. 2015;29:1859-68.

254. Wei C, Li L and Gupta S. NF-kappaB-mediated miR-30b regulation in cardiomyocytes cell death by targeting Bcl-2. *Molecular and cellular biochemistry*. 2014;387:135-41.

255. Shen Y, Shen Z, Miao L, Xin X, Lin S, Zhu Y, Guo W and Zhu YZ. miRNA-30 family inhibition protects against cardiac ischemic injury by regulating cystathionine-gamma-lyase expression. *Antioxid Redox Signal*. 2015;22:224-40.

256. Wang K, An T, Zhou LY, Liu CY, Zhang XJ, Feng C and Li PF. E2F1-regulated miR-30b suppresses Cyclophilin D and protects heart from ischemia/reperfusion injury and necrotic cell death. *Cell death and differentiation*. 2015;22:743-54.

257. Li T, Sun ZL and Xie QY. Protective effect of microRNA-30b on hypoxia/reoxygenation-induced apoptosis in H9C2 cardiomyocytes. *Gene*. 2015;561:268-75.

258. Winter J and Diederichs S. Argonaute-3 activates the let-7a passenger strand microRNA. *RNA biology*. 2013;10:1631-43.

259. Joshua-Tor L. The Argonautes. *Cold Spring Harbor symposia on quantitative biology*. 2006;71:67-72.

260. Zhang X, Wang X, Zhu H, Zhu C, Wang Y, Pu WT, Jegga AG and Fan GC. Synergistic effects of the GATA-4-mediated miR-144/451 cluster in protection against simulated ischemia/reperfusion-induced cardiomyocyte death. *Journal of molecular and cellular cardiology*. 2010;49:841-50.

261. Li F, Chen Q, Song X, Zhou L and Zhang J. MiR-30b Is Involved in the Homocysteine-Induced Apoptosis in Human Coronary Artery Endothelial Cells by Regulating the Expression of Caspase 3. *International journal of molecular sciences*. 2015;16:17682-95.

262. Cai Z ZH, Bosch-Marce M, Fox-Talbot K, Wang L, Wei C, Trush MA, Semenza GL. Complete loss of ischaemic preconditioning-induced cardioprotection in mice with partial deficiency of HIF-1 alpha. *Cardiovascular research*. 2008;77:463-470.

263. Eckle T KD, Lehmann R, El Kasmi K, Eltzschig HK. Hypoxia-inducible factor-1 is central to cardioprotection: a new paradigm for ischemic preconditioning. *Circulation*. 2008;118:166-175.

264. Liu Y, Nie H, Zhang K, Ma D, Yang G, Zheng Z, Liu K, Yu B, Zhai C and Yang S. A feedback regulatory loop between HIF-1alpha and miR-21 in response to hypoxia in cardiomyocytes. *FEBS letters*. 2014;588:3137-46.

265. Wei C, Li L, Kim IK, Sun P and Gupta S. NF-kappaB mediated miR-21 regulation in cardiomyocytes apoptosis under oxidative stress. *Free radical research*. 2014;48:282-91.

266. Kim HW, Mallick F, Durrani S, Ashraf M, Jiang S and Haider KH. Concomitant activation of miR-107/PDCD10 and hypoxamir-210/Casp8ap2 and their role in cytoprotection during ischemic preconditioning of stem cells. *Antioxid Redox Signal*. 2012;17:1053-65.

267. Kim HW, Haider HK, Jiang S and Ashraf M. Ischemic preconditioning augments survival of stem cells via miR-210 expression by targeting caspase-8-associated protein 2. *The Journal of biological chemistry*. 2009;284:33161-8.

268. Currie RW, Karmazyn M, Kloc M and Mailer K. Heat-shock response is associated with enhanced postischemic ventricular recovery. *Circulation research*. 1988;63:543-9.

269. Hutter JJ, Mestril R, Tam EK, Sievers RE, Dillmann WH and Wolfe CL. Overexpression of heat shock protein 72 in transgenic mice decreases infarct size in vivo. *Circulation*. 1996;94:1408-11.

270. Plumier JC, Ross BM, Currie RW, Angelidis CE, Kazlaris H, Kollias G and Pagoulatos GN. Transgenic mice expressing the human heat shock protein 70 have improved post-ischemic myocardial recovery. *The Journal of clinical investigation*. 1995;95:1854-60.

271. Trost SU, Omens JH, Karlon WJ, Meyer M, Mestril R, Covell JW and Dillmann WH. Protection against myocardial dysfunction after a brief ischemic period in transgenic mice expressing inducible heat shock protein 70. *The Journal of clinical investigation*. 1998;101:855-62.

272. Ray PS, Martin JL, Swanson EA, Otani H, Dillmann WH and Das DK. Transgene overexpression of alphaB crystallin confers simultaneous protection against cardiomyocyte apoptosis and necrosis during myocardial ischemia and reperfusion. *FASEB journal : official publication of the Federation of American Societies for Experimental Biology*. 2001;15:393-402.

273. Belke DD, Gloss B, Hollander JM, Swanson EA, Duplain H and Dillmann WH. In vivo gene delivery of HSP70i by adenovirus and adeno-associated virus preserves contractile function in mouse heart following ischemia-reperfusion. *Am J Physiol Heart Circ Physiol*. 2006;291:H2905-10.

274. Jayakumar J, Suzuki K, Khan M, Smolenski RT, Farrell A, Latif N, Raisky O, Abunasra H, Sammut IA, Murtuza B, Amrani M and Yacoub MH. Gene therapy for myocardial protection: transfection of donor hearts with heat shock protein 70 gene protects cardiac function against ischemia-reperfusion injury. *Circulation*. 2000;102:Iii302-6.

275. Jayakumar J, Suzuki K, Sammut IA, Smolenski RT, Khan M, Latif N, Abunasra H, Murtuza B, Amrani M and Yacoub MH. Heat shock protein 70 gene transfection protects mitochondrial and ventricular function against ischemia-reperfusion injury. *Circulation*. 2001;104:I303-7.

276. Wang JX, Gao J, Ding SL, Wang K, Jiao JQ, Wang Y, Sun T, Zhou LY, Long B, Zhang XJ, Li Q, Liu JP, Feng C, Liu J, Gong Y, Zhou Z and Li PF. Oxidative Modification of miR-184 Enables It to Target Bcl-xL and Bcl-w. *Molecular cell*. 2015;59:50-61.

277. Vekich JA, Belmont PJ, Thuerauf DJ and Glembotski CC. Protein disulfide isomerase-associated 6 is an ATF6-inducible ER stress response protein that protects cardiac myocytes from ischemia/reperfusion-mediated cell death. *Journal of molecular and cellular cardiology*. 2012;53:259-67.

278. Zhang K, Lindsberg PJ, Tatlisumak T, Kaste M, Olsen HS and Andersson LC. Stanniocalcin: A molecular guard of neurons during cerebral ischemia. *Proceedings of the National Academy of Sciences of the United States of America*. 2000;97:3637-42.

279. Kozomara A and Griffiths-Jones S. miRBase: annotating high confidence microRNAs using deep sequencing data. *Nucleic Acids Res*. 2014;42:D68-73.

280. Qiu H, Liu JY, Wei D, Li N, Yamoah EN, Hammock BD and Chiamvimonvat N. Cardiac-generated prostanoids mediate cardiac myocyte apoptosis after myocardial ischaemia. *Cardiovascular research*. 2012;95:336-45.

281. Stephanou A, Scarabelli TM, Brar BK, Nakanishi Y, Matsumura M, Knight RA and Latchman DS. Induction of apoptosis and Fas receptor/Fas ligand expression by ischemia/reperfusion in cardiac myocytes requires serine 727 of the STAT-1 transcription factor but not tyrosine 701. *The Journal of biological chemistry*. 2001;276:28340-7.

282. Polytarchou C, Iliopoulos D, Hatziapostolou M, Kottakis F, Maroulakou I, Struhl K and Tsichlis PN. Akt2 regulates all Akt isoforms and promotes resistance to hypoxia through induction of miR-21 upon oxygen deprivation. *Cancer research*. 2011;71:4720-31.

283. Palamarchuk A, Efanov A, Maximov V, Aqeilan RI, Croce CM and Pekarsky Y. Akt phosphorylates and regulates Pdcd4 tumor suppressor protein. *Cancer research*. 2005;65:11282-6.

284. Wang W, Zhao J, Wang H, Sun Y, Peng Z, Zhou G, Fan L, Wang X, Yang S, Wang R and Fang D. Programmed cell death 4 (PDCD4) mediates the sensitivity of gastric cancer cells to TRAIL-induced apoptosis by down-regulation of FLIP expression. *Experimental cell research*. 2010;316:2456-64.

285. Davidson SM, Stephanou A and Latchman DS. FLIP protects cardiomyocytes from apoptosis induced by simulated ischemia/reoxygenation, as demonstrated by short hairpin-induced (shRNA) silencing of FLIP mRNA. *Journal of molecular and cellular cardiology*. 2003;35:1359-64.

286. Marquez RT, Wendlandt E, Galle CS, Keck K and McCaffrey AP. MicroRNA-21 is upregulated during the proliferative phase of liver regeneration, targets Pellino-1, and inhibits NF-kappaB signaling. *American journal of physiology Gastrointestinal and liver physiology*. 2010;298:G535-41.

287. Khan M, Nickoloff E, Abramova T, Johnson J, Verma SK, Krishnamurthy P, Mackie AR, Vaughan E, Garikipati VN, Benedict C, Ramirez V, Lambers E, Ito A, Gao E, Misener S, Luongo T, Elrod J, Qin G, Houser SR, Koch WJ and Kishore R. Embryonic stem cell-derived exosomes promote endogenous repair mechanisms and enhance cardiac function following myocardial infarction. *Circulation research*. 2015;117:52-64.

288. Sahoo S and Losordo DW. Exosomes and cardiac repair after myocardial infarction. *Circulation research*. 2014;114:333-44.

289. Zhang Z, Yang J, Yan W, Li Y, Shen Z and Asahara T. Pretreatment of Cardiac Stem Cells With Exosomes Derived From Mesenchymal Stem Cells Enhances Myocardial Repair. *J Am Heart Assoc*. 2016;5.

VITA

Kristin (Lierl) Luther attended University of Cincinnati for her undergraduate degrees, with a dual major in Biology and Fine Arts. After graduation, she worked for two years as a research assistant in the laboratory of Dr. Kristen Page at Cincinnati Children's Hospital Medical Center in the department of Critical Care Medicine. Her project was to analyze the response of mice and bronchial cells to cockroach allergen, and resulted in new knowledge of the inflammatory signaling pathways that are activated.

In 2007, she attended University of Illinois at Chicago's Biomedical Visualization program, where she attained her MS degree. During her time at UIC, she joined the laboratory of Dr. Geula Gibori. There she helped to elucidate the transcription factors involved in expression of an enzyme during the response of breast cancer cells to estrogen. After attaining her MS, she worked as a freelance medical illustrator for two years, during which time she produced illustrations and graphic design.

She was accepted in 2011 to University of Cincinnati's Pharmacology program, where she began studying the role of miRNA in cardioprotection during ischemic preconditioning and stem cell therapy. She later transferred to Loyola University Chicago where she finished the project with a focus on pro-survival miRNA that is transferred from stem cells to cardiomyocytes via exosomes. She will continue this work during her postdoctoral fellowship at Cedars-Sinai Heart Institute in the laboratory of Dr. Eduardo Marbán.